

**Yeast-based assay systems for screening and
characterization of ligands targeting human glucose
transporters GLUT2 and GLUT3**

Dissertation
zur Erlangung des Doktorgrades
der Naturwissenschaften

vorgelegt beim Fachbereich Biowissenschaften
der Johann Wolfgang Goethe-Universität
in Frankfurt am Main

von
Sina Schmidl
aus Baden (Schweiz)

Frankfurt am Main, 2021
(D 30)

vom Fachbereich Biowissenschaften
der Johann Wolfgang Goethe-Universität
als Dissertation angenommen

Dekan: Prof. Dr. Sven Klimpel

1. Gutachter: Dr. Mislav Oreb
2. Gutachterin: Prof. Dr. Claudia Büchel

Datum der Disputation:

This thesis is based on the following publications:

Sina Schmidl, Cristina V. Iancu, Jun-yong Choe and Mislav Oreb (2018).

Ligand screening systems for human glucose transporters as tools in drug discovery. *Frontiers in Chemistry*, 6, 183. (published)

Sina Schmidl, Cristina V. Iancu, Mara Reifenrath, Jun-yong Choe and Mislav Oreb (2021). A label-free real-time method for measuring glucose uptake kinetics in yeast. *FEMS Yeast Research*, 21(1), foaa069. (published)

Sina Schmidl, Sebastian A. Tamayo Rojas, Cristina V. Iancu, Jun-yong Choe and Mislav Oreb (2021). Functional expression of the human glucose transporters GLUT2 and GLUT3 in yeast offers novel screening systems for GLUT-targeting drugs. *Frontiers in Molecular Bioscience*, 7, 598419. (published)

Sina Schmidl*, Oleg Ursu*, Cristina V. Iancu, Mislav Oreb, Tudor Oprea and Jun-yong Choe (2021). Identification of new GLUT2-selective inhibitors through *in silico* ligand screening and validation in a eukaryotic expression system. *Scientific Reports*, 11, 13751. (published)

* Shared first authorship

Contents

1	Summary	1
2	Introduction	4
2.1	Uptake of sugars in human cells	4
2.1.1	Structure and function of human GLUTs	6
2.1.2	GLUT-related diseases.....	7
2.1.2.1	GLUT1 deficiency syndrome.....	7
2.1.2.2	GLUT2-associated diseases	8
2.1.2.3	Diabetes.....	9
2.1.2.4	Cancer	10
2.2	Systems for assaying GLUT activity and identifying modulators	12
2.2.1	Cell-free systems.....	12
2.2.2	Animal cell-based systems	13
2.2.3	Yeast cell-based systems	14
2.2.3.1	The hexose transporter deficient yeast strain EBY.VW4000	15
2.2.3.2	Point mutations enable the functional expression of certain GLUTs in the hxt ⁰ yeast system.....	16
2.2.3.3	The lipid composition of the plasma membrane of yeast affects GLUT activity	17
2.2.3.4	Players that regulate phosphoinositide levels in membranes	18
2.2.3.5	Alterations in the ergosterol biosynthesis enable GLUT4 activity in yeast	20
2.2.4	Glucose uptake assays	24
2.3	Aim of this thesis	27
3	General discussion	28
3.1	The hxt ⁰ yeast system as a microbial investigation platform for transporters	28
3.1.1	The functional expression of GLUT2 and GLUT3 in a hxt ⁰ yeast strain	29

3.1.2	Expression of GLUTs with preserved functions	32
3.1.3	The sterol composition in yeast and its effect on the functional expression of human GLUTs	34
3.2	Structure-based GLUT-selective ligand screenings.....	38
3.2.1	GLUT2 screening and ideas for future GLUT-selective ligand screenings	39
3.2.2	Importance and application areas for GLUT-specific effectors	40
3.2.2.1	Application areas for GLUT2-specific inhibitors.....	42
3.3	Roles of soluble loops in transporters – more than just connectors.....	44
3.4	Advantages and restrictions of the pHluorin-based assay – a new, label-free method to measure sugar uptake	46
4	References	53
5	Additional results	71
5.1	Additional results and discussion – Impact of yeast PM modifications on the heterologous expression of human GLUTs	71
5.1.1	Construction of hxt ⁰ strains producing various sterols and evaluation of their ability to express native human GLUTs	71
5.1.2	Alterations of the PI production at the yeast PM and assessing the effects on functional expression of native human GLUTs	75
5.2	Additional results and discussion – Application of the hxt ⁰ yeast system as a screening platform for GLUT-specific inhibitors	78
5.2.1	Testing an HIV integrase inhibitor for inhibitory effects on GLUTs.....	78
5.2.2	Employing the pHluorin-based assay for inhibitor screenings.....	80
5.3	Materials and Methods	83
5.3.1	Plasmid construction.....	83
5.3.2	Strain construction	87
5.3.3	Media and growth conditions	88
5.3.4	Growth tests.....	89
5.3.5	C ¹⁴ glucose uptake assay	90

5.3.6	Platereader-assisted inhibitor screening with the pFluorin-based assay	91
5.4	References for the additional results	92
6	Publications	95
6.1	Ligand screening systems for human glucose transporters as tools in drug discovery	95
6.2	A label-free real-time method for measuring glucose uptake kinetics in yeast.....	103
6.3	Functional expression of the human glucose transporters GLUT2 and GLUT3 in yeast offers novel screening systems for GLUT-targeting drugs	117
6.4	Identification of new GLUT2-selective inhibitors through <i>in silico</i> ligand screening and validation in eukaryotic expression systems	140
7	Deutsche Zusammenfassung.....	173
8	Danksagung.....	178
9	Curriculum vitae	179

1 Summary

Human GLUTs represent a family of specialized transporters that facilitate the diffusion of hexoses through membranes along a concentration gradient. The 14 isoforms share high sequence identity but differ in substrate specificity and affinity, and tissue distribution. According to their structure similarity, GLUTs are divided into three classes, with class 1 comprising the most intensively studied isoforms GLUTs1-4. An abnormal function of different GLUT members has been related to the pathogenesis of various diseases, including cancer and diabetes. Hence, GLUTs are the subject of intensive research, and efforts concentrate on identifying GLUT-selective ligands for putative medical purposes and their application in studies aiming to further unravel the metabolic roles of these transporters.

The hexose transporter deficient (hxt^0) yeast strain EBY.VW4000 is devoid of all its endogenous hexose transporters and unable to grow on glucose or related hexoses. This strain has proven to be a valuable platform to investigate heterologous transporters due to its easy handling, increased robustness, and versatile applications. However, the functional expression of GLUTs in yeast requires certain modifications. Single point mutations of GLUT1 and GLUT5 led to their functional expression in EBY.VW4000, whereas the native GLUT1 was actively expressed in EBY.S7, a hxt^0 strain carrying the *fgy1* mutation that putatively reduces the phosphatidylinositol-4-phosphate (PI4P) content in the plasma membrane. GLUT4 was only actively expressed in the hxt^0 strain SDY.022, which also contains the *fgy1* mutation and in which *ERG4* is additionally deleted. Erg4 is one of the late enzymes in the ergosterol pathway, and therefore SDY.022 probably has an altered sterol composition in its membrane.

The goal of this thesis was to actively express GLUT2 and GLUT3 in a hxt^0 yeast strain, providing a convenient system for their ligand screening. A PCR-derived amino acid exchange in the sequence of GLUT3 enabled its functional expression in EBY.VW4000 and the unmodified GLUT3 protein was active in EBY.S7. Functional expression of GLUT2 was achieved by rational design. The extracellular loop between the transmembrane regions 1 and 2 is significantly larger in GLUT2 than in other class 1 GLUTs. By truncating this loop by 34 amino acids and exchanging an alanine for a serine, a GLUT3-like loop was implemented. The

resulting construct GLUT2 Δ loopS was functional in EBY.S7. With an additional point mutation in the transmembrane region 11, GLUT2 Δ loopS_Q455R was also actively expressed in EBY.VW4000. Inhibition studies with the known GLUT inhibitors phloretin and quercetin showed a reduced transporter activity for GLUT2 and GLUT3 in uptake assays and growth tests when inhibitors were present, demonstrating that both systems are amenable for ligand screening experiments.

The newly established GLUT2 yeast system was then used to screen a library of compounds pre-selected by *in silico* screening. Thereby, eleven identified GLUT2 inhibitors exhibited strong potencies with IC₅₀ values ranging from 0.61 to 19.3 μ M. By employing the other yeast systems, these compounds were tested for their effects on GLUT1, and GLUTs3-5, revealing that nine of the identified ligands were GLUT2-selective. In contrast, one was a pan-class 1 inhibitor (inhibiting GLUTs1-4), and one affected GLUT2 and GLUT5, the two fructose transporting isoforms. These compounds will serve as useful tools for investigations on the role of GLUT2 in metabolic diseases and might even evolve into pharmaceutical agents targeting GLUT2-associated diseases.

Due to the beneficial effect of the putatively changed sterol composition in SDY.022 (by *ERG4* deletion) on the functional expression of GLUT4, it was hypothesized that the presence of the human sterol cholesterol, or cholesterol-like sterols, might have a beneficial effect on GLUT expression, too. Thus, it was attempted to generate hxt⁰ strains that synthesize these sterols by genetic modifications targeting the ergosterol pathway. In the scope of these experiments, several strains with different sterol compositions were generated. Drop tests on glucose medium with the different strains expressing GLUT1 or GLUT4 revealed that the deletion of *ERG6* is clearly advantageous for a functional expression of GLUT1 (but not GLUT4). This indicates that the methyl group at the ergosterol side chain (introduced by Erg6 and reduced by Erg4) negatively influences GLUT1 activity. However, this effect on GLUT1 activity was less pronounced than the putative altered PI4P content in EBY.S7.

Additionally, in this thesis, a new tool to measure glucose transport rates of transporters expressed in the hxt⁰ yeast system was developed to facilitate their kinetic characterization. For this, the pH-sensitive GFP variant pHluorin was

employed as a biosensor for the cytosolic pH (pH_{cyt}) by measuring the ratio ($R_{390/470}$) of emission intensities at 512 nm from two different excitation wavelengths (390 and 470 nm). Sugar-starved cells exhibit a slightly acidic pH_{cyt} because ATP production is depleted, reducing the activity of ATP-dependent proton pumps. By reintroducing sugar, e.g., glucose, the pH_{cyt} rises to a normal pH_{cyt} of ~ 7 , as ATP production recovers. Within the first ~ 10 seconds, however, an initial further acidification takes place. This can be explained by the first step of glycolysis, in which glucose is phosphorylated to glucose-6-phosphate by a hexokinase, concomitantly hydrolyzing one ATP, which releases one proton that acidifies the cytosol. It was discovered that the velocity of this initial acidification is directly linked to the sugar uptake rate of the respective transporter expressed in the hxt^0 yeast strain. Thus, the linear decreasing slope of the acidification phase was defined as a parameter of sugar uptake velocity and used to fit the Michaelis-Menten equation, resulting in reliable K_M values. This method offers a great advantage over the conventionally used C^{14} glucose uptake assay as it does not require radiolabeled glucose, being safer, cheaper, and accessible to a broader scientific community.

In summary, this thesis expanded the hxt^0 yeast system with two important GLUTs, GLUT2 and GLUT3, providing a convenient and accessible platform for the screening of specific ligands. For GLUT2, this platform was successfully applied, resulting in the identification of eleven potent GLUT2 inhibitors, of which nine were GLUT2-specific. Moreover, a new label-free method was established that will facilitate and accelerate the kinetic characterization of transporters and will therefore be a valuable contribution to sugar transport-related research.

2 Introduction

2.1 Uptake of sugars in human cells

Hexoses, and mainly glucose, are the central substrates of mammalian energy metabolism and their transport across cell membranes via specialized transporters represents the first step. In human cells, three distinct sugar transporter families exist to fulfill this task; the glucose facilitator family (GLUTs) (Mueckler and Thorens, 2013), the secondary active sodium-glucose symporters (SGLTs) (Wright et al., 2011) and the glucose uniporter family (SWEETs) (Feng and Frommer, 2015).

The SGLT family comprises twelve members that differ in their substrate specificity and affinity, and their coupling ion preferences. They are also distributed in different tissues including the intestine, kidney, brain, muscles, and thyroid gland (Wright, 2013) and display varying stoichiometries, e.g., SGLT1 transports two sodium ions concomitant with one sugar molecule, whereas SGLT2 symports just one per molecule (Wright et al., 2011). SGLT1 and SGLT2 are the most extensively studied members and play crucial roles in the sugar absorption from the intestine and reabsorption in the kidney, respectively (Kellett and Brot-Laroche, 2005; Deng and Yan, 2016). As secondary active transporters, they rely on a sodium gradient across the membrane supplied by the primary active Na^+/K^+ pump (Wright et al., 2011). SWEET transporters are believed to be facilitative uniporters but information about their mode of action is still scarce (Feng and Frommer, 2015). Their name that derives from “sugar will eventually be exported transporters” indicates their important role in sugar export from photosynthetically active cells into the cell wall, in plants (Eom et al., 2015; Deng and Yan, 2016). While many representatives of the SWEET family exist in plants, only one homolog was identified in human cells (Feng and Frommer, 2015). Human SWEET1 shows weak glucose efflux activity and is ubiquitously synthesized but primarily found in oviduct, epididymis, intestine, and β -cell tissues (Eom et al., 2015).

The GLUT family comprises 14 members in humans that mediate the facilitated diffusion of glucose (and related substrates) along a concentration gradient (Holman, 2020). These transporters share high amino acid sequence identities (up to 65%) and similarities (up to 81%) (Iancu et al., 2013) but differ in substrate

specificity and affinity, thereby allowing a fine tuning of sugar transport corresponding to specific tissue requirements (Holman, 2020). In Table 1, predominant substrates, the affinity for their main substrate, and tissue distributions of all GLUTs are listed.

Table 1. The 14 GLUT isoforms. Predominant substrates for each GLUT and tissues in which they are primarily distributed are named. K_M values as a measure of affinity for the main substrates (underlined) are listed.

GLUT protein	Predominant substrates (Mueckler and Thorens, 2013)	Affinity (K_M values)	Tissue distribution (Mueckler and Thorens, 2013)
GLUT1	<u>Glucose</u> , galactose, mannose, glucosamine	3.4 mM (Kasahara and Kasahara, 1996)	Ubiquitous expression, main tissues: erythrocytes, brain, blood-brain barrier, blood-tissue barrier
GLUT2	<u>Glucose</u> , galactose, fructose, mannose, glucosamine	17 mM (Uldry et al., 2002)	Liver, β -cells, intestine, kidney, brain
GLUT3	<u>Glucose</u> , galactose, mannose, xylose	1.4 mM (Colville et al., 1993)	Brain (neurons), testis
GLUT4	<u>Glucose</u> , glucosamine	12 mM (Kasahara and Kasahara, 1997)	Adipose tissue, skeletal and cardiac muscle
GLUT5	<u>Fructose</u>	10 mM (Tripp et al., 2017)	Small intestine, kidney
GLUT6	<u>Glucose</u>	N/A	Brain, spleen, leucocytes
GLUT7	<u>Glucose</u> , fructose	0.3 mM (Li et al., 2004)	Small intestine, colon, testis, prostate
GLUT8	<u>Glucose</u> , fructose, galactose	2 mM (Schmidt et al., 2009)	Testis, brain, adrenal gland, liver, spleen, brown adipose tissue, lung
GLUT9	<u>Glucose</u> , fructose, <u>urate</u>	0.6 mM (glucose) (Manolescu et al., 2007) 1 mM (urate) (Caulfield et al., 2008)	Kidney, liver, small intestine, placenta, lung, leucocytes

GLUT10	<u>Glucose</u> , galactose	0.3 mM (Dawson et al., 2001)	Heart, lung, brain, liver, skeletal muscle pancreas, placenta, kidney
GLUT11	<u>Glucose</u> , fructose	0.16 mM (Manolescu et al., 2007)	Heart, muscle
GLUT12	<u>Glucose</u> , urate (Toyoda et al., 2020)	6.4 mM (Matsuo et al., 2020)	Heart, prostate, skeletal muscle, placenta
GLUT13/ HMIT	<u>Myo-inositol</u>	0.1 mM (Augustin, 2010)	Brain, adipose tissue
GLUT14	N/A	N/A	Testis

2.1.1 Structure and function of human GLUTs

GLUTs can be divided into three subclasses, according to their sequence and structure similarities (Joost et al., 2002). Class 1 GLUTs (GLUTs1-4, and GLUT14, a duplicon of GLUT3) are the most extensively studied isoforms. Class 2 comprises GLUT5, GLUT7, GLUT9, and GLUT11 and class 3 consists of GLUT6, GLUT8, GLUT10, GLUT12, and GLUT13 (Joost et al., 2002; Mueckler and Thorens, 2013). While GLUTs from class 1 and class 2 show a larger extracellular loop between the transmembrane regions (TM) 1 and TM2 containing a glycosylation site, this loop is shorter and lacks the glycosylation site in class 3 GLUTs. Instead, class 3 GLUTs possess a larger loop between TM9 and TM10, exhibiting such a site. Furthermore, an STSIF motif in the loop between TM7 and TM8 is a characteristic element of class 1 GLUTs, whereas class 2 GLUTs share the lack of tryptophan after the conserved GPXXXP motif in helix 10 (Joost and Thorens, 2009).

All GLUTs are furthermore members of the large major facilitator superfamily (MFS) and exhibit the distinct structure typical for MFS proteins (Thorens and Mueckler, 2010). Twelve transmembrane helices (TM1-TM12) are organized into two halves (N-terminal half: TM1-TM6 and C-terminal half: TM7-TM12), embedding the substrate cavity in the middle (Quistgaard et al., 2016). With most GLUTs presumably being uniporters (Iancu et al., 2013), they facilitate the diffusion across membranes of just one substrate molecule at a time along a concentration gradient supposedly by exposing the substrate cavity to each side of the membrane in an alternating manner. After binding of the substrate in the central

cavity, bending of α -helix ends induces occluded states in which the substrate site is shielded from either the cytoplasm (inside-occluded conformation) or the extracellular space (outward-occluded conformation) (Quistgaard et al., 2016). The rocker-switch movement, in which the two domains (N- and C-) rearrange around the substrate binding site in a rocking motion, then mediates a switch, and the substrate binding site opens to the other side of the membrane (Qureshi et al., 2020).

Elucidation of GLUT structure and the proposed alternating-access mechanism of transport was significantly advanced by crystal structures of GLUT1, GLUT3 and GLUT5 (Deng et al., 2014; Deng et al., 2015; Nomura et al., 2015) and their bacterial homologs XylE (Sun et al., 2012) and GlcP_{Se} (Iancu et al., 2013).

These achievements were challenging to obtain and represent a great success in sugar transport research, providing the basis for structure-based modelling of GLUTs (Thorens and Mueckler, 2010; Sun et al., 2012). They suggest the functions of particular amino acid residues and improve our understanding of disease-related mutations (Sun et al., 2012). With 3D models derived from existing GLUT crystal structures, *in silico* screening of ligands was enabled. Thereby, millions of compounds can be screened for their interactions with the active site or hydrophilic domains of specific GLUTs, depending on the investigation focus. A significantly reduced number of compounds can then be further investigated *in vitro* with the help of a convenient assay screening system (Schmidl et al., 2018).

2.1.2 GLUT-related diseases

Abnormal expression, localization, or function of GLUTs are related to the pathogenesis of several prevalent or also rare diseases, highlighting their significance for metabolic integrity.

2.1.2.1 GLUT1 deficiency syndrome

One GLUT-related disease is the GLUT1 deficiency syndrome (GLUT1 DS), formerly considered an extremely rare condition, with diverse symptoms that primarily comprise infantile seizures, developmental delay, acquired microcephaly, and complex movement disorders due to low glucose levels in the brain

(Brockmann, 2009; Tang et al., 2017). More recently, cases with milder symptoms and idiopathic epilepsies could be assigned to GLUT1 DS as well, suggesting a higher dimension of this condition (Tang et al., 2017). An insufficient glucose concentration in the cerebrospinal fluid with concomitant absence of hypoglycemia is used as a diagnostic marker for GLUT1 DS (Brockmann, 2009; Giorgis et al., 2016). The cause of this disease is a deficient transport of glucose to the brain, and, in most diagnosed patients (70-80%), mutations in the *SLC2A1* gene encoding for GLUT1 were found responsible (Giorgis et al., 2016). The only treatment for GLUT1 deficiency symptoms so far is a ketogenic diet, whereby ketone bodies enter the system via a monocarboxylic transport mechanism, independent from the transport via GLUT1, and provide an alternative source of energy to the brain (Pascual et al., 2004; Sandu et al., 2019). This treatment has been proven effective for diminishing seizures but only showed negligible improvements on cognitive dysfunctions (Pascual et al., 2004; Tang et al., 2017; Sandu et al., 2019). In mouse models, repletion of a functional *SLC2A1* gene at an early developmental stage to GLUT1 defective mice rescues brain microvasculature defects, another severe effect of GLUT1 DS, and is discussed as another therapeutic strategy (Tang et al., 2017).

2.1.2.2 GLUT2-associated diseases

The Fanconi-Bickel syndrome represents another rare disorder of carbohydrate metabolism due to mutations in a GLUT encoding gene. The disease was described for the first time in 1949 (Fanconi and Bickel, 1949). Several mutations distributed all over the *SLC2A2* gene, encoding GLUT2, without any mutational hot spots, have been related to this autosomal, recessive disease (Santer et al., 2002). These are putatively responsible for multiple typical symptoms like hepatomegaly, characteristic tubular nephropathy, glucose and galactose intolerance, hypoglycemia, rickets, and retarded growth. However, it has been shown that abnormal GLUT2 proteins also provoke atypical symptoms, like the failure to thrive, and the before-mentioned characteristic ones do not necessarily exist in Fanconi-Bickel syndrome patients (Santer et al., 2002). With its high degree of phenotypic heterogeneity and no existing drugs against the underlying cause, treatment of the

Fanconi-Bickel syndrome is challenging (Khandelwal et al., 2018; Sharari et al., 2020).

Besides mutations in the *SLC2A2* gene, other physiological effects can lead to GLUT2 malfunction as well, e.g., a disturbed anchoring to the cell membrane due to failed N- glycosylation, as it has been shown in murine β -cells (Ohtsubo et al., 2005). In mice (but not humans (McCulloch et al., 2011)), GLUT2 has been found responsible for glucose-stimulated insulin secretion in the pancreas (Ohtsubo et al., 2005). Due to its many regulatory functions (e.g., glucose-regulated gene expression in the liver (Guillemain et al., 2000), glucose reabsorption in the kidney (Ghezzi et al., 2018), glucose-sensing in the brain for a normal glucagon response (Koepsell, 2020), increased glucose uptake from the intestine after a meal (Kellett, 2001)), it might play multiple roles in the pathogenesis of diabetes or in symptoms of the metabolic syndrome (Thorens, 2001; Kellett and Brot-Laroche, 2005; Eny et al., 2008).

2.1.2.3 Diabetes

Multiple polygenic and environmental factors are believed to contribute to the development of diabetes (Ziesman, 2000). The insulin-dependent glucose transporter GLUT4 is considered a key player in the pathogenesis of this disease. This transporter is predominantly expressed in the adipose tissue, heart, and skeletal muscle and is stored in small vesicles in the cytoplasm until insulin triggers its translocation to the plasma membrane (PM), where it mediates glucose uptake (Hajiaghaalipour et al., 2015; Jaldin-Fincati et al., 2018). Diabetes mellitus type 2 is characterized by a resistance to insulin and a concomitant decrease in insulin production through the β -cells (Hajiaghaalipour et al., 2015), which leads to reduced GLUT4 levels at the PM, thus decreasing glucose uptake, resulting in elevated blood glucose levels. Moreover, other less-extensively studied glucose transporters were related to the pathogenesis of type 2 diabetes as well (Dawson et al., 2001; Maria et al., 2015). Hence, several GLUTs seem to play a crucial role in the development of diabetes.

In 2019, approximately 463 million adults had diabetes (www.idf.org), with an increasing proportion (more than 90%) of type 2 diabetes patients, and the

epidemic is constantly growing, evolving to a global health problem (Hajiaghaalipour et al., 2015). A healthy lifestyle, including diet, exercise, and weight control, can positively influence the pathogenesis of type 2 diabetes. In more severe cases, taking insulin or other anti-diabetes agents enables patients to control their disease. However, the maintenance of a normal blood glucose level requires strict management, and various complications may occur e.g., late consequences such as cardiovascular diseases, nephropathy, atherosclerosis, or retinopathy, which may severely diminish the patient's life quality (Hajiaghaalipour et al., 2015). Therefore, there is a great demand for anti-diabetic agents or treatments that may improve diabetes therapy and reduce the risk of further complications; enabling the manipulation of GLUTs is one approach for this purpose.

2.1.2.4 Cancer

The exploitation of GLUTs as drug targets is especially valuable in cancer therapy. An accelerated glycolysis rate with subsequent reduction of pyruvate to lactate usually only appears under anaerobic conditions in human cells when ATP production via the citric acid cycle is impeded. Tumor cells, however, show this metabolic abnormality under normoxic conditions (Danhier et al., 2017). This effect, called the "Warburg effect", causes a higher demand of glucose supply which is met by enhanced transport through increased expression of glucose transporters in these fast-proliferating cells (Cairns et al., 2011).

A higher expression rate of several GLUTs has already been identified in various kinds of tumors (Szablewski, 2013), and their entire role in cancer pathogenesis is likely not elucidated yet. Most prominently, higher expression rates of GLUT1 have been found in most cancer tissues (Godoy et al., 2006), and studies indicate that this overexpression is an early event in the course of the disease (Rudlowski et al., 2003; Macheda et al., 2005). In addition, expression of GLUT1 and GLUT3 seems to correlate with the malignancy of the tumor, and survival of patients decreases with increasing GLUT1 or GLUT3 expression (Macheda et al., 2005; Barron et al., 2016). Therefore, GLUTs have a high potential to serve as a biomarker in tumors revealing information about cancer aggressiveness and indicating an appropriate therapy. Besides an overexpression of constitutively expressed GLUTs in tumors,

GLUT isoforms were detected in malignant cells whereas those isoforms did not occur in the corresponding healthy tissue (Macheda et al., 2005). GLUT5, for example, was found in breast cancer but not in the normal tissue (Zamora-Leon et al., 1996). Intriguingly, the extensive expression of the fructose transporting proteins GLUT2 and GLUT5 in some malignant tissues like breast, stomach mucosa epithelium, or smooth muscle indicates that fructose is an attractive energy source for some tumors (Godoy et al., 2006). Various studies also related abnormal expression of other transporters, including GLUT4, GLUT6, GLUT7, GLUT8, GLUT11, and GLUT12, with the fast proliferation of cancer cells (Rogers et al., 2002; Godoy et al., 2006; McBrayer et al., 2012). Thus, members of the GLUT family have a high potential not only as biomarkers but also as drug targets for cancer treatment, which is bolstered by the fact that cancer cells die faster than normal cells under glucose-limiting conditions (Liu et al., 2010). Studies have already been performed in which GLUTs were inhibited to decrease cancer growth via different approaches, including the application of antisense oligonucleotides against *SLC2A* genes, usage of GLUT antibodies, and the inhibition of GLUT transporters with specifically binding substrates (Szablewski, 2013; Barron et al., 2016). Some inhibitors of GLUTs, predominantly GLUT1, have been discovered, as the selective GLUT1 inhibitor BAY-876 (Siebeneicher et al., 2016) and the non-selective but highly potent compounds glutor and glupin (Reckzeh and Waldmann, 2020), to name just a few, but they often do not meet the requirements like high specificity for certain GLUTs, sufficient tissue penetration, high potency, and negligible side-effects (Barron et al., 2016; George Thompson et al., 2016). Furthermore, most of the known inhibitors have not been tested in clinical trials yet, restricting the knowledge about their effects on cancer (Barron et al., 2016). Nevertheless, some recent studies show that GLUT inhibition indeed tackles cancer proliferation (Reckzeh et al., 2019; Shriwas et al., 2021) and further investigations in this field are desirable to improve the perspectives of cancer patients. Ultimately, this might lead to more clinical studies with GLUT effectors. However, many might fail in animal or clinical trials due to unexpected adverse effects and having a plethora of candidates is beneficial. Thus, the identification of further GLUT effectors is an important aim in combating cancer.

2.2 Systems for assaying GLUT activity and identifying modulators

Systematic discovery of GLUT-targeting drugs requires the analysis of high-quality 3D structures to identify active sites, *in silico* ligand screening of a large library of compounds, screening systems for further validation, and characterization of promising candidates (Schmidl et al., 2018). Increased availability of crystal structures for several transporters and homology models now allows *in silico* investigation of all GLUTs (Schmidl et al., 2018). Also, experimental, and computational techniques in the field of structure elucidation have improved (Colas et al., 2016), and efforts to provide a larger database of small compounds to a broader scientific community were successful (Schreiber et al., 2015). These factors led to better conditions for the virtual screening of possible effectors.

Although undoubtedly essential for narrowing down the number of possible effectors, *in silico* screening still results in a high number of candidates, e.g., 374 after GLUT5 screening (George Thompson et al., 2016) or >200 after GLUT2 screening (Schmidl et al., 2021c), revealing the demand for an additional, subsequent investigation platform. Requirements for such a system are high. It should be convenient to handle, quick, and cost-efficient, yielding reliable results while preserving the innate properties of the transporter (Schmidl et al., 2018).

2.2.1 Cell-free systems

Several cell-free, *in vitro* systems with different advantages have been employed to investigate membrane proteins, including GLUTs (Kraft et al., 2015). These systems generally aim to mimic the native lipid environment of the protein to maintain its natural conformation and function. Detergents self-assemble to micelles and are a widely used platform (Privé, 2007). Micelles can be easily modified in their size or chemical composition by varying detergents which influences protein interaction, but at the same time, they exhibit great complexity, and many factors like temperature and ionic strength must be considered (Privé, 2007; Kraft et al., 2015). Amphipols, a group of amphipathic polymers, stabilize membrane proteins by wrapping their hydrophobic core, enabling increased stability in an aqueous solution (in the absence of detergents) (Kleinschmidt and

Popot, 2014). Thereby, it allows the implementation of a series of experiments that require increased stability due to their length or destabilizing conditions. Specific poly(styrene-co-maleic acid) copolymers can bind to biological membranes, converting the protein of interest and its natural surrounding lipid environment into so-called nanodiscs (Overduin and Klumperman, 2019). These conserved lipid-protein complexes are advanced investigation tools as the natural environment of the target protein is preserved, and several studies indicate the significance of protein-lipid interactions in intrinsic membrane domains for the stability and activity of membrane proteins (van 't Klooster et al., 2020b). However, for direct transport activity assays, proteoliposomes are often the method of choice (Kraft et al., 2015). Thereby, the transporter is reconstituted in a lipid bilayer that offers two distinct compartments (outside and inside), which is necessary to quantify transport rates (Kraft et al., 2015). It also allows the adaptation of lipid lateral diffusion and the degree of membrane curvature by carefully selecting detergents (Seddon et al., 2004). Unfavorably, a considerable number of criteria (e.g., a homogenous size- and protein distribution of the liposomes, permeability of the membrane, and protein-to-lipid ratios) must be considered (Seddon et al., 2004), and a sufficient amount of pure protein must be obtained preliminary, making these experiments elaborate.

2.2.2 Animal cell-based systems

Apart from the described cell-free systems, cell-based systems have been widely used to assess GLUT activity, too. Obviously, human cell lines like HEK293 (Zutter et al., 2013) and many human cancer cell lines (e.g., MCF-7 (Zamora-Leon et al., 1996), Caco-2 (Mahraoui et al., 1994; Lee et al., 2015)) were utilized with the advantage that conditions like posttranslational modifications or lipid environment are most probable unchanged compared to native circumstances (Schmidl et al., 2018). However, the biggest drawback of human cell lines as investigation platform of GLUTs is the endogenous expression of sugar transporters in these cells (Schmidl et al., 2018). This background activity complicates the assessment of the GLUT in question, especially when the latter only shows a low affinity for its substrate, as is the case for GLUT2 (Schmidl et al., 2021c). *Xenopus laevis* oocytes exhibit a very low endogenous GLUT expression and provide the benefit

of a large cell size (enabling electrophysiological investigations) (Long et al., 2018). Thus, they were utilized in many studies to investigate GLUTs and their kinetic properties (Gould and Lienhard, 1989; Mueckler and Thorens, 2013; Long et al., 2018). Unfavorably for this platform, not all GLUTs insert in the PM sufficiently, and the amount of protein in the membrane needs to be determined via immunoprecipitation, which is labor-intensive and utilizes expensive antibodies (Gould and Lienhard, 1989; Keller et al., 1989). These factors and an insufficient robustness (César-Razquin et al., 2015) makes *Xenopus laevis* oocytes unsuitable as a high-throughput screening system for GLUTs.

2.2.3 Yeast cell-based systems

The baker's yeast *Saccharomyces cerevisiae* is a eukaryotic model organism. It has been used in numerous research areas (Nielsen, 2019). Consequently, information about its physiology and genetics is abundant, and many molecular biology tools to modify its genotype exist. Noteworthy, many cellular processes between yeast and humans are conserved, such as protein translocation and degradation processes, protein folding, chaperone function, and signal transduction events (Nielsen, 2019). The high conservation between human and yeast also becomes apparent on the gene level, as 47% of 414 essential yeast genes could be replaced with a human orthologue (Kachroo et al., 2015). Simple manipulation of the yeast genome, its short generation time, fast growth, and its advanced robustness (Nielsen, 2019) enable versatile experiments within short time frames and convenient experimental set-ups (e.g., less strict sterile conditions).

Thus, besides its exploitation as a production platform, yeast also plays an important role in unraveling the molecular processes of human diseases and in drug discovery efforts for many medical conditions (Mager and Winderickx, 2005; Verbandt et al., 2017). Approximately 30% of proteins associated with human pathologies have a yeast orthologue (Foury, 1997). Moreover, the development of so-called "humanized yeast models" by e.g., (over)expressing certain human proteins allows also to investigate pathological proteins and related processes without a known yeast counterpart (Winderickx et al., 2008). Yeast models were successfully applied to solve complex medical research questions and, being

amenable to high-throughput screenings, have helped to identify putative drugs (Winderickx et al., 2008). For example, effectors against (neuro)degenerative diseases that are mainly caused by excessive cell death such as Alzheimer's (Bharadwaj et al., 2010; Chen et al., 2020), Parkinson's (Flower et al., 2005), Huntington's (Meriin et al., 2002), or Wilson's disease (Hung et al., 1997) were identified with the help of yeast cell-based systems. Hence, to investigate human transporters and accelerate the discovery of relevant drugs, yeast offers many advantages compared to other systems (Schmidl et al., 2018).

2.2.3.1 The hexose transporter deficient yeast strain EBY.VW4000

The hexose transporter family in *S. cerevisiae* has 18 members (Hxt1-17 and Gal2) (Wieczorke et al., 1999), a surprisingly high number that raises questions about their roles and redundancy (Kruckeberg, 1996). It seems plausible that the variety of transporters is used by the yeast cell to respond to varying environmental conditions (Wieczorke et al., 1999; Levy et al., 2011). In addition, Snf3 and Rgt2 function as sensors for low or high glucose concentrations, respectively, which regulate the tailored expression of *HXTs* (Boles and Hollenberg, 1997).

In a CEN.PK2-1C strain background, Wieczorke et al. (1999) deleted successively all hexose transporter family genes *HXT1-16* (*HXT17* is absent in the CEN.PK family), *GAL2*, and the maltose transporter genes *AGT1*, *MPH2*, and *MPH3* via the LoxP-Cre recombinase system. The resulting *hxt*⁰ (hexose transporter deficient) strain was named EBY.VW4000 and is unable to grow on glucose and other hexoses (Wieczorke et al., 1999). Strain maintenance can be achieved by growth on maltose, a disaccharide that is taken up by specialized maltose symporters of the Malx1 family (Chow et al., 1989). Intriguingly, additional deletion of the low-glucose sensor *SNF3* in this strain partially restored its ability to grow on glucose, indicating the presence of another, so far unknown, hexose transporter that is repressed by Snf3 (Wieczorke et al., 1999). The iterative use of the LoxP-Cre recombinase system and many rounds of cultivation on selective and non-selective medium were most probably the reasons for chromosomal rearrangements and gene losses detected in the genome of EBY.VW4000 (Solis-Escalante et al., 2015). These genetic alterations most likely caused the sporulation deficiency discovered for EBY.VW4000 and might be the reason for more unanticipated

phenotypes (Solis-Escalante et al., 2015). Despite these characteristics, EBY.VW4000 has been proven to be a reliable system to investigate heterologous transporters from various organisms, including plants, insects, humans, and even bacteria (Wieczorke et al., 2002; Vignault et al., 2005; Price et al., 2010; Young et al., 2011; Xuan et al., 2013; Kim et al., 2017; Woodman et al., 2018; Zhang et al., 2020).

2.2.3.2 Point mutations enable the functional expression of certain GLUTs in the *hxt⁰* yeast system

Native human GLUTs are not actively expressed in a *hxt⁰* yeast strain without any further modifications. However, for GLUT1 (e.g., V69M, W65R, I71M (Wieczorke et al., 2002)), GLUT3 (S66Y (Schmidl et al., 2021b)) and GLUT5 (S72Y, S76I (Tripp et al., 2017)), single amino acid substitutions in the second transmembrane region, close to the first extracellular loop, led to a functional expression in a *hxt⁰* strain. These were discovered by different approaches. For GLUT1, *hxt⁰* yeast cell transformants expressing the transporter from a plasmid were plated on glucose medium and irradiated with UV-light in a sub-lethal dose (Wieczorke et al., 2002). After a prolonged incubation (7-14 days) at 30°C, suppressor colonies, which regained the ability to take up glucose, grew. After curing some of these colonies from their plasmids (by growing them on non-selective maltose medium for several generations), they lost the ability to grow on glucose again, proving that the presence of GLUT1 was the prerequisite for the earlier observed growth (Wieczorke et al., 2002). In one colony, endogenous mutations within the *hxt⁰* strain apparently led to a functional expression of GLUT1 (see chapter 2.2.3.3) (Wieczorke et al., 2002). In the four other suppressor colonies, point mutations within the GLUT1 coding sequence were discovered, namely W65R, I71M and two times V69M (Wieczorke et al., 2002). Reverse engineering of these and similar mutations (namely: W65R, V69M/T, A70M, I71M) validated that all of them enable a functional expression of GLUT1 in yeast (Wieczorke et al., 2002). In contrast to UV mutagenesis, for GLUT3 and GLUT5, PCR-born mutations led to the amino acid exchanges that allowed functional expression of these transporters and the concomitant cell growth on glucose (GLUT3) or fructose (GLUT5) medium (Tripp et al., 2017; Schmidl et al., 2021b).

The Q455R mutation (located at the end of TM11) in the modified GLUT2 Δ loopS variant likewise enabled GLUT2 Δ loopS_Q455R expression in EBY.VW4000 (Schmidl et al., 2021b). Structural models revealed that the mentioned residues in the TM2 and Q455R in TM11 are proximal in the three-dimensional structure, pointing out the significance of this region for the functional expression of GLUTs in yeast (Schmidl et al., 2021b). It was hypothesized that the beneficial effect of these mutations is caused by destabilization of the inward-facing conformation, thereby favoring the outward-facing one, leading to a better accessibility of the substrate cavity on the extracellular side (Schmidl et al., 2021b).

2.2.3.3 The lipid composition of the plasma membrane of yeast affects GLUT activity

Native GLUT1 was actively expressed in EBY.S7, a *hxt*⁰ strain, which additionally carries a *fgy1* (for functional expression of GLUT1 in yeast) mutation (Wieczorke et al., 2002) that was identified as the Efr3-encoding gene (Wieczorke, 2001). Efr3 is a scaffold protein located at the periphery of the yeast PM and part of the phosphatidylinositol-4-kinase Stt4 complex (Baird et al., 2008). A C-terminal interaction of Efr3 with Ypp1, which in turn interacts with Stt4, recruits Stt4 to the PM where it catalyzes the synthesis of phosphatidylinositol-4-phosphate (PI4P) (Wu et al., 2014). A frame-shift mutation in the *fgy1*-mutant led to a C-terminal truncation of 120 amino acids in the Efr3 sequence (Wieczorke, 2001), which probably hampers the PI4P synthesis at the PM and might result in an abnormal PI4P content.

Phosphoinositides, although representing a small fraction of lipids in the PM, play important roles in many processes, e.g., signaling, vesicle trafficking, cell proliferation, and cytoskeleton organization (Audhya et al., 2000). The possibility of (reversibly) phosphorylating three hydroxyl positions of the inositol head group individually (PI3P, PI4P, PI5P) or in combination (PI3,4P₂, PI3,5P₂, PI4,5P₂, PI3,4,5P₃) offers a variety of ways to generate signals that can be recognized and transmitted by specialized proteins (Baird et al., 2008). Phosphorylation at position 4 represents the first step in the biosynthesis of PI3,4P₂, PI4,5P₂, and PI3,4,5P₃. Hence, PI4P not only displays itself important regulatory functions but is also a precursor for other crucial phosphoinositides (D'Angelo et al., 2008). Furthermore,

a counterflow mechanism has been described in which lipid transfer proteins exchange sterols (cholesterol in humans and ergosterol in yeast) with PI4P between intracellular membranes resulting in an asymmetric sterol distribution between organelles (e.g., the cholesterol content in the PM of human cells is significantly higher than in the endoplasmic reticulum (ER) which allows specialized membrane functions) (Mesmin and Antonny, 2016). PI4P seems to be the driving force for this exchange and consequently for the distinct sterol distribution (Mesmin and Antonny, 2016). Similarly, it was shown that an exchange between PI4P and phosphatidylserine yields an enrichment of the latter in the PM (Moser von Filseck et al., 2015). Thus, an altered PI4P content in the membrane likely influences many crucial cellular processes, and it remains to be elucidated how exactly the *fyg1* mutation influences GLUT activity in yeast.

2.2.3.4 Players that regulate phosphoinositide levels in membranes

Other PI4P kinase enzymes exist in yeast (for an overview, see Figure 1). Like Stt4, Pik1 generates PI4P but is responsible for a distinct pool of this phosphoinositide in the trans-Golgi network and, therefore, plays discrete physiological roles (Audhya et al., 2000; Mesmin and Antonny, 2016). The two kinases Stt4 and Pik1 cannot complement each other's functions and are both essential for cell viability (Flanagan et al., 1993; Mesmin and Antonny, 2016). Lsb6 is another PM-associated enzyme with PI4P kinase activity but, in contrast to Stt4 and Pik1, is not essential for cell growth (Han et al., 2002). Nevertheless, overexpression of Lsb6 could partially restore the viability of $\Delta stt4$ mutant cells (Han et al., 2002). Han et al. (2002) reasoned that Lsb6 is responsible only for a small pool of PI4P at the PM or vacuolar membrane and that the activity of PI4P kinases is highly regulated *in vivo* to control phosphoinositide levels in the membranes. On the other hand, regulation of PI4P and its derivatives can also be achieved by PI4P degradation. Sac1 is a phosphatidylinositol (PI) phosphatase, localized primarily at the ER, that catalyzes the dephosphorylation of PI4P to PI (Zewe et al., 2018). Other players influencing the phosphoinositide levels in cellular membranes include, but are not limited to, Mss4, a PI4,5P₂ kinase that phosphorylates PI4P to produce PI4,5P₂ (Desrivières et al., 1998), or Ict1 a lysophosphatidic acid acyltransferase (generating phosphatidic acid) that has been

shown to enhance the production of overall phospholipids during organic solvent stress (Ghosh et al., 2008). In yeast, studies indicated that the PM protein Sfk1 is also involved in the proper localization of Stt4 to the membrane via C-terminal interaction (Audhya and Emr, 2002; Chung et al., 2015). Unlike Efr3, however, Sfk1 is not essential for Stt4 recruitment or activity, which further proves that its Stt4-related function can be fulfilled by other proteins (Audhya and Emr, 2002) and Sfk1 also comprises other functions. It has been found, for instance, that Sfk1 restricts the trans-bilayer movement of phospholipids and, thereby, takes on a role as a regulator of phospholipid asymmetry in the PM (Mioka et al., 2018). Evidently, the here-mentioned proteins (Figure 1) have regulatory functions for the phospholipid levels in intracellular membranes and might also influence sterol compositions. Hence, up- or downregulating their activity might alter the functional expression of human GLUTs in yeast and further elucidate the molecular basis behind this phenotype.

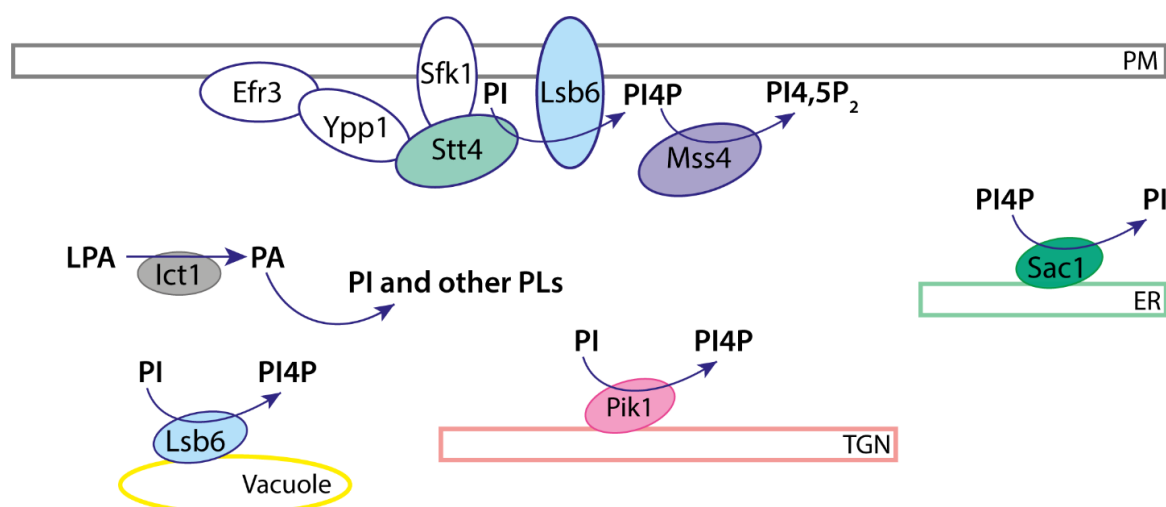


Figure 1. Selected proteins that regulate the phosphoinositide levels in membranes of yeast. Efr3 is a scaffold protein that, via interaction with Ypp1, recruits the PI4P-kinase Stt4 to the PM. Sfk1 is also involved in Stt4 proper localization. Lsb6 shows PI4P-kinase activity at the PM and vacuolar membrane and likely generates only a small pool of PI4P. Pik1 generates PI4P at the TGN, Sac1 dephosphorylates PI4P to PIP at the ER and Mss4 catalyzes the phosphorylation of PI4P to PI4,5P₂. Ict1 is a lysophosphatidic acyltransferase that enhances overall phospholipid production. PL= phospholipids, PI= phosphatidylinositol, PI4P= phosphatidylinositol-4-phosphate, PI4,5P₂= phosphatidylinositol-4,5-diphosphate, LPA= lysophosphatidic acid, PA= phosphatidic acid, PM= plasma membrane, ER= endoplasmic reticulum, TGN= trans Golgi network.

2.2.3.5 Alterations in the ergosterol biosynthesis enable GLUT4 activity in yeast

The second GLUT isoform that was actively expressed in a *hxt*⁰ yeast strain was GLUT4 and the mutation that enabled this (in combination with *fgy1*) was named *fgy4* (functional expression of GLUT4 in yeast). Screening with a gene bank for the *fgy4* complementing plasmid revealed that the gene encodes for Erg4, a C-24(28) sterol reductase that is one of the late enzymes of the ergosterol biosynthesis (Figure 2 A) (Zweytick et al., 2000; Dlugai, 2003). *ERG4* was then deleted in EBY.S7, resulting in the strain SDY.022 that actively expresses GLUT4 (Boles et al., 2004).

Ergosterol is the major sterol in fungal PMs and structurally similar to cholesterol, the main sterol in mammals (Figure 2 B), or the phytosterols from plants (Liu et al., 2019). Sterols are important determinants of membrane characteristics and functions. They are key players in processes like endocytosis, the stabilization of membrane proteins, protein sorting, development of membrane curvature and – barrier function, or regulation of receptors (Sokolov et al., 2019) and are engaged in the cellular response to multiple stressors (Liu et al., 2017).

Biosynthesis of ergosterol is a complex, multi-enzymatic process that can be divided into three modules (Hu et al., 2017). In the first mevalonate producing module, acetyl-CoA serves as a precursor and is transformed to mevalonate in three catalytic steps (Figure 2 A). In the subsequent farnesyl pyrophosphate pathway, six enzymes catalyze the synthesis of farnesyl pyrophosphate from mevalonate, which then enters the ergosterol pathway (Hu et al., 2017). While the first two modules take place at the vacuoles and the mitochondria, the ergosterol pathway mainly occurs in the ER and requires more steps and enzymes that ultimately lead to ergosterol as a product (Hu et al., 2017) (Figure 2 A). Enzymes catalyzing the early steps of this pathway (Erg9, Erg1, Erg7, Erg11, Erg24-27) are essential for cell viability, but later enzymes catalyzing the reactions from zymosterol via fecosterol and episterol to ergosterol (Erg2-6) are considered non-essential (Hu et al., 2017). Importantly, it has been shown that these last steps do not strictly follow a linear order of events (Souza et al., 2011; Liu et al., 2017). The Erg6-catalyzed reaction step that results in the methylation of the C24 residue was believed to precede the reaction steps of Erg2-5 (Liu et al., 2017). However, the

perceived-as-downstream reactions were also happening in an $\Delta erg6$ deletion strain except for the reduction of C24 (28), catalyzed by Erg4, which requires prior Erg6 activity (Souza et al., 2011). The conversion of fecosterol to ergosterol (via enzymatic activities of Erg2-5) does not change the number or localization of carbon atoms anymore (Figure 2 A). The loose substrate specificity of the late ergosterol enzymes, which allows the utilization of improperly modified substrates as precursors (Aguilar et al., 2010; Souza et al., 2011), is a probable reason why mutations in these genes are not lethal (Hu et al., 2017). Nevertheless, these mutations cause an altered sterol composition with sterol intermediates instead of ergosterol in the PM, resulting in interesting phenotypes (Hu et al., 2017; Liu et al., 2017). Cholesterol differs from ergosterol in the absence of the C24 methyl group and the two double bonds that ergosterol has at positions C7-8 and C22-23 (Souza et al., 2011; van 't Klooster et al., 2020b) (Figure 2 B). Both sterols can form lipid ordered domains (rafts) in membranes characterized by a high content of saturated acyl chains and important for numerous membrane functions (Xu et al., 2001). Thus, it was speculated that their overall physical properties are very similar, but their delicate structure differences might impose specific effects on membrane characteristics or lipid-protein interactions (Souza et al., 2011).

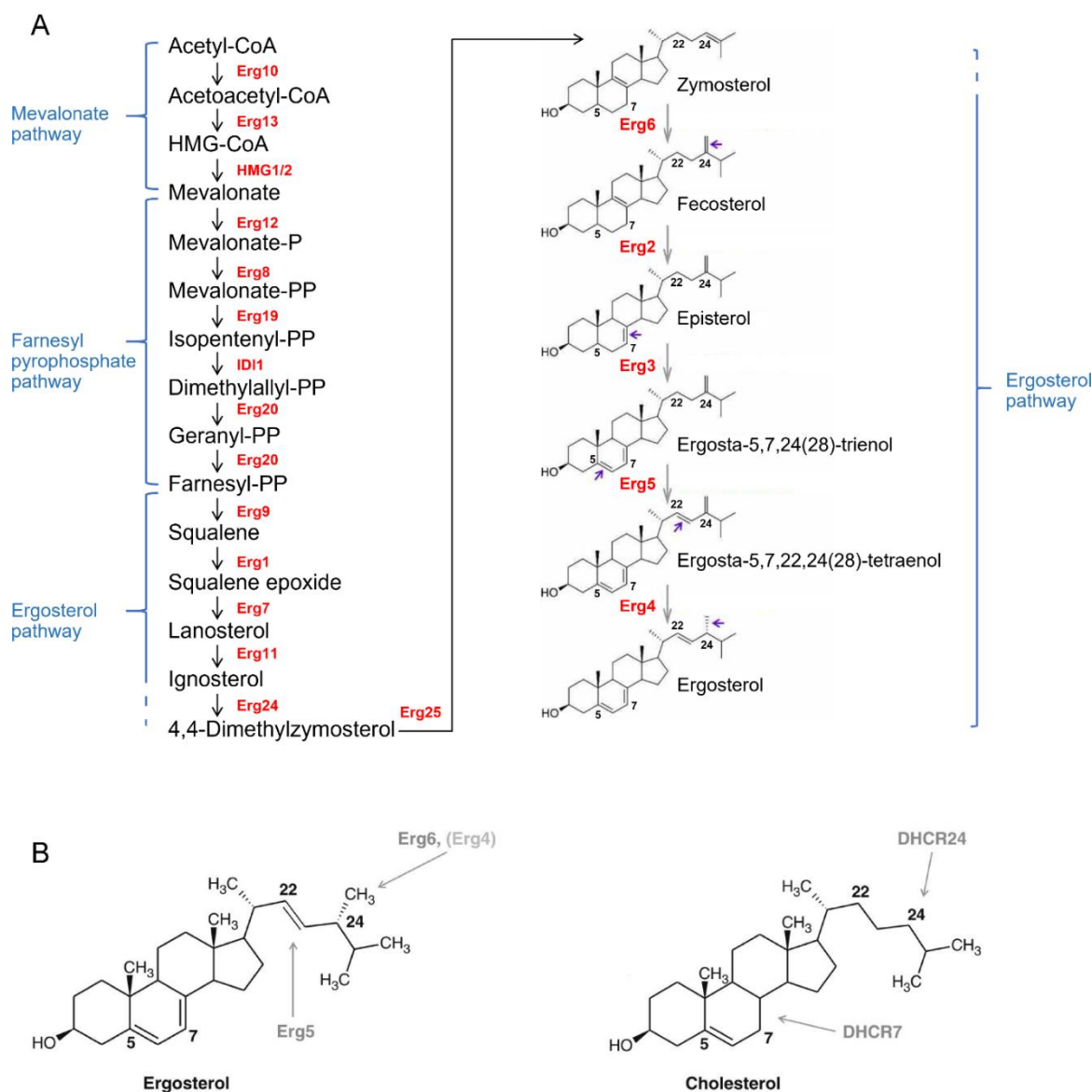


Figure 2. Steps and enzymes of the ergosterol pathway and structures of ergosterol and cholesterol. Ergosterol biosynthesis (A) can be divided into three modules. The first two modules, the mevalonate, and the farnesyl pyrophosphate pathway, take place in the vacuoles and mitochondria. The ergosterol pathway requires more enzymatic steps and mainly takes place at the endoplasmic reticulum. Enzymes are named in red. Structures of the late intermediates of the pathway are shown and the molecular alterations of each step are indicated with a purple arrow. The figure was modified after Kodedová and Sychrová (2015). The structures of ergosterol and cholesterol (B) differ, as ergosterol contains double bonds at positions C7-8 and C22-23 and a methyl group at position C24, which are absent in cholesterol. Dehydrocholesterol reductases (DHCR7 and DHCR24) saturate the double bonds at C7-8 and C24-25. Erg6 introduced a methylene group at C24 which was then saturated to the methyl group by Erg4, and Erg5 introduced the double bond at position C22-24. The figure was modified after Hirz et al. (2013).

Recently, more focus was given to the role of the lipidome of membrane proteins, which includes lipids in direct proximity and neighboring lipids that do not share direct contact with the protein (van 't Klooster et al., 2020a). Although the molecular

mechanisms remain to be elucidated, it has been shown that this lipidome is crucial for normal membrane protein activity. The yeast lysine transporter Lyp1, for example, needs ergosterol in its direct environment to function – a requirement that cannot be sufficiently replaced by its derivative cholesterol (van 't Klooster et al., 2020b). Furthermore, lipidomes show altered lipid compositions in comparison with overall membrane lipid distribution. In the case of Lyp1, phosphatidylserine was enriched, whereas ergosterol was depleted in its lipidome. It was speculated that this “disordered lipid environment” provides more flexibility which is crucial for the conformational change of transport proteins when translocating substrates (van 't Klooster et al., 2020b). These data also suggest that membrane transporters are susceptible to their lipid surroundings, and differences between human and fungal sterols likely prohibit the activity of heterologously expressed GLUTs in yeast.

As shown by density gradient centrifugation, in EBY.S7, GLUT4 seems to be held back in intracellular structures and does not localize at the PM (Dlugai, 2003). The additional *ERG4* deletion in SDY.022 enables the correct localization and activity of GLUT4 in yeast cells. Thus, the altered proteo-lipidome is likely not the cause for GLUT4 activity in this strain but can still be a contributing factor. With the help of the split-ubiquitin system, direct interaction between Erg4 and GLUT4 was verified. However, a similar interaction was also detected for other protein partners (GLUT1, Hxt1, Hxt9) indicating that the interaction is unspecific and probably not the cause for the altered localization in the $\Delta erg4$ strain (Dlugai, 2003).

The fact that just *ERG4* (or *ERG4/ERG5* double) deletion and not, e.g., an *ERG5* deletion combined with the *fgy1* mutation led to an active expression of GLUT4 suggests that the methylene group at the C24 carbon atom might play a crucial role (Dlugai, 2003). The reduction reaction, catalyzed by Erg4, eliminates the double bond, resulting in a methyl group (CH₃) (instead of methylene (CH₂)) (Figure 2 A). It was hypothesized that GLUT4 might interact specifically with this methylene group, and this colocalization leads to a translocation of GLUT4 at the PM when the respective sterols move from the ER to the PM (Dlugai, 2003). In humans, insulin triggers the translocation of GLUT4 from intracellular vesicles to the PM by a process that involves several proteins associated with lipid rafts (Chamberlain and Gould, 2002). These lipid rafts also trigger the recruitment and internalization of proteins in yeast membranes (Munn et al., 1999). Although, insulin and the

released signal cascade are absent in yeast, lipid rafts and their constituent ergosterol might be involved in the trafficking of GLUT4 to the PM via different mechanisms (Dlugai, 2003). The altered sterol composition might interfere with these processes, which in turn might affect the localization of the transporter. But the interplay between sterols and membrane proteins is highly complex and the molecular basis for GLUT4 activity in an $\Delta erg4$ strain is not resolved yet.

2.2.4 Glucose uptake assays

The hxt^0 yeast system also offers a platform for a more detailed characterization of the respective transporter, including its kinetic properties. For this, different methods exist (Yamamoto et al., 2015), but most studies rely on measuring the uptake of radiolabeled hexoses (Walsh et al., 1994b; Reifenberger et al., 1997; Farwick et al., 2014) because of its high reliability due to a good signal-to-noise ratio and high selectivity (Yamamoto et al., 2015).

One difficulty in these studies arises from the rapid metabolization of, e.g., glucose which makes the determination of an initial transport rate, independent of downstream metabolization, challenging. Attempts to circumvent this problem utilized non-metabolizable glucose analogs as, for example, 3-O-methyl-glucose (3MG), which cannot be phosphorylated by the hexokinase, preventing further degradation (Yamamoto et al., 2015). However, to exit, 3MG can permeate through the cell membrane. To prevent a fast equilibration of 3MG across the PM, applying a short incubation time and rapid cell separation from the medium is required. 3MG efflux can also be avoided by washing the cells with a mercuric chloride solution or ice-cold buffer (Yamamoto et al., 2015).

Radiolabeled 2-deoxy-glucose (2DG) is another non-metabolizable glucose analog but undergoes the initial phosphorylation step. The resulting 2-deoxy-glucose-6-phosphate (DG6P) is a stable product, unable to pass through the membrane and retained in the cell (Yamamoto et al., 2015). Furthermore, hexokinase deficient yeast cells were used for C^{14} glucose uptake assays to avoid further metabolization of the sugar. However, when conducted on a 5-s-timescale (according to the common protocol (Boles and Oreb, 2018)), the determined transporter capacities and apparent affinities were significantly decreased compared to wildtype cells

(Smits et al., 1996). This effect was not visible when glucose uptake was measured in a sub-second timescale (200 ms), using an advanced protocol that requires a specialized set-up (Walsh et al., 1994c). This shows that results from 5-s-timescale experiments are influenced by hexokinase activity, and removal of the substrate and factors (e.g., ATP depletion) that might decrease this activity should be considered (Walsh et al., 1994c; Smits et al., 1996).

In general, radioactive materials bear a risk for the experimenter and the environment; thus, special care must be taken when handling these. Additionally, the purchase and the disposal of radiolabeled chemicals are expensive, and elaborate management programs of universities aim to diminish radioactive waste (Ring et al., 1993). By (German) law, experiments with radiolabeled substances may only be conducted in separated and suitable laboratory spaces, and all persons in contact with these chemicals must receive prior training.

To avoid these negative concomitants, isotope-free assays to measure glucose uptake are used increasingly (Kim et al., 2012). One example is an enzymatic assay to measure the DG6P content in 2DG treated cells (Yamamoto and Ashida, 2012). When DG6P is oxidized to 6-phospho-2-deoxyglucuronic acid (6PDG) by a dehydrogenase, NADPH is generated from NADP, as a reduction equivalent. Thus, the NADPH content can be measured photometrically and relates to the amount of DG6P in the cell (Manchester, 1990; Sasson et al., 1993). Because NADPH fluorescence intensity is rather low, this method alone would require the cultivation of a large batch of cells and the generation of cell extract. By coupling this reaction with the oxidation of NADPH catalyzed by the enzyme diaphorase, which concomitantly transforms resazurin to resorufin, a strong fluorophore, the fluorescence signal can be accelerated (Yamamoto et al., 2006). In another approach, the NADPH that is produced during the conversion from DG6P to 6PDG is used to reduce a pro-luciferin to luciferin, thereby generating light proportional to the amount of 2DG that entered the cell (Valley et al., 2016). This bioluminescent assay shows a better signal-to-noise ratio and is more convenient because washing steps can be omitted compared to the fluorescent-based procedures (Valley et al., 2016).

Alternatively, the fluorescent glucose analogs, 2- and 6-NBDG ([N-(7-nitrobenz-2-oxa-1,3-diazol-4-yl) amino]-2-deoxyglucose)) (Speizer et al., 1985; Yoshioka et al.,

1996) can be directly used as uptake indicators, if applicable, combined with photomultipliers (Yamamoto and Ashida, 2012). The utilization of NBGDs has gained popularity in many cell types and experimental systems, including microplate assays, flow cytometry, and digital imaging fluorescence microscopy (Yamamoto et al., 2015). All mentioned glucose analogue-based methods are, however, not applicable for in-depth kinetic characterization of certain transporters since the chemical modification of the hexose moiety certainly affects the transport kinetics.

2.3 Aim of this thesis

Human GLUTs fulfill pivotal functions in sugar metabolism and are relevant drug targets in combatting important diseases. Different assay systems exist that allow broad research on these transporters. Among these, the *hxt⁰* yeast strains offer a valuable platform facilitating convenient and inexpensive research on selected GLUTs and enabling access to high-throughput screenings of large compound libraries. GLUT1, GLUT4 and GLUT5 were already actively expressed in yeast.

The aim of this thesis was to actively express the important human transporters GLUT2 and GLUT3 in a *hxt⁰* yeast strain, thereby extending the possible applications of a yeast cell-based platform. Subsequently, these systems should be used for the screening of possible ligand candidates (previously selected by *in silico* screening) in the attempt to identify compounds that would specifically affect the activity of the respective transporter.

Furthermore, previous studies have indicated that changes in the phospholipid or sterol composition in the yeast PM benefit the functional expression of some GLUTs. To improve our understanding of the molecular conditions or PM prerequisites for GLUT expression in yeast, the introduction of defined alterations in the phospholipid and ergosterol biosynthesis and their subsequent evaluation on GLUT expression were intended.

Moreover, several methods exist to examine glucose uptake in yeast cells or other systems, but they exhibit significant drawbacks as e.g., presumable aberrations due to the application of glucose analogues or the usage of radiolabeled sugars. To further facilitate research on GLUTs or other hexose transporters, this thesis intended to provide an alternative method to the commonly used glucose uptake assays by employing the pH-sensitive GFP variant pHluorin as a genetically encoded, ratiometric biosensor.

3 General discussion

3.1 The *hxt*⁰ yeast system as a microbial investigation platform for transporters

The easy manipulation and convenient handling of yeast made it the organism of choice for many research applications (Nielsen, 2019). In EBY.VW4000 twenty hexose (and maltose) transporter genes were deleted in a *Saccharomyces cerevisiae* CEN.PK2-1C strain background resulting in a *hxt*⁰ strain that is incapable of transporting glucose or related monosaccharides (Wieczorke et al., 1999). This offers an excellent opportunity to investigate endogenous Hxts separately or heterologous hexose transporters from various organisms (Wieczorke et al., 2002; Vignault et al., 2005; Schüßler et al., 2006; Price et al., 2010). It has been used for initial characterizations of newly found transporters (e.g., Schüßler et al., 2006), or to gain more information about substrate specificities or affinities of already known ones (e.g., Vignault et al., 2005). It is convenient for the application of several assays, including simple growth tests or radiolabeled glucose uptake assays (Boles and Oreb, 2018). Furthermore, the *hxt*⁰ system can be applied as a screening platform to examine compound libraries for their effects on the transporter in question as it has been performed for GLUT2, in this thesis (Schmidl et al., 2021c). Whereas for GLUT effectors, medical applications for metabolic diseases or their use in GLUT-related studies are conceivable more areas like the containment of infectious diseases could be tackled by using the *hxt*⁰ screening platform on other transporters. For example, the glucose transporter of the pathogen *Trypanosoma brucei* (THT1) has been identified as an advantageous drug target and hence, specific inhibition of THT1 could be a promising strategy to contain the African sleeping sickness, which is caused by *T. brucei* (Haanstra et al., 2017). With the help of virtual screening and subsequent verification of candidates in a *hxt*⁰ strain expressing THT1, putative drug candidates for this purpose could be identified. Also, PfHT1, the main hexose transporter of the malaria causative *Plasmodium falciparum* is considered the main target for “next-generation antimalarials” (Jiang et al., 2020). Its crystal structure has been obtained only recently which will facilitate *in silico* ligand design (Jiang et al., 2020), and the *hxt*⁰ yeast system could serve as a validation platform for this

objective, as well. This thesis focused on the functional expression of and further investigations on human GLUTs in the *hxt⁰* yeast system.

3.1.1 The functional expression of GLUT2 and GLUT3 in a *hxt⁰* yeast strain

GLUT2 is expressed in the liver, kidney, intestine, pancreas, and the brain and is unique among other GLUTs with its very low substrate affinities for the main hexoses glucose, fructose, galactose, and mannose (e.g., for glucose it has a $K_M=17$ mM) (Uldry et al., 2002; Thorens, 2015). Hence, it plays important roles in sugar sensing or signaling processes (Guillemain et al., 2000; Ohtsubo et al., 2005). GLUT2 malfunction is the underlying cause of the rare Fanconi-Bickel syndrome (Santer et al., 1997) and is likely also involved in more metabolic disfunctions (Thorens, 2015). GLUT3, on the other hand, transports glucose with high affinity ($K_M=1.4$ mM (Colville et al., 1993)) supporting cell types with a high energy demand such as sperm, white blood cells or neurons in the brain (Simpson et al., 2007). Many cancer cell types overexpress GLUT3 to sustain proliferation and its overexpression is a biomarker for grave tumor malignancy (Barron et al., 2016).

Because of their importance in certain diseases, it is desirable to obtain very detailed information about their precise physiological roles and to develop drugs targeting GLUT2 or GLUT3. Active expression of both transporters in an *hxt⁰* yeast strain was achieved in this thesis and thereby provides a convenient platform for further research.

Native GLUT3 was functionally expressed in the *hxt⁰ fgy1* yeast strain EBY.S7, suggesting that the assumed alteration of the PI4P composition in the PM of this strain is beneficial for GLUT3 activity, comparable to what has been observed with GLUT1 (Wieczorke et al., 2002). Additionally, as for GLUT1, a point mutation was identified for GLUT3 as well that allowed its active expression in EBY.VW4000, the *hxt⁰* strain with no further mutations (Wieczorke et al., 1999). This mutation (S66Y) lies in the second TM region, approaching the extracellular space (Schmidl et al., 2021b). Remarkably, mutations that led to an active expression of GLUT1 (W65R, V69M, A70M, I71M (Wieczorke et al., 2002)) and GLUT5 (S72Y, S76I (Tripp et al.,

2017)) in EBY.VW4000 were found in the same region which reveals a key role for this area for GLUT expression in yeast. Most of these mutations, except for W65R for GLUT1, replace a smaller residue with a bulkier one. Strikingly, for GLUT3 and GLUT5 all mutations conferring transporter activity targeted a serine, an especially small residue. Putatively, these mutations affect the interactions of TM regions 2 and 11 and force them to push away from each other (Tripp et al., 2017). This probably leads to a destabilization of the inward-facing conformation, hence favoring the outward-facing one which might improve the accessibility of the substrate cavity from outside the cell (Tripp et al., 2017). For W65R in GLUT1, a similar effect could be caused by the long side chain and the positive charge of arginine.

Correct localization of GLUT2 to the PM of the yeast cell was only achieved when the large extracellular loop between TM regions 1 and 2 was truncated by 34 amino acids (thereby resembling more the loop lengths of e.g., GLUT1 or GLUT3), including the removal of the glycosylation site at position 62 (Schmidl et al., 2021b). In GLUT2, this loop displays a significantly larger size than in other GLUTs (Schmidl et al., 2021b). This region may impose characteristic functions on GLUT2. However, functional studies on the GLUT2 $_{\Delta\text{loopS}_Q455R}$ variant in yeast revealed similar substrate specificities and affinities as those of the WT transporter (Schmidl et al., 2021c). Presumably, the large extracellular loop mediates a correct folding and protein trafficking to the membrane in human cells but impedes the same processes in yeast due to differences in the membrane composition and/or signaling reactions. The fact that very long extracellular loops are characteristic for eukaryotic proteins (and absent in prokaryotic ones) (van't Klooster et al., 2020c) could be interpreted as an indication that they play roles primarily in protein trafficking processes which are much less complex in bacteria. Although yeast and human cells exhibit many homologies in protein trafficking (Scheuring et al., 2001), differences exist, too (Phillips et al., 2001). Possibly, in yeast, putative signal molecules on the extended loop are not required and rather impede a normal transport to the PM. Determination of the subcellular location of native GLUT2 and GLUT2 $_{\Delta\text{loopS}}$ also revealed that the full-length transporter does not localize correctly at the PM (but resides in vacuoles) whereas the truncated version does, at least partly (Schmidl et al., 2021b). This also supports the hypothesis that the loop

impedes correct protein trafficking. To preserve the loop size, selective mutations in this area could be introduced and checked for benefits on the activity of the transporter in yeast. This was carried out in this thesis for the glycosylation site N62, in which the asparagine was mutated to glutamine (N62Q) without any observed effect (Schmidl et al., 2021b). Steric impediments could also prohibit the correct localization of GLUT2 to the PM, which would necessitate a more invasive loop truncation. Importantly, transport inhibition of the truncated GLUT2 by the well-known inhibitors, quercetin and phloretin, was unaffected, which confirmed its utility as a screening platform for GLUT2-affecting ligands. As for GLUT1, GLUT3, and GLUT5, a beneficial point mutation for active expression in yeast was found for GLUT2 as well, namely Q455R. While GLUT2 Δ loopS was already actively expressed in EBY.S7, the additional point mutation Q455R in GLUT2 Δ loopS_Q455R allowed its functionality also in EBY.VW4000 (Schmidl et al., 2021b). Although not located in TM2, it lies in TM11 and thereby approaches the same region as the mentioned mutations for GLUT1, GLUT3, and GLUT5 in the tertiary structure of the protein. Therefore, it likely fulfills a similar function and pushes the two TM regions 2 and 11 apart allowing a more stable outward facing conformation (Schmidl et al., 2021b).

With GLUT1 and GLUT4 already actively expressed in a hxt⁰ yeast strain in previous works (Wieczorke et al., 2002; Boles et al., 2004), now, all class 1 GLUTs (except for GLUT14, the duplicon of GLUT3 (Wu and Freeze, 2002)) are accessible in this platform. In addition, the class 2 member GLUT5 has been functionally expressed, before (Tripp et al., 2017). Although, GLUTs1-5 are already among the most studied isoforms (Thorens and Mueckler, 2010) several questions about their metabolic functions and distinct roles remain unanswered. It is intriguing, for example, that GLUTs differ extensively in their transport specificities and kinetic properties while presenting very high sequence similarities (Schmidl et al., 2021c). GLUT2, for instance, does not differ in its substrate binding site in comparison to GLUT1 or GLUT3 (Schmidl et al., 2021c). However, it transports glucose with a substantially lower affinity ($K_M=17$ mM for GLUT2, $K_M=1.4$ mM for GLUT3 (Colville et al., 1993; Uldry et al., 2002) and accepts fructose as a substrate in contrast to GLUT1 or GLUT3 (Mueckler and Thorens, 2013).

Some studies indicate that GLUTs in general depict the alternating mechanism of transport and it is presumed that most act as uniporters (Iancu et al., 2013; Deng et al., 2015). However, there is not much information about possible regulation systems that might adjust the transporters' mode of action according to metabolic needs, as for example a uniport/antiport switch that has been described for avian GLUT1 (Cloherty et al., 1996). Also, the detailed role of individual GLUTs in certain pathologies is still not clear and it is an overall objective of GLUT-related research to determine how modulation of sugar transport is involved in health and disease. Importantly, specific ligands uniquely acting on a particular GLUT are still very scarce. Identifying key residues and regions responsible for ligand binding and the establishment of high-throughput screening methods is therefore highly desirable. The co-existence of several GLUT isoforms in human cell lines complicates the analysis of a particular GLUT's role on sugar uptake (Schmidl et al., 2018), which is especially true for GLUTs with low transport affinities, like GLUT2. Having GLUTs 1-5 functionally expressed in the convenient *hxt⁰* yeast platform will facilitate research and ligand screening, eventually leading to the identification of specific effectors that will advance GLUT-related research.

3.1.2 Expression of GLUTs with preserved functions

The active expression of GLUTs 1, 3 and 5 in EBY.VW4000 is a valuable achievement for further studies and drug development. It cannot be completely excluded that the point mutations alter the properties of the transporter in some way. However, functional studies in yeast with GLUT1_{V69M}, GLUT3_{S66Y}, GLUT5_{S76I} or GLUT5_{S72Y} (Wieczorke et al., 2002; Tripp et al., 2017; Schmidl et al., 2021b) revealed that these mutated transporters show highly similar characteristics (e.g., for substrate specificity and -affinity or inhibitor response) as it is described for their native counterparts in literature (Kasahara and Kasahara, 1996; Zamora-Leon et al., 1996; Uldry et al., 2002; Augustin, 2010). This is a strong indication that the mutations probably do not influence the mechanism or rate of transport of the transporter and that their strongest effect concerns the transport activation in a foreign lipid environment. For GLUT2, however, the required alterations for its active expression were more invasive (Schmidl et al., 2021b). By truncating the extracellular loop between TM1 and TM2, one characteristic motif of this

transporter was eliminated. Since there is not much information about the specific roles of soluble loops it is not possible to make a reliable prediction which consequences such an alteration might impose on the transporter's functions. Nevertheless, with more studies concentrating on the hydrophilic regions of membrane proteins (Conseil et al., 2009; Aseervatham et al., 2015; van't Klooster et al., 2020c) the impression hardens that these regions play significant roles (see chapter 3.3). Also, regarding the fact that GLUT2 fulfills unique physiological roles in the human body, which distinguishes it clearly from other well-studied GLUTs (Thorens, 2001), one might consider the obvious structural differentiation of the extended first extracellular loop of GLUT2 as a possible factor for these roles. Still, functional studies that were performed with GLUT2 Δ loopS_Q455R constructs in yeast did not show significant differences in ligand response, substrate preferences or affinities (Schmidl et al., 2021b; Schmidl et al., 2021c). As a conclusion, GLUT2 Δ loopS_Q455R-expressing yeast systems can very well serve for investigations or ligand screenings. Identified ligands should then be validated in follow-up studies with other systems employing, for example, *Xenopus laevis* oocytes, proteoliposomes or cell cultures (Guillemain et al., 2000; Uldry et al., 2002) to show that their effect is not limited to the GLUT2 Δ loopS_Q455R-expressing yeast system but also applies to the native, full-length GLUT2 in other systems.

Regardless of the mentioned successes due to point mutations or GLUT2 loop alteration, a "universal" strain functionally expressing native GLUTs is doubtlessly useful for a higher certainty of unaffected functional properties. Native GLUT1 and GLUT3 are active in the hxt⁰ strain EBY.S7 which carries the additional *fgy1* mutation in its genome (Wieczorke et al., 2002; Schmidl et al., 2021b). This mutation affects the Stt4 complex, thereby putatively altering the PI4P content in the PM (Wieczorke, 2001). GLUT4 is actively expressed in the SDY.022 strain which, in addition to *fgy1*, carries a deletion of *ERG4* (Boles et al., 2004). Erg4 catalyzes one of the last steps in the ergosterol biosynthesis (Zweytick et al., 2000). These findings point to the membrane lipid and/or sterol composition as a central factor for active expression of native GLUTs in yeast.

Native GLUT2, GLUT5 or GLUT9 (this thesis, data not shown) are not actively expressed in either EBY.S7 nor SDY.022 (Tripp et al., 2017; Schmidl et al., 2021b).

It is conceivable that further specific alterations of the membrane lipid composition of the yeast strain would enable their activity, as well.

3.1.3 The sterol composition in yeast and its effect on the functional expression of human GLUTs

As cholesterol for mammalian cells, ergosterol is the main sterol in fungal PMs (Liu et al., 2019). Both sterols depict a similar structure. Ergosterol differs from cholesterol by having an extra methyl group at position C24 (at the side chain) and two additional double bonds, one between C7-8 (B-ring) and one at C22-23 (side chain) (Figure 2 B) (Bloch, 1983). The hydroxyl group at C3 is viewed as an obligatory structural feature of membrane sterols that imposes the amphipathic character to these molecules and orients it in the membrane bilayer (Nes et al., 1978; Bloch, 1983). The variability of cholesterol and ergosterol concentrates mostly on the side chain. The cholesterol side chain facilitates the highest membrane order compared to analogues with differing side chain lengths (Bloch, 1983). In contrast, higher concentrations of ergosterol (more than 8 mol %) impose a membrane disorder which is possibly mediated by the C24-methyl group, and it seems to be beneficial for cell growth (Bloch, 1983). Membrane disorder allows for a greater mobility of acyl chains, thereby reducing viscosity and increasing permeability (Bloch, 1983). The extra methyl group in ergosterol therefore likely influences the physical property of the PM to some extent. It was discussed that the preference for ergosterol (and the coherent viscosity-decreasing effect) might be related to the lower optimal growth temperature of yeast (30°C, compared to mammalian body temperature of ~37°C) that would lead to a higher membrane viscosity (Bloch, 1983).

When grown under anaerobic conditions, *S. cerevisiae* is strictly sterol auxotroph (Wiersma et al., 2020) and only the feeding of ergosterol intermediates that possess C24-methyl groups (e.g., brassicasterol or 24-methylcholesterol) enable their growth (Bloch, 1983; Wiersma et al., 2020). However, sterols lacking this configuration (as e.g., cholesterol) could restore growth by complementing the “bulk function”, if very small quantities of ergosterol were supplied as well for specific sterol-protein interactions (Wiersma et al., 2020). Consistent with this, it is generally believed that the physical properties between ergosterol and cholesterol

are neglectable and that the two sterols impose specific direct effects that might be essential for certain membrane proteins (Xu et al., 2001; Souza et al., 2011). Surprisingly, a *S. cerevisiae* strain in which ergosterol production is abolished, and which instead produces tetrahymanol, a sterol surrogate that is formed by cyclization from squalene, shows a growth advantage under anaerobic conditions and in the absence of sterol supplementation (Wiersma et al., 2020). This indicates that with tetrahymanol the mentioned requirements for specific sterols are absent, but the underlying mechanisms are not yet known (Wiersma et al., 2020).

A growing body of evidence shows that membrane proteins require a certain lipid environment (Souza et al., 2011; van 't Klooster et al., 2020b; van 't Klooster et al., 2020a) and in yeast, Δerg mutants show diverse phenotypes (Souza et al., 2011). Some membrane proteins seem to be more susceptible to the sterol composition of the membrane than others (Souza et al., 2011). Souza et al. (2011) have shown, for example, that the yeast arginine permease Can1 functions normally in strains with sterol intermediates, whereas the ABC transporter Pdr12 seems to require ergosterol for normal activity. The high affinity tryptophan permease Tat2, on the other hand, also shows reduced functionality in strains with sterol intermediates different from ergosterol, except for cholesterol which seems to complement the ergosterol-related condition necessary for the activity of Tat2 (Souza et al., 2011). Considering this, one might hypothesize that human GLUTs, too, specifically interact with cholesterol, as the main human sterol and require it for their normal activity. Therefore, it was attempted in this thesis to create a hxt^0 strain that stably produces cholesterol instead of ergosterol by deleting *ERG5* and *ERG6* while integrating the genes encoding for the dehydrocholesterol reductases (DHCR) 7 and 24 (as it was done before in *S. cerevisiae* (Souza et al., 2011)) in the hxt^0 strain EBY.VW4000. It was achieved to produce various strains with sterol intermediates (see chapter 5.1.1, Table 2), but since the deletion of both *ERG5* and *ERG6* within the same strain was not successful, a cholesterol producing strain was not generated. Nevertheless, according to Souza et al. (2011), Erg5 is supposedly much less active in a $\Delta erg6$ strain which supports the hypothesis that the strain SSY63 (with *DHCR7* and *DHCR24* integrated and *ERG6* deleted) might, at least partly, also produce cholesterol. Strikingly, obtaining $\Delta erg6$ mutants was in general challenging and finally only worked for strains that had *DHCR24* already integrated

in their genome. It has been published previously, that $\Delta erg6$ mutants do not take up tryptophan as efficiently (Gaber, R., F. et al., 1989; Parks et al., 1995), which might be one contributing reason. As the employed strain (EBY.VW4000) is auxotrophic for certain amino acids, including tryptophan, it requires its efficient uptake for cell growth (Wieczorke et al., 1999). This tryptophan uptake deficiency is related with a misrouting of Tat2 to the vacuole, even under low tryptophan concentrations in the medium, when Tat2 is required for the uptake of this amino acid (Souza et al., 2011). A higher supply of tryptophane in the medium might have addressed this issue, as the Tat1 transporter might still take up tryptophane with low affinity (Schmidt et al., 1994), but was not tested. However, Souza et al. (2011) showed that this mislocalization and concomitant malfunction of Tat2 only appears in $\Delta erg5/erg6$ strains (producing ergosterol intermediates different from cholesterol), but that cholesterol can complement for ergosterol in this matter. In other words, a cholesterol-producing strain functionally expresses Tat2 and shows almost normal tryptophan uptake compared to an ergosterol-producing strain. The fact that an *ERG6* deletion only worked in a *DHCR24*-containing strain might, therefore, indicate that a sterol with a double bond at C24 (in *DHCR24*-deficient, *ERG6* deletion strains) is unbeneficial for the proper location of Tat2, that rather requires the saturation of this double bond, which lacks in both cholesterol and ergosterol. It fails to explain, however, why it was unsuccessful to also delete *ERG5* in SSY63 as this would have yielded a stable cholesterol-producing strain which should have led to a normal Tat2 activity as well, according to these findings (Souza et al., 2011). Furthermore, to compensate for possible growth defects due to sterol anomalies, ergosterol was supplied in the medium on which the transformants were plated but apparently not taken up efficiently. Deleting *ERG5* would have removed the C22-23 double bond that could have affected the stereochemistry of the molecule which also might be unpreferable for some transporters or the physical membrane properties. The fact that a (tryptophan auxotrophic) strain containing both deletions (*ERG5* and *ERG6*) has been generated in other studies (Souza et al., 2011) shows that it is generally possible to combine both deletions. Yet, it is conceivable that due to the usage of a different strain background here, the initial lipid/sterol composition of the membrane already differs between EBY.VW4000 and the strains used in other studies (Souza et al., 2011) and that, therefore, alterations in the sterol compositions have more critical

effects. Evidently, the repeated use of LoxP-Cre recombinase system in EBY.VW4000 to delete all hexose transporters, led to chromosomal rearrangements and gene loss (Solis-Escalante et al., 2015) and might have already influenced the membrane conditions. Also, the phenotypes of sterol-affecting mutations are diverse, and the sterol composition furthermore influences the lipid composition of the membrane suggesting that *ERG* deletions provoke an impact on various cellular processes which makes it difficult to analyze cause-and-effect relationships.

Concerning the functional expression of GLUTs, an effect was visible for both $\Delta erg6$ strains SSY61 and SSY63. Drop tests revealed that native GLUT1 is actively expressed in these two strains in contrast to the EBY.VW4000 strain or also the other sterol-affected strains (SSY53 – SSY58) that did not show growth with GLUT1 (or GLUT4) on glucose medium. This indicates that a more cholesterol-like sterol (which does not contain the C24 methyl group) is beneficial for GLUT1 expression. However, the effect was less prominent as for the *fgy1* strain EBY.S7 (and *fgy1*/ $\Delta erg4$ strain SDY.022) that supposedly contain an altered PI4P composition in the PM and showed stronger growth with GLUT1 on glucose. If the observed beneficial effect of the *ERG6* deletion on GLUT expression is, in fact, due to an altered sterol composition, or if the altered sterol composition in turn led to an altered phospholipid composition which provoked the effect (Mesmin and Antony, 2016), could not be evaluated at this point since lipid profiles were not determined.

3.2 Structure-based GLUT-selective ligand screenings

Computer-aided drug design has accelerated drug discoveries since the 1980s (Baig and Ahmad, 2016). To identify ligands that bind and affect GLUTs, *in silico* screening systems have been employed as well. Ideally, structural models for these assays are created from experimentally determined crystal structures. However, when these are not available, homology models from related proteins can be generated (Colas et al., 2016). In early studies that aimed to determine GLUT-interacting ligands, structural models were generated from crystal structures of bacterial GLUT homologs (George Thompson et al., 2016; Ung et al., 2016) or other MFS transporters (Mishra et al., 2015). In these studies, up to 10 million compounds were screened and ultimately ligands for GLUT1, GLUT4, and GLUT5 were identified (Mishra et al., 2015; George Thompson et al., 2016; Ung et al., 2016). For example, the first potent and specific GLUT5 inhibitor (N-[4-(methylsulfonyl)-2-nitrophenyl]-1,3-benzodioxol-5-amine (MSNBA)) was found by virtual ligand screening with a GLUT5 model in the inward-facing conformation based on the crystal structure of the bacterial GLUT homolog GlcP_{Se} (Iancu et al., 2013) and investigation of the resulting candidates in proteoliposomes (George Thompson et al., 2016).

Currently available crystal structures of GLUT1, GLUT3, and GLUT5 (Deng et al., 2014; Deng et al., 2015; Nomura et al., 2015) improve the structural models of other GLUTs and make *in silico* screening for all GLUTs accessible. To identify GLUT2-specific ligands, a structural model of the inward-facing conformation of GLUT2 was created based on the crystal structure of GLUT1. The two homologs share high protein sequence identity and similarity (52% and 68%, respectively), which benefitted the modeling (Schmidl et al., 2021c). With structure-based *in silico* screenings, the vast plethora of small molecules can be significantly reduced to a number that is amenable for experimental validations (e.g., for GLUT2, the ChemNavigator library consisting of more than 6 million compounds was used for screening). However, in most cases, virtual screening still leaves a considerable high number of putative ligands (George Thompson et al., 2016; Schmidl et al., 2021c), which requires a convenient high-throughput system for fast and reliable validation. Therefore, studies concentrating on GLUT-selective ligand identification benefit from developing a yeast cell-based system that solely expresses the

respective GLUT, now available for all class 1 GLUTs (GLUTs1-4) and the class 2 member GLUT5.

3.2.1 GLUT2 screening and ideas for future GLUT-selective ligand screenings

In this thesis, active expression of GLUT2 in a *hxt⁰* strain was achieved and subsequently used to test 163 of the top 200 compounds priorly selected by *in silico* screening and accessibility (Schmidl et al., 2021c). As a result, eleven potent GLUT2 inhibitors with IC₅₀ values ranging from 0.61 to 19.3 μM were identified; from these nine seem to be GLUT2-specific as they did not affect the closely related GLUT1, GLUT3, and GLUT4, or the class 2 GLUT, GLUT5 (Schmidl et al., 2021c). The high selectivity of most of the inhibitors might seem surprising at first sight, given the high sequence identities and similarities between class 1 GLUTs (Thorens and Mueckler, 2010) especially in the substrate binding site (Schmidl et al., 2021c). But the identified compounds docked to the upper portion of the substrate cavity without the substrate binding site, which shows significantly lower conservation among GLUTs. Indeed, kinetic analysis of the most potent GLUT2 inhibitors showed that they are noncompetitive with glucose, confirming the ligand docking (Schmidl et al., 2021c). This cytosolic entrance is in proximity to soluble loops, especially the large loop between TM6 and TM7 that connects the two protein domains, which generally show higher sequence variabilities among GLUTs than hydrophobic TM regions (Schmidl et al., 2021c). These findings indicate that targeting the entrance of the substrate cavity might improve the chances of finding selective inhibitors for GLUTs in future studies. Coupling these inhibitors with a glycosyl group might lead to an even more potent inhibition, as inhibitor-binding and glucose-binding sites would be occupied simultaneously, and selectivity would be maintained (Schmidl et al., 2021c). Moreover, such glycosyl-bound inhibitors might be exploited to stabilize the protein during crystallization and generate new crystal structures of transporters or their conformations (e.g., the GLUT2 structure) (Schmidl et al., 2021c). By binding distantly from the substrate binding site, the ligands confer allosteric inhibition. Also accelerating transport activity requires allosteric events, but the discovery of activators is more challenging because it requires a more complex mode of action. For the bacterial

lactose permease LacY, an MFS member, nanobodies were identified that were able to increase the transport affinity of LacY for lactose by a factor of 200, via interaction with exofacial loops (Smirnova et al., 2014). This increase in affinity putatively derives from the stabilization of the substrate-bound conformation and a consequential decrease in sugar dissociation rates (Smirnova et al., 2014). Similar effects by ligand interactions with extracellular loops are conceivable for GLUTs as well. The virtual screening for GLUT2 (Schmidl et al., 2021c) concentrated on protein-ligand interaction in the substrate cavity, therefore inhibitors, but no activators were found. Moreover, only the inward-facing conformation of GLUT2 was used for the *in silico* screening. It is generally believed that ligands preferentially interact with a specific transporter conformation (Loland et al., 2002); the usage of an outward-facing structural model might have revealed different inhibitors. To find allosteric effectors, including activators, regions of special focus are the soluble intra- and extracellular loops or hydrophilic termini.

3.2.2 Importance and application areas for GLUT-specific effectors

With a growing awareness that GLUTs play a major role in health and disease, they have been declared as important drug targets. Naturally, based on the knowledge on the metabolic roles of certain GLUTs, efforts concentrated on targeting these by identifying and applying small GLUT-affecting compounds. One prominent area of application is the treatment of cancer cells. For example, many studies and preclinical trials have shown that diminishing glucose-uptake in cells via inhibition of GLUTs, and in particular GLUT1 or GLUT3, can decrease tumor growth (Barron et al., 2016; Reckzeh et al., 2019; Shriwas et al., 2021). Unspecific GLUT inhibitors like phloretin have demonstrated anti-tumor effects as well (Wu et al., 2009; Lin et al., 2016). Thus, other ligands inhibiting several GLUTs to reduce overall glucose uptake are interesting candidates for putative anti-cancer drugs, including the pan class 1 inhibitor G2iF detected within the scope of the GLUT2 ligand screening (Schmidl et al., 2021c). Furthermore, it is hypothesized that certain tumors preferably use fructose for proliferation (as indicated by overexpression of fructose transporters) (Godoy et al., 2006). Specific inhibition of fructose transporters might therefore be a useful tool in specialized cancer treatment. This notion is supported by studies illustrating that antisense

oligonucleotides against GLUT5 mRNA have anti-proliferative effects on breast tumor cell lines (Chan et al., 2004). The GLUT2/GLUT5 inhibiting ligand G2il, that was also identified (Schmidl et al., 2021c), is likely a valuable contribution to such approaches.

The most dominant method to tackle malignant tumor growth is chemotherapy which is widely used with often successful outcomes. However, after a prolonged exposure to chemotherapeutics, tumor cells of many patients develop a resistance which accounts for the most common reason for chemotherapy failure (Ma and Zong, 2020). This event is often related to an upregulated GLUT expression and GLUT inhibition can be used to reduce or delay this unwanted resistance, as it has been shown for GLUT3 inhibition in glioblastoma cells (Le Calvé et al., 2010). Therefore, GLUT inhibitors can also be useful as therapeutic agents in combination with chemotherapy to re-sensitize malignant cells to the applied toxin.

Apart from cancer, many other diseases in which GLUTs are involved exist, such as GLUT1 DS (Brockmann, 2009), the Fanconi-Bickel syndrome (Santer et al., 2002) or diabetes (Hajiaghaalipour et al., 2015). Most of these would benefit rather from compounds that improve the activity of the respective GLUT instead of inhibiting them. However, activators are very scarce. Ligand screening approaches also mostly concentrate on the substrate cavities of the transporter and compounds that interact with these sites are predetermined to inhibit. For activating compounds, regions apart from this central cavity should be considered, including polar loops or termini. More information about these regions would therefore fuel the discovery of GLUT activators. Furthermore, to specifically address e.g., GLUT1 DS, known mutations within GLUT1 should be reconstituted in virtual models as well as in the experimental platform to identify compounds that can complement the deficiencies. A mutation of a tyrosine residue to alanine in an intracellular loop of the dopamine transporter has been shown to alter the conformational equilibrium and thereupon convert the effect of extracellular binding zinc ions from a former inhibiting to a now activating shift (Loland et al., 2002). Conceivably, similar effects might be found for defective GLUT1 or GLUT2 transporters present in GLUT1 DS or Fanconi-Bickel syndrome patients that might tremendously improve the therapeutic perspectives.

Several inhibiting compounds for GLUTs are known, including unspecific ones like phloretin and quercetin (Johnston et al., 2005) or specific ones as for example MSNBA (George Thompson et al., 2016) for GLUT5. Nevertheless, it is desirable to extend this list to have a plethora of compounds with varying potency and specificities but also to provide several substances for putative clinical trials. The success rate of a drug entering clinical trials is very low and even lower in the area of oncology (Wong et al. calculated a probability of success of only 3.4% for oncology drugs (Wong et al., 2019)). One problem is the fact that cancer cells derive from healthy cells and therefore lack specific targets that are distinctive for the malignant tissue but absent in healthy tissues (Haanstra et al., 2017). Drugs targeting GLUTs likely show unwanted off-target effects that might impair the health status of the patient. These unanticipated side effects are often not encountered in preclinical trials and having more test candidates improves the chance to accomplish the development of a safe pharmaceutical product that can be used in patients.

Finally, the usage of effectors is not limited to a possible development into drugs. Numerous studies try to further unravel the molecular mechanisms and correlations of GLUTs in health and disease. While some GLUT-disease relationships are more evident (as e.g., an overexpression of GLUT1 and GLUT3 in cancer tissues (Macheda et al., 2005)), others are still more elusive. For GLUT2, for instance, substantial evidence exists that it is involved in many metabolic processes and maintains glucose or fructose homeostasis in e.g., the lumen, kidney and liver (Kellett and Brot-Laroche, 2005; Patel et al., 2015; Ghezzi et al., 2018) but its distinct role remains to be a subject of many investigations. These studies benefit from specific inhibitors to analyze effects of GLUT malabsorption in different tissues.

3.2.2.1 Application areas for GLUT2-specific inhibitors

Within this work, eleven compounds with an inhibiting effect on GLUT2 of which nine are putatively GLUT2-specific could be identified (Schmidl et al., 2021c). Therefore, highly potent, and specific inhibitors for GLUT2 are now available for the first time. The role of GLUT2 in several diseases is partly ambiguous and not

fully elucidated, yet. Its extraordinary low affinity for glucose ($K_M \sim 17$ mM (Uldry et al., 2002)) likely imposes functions apart from transport, like glucose sensing or signaling (Guillemain et al., 2000; Ohtsubo et al., 2005) to this unique transporter. Like other GLUTs, GLUT2 has also been found to be overexpressed in certain cancer types like pancreatic, hepatic, micropapillary, or colon cancer (Godoy et al., 2006) and its inhibition diminished tumor growth of colon or hepatic cancer as shown in studies with human cell lines (Wu et al., 2009; Lin et al., 2016). The idea of GLUT inhibition to combat cancer proliferation therefore also encloses GLUT2.

GLUT2 supports SGLT1 to take up glucose from the lumen after a meal but is not present at the apical site of the brush-boarder membrane in fasting states, in healthy individuals (Kellett and Brot-Laroche, 2005). However, a constant presence of GLUT2 at this location was observed in morbidly obese patients and this abnormality was related to insulin resistance (Ait-Omar et al., 2011). Because GLUT2 is a facilitator that transports glucose along a concentration gradient, the continuous presence of the transporter at the apical membrane enables transport from the blood through the basolateral membrane to the intestine. Higher blood glucose levels due to insulin resistance might result in higher glucose levels in the lumen in fasting states. The abnormal sugar supply supports bacterial growth and might interfere with a healthy gut microbiome (Ait-Omar et al., 2011).

Further studies revealed that GLUT2 deletion in the murine intestine leads to favorable effects like an improved glucose tolerance or decreased body weight gain (Schmitt et al., 2017). Together, these findings indicate that GLUT2 inhibition might yield health benefits for morbidly obese and/or diabetes type 2 patients or could be applied to rehabilitate a healthy gut microbiome. In addition, certain viruses induce an overexpression of GLUT2 to enhance viral replication (Dai et al., 2016) and inhibitors could putatively contain this. Although the idea to use GLUT2 inhibitors to help with the here-described health problems is tempting, one must consider the many regulating functions GLUT2 putatively holds in different tissues. Elucidating these roles in detail is fundamental to shed light on several metabolic conditions and to predict possible, unwanted side effects of GLUT2 inhibitors as drugs.

Among many studies aiming to determine the role of GLUT2, some employed the unspecific inhibitor phloretin but its effects on other GLUTs necessitate great efforts to prove a GLUT2-specific effect (Wu et al., 2009; Lin et al., 2016). The nine specific, easily accessible, and very potent inhibitors determined in the scope of this work (e.g., G2iA with an $IC_{50}=0.61 \mu\text{M}$ (Schmidl et al., 2021c)) will significantly improve the design of future GLUT2-related studies.

3.3 Roles of soluble loops in transporters – more than just connectors

Although recent studies with diverse transporters indicate an important role of hydrophilic regions in transport processes (Katagiri et al., 1992; Aseervatham et al., 2015; van't Klooster et al., 2020c), information about the distinct functions of soluble loops is still scarce. In addition, modeling their structure is challenging as they are often not well resolved in crystal structures (van't Klooster et al., 2020c). Also, alignments of prokaryotic and eukaryotic homologs of membrane proteins revealed that the soluble loops in prokaryotic transporters are generally shorter, which impedes the structural modeling of eukaryotic loops from bacterial homologs (Beuming et al., 2006; van't Klooster et al., 2020c). Various studies have illustrated that hydrophilic regions of transporters can affect the folding, trafficking to the PM, stability, activity, affinity, and even substrate specificity of the protein (Kanner et al., 1994; Loland et al., 2002; Cohen et al., 2003; Conseil et al., 2009; Aseervatham et al., 2015; Papadaki et al., 2017; van't Klooster et al., 2020c).

Several mutations in the extracellular loops of the lysine transporter Lyp1 have negatively influenced protein trafficking or led to an increased turnover, which indicates a compromised stability (van't Klooster et al., 2020c). Similarly, the two large loops of human equilibrative nucleoside transporters were not essential but contributed to higher efficiency of protein folding, trafficking, and targeting (Aseervatham et al., 2015). In human organic cation transporters, cysteine residues in the soluble loops facilitate protein oligomerization, influencing the protein's quaternary structure and its insertion into the PM (Keller et al., 2011; Brast et al., 2012). Furthermore, amino acid substitutions in the first extracellular loop of the mammalian metal ion transporter DCT1 led to drastic changes in the uptake of

different metal ions, indicating a distinct role of this region for metal ion binding (Cohen et al., 2003). A mutation of a tyrosine residue in an intracellular loop of the dopamine transporter led to an altered preference of conformational states, indicating that soluble loops are conformationally active and play a role in the substrate gating process (Loland et al., 2002). Strikingly, Qureshi et al. showed that, in *Plasmodium falciparum* hexose transporter (PfHT1), polar contacts between TM regions 1 and 7b induce the formation of the occluded-state conformation after substrate binding, which is a prerequisite for the alternating access mechanism (Qureshi et al., 2020). Hence, these interactions are involved in the substrate gating process. Interestingly, PfHT1 shares a high sequence similarity of its sugar binding site with GLUT3 and GLUT5 but exhibits a more relaxed substrate specificity (it transports both glucose and fructose, whereas GLUT3 and GLUT5 transport one substrate, respectively) (Qureshi et al., 2020). Qureshi et al. (2020), therefore, conclude that the evolved substrate-gating dynamics, which rely on polar interactions, lead to an easier transition to the occluded state, which in turn favors a more robust and promiscuous sugar transport. Another example illustrating the significance of polar residues for transport processes derives from the yeast hexose transporters Hxt15 and Hxt16. Both are polyol transporters that share very high (99%) sequence similarity (Jordan et al., 2016). In fact, they only differ in two amino acids (D276 and T520 in Hxt16) which are both located in cytosolic regions (Jordan et al., 2016). Despite of these mere differences, Hxt15 transports mannitol and sorbitol with a significant increased affinity (~50-fold and 4-fold, respectively) demonstrating the importance of these cytosolic loops on transport activity (Jordan et al., 2016).

Albeit their high sequence similarities and especially their conservation at the sugar binding sites, GLUT homologs demonstrate individual substrate preferences and affinities (Joost and Thorens, 2009; Schmidl et al., 2021c), which indicates that the molecular basis for these differences probably lies apart from the substrate binding site and might involve hydrophilic areas. This hypothesis is supported by the finding that the C-terminal intracellular domain of GLUT2 is responsible for the low affinity of the transporter for glucose (Katagiri et al., 1992). Furthermore, a mutation of an isoleucine residue (Ile314) (a residue conserved among fructose-transporting GLUTs) in GLUT7 to valine abolished fructose transport but left glucose transport

unaffected (Manolescu et al., 2005). Although Ile314 (GLUT7) lies in the TM region 7, it is apart from the sugar binding site and approaches the extracellular loop between TM7 and TM8 (Manolescu et al., 2005). Interestingly, one frequent missense mutation in GLUT1 encountered for GLUT1 DS patients is the mutation of the threonine residue Thr310 (GLUT1) to isoleucine (Iserovich et al., 2002). This residue is in TM region 8 and, like Ile314 of GLUT7, close to the loop connecting TM helices 7 and 8, and compromises glucose transport (Iserovich et al., 2002). In conclusion, these findings indicate that for GLUTs also, residues apart from the lower substrate cavity impact substrate specificities or affinities and transport activity.

In yeast, a (partly) correct localization of GLUT2 to the PM was only achieved when the large extracellular loop between TM regions 1 and 2 was truncated by 34 amino acids (Schmidl et al., 2021b). Full-length GLUT2 was not present at the cell periphery but localized in intracellular vesicles, indicating that the extended loop size impedes a correct protein trafficking (Schmidl et al., 2021b). It cannot be completely excluded that this invasive alteration affects GLUT2 in some way, however, functional studies revealed similar characteristics of GLUT2 Δ loopS_Q455R in yeast compared to full-length GLUT2 in other systems (Schmidl et al., 2021b; Schmidl et al., 2021c), proving that the GLUT2 Δ loopS_Q455R yeast system is applicable for ligand screening purposes.

3.4 Advantages and restrictions of the pHluorin-based assay – a new, label-free method to measure sugar uptake

In this thesis, a new method was established to measure the glucose uptake of *hxt*⁰ yeast cells selectively expressing a specific transporter, by employing the pH-sensitive GFP variant pHluorin as a biosensor. pHluorin and the respective transporter were co-expressed, on separate plasmids, in a *hxt*⁰ yeast strain and the cytosolic pH (pH_{cyt}) of these cells was monitored. For this, the ratio (R_{390/470}) of emission intensities at 512 nm from two different excitation wavelengths (390 and 470 nm) was calculated and used as a proxy for pH_{cyt} (Orij et al., 2009).

When yeast cells are deprived from sugar, their cytosol acidifies to a pH_{cyt} of approximately 6 (Orij et al., 2009). This is, most likely, caused by a reduced activity

of the PM ATPase and the vacuolar V-ATPase (both remove protons from the cytosol) due to a lower ATP level (Orij et al., 2011). Naturally, the reintroduction of glucose to starved cells will ultimately increase the ATP pool again and lead to the recovery to a normal pH_{cyt} of ~ 7 . However, directly after supplying glucose to starved cells, the pH_{cyt} decreases further rapidly, before it gradually increases (Ramos et al., 1989; Orij et al., 2009). When looking at the consecutive metabolic reactions of glycolysis, the basis of this phenomenon becomes evident. In the first step, glucose is phosphorylated by the hexokinase to glucose-6-phosphate. In this step one ATP is hydrolyzed under the release of one proton which leads to the observed initial acidification (Orij et al., 2011). The in this thesis established method utilizes these correlations to determine the glucose uptake rates of the transporter in question (Schmidl et al., 2021a). The linear decreasing slope of the acidification phase, measured with hxt^0 yeast cells that, besides pHluorin, express the respective transporter and are pulsed with a defined glucose concentration, is used as a parameter of velocity. Reciprocal values derived from cells pulsed with a range of different glucose concentrations were then used to fit the Michaelis Menten equation and calculate K_M values (Schmidl et al., 2021a).

Results obtained with this method for the high-affinity/low-capacity yeast transporter Hxt7 ($K_M=1.3$ mM) and the medium-affinity/medium-capacity yeast transporter Hxt5 ($K_M=3.3$ mM) were in good agreement with the results published (Reifenberger et al., 1997; Diderich et al., 2001; Buziol et al., 2002) or determined in this work with the conventional C^{14} uptake assay (Schmidl et al., 2021a). However, for the low-affinity/high-capacity transporter Hxt1 a severe discrepancy was observed ($K_M=6.2$ mM with the pHluorin-based assay (Schmidl et al., 2021a) vs. $K_M\sim 100$ mM with the C^{14} uptake assay (Reifenberger et al., 1997)) which presumably derived from the high capacity of Hxt1 expressed from a high-copy plasmid and under the control of a strong promotor. These results indicate that, for very high transport rates, other factors become rate limiting and thereby glucose concentrations inducing transport saturation are underestimated. Fortunately, transport capacities can be easily modulated in the experimental set-ups used in this study by choosing a weaker promotor, integrating the transporter gene into the genome, or expressing the transporter from a low-copy plasmid (Schmidl et al., 2021a). However, if it is the aim to determine transport kinetics of, for example,

wildtype strains, capacities cannot be reduced which might prevent the usage of our method in these cases. In the performed experiments of this thesis, Hxt1 was expressed from a low-copy plasmid to reduce its capacity which yielded significantly higher K_M values for Hxt1 ($K_M=99.1$ mM) that agreed with the published values and the ones obtained previously with the C^{14} uptake assay (Reifenberger et al., 1997; Schmidl et al., 2021a). By setting the initial transport velocity (V_0) values measured by both methods (pHluorin-based assay and C^{14} uptake assay) for Hxt5 and Hxt1, respectively, into relation in one graph, a linear correlation up to a certain threshold ($\sim 0.006 R_{390/470} s^{-1}$ or $1.5 \text{ nmol min}^{-1} \text{ mg}_{\text{cdw}}^{-1}$) is visible (Schmidl et al., 2021a). Values exceeding this threshold did not correlate linearly anymore. Therefore, it was reasoned that the pHluorin-based method is accurate if the capacity stays within this determined range which can be easily achieved for every transporter by the before-mentioned options. Also, kinetic characteristics of unknown transporters can be determined with the pHluorin-based assay under consideration of this threshold. Ideally, when working with an unknown transporter one should intend a lower expression level from the beginning by e.g., choosing a weaker promoter or a low-copy plasmid. It should be noted that the integration of just one gene into the genome might not be sufficient for effective glucose uptake for many transporters as it has been observed in this thesis for e.g., the heterologous transporter GLUT4 but also the endogenous transporters Hxt1, Hxt5 and Hxt7. Therefore, genomic integration should not be the method of choice for lowering the expression levels.

It is not entirely clear what imposes the assay limitation when transport rates are high. It has been proposed earlier that, in yeast, sugar transport and phosphorylation are tightly intertwined (Walsh et al., 1994c) and even the option of a physical interaction between transporter and kinase was discussed (Clifton et al., 1993). Thus, it was tested if the hexokinase activity might be the limiting factor by additionally overexpressing Hxk2 in a Hxt1- and pHluorin overexpressing hxt⁰ strain (all three from separate multi-copy plasmids). The K_M values obtained from these cells with the pHluorin-based assay were not higher, even though a higher expression of Hxk2 was confirmed (Schmidl et al., 2021a). However, ATP depletion, caused by the prior starving conditions, could also negatively affect

hexokinase activity. In this case, an overexpression of the enzyme would not increase the phosphorylation activity.

A role of ATP in hexose transport measured by C¹⁴ uptake assays was observed before (Schuddemat et al., 1988; Walsh et al., 1994c). Respiratory inhibitors have been shown to reduce sugar uptake (Schuddemat et al., 1988), but this effect was only observed when measured on a 5 s timescale, not when the extra fast quench-flow technique (200 ms) (Walsh et al., 1994a) was used (Walsh et al., 1994c), indicating that it affects the metabolizing steps and not the true initial uptake rate (Walsh et al., 1994c). Walsh et al. (1994c) hypothesized that the lower ATP pool causes a reduction of hexokinase activity leading to an accumulation of internal sugar which in turn slows down the transport rate. Therefore, it is likely that in the experiments of this thesis, too, ATP is the limiting factor, but other bottlenecks cannot be completely excluded at this point.

Because the pHluorin-based assay measures pH changes as a parameter of sugar entry, it is directly dependent on a normal sugar phosphorylation at least for most transporters. The co-transport of protons by some symporters might serve as a sufficient signal for these calculations as well but this has not been tested, yet. Hence, for uniporters, the transport rates of substrates that do not undergo the initial phosphorylation step like xylose, lactose, glucosamine, or arabinose cannot be determined with this method. Disaccharides like maltose and sucrose are cleaved into monosaccharides (2x glucose and 1x glucose/1x fructose, respectively) first, before these substrates are phosphorylated (Fraenkel, 2011). Furthermore, maltose is transported via specialized symporters that introduce one proton along with one maltose molecule (Loureiro-Dias and Peinado, 1984) which would affect the pH_{cyt}. Supposedly, this would lead to a stronger acidification, but should not tamper with the results and so the pHluorin-based assay could, in theory, be applied to measure the uptake of these disaccharides, as well. However, this was not tested yet and remains to be confirmed by practical experiments. In yeast, the most abundant sugar glucose, and its widespread derivatives fructose and mannose, are phosphorylated by the hexokinases Hxk1 and Hxk2 (glucose and mannose can additionally be phosphorylated by the glucokinase Glk1) (Fraenkel, 2011). Galactose is phosphorylated by Gal1 (Fraenkel, 2011).

Therefore, the here-established method applies for the largest fraction of sugars and preferred substrates of most organisms.

One major advantage of the pHluorin-based assay over the commonly used C¹⁴-glucose uptake assay, is the fact that it does not require radiolabeled compounds. In Germany, the Radiation Protection Ordinance (Strahlenschutzverordnung) regulates the handling of radioisotopes to minimize the exposure to radiation, thereby reducing the risk of health detriments. Hence, experiments employing such isotopes can only be executed in specialized laboratories from healthy, non-pregnant individuals that conducted prior training. Not all groups have access to such laboratories which prevents them to experiment with isotopes. Moreover, the purchase, storage and disposal of radio-chemicals is not only expensive but requires special management (Ring et al., 1993), making these experiments costly and elaborate. Although biological experiments only contribute a small percentage to the general radioactive waste (significantly higher amounts accumulate in e.g., the generation of nuclear energy or mining (Natarajan et al., 2020)), its reduction is desirable for environmental protection. Moreover, C¹⁴ uptake assays require a significant amount of single-use scintillation vials and plastic containers for disposal. By using the pHluorin-based assay instead of the C¹⁴ sugar uptake assay, radio-chemicals and plastic wastes are reduced, making this method more environmentally friendly.

In this thesis, all kinetic determinations of transport rates by the pHluorin-based assay were conducted with the PTI QuantaMaster™ 8000 (Model QM-8075-11-C, Horiba Scientific). Two other devices, Fluorolog®-3 and Duetta™ (Horiba Scientific), were tried for these purposes during this thesis, as well. However, it became apparent that with these latter two, kinetics cannot be determined because the output of the ratio R_{390/470} is too slow. Either the switch between the excitation wavelength 390 nm and 470 nm was conducted too slow (for Fluorolog®-3) or when the device was able to operate this switch faster, the software required prolonged intervals between the output of ratios (R_{390/470}) (for Duetta™). The PTI QuantaMaster™ 800-series incorporates a superior DeltaRam X™ technology which allows for high-speed wavelength switching and rapid signal output (<https://www.horiba.com/>). In our experiments with the PTI QuantaMaster™ 8000, we obtained one value every 2.2 s. This very fast output of R_{390/470} values was

necessary because the initial acidification reaction is a very fast process that reaches its peak after only approximately ten seconds (Schmidl et al., 2021a). For a reliable determination of the linear slope ($\Delta R_{390/470}/\Delta t$) more values in this time frame are favorable. This requirement also unfortunately excludes the usage of platereaders (such as CLARIOstar®, BMG Labtech, Ortenberg, Germany) as devices for kinetic characterization via the pHluorin-based assay, as its signal output depends on the number of samples and always requires several minutes. Mostly, the initial acidification after the glucose pulse is not even visible, when measured with the platereader (Reifenrath and Boles, 2018). The apparent strict requirement of the PTI QuantaMaster™ 8000 or a technically comparable device with advanced wavelength switching speed for kinetic determinations can be viewed as a disadvantage of the pHluorin-based assay, considering that this device is expensive and so far not widely distributed among research laboratories. It is noteworthy, however, that a scintillation counter requires a comparable financial investment. Thus, with more technological improvements and expansion of research fields in which this method can be applied, the pHluorin-based assay will likely become a method of choice for many laboratories.

For qualitative measurements, however, e.g., to test if a transporter is active in the *hxt⁰* yeast system or to investigate the effect of certain compounds on transporters, timepoints on a minute scale, measured by the platereader, would be sufficient. In this case, not the initial acidification would be measured but the recovery to a normal pH_{cyt} . A proof of concept was given in this thesis, when pHluorin- and GLUT1_{V69M}-coexpressing *hxt⁰* cells were starved and then exposed to different concentrations of the class 1 GLUT inhibitor phloretin and their pH_{cyt} response to a glucose pulse was measured with the platereader (see chapter 5.2.2). With high concentrations of the inhibitor (300 μM) the recovery to a near-neutral pH is completely absent, whereas with lower concentrations (20 μM or 50 μM), the pH rises after the pulse, but to a lower level compared to the control (no phloretin). This shows that also the recovery phase could be used to analyze transport activity qualitatively, but the sensitivity of these measurements is lower compared to tests using the initial acidification phase as a parameter. Also, it should be noted that many compounds (e.g., the GLUT5 inhibitor MSNBA) exhibit a strong color and it

was experienced in this work that colorful compounds often interfere with the emission signal which might falsify the results.

In general, the newly established pHluorin-based assay represents an attractive alternative to the commonly used C¹⁴ sugar uptake assay. It abstains from the use of radio-chemicals and requires less expandable materials, making it safer, cheaper, and environmentally more friendly. The results are obtained in real-time which allows a quick analysis and adjustment of experimental conditions if necessary. On the contrary, the C¹⁴ uptake assay usually requires several hours (>5 hours for a typical kinetic characterization of a transporter) until the raw data is obtained and the success of the experiment can only be assessed subsequently (Schmidl et al., 2021a). In addition, also the experimental steps are easily conducted and less time consuming (Schmidl et al., 2021a).

The versatile biosensor pHluorin was initially developed to investigate the pH changes in secretory vesicles in neurons during synaptic transmission events (Miesenböck et al., 1998). Since its development it was used extensively, not only in cultured cells (Miesenböck et al., 1998) but also e.g., in the nematode *Caenorhabditis elegans* (Nehrke, 2006), in yeast (Brito et al., 2020) and in the parasite *Plasmodium falciparum* (Kuhn et al., 2007). Its expansive use is a strong indicator that the here-established method is likely not restricted to the hxt⁰ yeast system but might also be applied in, for instance, cell cultures or *Xenopus laevis* oocytes.

4 References

- Aguilar, P. S., Heiman, M. G., Walther, T. C., Engel, A., Schwudke, D., Gushwa, N., et al. (2010). Structure of sterol aliphatic chains affects yeast cell shape and cell fusion during mating. *P Natl Acad Sci USA* 107, 4170–4175. doi: 10.1073/pnas.0914094107
- Ait-Omar, A., Monteiro-Sepulveda, M., Poitou, C., Le Gall, M., Cotillard, A., Gilet, J., et al. (2011). GLUT2 accumulation in enterocyte apical and intracellular membranes. A study in morbidly obese human subjects and ob/ob and high fat-fed mice. *Diabetes* 60, 2598–2607. doi: 10.2337/db10-1740
- Aseervatham, J., Tran, L., Machaca, K., and Boudker, O. (2015). The role of flexible loops in folding, trafficking and activity of equilibrative nucleoside transporters. *PLoS ONE* 10, e0136779. doi: 10.1371/journal.pone.0136779
- Audhya, A., and Emr, S. D. (2002). Stt4 PI 4-kinase localizes to the plasma membrane and functions in the Pkc1-mediated MAP kinase cascade. *Dev Cell* 2, 593–605. doi: 10.1016/s1534-5807(02)00168-5
- Audhya, A., Foti, M., and Emr, S. D. (2000). Distinct roles for the yeast phosphatidylinositol 4-kinases, Stt4p and Pik1p, in secretion, cell growth, and organelle membrane dynamics. *Mol Biol Cell* 11, 2673–2689. doi: 10.1091/mbc.11.8.2673
- Augustin, R. (2010). The protein family of glucose transport facilitators: It's not only about glucose after all. *IUBMB Life* 62, 315–333. doi: 10.1002/iub.315
- Baig, M. H., and Ahmad, K. (2016). Computer aided drug design: Success and limitations. *Curr Pharm Des* 22, 572–581. doi: 10.2174/1381612822666151125000550
- Baird, D., Stefan, C., Audhya, A., Weys, S., and Emr, S. D. (2008). Assembly of the PtdIns 4-kinase Stt4 complex at the plasma membrane requires Ypp1 and Efr3. *J Cell Biol* 183, 1061–1074. doi: 10.1083/jcb.200804003
- Barron, C. C., Bilan, P. J., Tsakiridis, T., and Tsiani, E. (2016). Facilitative glucose transporters: Implications for cancer detection, prognosis and treatment. *Metab Clin Exp* 65, 124–139. doi: 10.1016/j.metabol.2015.10.007
- Beuming, T., Shi, L., Javitch, J. A., and Weinstein, H. (2006). A comprehensive structure-based alignment of prokaryotic and eukaryotic neurotransmitter/Na⁺ symporters (NSS) aids in the use of the LeuT structure to probe NSS structure and function. *Mol Pharmacol* 70, 1630–1642. doi: 10.1124/mol.106.026120
- Bharadwaj, P., Martins, R., and Macreadie, I. (2010). Yeast as a model for studying Alzheimer's disease. *FEMS Yeast Res* 10, 961–969. doi: 10.1111/j.1567-1364.2010.00658.x
- Bloch, K. E. (1983). Sterol, structure and membrane function. *Crit Rev Biochem Mol* 14, 47–92. doi: 10.3109/10409238309102790
- Boles, E., Dlugai, S., Mueller, G., and Voss, D. (2004). Use of *Saccharomyces cerevisiae* ERG4 mutants for the expression of glucose transporters from mammals. Geneva, Switzerland: World Intellectual Property Organisation. WO002004026907A3.

References

- Boles, E., and Hollenberg, C. P. (1997). The molecular genetics of hexose transport in yeasts. *FEMS Microbiol Rev* 21, 85–111. doi: 10.1111/j.1574-6976.1997.tb00346.x
- Boles, E., and Oreb, M. (2018). A growth-based screening system for hexose transporters in yeast. *Methods Mol Biol* 1713, 123–135. doi: 10.1007/978-1-4939-7507-5_10
- Brast, S., Grabner, A., Sucic, S., Sitte, H. H., Hermann, E., Pavenstädt, H., et al. (2012). The cysteines of the extracellular loop are crucial for trafficking of human organic cation transporter 2 to the plasma membrane and are involved in oligomerization. *FASEB J* 26, 976–986. doi: 10.1096/fj.11-180679
- Brito, A. S., Neuhäuser, B., Wintjens, R., Marini, A. M., and Boeckstaens, M. (2020). Yeast filamentation signaling is connected to a specific substrate translocation mechanism of the Mep2 transceptor. *PLoS Genet* 16, e1008634. doi: 10.1371/journal.pgen.1008634
- Brockmann, K. (2009). The expanding phenotype of GLUT1-deficiency syndrome. *Brain Dev* 31, 545–552. doi: 10.1016/j.braindev.2009.02.008
- Buziol, S., Becker, J., Baumeister A., jung, S., Mauch, K., Reuss, M., et al. (2002). Determination of *in vivo* kinetics of the starvation-induced Hxt5 glucose transporter of *Saccharomyces cerevisiae*. *FEMS Yeast Res* 2, 283–291. doi: 10.1016/S1567-1356(02)00113-7
- Cairns, R. A., Harris, I. S., and Mak, T. W. (2011). Regulation of cancer cell metabolism. *Nat Rev Cancer* 11, 85–95. doi: 10.1038/nrc2981
- Caulfield, M. J., Munroe, P. B., O'Neill, D., Witkowska, K., Charchar, F. J., Doblado, M., et al. (2008). SLC2A9 is a high-capacity urate transporter in humans. *PLoS Med* 5, e197. doi: 10.1371/journal.pmed.0050197
- César-Razquin, A., Snijder, B., Frappier-Brinton, T., Isserlin, R., Gyimesi, G., Bai, X., et al. (2015). A call for systematic research on solute carriers. *Cell* 162, 478–487. doi: 10.1016/j.cell.2015.07.022
- Chamberlain, L. H., and Gould, G. W. (2002). The vesicle- and target-SNARE proteins that mediate GLUT4 vesicle fusion are localized in detergent-insoluble lipid rafts present on distinct intracellular membranes. *J Biol Chem* 277, 49750–49754. doi: 10.1074/jbc.M206936200
- Chan, K. K., Chan, J. Y. W., Chung, K. K. W., and Fung, K.-P. (2004). Inhibition of cell proliferation in human breast tumor cells by antisense oligonucleotides against facilitative glucose transporter 5. *J Cell Biochem* 93, 1134–1142. doi: 10.1002/jcb.20270
- Chen, X., Ji, B., Hao, X., Li, X., Eisele, F., Nyström, T., et al. (2020). FMN reduces Amyloid- β toxicity in yeast by regulating redox status and cellular metabolism. *Nat Commun* 11, 867. doi: 10.1038/s41467-020-14525-4
- Chow, T. H., Sollitti, P., and Marmur, J. (1989). Structure of the multigene family of MAL loci in *Saccharomyces*. *Mol Gen Genet* 217, 60–69. doi: 10.1007/BF00330943

- Chung, J., Nakatsu, F., Baskin, J. M., and Camilli, P. de (2015). Plasticity of PI4KIII α interactions at the plasma membrane. *EMBO Rep* 16, 312–320. doi: 10.15252/embr.201439151
- Clifton, D., Walsh, R. B., and Fraenkel, D. G. (1993). Functional studies of yeast glucokinase. *J Bacteriol* 175, 3289–3294. doi: 10.1128/jb.175.11.3289-3294.1993
- Cloherty, E. K., Diamond, D. L., Heard, K. S., and Caruthers, A. A. C. (1996). Regulation of GLUT1-mediated sugar transport by an antiport/uniport switch mechanism. *Biochemistry* 35, 13231–13239. doi: 10.1021/bi961208t
- Cohen, A., Nevo, Y., and Nelson, N. (2003). The first external loop of the metal ion transporter DCT1 is involved in metal ion binding and specificity. *P Natl Acad Sci USA* 100, 10694–10699. doi: 10.1073/pnas.1934572100
- Colas, C., Ung, P. M.-U., and Schlessinger, A. (2016). SLC transporters: Structure, function, and drug discovery. *Medchemcomm* 7, 1069–1081. doi: 10.1039/C6MD00005C
- Colville, C. A., Seatter, M. J., Jess, T. J., Gould, G. W., and Thomas, H. M. (1993). Kinetic analysis of the liver-type (GLUT2) and brain-type (GLUT3) glucose transporters in *Xenopus oocytes*: Substrate specificities and effects of transport inhibitors. *Biochem J* 290, 701–706. doi: 10.1042/bj2900701
- Conseil, G., Rothnie, A. J., Deeley, R. G., and Cole, S. P. C. (2009). Multiple roles of charged amino acids in cytoplasmic loop 7 for expression and function of the multidrug and organic anion transporter MRP1 (ABCC1). *Mol Pharmacol* 75, 397–406. doi: 10.1124/mol.108.052860
- Dai, L., Hu, W. W., Xia, L., Xia, M., and Yang, Q. (2016). Transmissible gastroenteritis virus infection enhances SGLT1 and GLUT2 expression to increase glucose uptake. *PLoS ONE* 11, e0165585. doi: 10.1371/journal.pone.0165585
- D'Angelo, G., Vicinanza, M., Di Campli, A., and Matteis, M. A. de (2008). The multiple roles of PtdIns(4)P– not just the precursor of PtdIns(4,5)P₂. *J Cell Sci* 15, 1955–1963. doi: 10.1242/jcs.023630
- Danhier, P., Bański, P., Payen, V. L., Grasso, D., Ippolito, L., Sonveaux, P., et al. (2017). Cancer metabolism in space and time: Beyond the Warburg effect. *BBA Bioenerg* 1858, 556–572. doi: 10.1016/j.bbabi.2017.02.001
- Dawson, P. A., Mychaleckyj, J. C., Fossey, S. C., Mihic, S. J., Craddock, A. L., and Bowden, D. W. (2001). Sequence and functional analysis of GLUT10: A glucose transporter in the Type 2 diabetes-linked region of chromosome 20q12-13.1. *Mol Genet Metab* 74, 186–199. doi: 10.1006/mgme.2001.3212
- Deng, D., Sun, P., Yan, C., Ke, M., Jiang, X., Xiong, L., et al. (2015). Molecular basis of ligand recognition and transport by glucose transporters. *Nature* 526, 391–396. doi: 10.1038/nature14655
- Deng, D., Xu, C., Sun, P., Wu, J., Yan, C., Hu, M., et al. (2014). Crystal structure of the human glucose transporter GLUT1. *Nature* 510, 121–125. doi: 10.1038/nature13306

References

- Deng, D., and Yan, N. (2016). GLUT, SGLT, and SWEET: Structural and mechanistic investigations of the glucose transporters. *Protein Sci* 25, 546–558. doi: 10.1002/pro.2858
- Desrivières, S., Cooke, F. T., Parker, P. J., and Hall, M. N. (1998). MSS4, a phosphatidylinositol-4-phosphate 5-kinase required for organization of the actin cytoskeleton in *Saccharomyces cerevisiae*. *J Biol Chem* 273, 15787–15793. doi: 10.1074/jbc.273.25.15787
- Diderich, J. A., Schuurmans, J. M., van Gaalen, M. C., Kruckeberg, A. L., and van Dam, K. (2001). Functional analysis of the hexose transporter homologue HXT5 in *Saccharomyces cerevisiae*. *Yeast* 18, 1515–1524. doi: 10.1002/yea.779
- Dlugai, S. (2003). Untersuchungen zur funktionellen Expression des humanen Glukosetransporters GLUT4 in der Hefe *Saccharomyces cerevisiae* und der Nachweis möglicher Interaktionspartner. Dissertation, Heinrich-Heine-Universität Düsseldorf.
- Eny, K. M., Wolever, T. M. S., Fontaine-Bisson, B., and El-Soheemy, A. (2008). Genetic variant in the glucose transporter type 2 is associated with higher intakes of sugars in two distinct populations. *Physiol Genomics* 33, 355–360. doi: 10.1152/physiolgenomics.00148.2007
- Eom, J.-S., Chen, L.-Q., Sosso, D., Julius, B. T., Lin, I. W., Qu, X.-Q., et al. (2015). SWEETs, transporters for intracellular and intercellular sugar translocation. *Curr Opin Plant Biol* 25, 53–62. doi: 10.1016/j.pbi.2015.04.005
- Fanconi, G., and Bickel, H. (1949). Die chronische Aminoacidurie (Aminosäurediabetes oder nephrotisch-glukosurischer Zwergwuchs) bei der Glykogenose und der Cystinkrankheit. *Helv Paediatr Acta* 4, 359–396.
- Farwick, A., Bruder, S., Schadoweg, V., Oreb, M., and Boles, E. (2014). Engineering of yeast hexose transporters to transport D-xylose without inhibition by D-glucose. *P Natl Acad Sci USA* 111, 5159–5164. doi: 10.1073/pnas.1323464111
- Feng, L., and Frommer, W. B. (2015). Structure and function of SemiSWEET and SWEET sugar transporters. *Trends Biochem Sci* 40, 480–486. doi: 10.1016/j.tibs.2015.05.005
- Flanagan, C. A., Schnieders, E. A., Emerick, A. W., Kunisawa, R., Admon, A., and Thorner, J. (1993). Phosphatidylinositol 4-kinase: Gene structure and requirement for yeast cell viability. *Science* 262, 1444–1448. doi: 10.1126/science.8248783
- Flower, T. R., Chesnokova, L. S., Froelich, C. A., Dixon, C., and Witt, S. N. (2005). Heat shock prevents alpha-synuclein-induced apoptosis in a yeast model of Parkinson's disease. *J Mol Biol* 351, 1081–1100. doi: 10.1016/j.jmb.2005.06.060
- Foury, F. (1997). Human genetic diseases: A cross-talk between man and yeast. *Gene* 195, 1–10. doi: 10.1016/s0378-1119(97)00140-6
- Fraenkel, D. G. (2011). Yeast intermediary metabolism. *Cold Spring Harb Lab Press. New York*.

- Gaber, R., F., Copple, Deborah, M., Kennedy, Brian, K., Vidal, M., and Bard, M. (1989). The yeast gene *ERG6* is required for normal membrane function but is not essential for biosynthesis of the cell-cycle-sparking sterol. *Mol Cell Biol* 9, 3447–3456. doi: 10.1128/mcb.9.8.3447-3456
- George Thompson, A. M., Ursu, O., Babkin, P., Iancu, C. V., Whang, A., Oprea, T. I., et al. (2016). Discovery of a specific inhibitor of human GLUT5 by virtual screening and *in vitro* transport evaluation. *Sci Rep* 6, 24240. doi: 10.1038/srep24240
- Ghezzi, C., Loo, D. D. F., and Wright, E. M. (2018). Physiology of renal glucose handling via SGLT1, SGLT2 and GLUT2. *Diabetologia* 61, 2087–2097. doi: 10.1007/s00125-018-4656-5
- Ghosh, A. K., Ramakrishnan, G., and Rajasekharan, R. (2008). YLR099C (ICT1) encodes a soluble Acyl-CoA-dependent lysophosphatidic acid acyltransferase responsible for enhanced phospholipid synthesis on organic solvent stress in *Saccharomyces cerevisiae*. *J Biol Chem* 283, 9768–9775. doi: 10.1074/jbc.M708418200
- Giorgis, V. de, Varesio, C., Baldassari, C., Piazza, E., Olivotto, S., Macasaet, J., et al. (2016). Atypical manifestations in GLUT1 deficiency syndrome. *J Child Neurol* 31, 1174–1180. doi: 10.1177/0883073816650033
- Godoy, A., Ulloa, V., Rodríguez, F., Reinicke, K., Yañez, A. J., García, M. d. I. A., et al. (2006). Differential subcellular distribution of glucose transporters GLUT1-6 and GLUT9 in human cancer: Ultrastructural localization of GLUT1 and GLUT5 in breast tumor tissues. *J Cell Physiol* 207, 614–627. doi: 10.1002/jcp.20606
- Gould, G. W., and Lienhard, G. E. (1989). Expression of a functional glucose transporter in *Xenopus oocytes*. *Biochemistry* 28, 9447–9452. doi: 10.1021/bi00450a030
- Guillemain, G., Loizeau, M., Pinnçon-Raymond, M., Girard, J., and Leturque, A. (2000). The large intracytoplasmic loop of the glucose transporter GLUT2 is involved in glucose signaling in hepatic cells. *J Cell Sci* 113, 841–847.
- Haanstra, J. R., Gerding, A., Dolga, A. M., Sorgdrager, F. J. H., Buist-Homan, M., Du Toit, F., et al. (2017). Targeting pathogen metabolism without collateral damage to the host. *Sci Rep* 7, 40406. doi: 10.1038/srep40406
- Hajiaghaalipour, F., Khalilpourfarshbafi, M., and Arya, A. (2015). Modulation of glucose transporter protein by dietary flavonoids in type 2 diabetes mellitus. *Int J Biol Sci* 11, 508–524. doi: 10.7150/ijbs.11241
- Han, G.-S., Audhya, A., Markley, D. J., Emr, S. D., and Carman, G. M. (2002). The *Saccharomyces cerevisiae* LSB6 gene encodes phosphatidylinositol 4-kinase activity. *J Biol Chem* 277, 47709–47718. doi: 10.1074/jbc.M207996200
- Hirz, M., Richter, G., Leitner, E., Wriessnegger, T., and Pichler, H. (2013). A novel cholesterol-producing *Pichia pastoris* strain is an ideal host for functional expression of human Na,K-ATPase $\alpha\beta 1$ isoform. *Appl Microbiol Biotechnol* 97, 9465–9478. doi: 10.1007/s00253-013-5156-7

References

- Holman, G. D. (2020). Structure, function and regulation of mammalian glucose transporters of the SLC2 family. *Pflugers Arch* 472, 1155–1175. doi: 10.1007/s00424-020-02411-3
- Hu, Z., He, B., Ma, L., Sun, Y., Niu, Y., and Zeng, B. (2017). Recent advances in ergosterol biosynthesis and regulation mechanisms in *Saccharomyces cerevisiae*. *Indian J Microbiol* 57, 270–277. doi: 10.1007/s12088-017-0657-1
- Hung, I. H., Suzuki, M., Yamaguchi, Y., Yuan, D. S., Klausner, R. D., and Gitlin, J. D. (1997). Biochemical characterization of the Wilson disease protein and functional expression in the yeast *Saccharomyces cerevisiae*. *J Biol Chem* 272, 21461–21466. doi: 10.1074/jbc.272.34.21461
- Iancu, C. V., Zamoon, J., Woo, S. B., Aleshin, A., and Choe, J. (2013). Crystal structure of a glucose/H⁺ symporter and its mechanism of action. *P Natl Acad Sci USA* 110, 17862–17867. doi: 10.1073/pnas.1311485110
- Iserovich, P., Wang, D., Ma, L., Yang, H., Zuniga, F. A., Pascual, J. M., et al. (2002). Changes in glucose transport and water permeability resulting from the T310I pathogenic mutation in GLUT1 are consistent with two transport channels per monomer. *J Biol Chem* 277, 30991–30997. doi: 10.1074/jbc.M202763200
- Jaldin-Fincati, J. R., Bilan, P. J., and Klip, A. (2018). GLUT4 translocation in single muscle cells in culture: Epitope detection by immunofluorescence. *Methods Mol Biol* 1713, 175–192. doi: 10.1007/978-1-4939-7507-5_14
- Jiang, X., Yuan, Y., Huang, J., Zhang, S., Luo, S., Wang, N., et al. (2020). Structural basis for blocking sugar uptake into the malaria parasite *Plasmodium falciparum*. *Cell* 183, 258–268.e12. doi: 10.1016/j.cell.2020.08.015
- Johnston, K., Sharp, P., Clifford, M., and Morgan, L. (2005). Dietary polyphenols decrease glucose uptake by human intestinal Caco-2 cells. *FEBS Lett* 579, 1653–1657. doi: 10.1016/j.febslet.2004.12.099
- Joost, H.-G., Bell, G. I., Best, J. D., Birnbaum, M. J., Charron, M. J., Chen, Y. T., et al. (2002). Nomenclature of the GLUT/SLC2A family of sugar/polyol transport facilitators. *Am J Physiol Endocrinol Metab* 282, E974–E976. doi: 10.1152/ajpendo.00407.2001
- Joost, H.-G., and Thorens, B. (2009). The extended GLUT-family of sugar/polyol transport facilitators: Nomenclature, sequence characteristics, and potential function of its novel members. *Mol Membr Biol* 18, 247–256. doi: 10.1080/09687680110090456
- Jordan, P., Choe, J., Boles, E., and Oreb, M. (2016). Hxt13, Hxt15, Hxt16 and Hxt17 from *Saccharomyces cerevisiae* represent a novel type of polyol transporters. *Sci Rep* 6, 23502. doi: 10.1038/srep23502
- Kachroo, A. H., Laurent, J. M., Yellman, C. M., Meyer, A. G., Wilke, C. O., and Marcotte, E. M. (2015). Systematic humanization of yeast genes reveals conserved functions and genetic modularity. *Science* 348, 921–925. doi: 10.1126/science.aaa0769
- Kanner, B. I., Bendahan, A., Pantanowitz, S., and Su, H. (1994). The number of amino acid residues in hydrophilic loops connecting transmembrane domains of the GABA

- transporter GAT-1 is critical for its function. *FEBS Lett* 356, 191–194. doi: 10.1016/0014-5793(94)01255-5
- Kasahara, T., and Kasahara, M. (1996). Expression of the rat GLUT1 glucose transporter in the yeast *Saccharomyces cerevisiae*. *Biochem J* 315, 177–182. doi: 10.1042/bj3150177
- Kasahara, T., and Kasahara, M. (1997). Characterization of rat GLUT4 glucose transporter expressed in the yeast *Saccharomyces cerevisiae*: Comparison with GLUT1 glucose transporter. *Biochim Biophys Acta* 1324, 111–119. doi: 10.1016/S0005-2736(96)00217-9
- Katagiri, H., Asano, T., Ishihara, H., Tsukuda, K., Lin, J.-L., Inukai, K., et al. (1992). Replacement of intracellular C-terminal domain of GLUT1 glucose transporter with that of GLUT2 increases V_{\max} and K_m of transport activity. *J Biol Chem* 267, 22550–22555.
- Keller, K., Strube, M., and Mueckler, M. (1989). Functional expression of the human HepG2 and rat adipocyte glucose transporters in *Xenopus oocytes*. *J Biol Chem* 264, 18884–18889.
- Keller, T., Egenberger, B., Gorboulev, V., Bernhard, F., Uzelac, Z., Gorbunov, D., et al. (2011). The large extracellular loop of organic cation transporter 1 influences substrate affinity and is pivotal for oligomerization. *J Biol Chem* 286, 37874–37886. doi: 10.1074/jbc.M111.289330
- Kellett, G. L. (2001). The facilitated component of intestinal glucose absorption. *J Physiol* 531, 585–595. doi: 10.1111/j.1469-7793.2001.0585h.x
- Kellett, G. L., and Brot-Laroche, E. (2005). Apical GLUT2. A major pathway of intestinal sugar absorption. *Diabetes* 54, 3056–3062. doi: 10.2337/diabetes.54.10.3056
- Khandelwal, P., Sinha, A., Jain, V., Houghton, J., Hari, P., and Bagga, A. (2018). Fanconi syndrome and neonatal diabetes: Phenotypic heterogeneity in patients with GLUT2 defects. *CEN Case Rep* 7, 1–4. doi: 10.1007/s13730-017-0278-x
- Kim, H., Lee, H.-S., Park, H., Lee, D.-H., Boles, E., Chung, D., et al. (2017). Enhanced production of xylitol from xylose by expression of *Bacillus subtilis* arabinose: H⁺ symporter and *Scheffersomyces stipitis* xylose reductase in recombinant *Saccharomyces cerevisiae*. *Enzyme Microb Technol* 107, 7–14. doi: 10.1016/j.enzmictec.2017.07.014
- Kim, W. H., Lee, J., Jung, D.-W., and Williams, D. R. (2012). Visualizing sweetness: Increasingly diverse applications for fluorescent-tagged glucose bioprobes and their recent structural modifications. *Sensors Basel* 12, 5005–5027. doi: 10.3390/s120405005
- Kleinschmidt, J. H., and Popot, J.-L. (2014). Folding and stability of integral membrane proteins in amphipols. *Arch Biochem Biophys* 564, 327–343. doi: 10.1016/j.abb.2014.10.013
- Kodedová, M., and Sychrová, H. (2015). Changes in the sterol composition of the plasma membrane affect membrane potential, salt tolerance and the activity of multidrug

References

- resistance pumps in *Saccharomyces cerevisiae*. *PLoS ONE* 10, e0139306. doi: 10.1371/journal.pone.0139306
- Koepsell, H. (2020). Glucose transporters in brain in health and disease. *Pflugers Arch* 472, 1299–1343. doi: 10.1007/s00424-020-02441-x
- Kraft, T. E., Hresko, R. C., and Hruz, P. W. (2015). Expression, purification, and functional characterization of the insulin-responsive facilitative glucose transporter GLUT4. *Protein Sci* 24, 2008–2019. doi: 10.1002/pro.2812
- Kruckeberg, A. (1996). The hexose transporter family of *Saccharomyces cerevisiae*. *Arch Microbiol* 166, 283–292. doi: 10.1007/s002030050385
- Kuhn, Y., Rohrbach, P., and Lanzer, M. (2007). Quantitative pH measurements in *Plasmodium falciparum*-infected erythrocytes using pHluorin. *Cell Microbiol* 9, 1004–1013. doi: 10.1111/j.1462-5822.2006.00847.x
- Le Calvé, B., Rynkowski, M., Le Mercier, M., Bruyère, C., Lonez, C., Gras, T., et al. (2010). Long-term *in vitro* treatment of human glioblastoma cells with temozolomide increases resistance *in vivo* through up-regulation of GLUT transporter and aldo-keto reductase enzyme AKR1C expression. *Neoplasia* 12, 727–739. doi: 10.1593/neo.10526
- Lee, Y., Lim, Y., and Kwon, O. (2015). Selected phytochemicals and culinary plant extracts inhibit fructose uptake in Caco-2 cells. *Molecules* 20, 17393–17404. doi: 10.3390/molecules200917393
- Levy, S., Kafri, M., Carmi, M., and Barkai, N. (2011). The competitive advantage of a dual-transporter system. *Science* 334, 1408–1412. doi: 10.1126/science.1207154
- Li, Q., Manolescu, A., Ritzel, M., Yao, S., Slugoski, M., Young, J. D., et al. (2004). Cloning and functional characterization of the human GLUT7 isoform SLC2A7 from the small intestine. *Am J Physiol Gastrointest Liver Physiol* 287, G236-G242. doi: 10.1152/ajpgi.00396.2003
- Lin, S.-T., Tu, S.-H., Yang, P.-S., Hsu, S.-P., Lee, W.-H., Ho, C.-T., et al. (2016). Apple polyphenol phloretin inhibits colorectal cancer cell growth via inhibition of the type 2 glucose transporter and activation of p53-mediated signaling. *J Agric Food Chem* 64, 6826–6837. doi: 10.1021/acs.jafc.6b02861
- Liu, G., Chen, Y., Færgeman, N. J., and Nielsen, J. (2017). Elimination of the last reactions in ergosterol biosynthesis alters the resistance of *Saccharomyces cerevisiae* to multiple stresses. *FEMS Yeast Res* 17, fox063. doi: 10.1093/femsyr/fox063
- Liu, J.-F., Xia, J.-J., Nie, K.-L., Wang, F., and Deng, L. (2019). Outline of the biosynthesis and regulation of ergosterol in yeast. *World J Microbiol Biotechnol* 35, 98. doi: 10.1007/s11274-019-2673-2
- Liu, Y., Zhang, W., Cao, Y., Liu, Y., Bergmeier, S., and Chen, X. (2010). Small compound inhibitors of basal glucose transport inhibit cell proliferation and induce apoptosis in cancer cells via glucose-deprivation-like mechanisms. *Cancer Lett* 298, 176–185. doi: 10.1016/j.canlet.2010.07.002

- Loland, C. J., Norregaard, L., Litman, T., and Gether, U. (2002). Generation of an activating Zn²⁺ switch in the dopamine transporter: Mutation of an intracellular tyrosine constitutively alters the conformational equilibrium of the transport cycle. *P Natl Acad Sci USA* 99, 1683–1688. doi: 10.1073/pnas.032386299
- Long, W., O'Neill, D., and Cheeseman, C. I. (2018). GLUT characterization using frog *Xenopus laevis* oocytes. *Methods Mol Biol* 1713, 45–55. doi: 10.1007/978-1-4939-7507-5_4
- Loureiro-Dias, M. C., and Peinado, J. M. (1984). Transport of maltose in *Saccharomyces cerevisiae*: Effect of pH and potassium loss. *Biochem J* 222, 293–298. doi: 10.1042/bj2220293
- Ma, L., and Zong, X. (2020). Metabolic symbiosis in chemoresistance: Refocusing the role of aerobic glycolysis. *Front Oncol* 10, 5. doi: 10.3389/fonc.2020.00005
- Macheda, M. L., Rogers, S., and Best, J. D. (2005). Molecular and cellular regulation of glucose transporter (GLUT) proteins in cancer. *J Cell Physiol* 202, 654–662. doi: 10.1002/jcp.20166
- Mager, W. H., and Winderickx, J. (2005). Yeast as a model for medical and medicinal research. *Trends Pharmacol Sci* 26, 265–273. doi: 10.1016/j.tips.2005.03.004
- Mahraoui, L., Takeda, J., Mesonero, J., Chantret, I., Dussaulx, E., Bell, G. I., et al. (1994). Regulation of expression of the human fructose transporter (GLUT5) by cyclic AMP. *Biochem J* 301, 169–175. doi: 10.1042/bj3010169
- Manchester, J. K. (1990). Measurement of 2-deoxyglucose and 2-deoxyglucose 6-phosphate in tissues. *Anal Biochem* 185, 118–124. doi: 10.1016/0003-2697(90)90265-b
- Manolescu, A., Salas-Burgos, A. M., Fischbarg, J., and Cheeseman, C. I. (2005). Identification of a hydrophobic residue as a key determinant of fructose transport by the facilitative hexose transporter SLC2A7 (GLUT7). *J Biol Chem* 280, 42978–42983. doi: 10.1074/jbc.M508678200
- Manolescu, A. R., Augustin, R., Moley, K., and Cheeseman, C. (2007). A highly conserved hydrophobic motif in the exofacial vestibule of fructose transporting SLC2A proteins acts as a critical determinant of their substrate selectivity. *Mol Membr Biol* 24, 455–463. doi: 10.1080/09687680701298143
- Maria, Z., Campolo, A. R., and Lacombe, V. A. (2015). Diabetes alters the expression and translocation of the insulin-sensitive glucose transporters 4 and 8 in the atria. *PLoS ONE* 10, e0146033. doi: 10.1371/journal.pone.0146033
- Matsuo, S., Hiasa, M., and Omote, H. (2020). Functional characterization and tissue localization of the facilitative glucose transporter GLUT12. *J Biochem* 168, 611–620. doi: 10.1093/jb/mvaa090
- McBrayer, S. K., Cheng, J. C., Singhal, S., Krett, N. L., Rosen, S. T., and Shanmugam, M. (2012). Multiple myeloma exhibits novel dependence on GLUT4, GLUT8, and GLUT11:

References

- Implications for glucose transporter-directed therapy. *Blood* 119, 4686–4697. doi: 10.1182/blood-2011-09-377846
- McCulloch, L. J., van de Bunt, M., Braun, M., Frayn, K. N., Clark, A., and Gloyn, A. L. (2011). GLUT2 (SLC2A2) is not the principal glucose transporter in human pancreatic beta cells: Implications for understanding genetic association signals at this locus. *Mol Genet Metab* 104, 648–653. doi: 10.1016/j.ymgme.2011.08.026
- Meriin, A. B., Zhang, X., He, X., Newnam, G. P., Chernoff, Y. O., and Sherman, M. Y. (2002). Huntington toxicity in yeast model depends on polyglutamine aggregation mediated by a prion-like protein Rnq1. *J Cell Biol* 157, 997–1004. doi: 10.1083/jcb.200112104
- Mesmin, B., and Antonny, B. (2016). The counterflow transport of sterols and PI4P. *Biochim Biophys Acta* 1861, 940–951. doi: 10.1016/j.bbalip.2016.02.024
- Miesenböck, G., Angelis, D. A. de, and Rothman, J. E. (1998). Visualizing secretion and synaptic transmission with pH-sensitive green fluorescent proteins. *Nature* 394, 192–195. doi: 10.1038/28190
- Mioka, T., Fujimura-Kamada, K., Mizugaki, N., Kishimoto, T., Sano, T., Nunome, H., et al. (2018). Phospholipid flippases and Sfk1p, a novel regulator of phospholipid asymmetry, contribute to low permeability of the plasma membrane. *Mol Biol Cell* 29, 1203–1218. doi: 10.1091/mbc.E17-04-0217
- Mishra, R. K., Wei, C., Hresko, R. C., Bajpai, R., Heitmeier, M., Matulis, S. M., et al. (2015). *In silico* modeling-based identification of glucose transporter 4 (GLUT4)-selective inhibitors for cancer therapy. *J Biol Chem* 290, 14441–14453. doi: 10.1074/jbc.M114.628826
- Moser von Filseck, J., Čopič, A., Delfosse, V., Vanni, S., Jackson, C. L., Bourguet, W., et al. (2015). Phosphatidylserine transport by ORP/Osh proteins is driven by phosphatidylinositol 4-phosphate. *Science* 349, 432–436. doi: 10.1126/science.aab1346
- Mueckler, M., and Thorens, B. (2013). The SLC2 (GLUT) family of membrane transporters. *Mol Aspects Med* 34, 121–138. doi: 10.1016/j.mam.2012.07.001
- Munn, A. L., Heese-Peck, A., Stevenson, B. J., Pichler, H., and Riezman, H. (1999). Specific sterols required for the internalization step of endocytosis in yeast. *Mol Biol Cell* 10, 3943–3957. doi: 10.1091/mbc.10.11.3943
- Natarajan, V., Karunanidhi, M., and Raja, B. (2020). A critical review on radioactive waste management through biological techniques. *Environ Sci Pollut R* 27, 29812–29823. doi: 10.1007/s11356-020-08404-0
- Nehrke, K. (2006). Intracellular pH measurements *in vivo* using green fluorescent protein variants. *Methods Mol Biol* 351, 223–239. doi: 10.1385/1-59745-151-7:223
- Nes, W. R., Sekula, B. C., Nes, W. D., and Adler, J. H. (1978). The functional importance of structural features of ergosterol in yeast. *J Biol Chem* 253, 6218–6225. doi: 10.1016/S0021-9258(17)34602-1

- Nielsen, J. (2019). Yeast systems biology: Model organism and cell factory. *Biotechnol J* 14, e1800421. doi: 10.1002/biot.201800421
- Nomura, N., Verdon, G., Kang, H. J., Shimamura, T., Nomura, Y., Sonoda, Y., et al. (2015). Structure and mechanism of the mammalian fructose transporter GLUT5. *Nature* 526, 397–401. doi: 10.1038/nature14909
- Ohtsubo, K., Takamatsu, S., Minowa, M. T., Yoshida, A., Takeuchi, M., and Marth, J. D. (2005). Dietary and genetic control of glucose transporter 2 glycosylation promotes insulin secretion in suppressing diabetes. *Cell* 123, 1307–1321. doi: 10.1016/j.cell.2005.09.041
- Orij, R., Brul, S., and Smits, G. J. (2011). Intracellular pH is a tightly controlled signal in yeast. *Biochim Biophys Acta* 1810, 933–944. doi: 10.1016/j.bbagen.2011.03.011
- Orij, R., Postmus, J., Ter Beek, A., Brul, S., and Smits, G. J. (2009). *In vivo* measurement of cytosolic and mitochondrial pH using a pH-sensitive GFP derivative in *Saccharomyces cerevisiae* reveals a relation between intracellular pH and growth. *Microbiology* 155, 268–278. doi: 10.1099/mic.0.022038-0
- Overduin, M., and Klumperman, B. (2019). Advancing membrane biology with poly(styrene-co-maleic acid)-based native nanodiscs. *Eur Polym J* 110, 63–68. doi: 10.1016/j.eurpolymj.2018.11.015
- Papadaki, G. F., Amillis, S., and Diallinas, G. (2017). Substrate specificity of the FurE transporter is determined by cytoplasmic terminal domain interactions. *Genetics* 207, 1387–1400. doi: 10.1534/genetics.117.300327
- Parks, L. W., Smith, S. J., and Crowley, J. H. (1995). Biochemical and physiological effects of sterol alterations in yeast—a review. *Lipids* 30, 227–230. doi: 10.1007/BF02537825
- Pascual, J., Wang, D., Lecumberri, B., Yang, H., Mao, X., Yang, R., et al. (2004). GLUT1 deficiency and other glucose transporter diseases. *Eur J Endocrinol* 150, 627–633. doi: 10.1530/eje.0.1500627
- Patel, C., Sugimoto, K., Douard, V., Shah, A., Inui, H., Yamanouchi, T., et al. (2015). Effect of dietary fructose on portal and systemic serum fructose levels in rats and in KHK^{-/-} and GLUT5^{-/-} mice. *Am J Physiol Gastrointest Liver Physiol* 309, G779–G790. doi: 10.1152/ajpgi.00188.2015
- Phillips, S. A., Barr, V. A., Haft, D. H., Taylor, S. I., and Haft, C. R. (2001). Identification and characterization of SNX15, a novel sorting nexin involved in protein trafficking. *J Biol Chem* 276, 5074–5084. doi: 10.1074/jbc.M004671200
- Price, D. R. G., Tibbles, K., Shigenobu, S., Smertenko, A., Russell, C. W., Douglas, A. E., et al. (2010). Sugar transporters of the major facilitator superfamily in aphids; from gene prediction to functional characterization. *Insect Mol Biol* 19, 97–112. doi: 10.1111/j.1365-2583.2009.00918.x
- Privé, G. G. (2007). Detergents for the stabilization and crystallization of membrane proteins. *Methods* 41, 388–397. doi: 10.1016/j.ymeth.2007.01.007

References

- Quistgaard, E. M., Löw, C., Guettou, F., and Nordlund, P. (2016). Understanding transport by the major facilitator superfamily (MFS): Structures pave the way. *Nat Rev Mol Cell Biol* 17, 123–132. doi: 10.1038/nrm.2015.25
- Qureshi, A. A., Suades, A., Matsuoka, R., Brock, J., McComas, S. E., Nji, E., et al. (2020). The molecular basis for sugar import in malaria parasites. *Nature* 578, 321–325. doi: 10.1038/s41586-020-1963-z
- Ramos, S., Balbin, M., Raposo, M., Valle E., and Pardo, L. A. (1989). The mechanism of intracellular acidification induced by glucose in *Saccharomyces cerevisiae*. *J Gen Microbiol* 135, 2413–2422. doi: 10.1099/00221287-135-9-2413
- Reckzeh, E. S., Karageorgis, G., Schwalfenberg, M., Ceballos, J., Nowacki, J., Stroet, M. C. M., et al. (2019). Inhibition of glucose transporters and glutaminase synergistically impairs tumor cell growth. *Cell Chem Biol* 26, 1214–1228. doi: 10.1016/j.chembiol.2019.06.005
- Reckzeh, E. S., and Waldmann, H. (2020). Small-molecule inhibition of glucose transporters GLUT-1-4. *ChemBioChem* 21, 45–52. doi: 10.1002/cbic.201900544
- Reifenberger, E., Boles, E., and Ciriacy, M. (1997). Kinetic characterization of individual hexose transporters of *Saccharomyces cerevisiae* and their relation to the triggering mechanisms of glucose repression. *Eur J Biochem* 245, 324–333. doi: 10.1111/j.1432-1033.1997.00324.x
- Reifenrath, M., and Boles, E. (2018). A superfolder variant of pH-sensitive pHluorin for *in vivo* pH measurements in the endoplasmic reticulum. *Sci Rep* 8, 11985. doi: 10.1038/s41598-018-30367-z
- Ring, J., Osborne, F., Shapiro, J., and Johnson, R. (1993). Radioactive waste management at a large university and medical research complex. *Health Phys* 65, 193–199. doi: 10.1097/00004032-199308000-00011
- Rogers, S., Macheda, M. L., Docherty, S. E., Carty, M. D., Henderson, M. A., Soeller, W. C., et al. (2002). Identification of a novel glucose transporter-like protein-GLUT-12. *Am J Physiol Endocrinol Metab* 282, E733–E738. doi: 10.1152/ajpendo.2002.282.3.E733
- Rudlowski, C., Becker, A. J., Schroder, W., Rath, W., Büttner, R., and Moser, M. (2003). GLUT1 messenger RNA and protein induction relates to the malignant transformation of cervical cancer. *Am J Clin Pathol* 120, 691–698. doi: 10.1309/4KYNQM5862JW2GD7
- Sandu, C., Burloiu, C. M., Barca, D. G., Magureanu, S. A., and Craiu, D. C. (2019). Ketogenic diet in patients with GLUT1 deficiency syndrome. *Maedica* 14, 93–97. doi: 10.26574/maedica.2019.14.2.93
- Santer, R., Groth, S., Kinner, M., Dombrowski, A., Berry, G. T., Brodehl, J., et al. (2002). The mutation spectrum of the facilitative glucose transporter gene SLC2A2 (GLUT2) in patients with Fanconi-Bickel syndrome. *Hum Genet* 110, 21–29. doi: 10.1007/s00439-001-0638-6

- Santer, R., Schneppenheim, R., Dombrowski, A., Götze, H., Steinmann, B., and Schaub, J. (1997). Mutations in GLUT2, the gene for the liver-type glucose transporter, in patients with Fanconi-Bickel syndrome. *Nat Genet* 3, 324–326. doi: 10.1038/ng1197-324
- Sasson, S., Oron, R., and Cerasi, E. (1993). Enzymatic assay of 2-deoxyglucose 6-phosphate for assessing hexose uptake rates in cultured cells. *Anal Biochem* 215, 309–311. doi: 10.1006/abio.1993.1594
- Scheuring, S., Röhricht, R. A., Schöning-Burkhardt, B., Beyer, A., Müller, S., Abts, H. F., et al. (2001). Mammalian cells express two VPS4 proteins both of which are involved in intracellular protein trafficking. *J Mol Biol* 312, 469–480. doi: 10.1006/jmbi.2001.4917
- Schmidl, S., Iancu, C. V., Choe, J., and Oreb, M. (2018). Ligand screening systems for human glucose transporters as tools in drug discovery. *Front Chem* 6, 183. doi: 10.3389/fchem.2018.00183
- Schmidl, S., Iancu, C. V., Reifenrath, M., Choe, J., and Oreb, M. (2021a). A label-free real-time method for measuring glucose uptake kinetics in yeast. *FEMS Yeast Res* 21, foaa069. doi: 10.1093/femsyr/foaa069
- Schmidl, S., Tamayo Rojas, S. A., Iancu, C. V., Choe, J., and Oreb, M. (2021b). Functional expression of the human glucose transporters GLUT2 and GLUT3 in yeast offers novel screening systems for GLUT-targeting drugs. *Front Mol Biosci* 7, 598419. doi: 10.3389/fmolb.2020.598419
- Schmidl, S., Ursu, O., Iancu, C. V., Oreb, M., Oprea, T. I., and Choe, J. (2021c). Identification of new GLUT2-selective inhibitors through *in silico* ligand screening and validation in eukaryotic expression systems. *Sci Rep* 11, 13751. doi: 10.1038/s41598-021-93063-5
- Schmidt, A., Hall, M. N., and Koller, A. (1994). Two FK506 resistance-conferring genes in *Saccharomyces cerevisiae*, TAT1 and TAT2, encode amino acid permeases mediating tyrosine and tryptophan uptake. *Mol Cell Biol* 14, 6597–6606. doi: 10.1128/mcb.14.10.6597-6606.1994
- Schmidt, S., Joost, H.-G., and Schürmann, A. (2009). GLUT8, the enigmatic intracellular hexose transporter. *Am J Physiol Endocrinol Metab* 296, E614-E618. doi: 10.1152/ajpendo.91019.2008
- Schmitt, C. C., Arantias, T., Viel, T., Chateau, D., Le Gall, M., Waligora-Dupriet, A.-J., et al. (2017). Intestinal invalidation of the glucose transporter GLUT2 delays tissue distribution of glucose and reveals an unexpected role in gut homeostasis. *Mol Metab* 6, 61–72. doi: 10.1016/j.molmet.2016.10.008
- Schreiber, S. L., Kotz, J. D., Li, M., Aubé, J., Austin, C. P., Reed, J. C., et al. (2015). Advancing biological understanding and therapeutics discovery with small-molecule probes. *Cell* 161, 1252–1265. doi: 10.1016/j.cell.2015.05.023
- Schuddemat, J., van den Broek, P., and van Steveninck, J. (1988). The influence of ATP on sugar uptake mediated by the constitutive glucose carrier of *Saccharomyces cerevisiae*. *Biochim Biophys Acta* 937, 81–87. doi: 10.1016/0005-2736(88)90229-5

References

- Schüßler, A., Martin, H., Cohen, D., Fitz, M., and Wipf, D. (2006). Characterization of a carbohydrate transporter from symbiotic glomeromycotan fungi. *Nature* 444, 933–936. doi: 10.1038/nature05364
- Seddon, A. M., Curnow, P., and Booth, P. J. (2004). Membrane proteins, lipids and detergents: Not just a soap opera. *Biochim Biophys Acta* 1666, 105–117. doi: 10.1016/j.bbamem.2004.04.011
- Sharari, S., Abou-Alloul, M., Hussain, K., and Ahmad Khan, F. (2020). Fanconi-Bickel syndrome: A review of the mechanisms that lead to dysglycaemia. *Int J Mol Sci* 21, 6286. doi: 10.3390/ijms21176286
- Shriwas, P., Roberts, D., Li, Y., Wang, L., Qian, Y., Bergmeier, S., et al. (2021). A small-molecule pan-class I glucose transporter inhibitor reduces cancer cell proliferation *in vitro* and tumor growth *in vivo* by targeting glucose-based metabolism. *Cancer Metab* 9, 14. doi: 10.1186/s40170-021-00248-7
- Siebeneicher, H., Cleve, A., Rehwinkel, H., Neuhaus, R., Heisler, I., Müller, T., et al. (2016). Identification and optimization of the first highly selective GLUT1 inhibitor BAY-876. *ChemMedChem* 11, 2261–2271. doi: 10.1002/cmdc.201600276
- Simpson, I. A., Carruthers, A., and Vannucci, S. J. (2007). Supply and demand in cerebral energy metabolism: The role of nutrient transporters. *J Cereb Blood Flow Metab* 27, 1766–1791. doi: 10.1038/sj.jcbfm.9600521
- Smirnova, I., Kasho, V., Jiang, X., Pardon, E., Steyaert, J., and Kaback, H. R. (2014). Outward-facing conformers of LacY stabilized by nanobodies. *P Natl Acad Sci USA* 111, 18548–18553. doi: 10.1073/pnas.1422265112
- Smits, H. P., Smits, G. J., postma, P. W., Walsh, M. C., and van Dam, K. (1996). High-affinity glucose uptake in *Saccharomyces cerevisiae* is not dependent on the presence of glucose-phosphorylating enzymes. *Yeast* 12, 439–477. doi: 10.1002/(SICI)1097-0061(199604)
- Sokolov, S. S., Trushina, N. I., Severin, F. F., and Knorre, D. A. (2019). Ergosterol turnover in yeast: An interplay between biosynthesis and transport. *Biochemistry Moscow* 84, 346–357. doi: 10.1134/S0006297919040023
- Solis-Escalante, D., van den Broek, M., Kuijpers, N. G. A., Pronk, J. T., Boles, E., Daran, J.-M., et al. (2015). The genome sequence of the popular hexose-transport-deficient *Saccharomyces cerevisiae* strain EBY.VW4000 reveals LoxP/Cre-induced translocations and gene loss. *FEMS Yeast Res* 15, 1–12. doi: 10.1093/femsyr/fou004
- Souza, C. M., Schwabe, T. M. E., Pichler, H., Ploier, B., Leitner, E., Guan, X. L., et al. (2011). A stable yeast strain efficiently producing cholesterol instead of ergosterol is functional for tryptophan uptake, but not weak organic acid resistance. *Metab Eng* 13, 555–569. doi: 10.1016/j.ymben.2011.06.006
- Speizer, L., Haugland, R., and Kutchai, H. (1985). Asymmetric transport of a fluorescent glucose analogue by human erythrocytes. *Biochim Biophys Acta* 815, 75–84. doi: 10.1016/0005-2736(85)90476-6

- Sun, L., Zeng, X., Yan, C., Sun, X., Gong, X., Rao, Y., et al. (2012). Crystal structure of a bacterial homologue of glucose transporters GLUT1-4. *Nature* 490, 361–366. doi: 10.1038/nature11524
- Szablewski, L. (2013). Expression of glucose transporters in cancers. *Biochim Biophys Acta* 1835, 164–169. doi: 10.1016/j.bbcan.2012.12.004
- Tang, M., Gao, G., Rueda, C. B., Yu, H., Thibodeaux, D. N., Awano, T., et al. (2017). Brain microvasculature defects and GLUT1 deficiency syndrome averted by early repletion of the glucose transporter-1 protein. *Nat Commun* 8, 14152. doi: 10.1038/ncomms14152
- Thorens, B. (2001). GLUT2 in pancreatic and extra-pancreatic gluco-detection (review). *Mol Membr Biol* 18, 265–273. doi: 10.1080/09687680110100995
- Thorens, B. (2015). GLUT2, glucose sensing and glucose homeostasis. *Diabetologia* 58, 221–232. doi: 10.1007/s00125-014-3451-1
- Thorens, B., and Mueckler, M. (2010). Glucose transporters in the 21st Century. *Am J Physiol Endocrinol Metab* 298, E141-E145. doi: 10.1152/ajpendo.00712.2009
- Toyoda, Y., Takada, T., Miyata, H., Matsuo, H., Kassai, H., Nakao, K., et al. (2020). Identification of GLUT12/SLC2A12 as a urate transporter that regulates the blood urate level in hyperuricemia model mice. *P Natl Acad Sci USA* 117, 18175–18177. doi: 10.1073/pnas.2006958117
- Tripp, J., Essl, C., Iancu, C. V., Boles, E., Choe, J., and Oreb, M. (2017). Establishing a yeast-based screening system for discovery of human GLUT5 inhibitors and activators. *Sci Rep* 7, 6197. doi: 10.1038/s41598-017-06262-4
- Uldry, M., Ibberson, M., Hosokawa, M., and Thorens, B. (2002). GLUT2 is a high affinity glucosamine transporter. *FEBS Lett* 524, 199–203. doi: 10.1016/s0014-5793(02)03058-2
- Ung, P. M.-U., Song, W., Cheng, L., Zhao, X., Hu, H., Chen, L., et al. (2016). Inhibitor discovery for the human GLUT1 from homology modeling and virtual screening. *ACS Chem Biol* 11, 1908–1916. doi: 10.1021/acscchembio.6b00304
- Valley, M. P., Karassina, N., Aoyama, N., Carlson, C., Cali, J. J., and Vidugiriene, J. (2016). A bioluminescent assay for measuring glucose uptake. *Anal Biochem* 505, 43–50. doi: 10.1016/j.ab.2016.04.010
- van 't Klooster, J. S., Cheng, T.-Y., Sikkema, H. R., Jeucken, A., Moody, B., and Poolman, B. (2020a). Periprotein lipidomes of *Saccharomyces cerevisiae* provide a flexible environment for conformational changes of membrane proteins. *Elife* 9, e57003. doi: 10.7554/eLife.57003
- van 't Klooster, J. S., Cheng, T.-Y., Sikkema, H. R., Jeucken, A., Moody, D. B., and Poolman, B. (2020b). Membrane lipid requirements of the lysine transporter Lyp1 from *Saccharomyces cerevisiae*. *J Mol Biol* 432, 4023–4031. doi: 10.1016/j.jmb.2020.04.029
- van't Klooster, J. S., Bianchi, F., Doorn, R. B., Lorenzon, M., Lusseveld, J. H., Punter, C. M., et al. (2020c). Extracellular loops matter - subcellular location and function of the

References

- lysine transporter Lyp1 from *Saccharomyces cerevisiae*. *FEBS J* 287, 4401–4414. doi: 10.1111/febs.15262
- Verbandt, S., Cammue, B. P. A., and Thevissen, K. (2017). Yeast as a model for the identification of novel survival-promoting compounds applicable to treat degenerative diseases. *Mech Ageing Dev* 161, 306–316. doi: 10.1016/j.mad.2016.06.003
- Vignault, C., Vachaud, M., Cakir, B., Glissant, D., Dédaldéchamp, F., Büttner, M., et al. (2005). VvHT1 encodes a monosaccharide transporter expressed in the conducting complex of the grape berry phloem. *J Exp Bot* 56, 1409–1418. doi: 10.1093/jxb/eri142
- Walsh, M. C., Smits, H. P., Scholte, M., Smits, G., and van Dam, K. (1994a). Rapid kinetics of glucose uptake in *Saccharomyces cerevisiae*. *Folia Microbiol* 39, 557–559. doi: 10.1007/BF02814107
- Walsh, M. C., Smits, H. P., Scholte, M., and van Dam, K. (1994b). Affinity of glucose transport in *Saccharomyces cerevisiae* is modulated during growth on glucose. *J Bacteriol* 176, 953–958. doi: 10.1128/jb.176.4.953-958.1994
- Walsh, M. C., Smits, H. P., and van Dam, K. (1994c). Respiratory inhibitors affect incorporation of glucose into *Saccharomyces cerevisiae* cells, but not the activity of glucose transport. *Yeast* 10, 1553–1558. doi: 10.1002/yea.320101204
- Wieczorke, R. (2001). Molekulargenetische und physiologische Untersuchungen zur Funktion von FGY1 bei der heterologen Expression von Glukosetransportern in der Hefe *Saccharomyces cerevisiae*. Dissertation, Heinrich-Heine-Universität Düsseldorf.
- Wieczorke, R., Dlugai, S., Krampe, S., and Boles, E. (2002). Characterisation of mammalian GLUT glucose transporters in a heterologous yeast expression system. *Cell Physiol Biochem* 13, 123–134. doi: 10.1159/000071863
- Wieczorke, R., Krampe, S., Weierstall, T., Freidel, K., Hollenberg, C. P., and Boles, E. (1999). Concurrent knock-out of at least 20 transporter genes is required to block uptake of hexoses in *Saccharomyces cerevisiae*. *FEBS Lett* 464, 123–128. doi: 10.1016/S0014-5793(99)01698-1
- Wiersma, S. J., Mooiman, C., Giera, M., and Pronk, J. T. (2020). Squalene-tetrahymanol cyclase expression enables sterol-independent growth of *Saccharomyces cerevisiae*. *Appl Environ Microbiol* 86, e00672-20. doi: 10.1128/AEM.00672-20
- Winderickx, J., Delay, C., Vos, A. de, Klinger, H., Pellens, K., Vanhelmont, T., et al. (2008). Protein folding diseases and neurodegeneration: lessons learned from yeast. *Biochim Biophys Acta* 1783, 1381–1395. doi: 10.1016/j.bbamcr.2008.01.020
- Wong, C. H., Siah, K. W., and Lo, A. W. (2019). Estimation of clinical trial success rates and related parameters. *Biostatistics* 20, 273–286. doi: 10.1093/biostatistics/kxx069
- Woodman, B. S., Trousdale, C., Conover, J., and Kim, K. (2018). Yeast membrane lipid imbalance leads to trafficking defects toward the Golgi. *Cell Biol Int* 42, 890–902. doi: 10.1002/cbin.10956

- Wright, E. M. (2013). Glucose transport families SLC5 and SLC50. *Mol Aspects Med* 34, 183–196. doi: 10.1016/j.mam.2012.11.002
- Wright, E. M., Loo, D. D. F., and Hirayama, B. A. (2011). Biology of human sodium glucose transporters. *Physiol Rev* 91, 733–794. doi: 10.1152/physrev.00055.2009
- Wu, C.-H., Ho, Y.-S., Tsai, C.-Y., Wang, Y.-J., Tseng, H., Wei, P.-L., et al. (2009). *In vitro* and *in vivo* study of phloretin-induced apoptosis in human liver cancer cells involving inhibition of type II glucose transporter. *Int J Cancer* 124, 2210–2219. doi: 10.1002/ijc.24189
- Wu, X., Chi, R. J., Baskin, J. M., Lucast, L., Burd, C. G., De Camilli, P., et al. (2014). Structural insights into assembly and regulation of the plasma membrane phosphatidylinositol 4-kinase complex. *Dev Cell* 28, 19–29. doi: 10.1016/j.devcel.2013.11.012
- Wu, X., and Freeze, H. H. (2002). GLUT14, a duplicon of GLUT3, is specifically expressed in testis as alternative splice forms. *Genomics* 80, 553–557. doi: 10.1006/geno.2002.7010
- Xu, X., Bittman, R., Duportail, G., Heissler, D., Vilcheze, C., and London, E. (2001). Effect of the structure of natural sterols and sphingolipids on the formation of ordered sphingolipid/sterol domains (rafts). Comparison of cholesterol to plant, fungal, and disease-associated sterols and comparison of sphingomyelin, cerebroside, and ceramide. *J Biol Chem* 276, 33540–33546. doi: 10.1074/jbc.M104776200
- Xuan, Y. H., Hu, Y. B., Chen, L.-Q., Sosso, D., Ducat, D. C., Hou, B.-H., et al. (2013). Functional role of oligomerization for bacterial and plant SWEET sugar transporter family. *P Natl Acad Sci USA* 110, E3685–E3694. doi: 10.1073/pnas.1311244110
- Yamamoto, N., and Ashida, H. (2012). Evaluation methods for facilitative glucose transport in cells and their applications. *Food Sci Technol Res* 18, 493–503. doi: 10.3136/fstr.18.493
- Yamamoto, N., Sato, T., Kawasaki, K., Murosaki, S., and Yamamoto, Y. (2006). A nonradioisotope, enzymatic assay for 2-deoxyglucose uptake in L6 skeletal muscle cells cultured in a 96-well microplate. *Anal Biochem* 351, 139–145. doi: 10.1016/j.ab.2005.12.011
- Yamamoto, N., Ueda-Wakagi, M., Sato, T., Kawasaki, K., Sawada, K., Kawabata, K., et al. (2015). Measurement of glucose uptake in cultured cells. *Curr Protoc Pharmacol* 71, 12.14.1–12.14.26. doi: 10.1002/0471141755.ph1214s71
- Yoshioka, K., Takahashi, H., Homma, T., Saito, M., Oh, K.-B., Nemoto, Y., et al. (1996). A novel fluorescent derivative of glucose applicable to the assessment of glucose uptake activity of *Escherichia coli*. *BBA Gen Subjects* 1289, 5–9. doi: 10.1016/0304-4165(95)00153-0
- Young, E., Poucher, A., Comer, A., Bailey, A., and Alper, H. (2011). Functional survey for heterologous sugar transport proteins, using *Saccharomyces cerevisiae* as a host. *Appl Environ Microbiol* 77, 3311–3319. doi: 10.1128/AEM.02651-10

References

- Zamora-Leon, S. P., Golde, D. W., Concha, I. I., Rivas, C. I., Delgado-Lopez, F., Baselga, J., et al. (1996). Expression of the fructose transporter GLUT5 in human breast cancer. *P Natl Acad Sci USA* 93, 1847–1852. doi: 10.1073/pnas.93.5.1847
- Zewe, J., Wills, R. C., Sangappa, S., Goulden, B. D., and Hammond, G. R. V. (2018). SAC1 degrades its lipid substrate PtdIns4P in the endoplasmatic reticulum to maintain a steep chemical gradient with donor membranes. *Elife* 7, e35588. doi: 10.7554/eLife.35588.001
- Zhang, Q., Hua, X., Liu, H., and Shi, Y. (2020). Evolutionary expansion and functional divergence of sugar transporters in *Saccharum* (*S. spontaneum* and *S. officinarum*). *Plant J* 105, 884–906. doi: 10.1111/tpj.15076
- Ziesman (2000). Targeted disruption of the glucose transporter 4 selectively in muscle causes insulin resistance and glucose intolerance. *Nat Med* 6, 924–928. doi: 10.1038/78693
- Zutter, J. K. de, Levine, K. B., Di Deng, and Carruthers, A. (2013). Sequence determinants of GLUT1 oligomerization: Analysis by homology-scanning mutagenesis. *J Biol Chem* 288, 20734–20744. doi: 10.1074/jbc.M113.469023
- Zweytick, D., Hrastnik, C., Kohlwein, Sepp, D., and Daum, G. (2000). Biochemical characterization and subcellular localization of the sterol C-24(28) reductase, Erg4p, from the yeast *Saccharomyces cerevisiae*. *FEBS Lett* 470, 83–87. doi: 10.1016/s0014-5793(00)01290-4

5 Additional results

5.1 Additional results and discussion – Impact of yeast PM modifications on the heterologous expression of human GLUTs

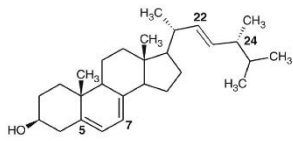
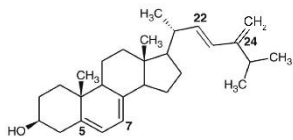
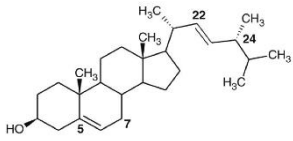
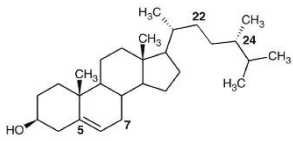
The active expression of GLUT1 and GLUT3 in the *fgy1 hxt⁰* yeast strain EBY.S7 and of GLUT4 in the *fgy1/Δerg4 hxt⁰* yeast strain SDY.022 (Wieczorke et al., 2002; Boles et al., 2004; Schmidl et al., 2021b) indicates that an altered phospholipid and/or sterol composition in the PM of yeast cells might benefit the functional expression of GLUTs in such a strain. Since a counterflow transport of PI4P and sterols occurs in yeast (Mesmin and Antonny, 2016) intended modifications of one aspect (e.g., the PI4P content in the PM) might also affect the other one (e.g., the ergosterol composition in the PM) so that it is difficult to define the exact molecular basis for the observed effects of e.g., Δerg mutants. In general, several studies show that many membrane proteins are susceptible to changes in their lipid environment (Souza et al., 2011; van 't Klooster et al., 2020a; van 't Klooster et al., 2020b). Thus, it is conceivable that GLUTs require a certain lipid environment for their normal function, too.

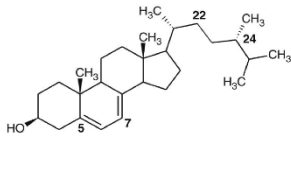
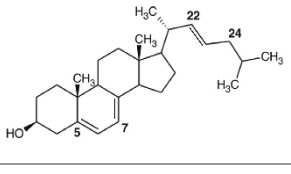
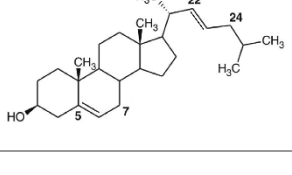
5.1.1 Construction of *hxt⁰* strains producing various sterols and evaluation of their ability to express native human GLUTs

In this thesis, it was intended to generate a cholesterol-producing *hxt⁰* yeast strain to create a more “human-like” PM. For this, it was attempted to delete the two late ergosterol biosynthesis genes *ERG5* and *ERG6* and concomitantly integrate *DHCR7* and *DHCR24* (whose gene products reduce double bonds to generate cholesterol) in the strain background EBY.VW4000 by following the example of Souza et al. (2011), who have conducted this in *S. cerevisiae*, before. In this process, several intermediate strains were generated that putatively exhibit a range of sterol compositions in their membranes, including cholesterol-like sterols (see Table 2). Unfortunately, the simultaneous deletion of *ERG5* and *ERG6* in the same strain was not successful and therefore a stably producing cholesterol strain was not obtained. However, it was reported before that Erg5 is much less active in an $\Delta erg6$ strain (Souza et al., 2011) which allows the presumption that a $\Delta erg6$ strain

expressing both, DHCR7 and DHCR24, (SSY63) produces cholesterol to some extent. Furthermore, *ERG6* deletion was only achieved for strains already containing *DHCR24*. Thus, a double bond at the C24 (25) position (when not reduced by DHCR24) seems to be unfavorable for cell viability. It should be noted that ergosterol was supplied in the medium on which transformants were plated and in case of an efficient uptake and successful integration into the PM, this should have allowed cell growth of strains with the inability to produce ergosterol themselves, as well. The absence of colonies for some sterol mutants suggests that an efficient uptake did not take place.

Table 2. Strains used (EBY.VW4000, EBY.S7, SDY.022) or constructed and used (SSY53 – SSY58, SSY61, SSY63) in the additional results. Strain names, genotypes and the names and structures of the varying putative main sterols in their membranes are listed.

Strain name	Genotype	Reference	Putative main sterol	Sterol structure
EBY.VW4000	<i>MATa leu2-3,112 ura3-52 trp1-289 his3-1 MAL2-8c SUC2 Δhxt1-17 Δgal2 Δstl1 Δagt1 Δmph2 Δmph3</i>	(Wieczorke et al., 1999)	Ergosterol	
EBY.S7	<i>MATa leu2-3,112 ura3-52 trp1-289 his3-1 MAL2-8c SUC2 Δhxt1-17 Δgal2 Δstl1 Δagt1 fgy1-1</i>	(Wieczorke et al., 2002)		
SDY.022	<i>MATa leu2-3,112 ura3-52 trp1-289 his3-1 MAL2-8c SUC2 Δhxt1-17 Δgal2 Δstl1 Δagt1 fgy1-1 erg4::KanMX</i>	(Boles et al., 2004)	Ergosta-5,7,22,24(28)-tetraenol	
SSY53	EBY.VW4000 <i>ΔURA3::TDH3-DHCR7</i>	This thesis	Brassicasterol	
SSY54	EBY.VW4000 <i>ΔHO::TDH3-DHCR24 ΔURA3::TDH3-DHCR7</i>		(Ergosta-5,22-dienol)	
SSY55	EBY.VW4000 <i>ΔHO::TDH3-DHCR24</i>		Ergosterol	See first structure
SSY56	EBY.VW4000 <i>ΔURA3::TDH3-DHCR7 Δerg5</i>		Campesterol	(Ergosta-5-enol)
SSY57	EBY.VW4000 <i>ΔHO::TDH3-DHCR24 ΔURA3::TDH3-DHCR7 Δerg5</i>			

SSY58	EBY.VW4000 $\Delta HO::TDH3-DHCR24$ $\Delta erg5$	This thesis	Ergosta-5,7-dienol	
SSY61	EBY.VW4000 $\Delta HO::TDH3-DHCR24$ $\Delta erg6$		Cholest-5,7,22-trienol	
SSY63	EBY.VW4000 $\Delta HO::TDH3-DHCR24$ $\Delta URA3::TDH3-DHCR7$ $\Delta erg6$		Cholest-5,22-dienol	

The efforts to create strains with differing sterol compositions yielded the strains SSY53 – SSY58, SSY61 and SSY63 (Table 2) and their ability to functionally express the native, human GLUT1 and GLUT4 was tested via drop tests. For this, all strains were transformed with one plasmid, expressing either GLUT1 or GLUT4 or, as a positive control, the endogenous transporter Hxt1. An empty plasmid was also included as a negative control. In a first test, all here-generated strains were compared with EBY.VW4000, the *hxt*⁰ strain with no further membrane modifications. Pre-cultures were harvested, washed twice with ddH₂O, and dissolved in ddH₂O to an OD_{600nm} of 1. Serial dilutions (10⁰, 10⁻¹, 10⁻², 10⁻³) were prepared and 4 μ l of each dilution was applied onto the solid media. All cells showed normal growth on maltose medium (data not shown), excluding general limitations on cell viability. The strains SSY53 – SSY58 only grew on glucose plates (2% (w/v) or 0.2% (w/v)) when expressing the endogenous transporter Hxt1, whereas no growth was detected for GLUT1 or GLUT4-expressing cells (data not shown), demonstrating that the putative sterol alterations in SSY53 – SSY58 do not contribute to a functional expression of these GLUTs. For SSY61 and SSY63 cells that expressed GLUT1 from a plasmid, clear growth was visible even in spots of higher dilutions, on 0.2% (w/v) glucose containing medium (Figure 3). Growth of the same cells on 2% (w/v) glucose was less pronounced (data not shown).

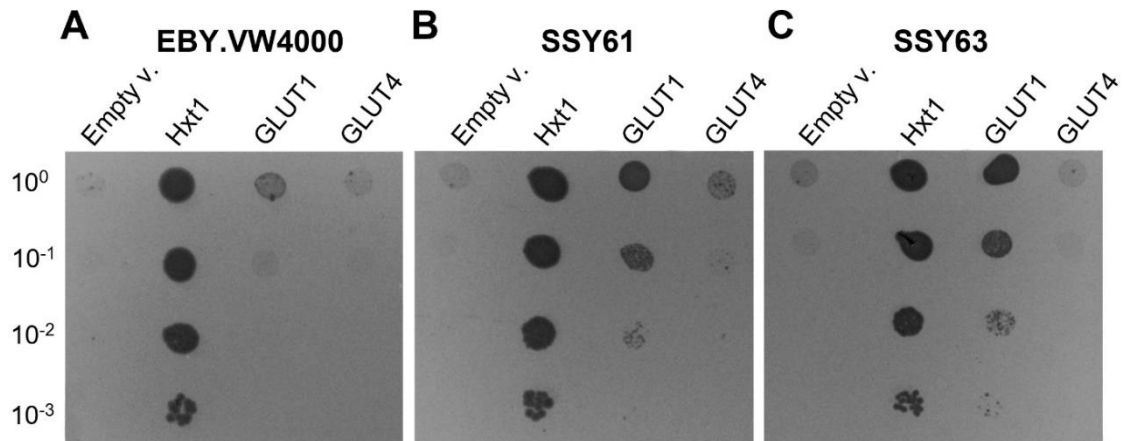


Figure 3. Growth test of *hxt*⁰ yeast strains producing different sterols.

Growth of EBY.VW4000 (A), SSY61 (B) and SSY63 (C) cells expressing the empty vector p426H7, the endogenous transporter *Hxt1*, or the two human GLUTs; GLUT1 and GLUT4, respectively, was assessed on SC -URA medium containing 0.2% (w/v) glucose. Pre-cultures were grown over night in SC -URA medium with 1% (w/v) maltose, washed and adjusted to an OD_{600nm} of 1 in ddH₂O. Dilutions (10⁻¹, 10⁻², 10⁻³) were prepared and 4 μl of each were dropped onto the solid medium. The plates were incubated at 30°C for six days.

Since GLUT1-expressing EBY.VW4000 cells grew much worse on 0.2% (w/v) glucose medium compared to GLUT1-expressing SSY61 or SSY63 cells, these results indicate that the alterations in the sterol biosynthesis in these two strains positively affect the functional expression of GLUT1. In both strains *ERG6* was successfully deleted, resulting in the absence of the methyl group at C24 (Table 2). Thus, these results suggest that the absence of the methyl group and therefore a more cholesterol-like sterol is beneficial for GLUT expression. However, when compared to EBY.S7 and SDY.022 (the two *hxt*⁰ strains with additional mutations affecting the PM lipid composition, see Table 2), GLUT1-expressing SSY63 cells showed inferior growth (Figure 4). The putatively reduced PI4P content in EBY.S7 and SDY.022 PMs therefore seems to have a stronger impact on functional GLUT expression. Future efforts to create *hxt*⁰ strains with modifications that benefit the functional expression of native human GLUTs should therefore rather focus on the phospholipid biosynthesis.

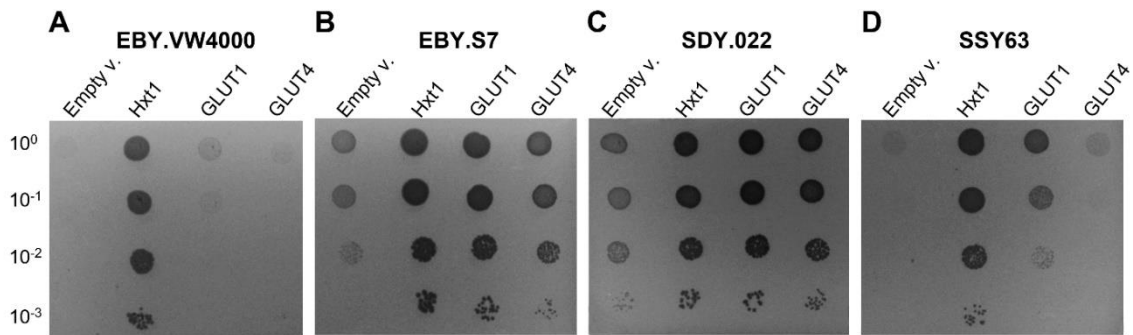


Figure 4. Growth test of *hxt*⁰ yeast strains with different membrane lipid modifications. Growth of EBY.VW4000 (A), EBY.S7 (B), SDY.022 (C) and SSY63 (D) cells expressing the empty vector p426H7, the endogenous transporter Hxt1, or the two human GLUTs; GLUT1 and GLUT4, respectively, was assessed on SC -URA medium containing 0.2% (w/v) glucose. Pre-cultures were grown over night in SC -URA medium with 1% (w/v) maltose, washed and adjusted to an OD_{600nm} of 1 in ddH₂O. Dilutions (10⁻¹, 10⁻², 10⁻³) were prepared and 4 μ l of each were dropped onto the solid medium. The plates were incubated at 30°C for six days.

5.1.2 Alterations of the PI production at the yeast PM and assessing the effects on functional expression of native human GLUTs

The C-terminal truncation of Efr3 in the strain EBY.S7 has been proven to be beneficial for heterologous GLUT expressions in this strain (Wieczorke, 2001). Presumably, this truncation impedes the normal localization of the PI4P kinase Stt4 to the PM which would result in lower levels of PI4P at the membrane (Baird et al., 2008). Therefore, it was intended in this thesis to manipulate PI levels at the PM of a *hxt*⁰ yeast strain in different ways with the aim to further elucidate the linkage between PI(4P) content and functional GLUT expression. Several enzymes exist that are involved in the generation or degradation of PI4P (see chapter 2.2.3.4, Figure 1). In this thesis, Stt4, Lsb6, Sac1, Sfk1, Ict1 and Mss4 were overexpressed on a plasmid in EBY.VW4000 and EBY.S7 cells. Additionally, these cells were transformed with either an empty plasmid (negative control), the endogenous transporter Hxt1 (positive control) or GLUT1, to test their effect of functionally expressing this transporter. As an altered functional expression would result in improved or worse growth on the substrates used by the transporter, the effects were tested via drop tests on 0.2% (w/v) glucose and 0.2% (w/v) mannose, respectively. Maltose medium (1% (w/v)) was included as well, on which all cells grew normally (data not shown), which excludes effects on overall cell viability. Cell growth on glucose or mannose medium was highly similar and Table 3 illustrates the observed cell growth on these two sugars.

Table 3. Effect of the overexpression of PI processing enzymes on functional GLUT1 expression. EBY.VW4000 and EBY.S7 cells were transformed with two plasmids, containing the gene for an enzyme that affects the content of PI(4P) in the PM (plasmid 1) and the native human GLUT1 (plasmid 2). Pre-cultures were grown over night in SC -URA -HIS -MET medium with 1% (w/v) maltose, washed and adjusted to an OD_{600nm} of 1 in ddH₂O. Dilutions (10⁻¹, 10⁻², 10⁻³) were prepared and 4 µl of each were dropped onto the solid SC -URA -HIS -MET medium with 0.2% (w/v) glucose or 0.2% (w/v) mannose, respectively. Plates were incubated at 30°C for five days. Either no/very weak growth (-) or good growth (+) was observed for the different cells, and these observations were consistent on both media (glucose and mannose). These results were obtained by Julia Heine (Master student) under supervision of the author.

Strain	Plasmid 1: p423MET25_	Plasmid 2: p426H7_	Growth on 0.2 % (w/v) glucose and mannose
EBY.VW4000	Empty plasmid	GLUT1	-
	Stt4		-
	Lsb6		-
	Sac1		-
	Sfk1		-
	Ict1		-
	Mss4		-
EBY.S7	Empty plasmid	GLUT1	+
	Stt4		+
	Lsb6		+
	Sac1		+
	Sfk1		-
	Ict1		+
	Mss4		+

Most of the overexpressed enzymes had no or little effect on the growth of GLUT1-expressing hxt⁰ strains on glucose or mannose (Table 3). However, when Sfk1 was overexpressed in EBY.S7, GLUT1-expressing cells showed significantly reduced growth on glucose or mannose medium, compared to GLUT1-expressing cells harboring an empty vector as the first plasmid (Table 3 and Figure 5 A).

In yeast, Sfk1 acts as an additional regulator of the PI4P kinase Stt4 and is, like Efr3, involved in its proper localization to the PM (Audhya and Emr, 2002). Physical interactions between Stt4 and Sfk1 have been detected in crosslinking experiments (Audhya and Emr, 2002) and it has been shown that these interactions were mediated by the C-terminus of Sfk1 (Mioka et al., 2018). Nevertheless, $\Delta sfk1$ cells are viable, unlike $\Delta stt4$ cells, suggesting that Sfk1 plays only a minor or auxiliary role in the recruitment of Stt4 to the PM. Thus, unlike Efr3 and Ypp1, Sfk1 is not

essential for the formation of a functional Stt4 complex (Audhya and Emr, 2002; Mioka et al., 2018).

The results obtained in this thesis, indicate that an overexpression of Sfk1 might compensate for the incapability of the truncated Efr3 to efficiently recruit Stt4 to the membrane. In other words, Sfk1 overexpression in EBY.S7 might improve the generation of PI4P at the PM, which in turn negatively influences the functional expression of GLUTs. As the C-terminus of Sfk1 was defined as the region for Stt4 interaction (Mioka et al., 2018), this region was truncated by 64 amino acids, yielding Sfk1 Δ C. To further investigate the hypothesis that an improved assembly of the Stt4 complex via Sfk1 interaction is the reason for the reduced growth of Sfk1- and GLUT1-coexpressing EBY.S7 cells on glucose, Sfk1 Δ C was overexpressed along with GLUT1 in this strain as well. Growth in liquid glucose (0.2 % (w/v)) medium, assessed with the Cell Growth Quantifier (Aquila Biolabs), confirmed that the overexpression of Sfk1 crucially reduces cell growth of GLUT1-expressing EBY.S7 cells (maximal growth rate 0.023 h⁻¹, compared to 0.042 h⁻¹ for cells expressing the empty vector instead of Sfk1), whereas overexpression of Sfk1 Δ C did not (maximal growth rate 0.040 h⁻¹) (Figure 5 B). Controls with cells expressing each plasmid (empty, Sfk1 or Sfk1 Δ C), respectively with an empty vector instead of GLUT1 were tested as well and did not show growth on glucose medium, confirming that cell growth on this medium was related to sugar uptake via GLUT1. On maltose medium, however, all cells grew equally good, independent from the plasmids they harbored (data not shown). These results indicate that the C-terminal interaction of Sfk1 with Stt4 in Sfk1-overexpressing cells, indeed complements the Efr3 defect in EBY.S7 and that the putatively resulting PI4P increase negatively influences functional GLUT1 expression.

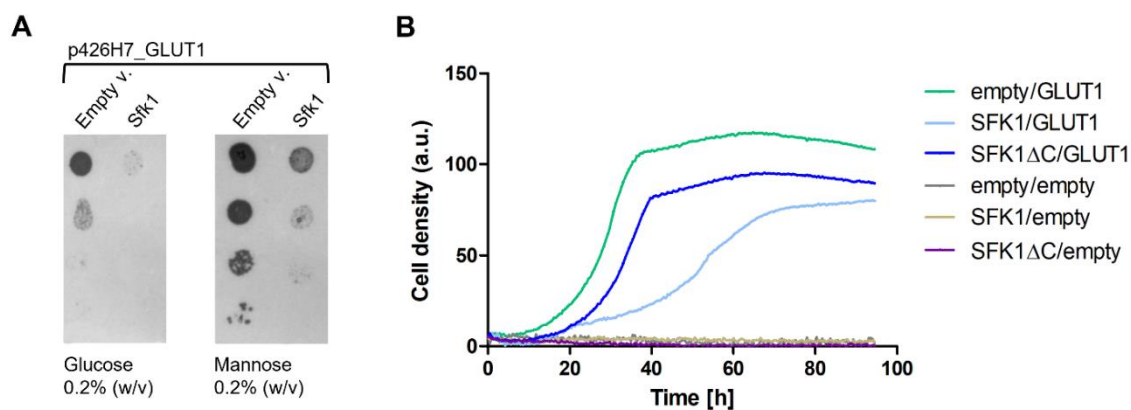


Figure 5. Overexpression of (full-length) Sfk1 reduces the functional expression of GLUT1 in EBY.S7. Growth of EBY.S7 cells expressing either the empty p423MET25 vector or p423MET25_Sfk1, respectively, along with GLUT1 from a second plasmid (p426H7) was assessed by a drop test on SC -URA -HIS -MET medium containing either 0.2% (w/v) glucose or 0.2% (w/v) mannose (A). The same cells, in addition to GLUT1-expressing EBY.S7 cells that co-express Sfk1 Δ C, in which 64 amino acids from the C-terminus were truncated, were grown in liquid SC -URA -HIS -MET medium with 0.2% (w/v) glucose (B). Empty vector controls (instead of GLUT1) were included. Cell growth was measured with the Cell Growth Quantifier (Aquila Biolabs). The results shown here were obtained by Julia Heine (Master student) (A) and Okbai Tesfamichael (practical course) (B) under supervision of the author.

5.2 Additional results and discussion – Application of the hxt⁰ yeast system as a screening platform for GLUT-specific inhibitors

Human GLUTs are the subject of intensive research because of their involvement in several metabolic diseases and the identification of GLUT-specific inhibitors is desirable not only for putative medical purposes but also as tools to further elucidate their specific role. Therefore, the available hxt⁰ yeast platforms were also applied in this thesis for different screening approaches, and it was intended to develop advanced methods that would facilitate the screening processes with the perspective to accelerate the discovery of GLUT-selective ligands.

5.2.1 Testing an HIV integrase inhibitor for inhibitory effects on GLUTs

In this thesis, the hypothesis was brought up that the human immunodeficiency virus (HIV) integrase inhibitor dolutegravir (DTG), a first-line treatment against HIV (Kouanfack et al., 2019), shows inhibitory effects on one or more GLUTs. During the DoIPHIN-2 study (Kintu et al., 2020), DTG was applied to women in their late pregnancies to avoid mother-to-child transmission of HIV and elevated blood

glucose levels in a small percentage of patients receiving DTG was observed (personal communication Prof. Saye Khoo). Therefore, DTG and, as controls, the two other HIV integrase inhibitors bictegravir and raltegravir were tested in this work for their effects on GLUT1, GLUT3 and GLUT4 in growth tests and with C¹⁴-glucose uptake assays (for details, see chapters 5.3.4 and 5.3.5). As the compounds were resolved in a dimethyl sulfoxide (DMSO)-based solvent, this chemical was applied to the negative control to rule out putative inhibitory effects of the solvent.

Only for GLUT4 (and not for GLUT1 nor GLUT3, data not shown), a minor inhibition of DTG (and bictegravir and raltegravir) on glucose uptake (measured by the C¹⁴-glucose uptake assay with 10 μ M of the applied compounds) was observed (Figure 6 A). However, the observed variance is statistically not significant (p -value=0.168, significance level: 0.05). Moreover, this effect was not visible in the growth test performed in glucose containing liquid medium (SC-URA D 0.2% (w/v)) when 10 μ M ($\sim \geq 4$ -fold of the daily dose applied to women during the DoIPHIN-2 study (Kintu et al., 2020)) of the HIV integrase inhibitors were applied (Figure 6 B). Cells that were exposed to bictegravir did not show any growth on glucose medium (Figure 6 B). But the same absence of growth was observed on ethanol medium (data not shown), which was tested as a control because ethanol is taken up by yeast cells independently from sugar transporters and is metabolized via different enzymatic reactions (Fraenkel, 2011). Thus, bictegravir seems to have a toxic effect on yeast cells which is not related to glucose uptake (or metabolism) and inhibits cell growth on various carbon sources, impeding a conclusion of its specific effect on GLUTs from simple growth tests. On the other hand, yeast cells that were grown in media containing either DTG or raltegravir did not exhibit any growth deficits (Figure 6 B). Still, a minor inhibitory effect of DTG on GLUT4 should not be completely excluded, by these experiments. If slight inhibition of GLUT4 is the underlying reason of the observed higher blood glucose levels of a small percentage of pregnant women who received DTG treatment should be further analyzed, for example in *in vivo* studies with mouse models. Conceivably, it is a contributing factor that might, together with e.g., genetic predispositions for insulin resistance or other physiological conditions, favor a lower GLUT4 activity and should be considered when prescribed. It has been found previously that indinavir

and other HIV protease inhibitors act as GLUT4 inhibitors (Hresko and Hruz, 2011) which favors the development of diabetes for patients following this antiretroviral therapy. The possibility that DTG has a (minor) inhibitory effect on GLUT4 as well might be a significant drawback for therapies against HIV.

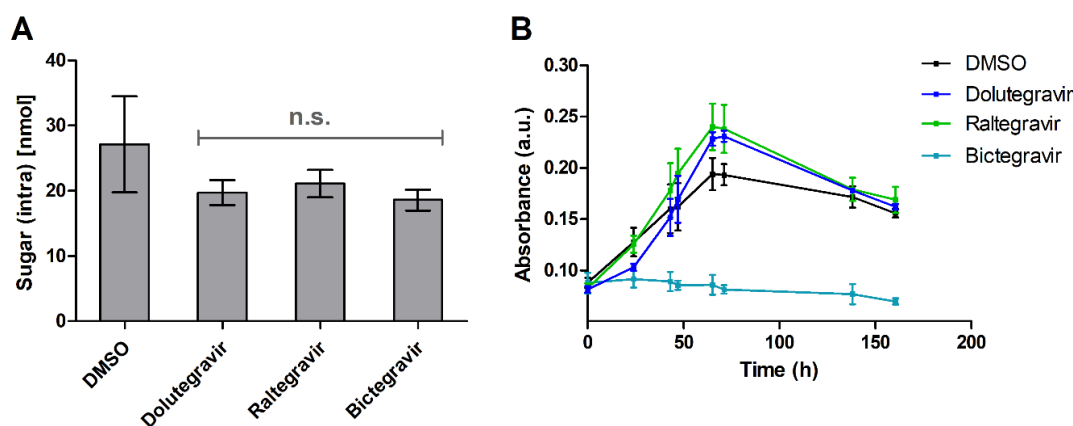


Figure 6. Effects of HIV integrase inhibitors dolutegravir, raltegravir, and bictegravir on GLUT4. Glucose uptake of SDY.022 cells expressing GLUT4 was tested via the C^{14} glucose uptake assay whereat cells were exposed to 10 μ M HIV integrase inhibitor (dolutegravir, raltegravir, or bictegravir, respectively), or DMSO as a control, 35 s prior to the addition of 50 μ M radiolabeled glucose (A). Mean values and standard deviations of three replicates are shown. n.s.= not significant. Growth test of SDY.022 cells expressing GLUT4 from a multicopy plasmid (p426H7) in SC -URA medium with glucose (0.2% (w/v)), containing either 10 μ M of each HIV integrase inhibitor, respectively, or the solvent DMSO as a control (B). Cells were cultured in a volume of 500 μ l in 24-well plates and growth was measured with the platereader (CLARIOstar®, BMG Labtech, Ortenberg, Germany). Mean values and standard deviations of two biological and two technical replicates (in total four replicates) are depicted.

5.2.2 Employing the pHluorin-based assay for inhibitor screenings

The here-established label-free, pHluorin-based method to measure glucose uptake is an attractive alternative to the conventional glucose uptake measurements for the determination of kinetic properties of transporters (Schmidl et al., 2021a). To calculate these precise parameters (e.g., K_M values), the slope of the initial acidification that occurs after the glucose pulse to glucose-starved cells must be carefully determined for which more time points are beneficial. Since the initial acidification is a rapid progress that happens within the first ten seconds after the sugar pulse, a very fast signal output and detection is required. Not all currently available fluorimeters and much less platereaders are capable of such a quick signal output, excluding these devices as operating resources for kinetic

characterizations via the pHluorin-based assay. Nevertheless, valuable information can be obtained also from the recovery phase to a neutral pH that follows the initial acidification after a glucose pulse. This reaction is visible still after several minutes, allowing measurements with platereaders or other, “slower” devices. Hypothetically, the pH_{cyt} of cells expressing a fully active transporter should recover to a near neutral pH_{cyt} several minutes after the reintroduction of sugar (Orij et al., 2009). Therefore, the recovery phase should allow qualitative conclusions about the activity of the transporter (e.g., if a heterologous expressed human GLUT is functional in the chosen yeast strain). Likewise, a restricted activity should be visible by a reduced recovery, a fact that could be exploited for the screening of inhibitors. To test this hypothesis, GLUT1_{V69M} and pHluorin were expressed in EB.Y.VW4000 cells from separate plasmids. As controls the empty vector p426H7 and the endogenous yeast transporter Hxt1 were expressed in EB.Y.VW4000 cells, along with pHluorin, as well. Pre-cultures were harvested, starved (3-4 h) and adjusted to a cell density of $\text{OD}_{600\text{nm}}$ of 1. 180 μl of this cell suspension were then dispensed in the wells of a 96-well plate. Measuring the ratio of the emission intensities at the two different excitation wavelengths 390 nm and 470 nm ($R_{390/470}$) allowed the determination of the pH_{cyt} with the help of a previously generated calibration curve. Thus, the initial pH_{cyt} was determined (time point -5). Different concentrations (0 μM , 20 μM , 50 μM and 300 μM) of the known GLUT1-inhibitor phloretin (Tsujiyama et al., 1996) were subsequently applied simultaneously with 1% (w/v) glucose and the pH_{cyt} was determined again (time point 0). Over a time span of 17 min the pH_{cyt} was determined every ~ 5.7 min with the platereader (CLARIOstar®, BMG Labtech, Ortenberg, Germany) to track the pH_{cyt} recovery of the cells (Figure 7). As expected, the lack of an active transporter (empty vector control) precluded the pH_{cyt} recovery after the addition of glucose (Figure 7 A). On the other hand, cells expressing the endogenous Hxt1 transporter exhibited a continuous rise of the pH_{cyt} after the pulse, independently from the presence of phloretin (Figure 7 B). The pH_{cyt} of GLUT1_{V69M} expressing cells also recovered, but this process was significantly affected by the addition of phloretin in a concentration dependent manner (Figure 7 C). A high concentration of phloretin (300 μM) abolished the recovery completely, whereas lower concentrations (20 μM and 50 μM) reduced the rate of the pH_{cyt} rise (Figure 7 C). For the first time point (0) after the sugar pulse, the pH_{cyt} of Hxt1 expressing cells was apparently lower

than for all GLUT1_{V69M} expressing cells (Figure 7 B, C). This likely originates from the initial acidification which is supposedly stronger when Hxt1 is present in comparison to GLUT1_{V69M}, as the endogenous transporter exhibits a higher sugar uptake capacity (measured in this thesis, data not shown). Hence, the lower pH_{cyt} after the initial acidification (for Hxt1 expressing cells) would need more time to rise again resulting in a lower pH_{cyt} at the first time point which is already balanced out at the second time point (after approximately ten min after the pulse) (Figure 7).

In general, this experiment shows that it is possible to use the pHluorin-based assay to test for inhibitory effects of compounds on transporters expressed in a hxt⁰ yeast strain by tracking the pH_{cyt} recovery phase. For this, signal recording on a time frame of several minutes is sufficient, allowing the measurement with a multi-well plater reader. Thus, an important prerequisite for high-throughput screenings is fulfilled. In comparison to growth tests, results are also obtained much quicker (3-4 h starving plus ~30 min for the measurement = ~4.5 hours vs. ~3 days). Moreover, this method is not susceptible to suppressor mutations, as the growth-based screening might be. In conclusion, these results provide a proof of concept for using the pHluorin-based method in GLUT-ligand screenings, at least in a qualitative or semi-quantitative manner.

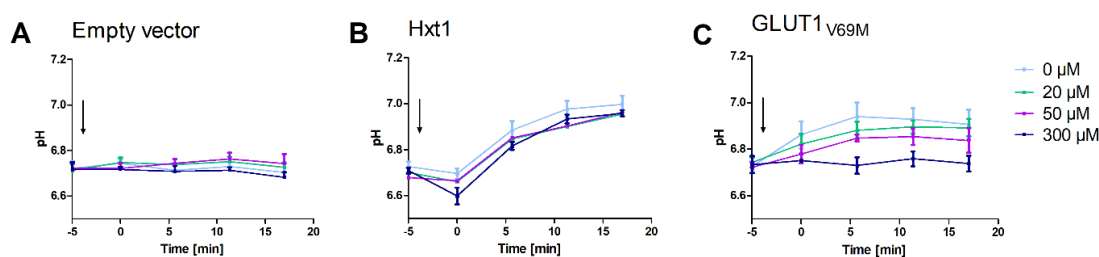


Figure 7. Transport inhibitor screening with the pHluorin-based assay.

EBY.VW4000 cells expressing the empty vector p426H7 (A), the endogenous transporter Hxt1 (B), or the human GLUT1_{V69M} (C) along with pHluorin, on a separate plasmid, were grown over night in If SC -URA -LEU M (1% (w/v)) medium, harvested, and starved for 3-4 hours in medium with no sugar. 180 μ l of cells ($OD_{600nm}=1$) were prepared in a 96-well plate. The pH_{cyt} of the cells was determined by measuring the ratio of the emission intensities (at 512 nm) at the two different excitation wavelengths 390 nm and 470 nm with the plater reader (CLARIOstar®, BMG Labtech) and with the help of a previously generated calibration curve. A mix (volume of 20 μ l) of 10% (w/v) glucose (final concentration 1% (w/v)) and different concentrations of the GLUT1 inhibitor phloretin (final concentrations: 0 μ M, 20 μ M, 50 μ M and 100 μ M) were then added simultaneously and the pH_{cyt} was determined every ~5.7 min for the next ~17 min. The time point of the glucose pulse is indicated by the arrow. Mean values and standard deviations of biological triplicates are shown.

5.3 Materials and Methods

5.3.1 Plasmid construction

All plasmids used in the additional results are listed in Table 4. The DNA sequences of *DHCR7* (GenBank NM201330) and *DHCR24* (GenBank BC086711) were codon-optimized for expression in yeast with the JCat tool (Grote et al., 2005). Overhangs for implementation in the Golden Gate system (Lee et al., 2015) were added and the BsmB1 cutting site within the open reading frame (ORF) of both genes was removed to avoid a cutting of the Golden Gate enzymes within the ORF. These oligonucleotides were then ordered from Twist Bioscience (San Francisco, CA, USA). Golden Gate entry plasmids and cassette plasmids were created as described before (Lee et al., 2015). CRISPR/Cas9 plasmids were amplified each in two PCR fragments, assembled *in vitro* in an isothermal reaction using T5 exonuclease, polymerase, and ligase (Gibson et al., 2010) and transformed into *E. coli* DH10 β . All other plasmids were assembled via homologous recombination according to Oldenburg et al. (1997). For this, PCR fragments with overhangs to promotor and terminator regions were generated and transformed together with the BamH1/EcoR1 linearized vector backbone into EBY.VW4000 cells. To delete 64 amino acids from the Sfk1 C-terminus, the second (reverse) primer was designed to bind in the terminator region but continued 192 bp upstream of the stop codon of Sfk1 and a new stop codon was inserted at the new sequence ending. The PCR derived from this and the regular forward primer (binding at the sequence start with an overhang to the promotor region) was transformed as well with the linearized p423MET25 plasmid into EBY.VW4000 cells to allow for homologous recombination. Verification was carried out via Sanger sequencing. PCRs were performed with Phusion polymerase (New England Biolabs GmbH), and primers listed in Table 5.

Table 4. Plasmids used in the additional results.

Plasmid name	Relevant properties	Reference
p425H7	2μ , <i>LEU2</i> , <i>Amp^R</i> , <i>HXT7p¹⁻³⁹²</i> , <i>CYC1t</i>	(Becker and Boles, 2003)
p426H7	2μ , <i>URA3</i> , <i>Amp^R</i> , <i>HXT7p¹⁻³⁹²</i> , <i>CYC1t</i>	(Becker and Boles, 2003)

Additional results

p423MET24	<i>2μ, HIS3, Amp^R, MET25p, CYC1t</i>	(Becker and Boles, 2003)
JHeV1	p423MET25_Stt4	This group
JHeV2	p423MET25_Sac1	This group
JHeV3	p423MET25_Sfk1	This group
JHeV4	p423MET25_Lsb6	This group
JHeV5	p423MET25_Mss4	This group
JHeV6	p423MET25_lct1	This group
SSV52	p423MET25_Sfk1ΔC	This thesis
SSV20	p426H7_Hxt1	This group
SSV16	p426H7_Glut1	This group
SSV66	p426H7_Glut1 _{V69M}	This group
SSV19	p426H7_optGlut3 _{S66Y}	This thesis
SSV14	p426H7_Glut4	This group
SSV61	p425H7_pHluorin	This thesis
pYTK001	Golden Gate entry vector, <i>Cam^R</i>	(Lee et al., 2015)
SSV78	pYTK001_DHCR7	This thesis
SSV79	pYTK001_DHCR24	This thesis
pYTK009	Golden Gate entry vector with <i>TDH3</i> promoter, <i>Cam^R</i>	(Lee et al., 2015)
pGG4.12	Golden Gate entry vector with <i>CYC1</i> terminator, <i>Cam^R</i>	This group
ALV001	Golden Gate plasmid for genomic integration into the <i>URA3</i> locus, <i>Kan^R</i>	Álvaro Furones Cuadrado, this group
SSV80	ALV1_TDH3p-DHCR7-CYC1t	This thesis
SiHV111	Golden Gate plasmid for genomic integration into the <i>HO</i> locus, <i>Kan^R</i>	Simon Harth, this group
SSV101	SiHV111_TDH3p-DHCR24-CYC1t	This thesis
pRCC-K	<i>2μ, kanMX, Amp^R, ROX3p-Cas9opt-CYC1t, SNR52p-gRNA</i>	(Generoso et al., 2016)
MRV02	pRCC-K with gRNA for <i>URA3</i> locus	Mara Reifenrath, this group
SSV100	pRCC-K with gRNA for <i>ERG5</i> locus	This thesis
SSV98	pRCC-K with gRNA for <i>ERG6</i> locus	This thesis

Table 5. Primers used in the additional results.

Primer name	Sequence 5'-3'	Application
MOP289	CAAGAACAACAAGCTCAAC	Sequencing primer forward, binds in <i>HXT7</i> promotor region
MOP290	ACCTAGACTTCAGGTTGTC	Sequencing primer reverse, binds in <i>CYC1</i> terminator region
MOP291	GCGTCTGTTAGAAAGGAAGTTTTTCC	Sequencing primer forward, binds in <i>MET25</i> promotor region
SSP107	TCGGTAAGTGGTTCGACTTC	Sequencing primer forward, binds in <i>DHCR7</i>
SSP108	GTTATGACTGACCACGCTGAAC	Sequencing primer forward, binds in <i>DHCR24</i>
SSP109	GTGGTCGTGACAGATGTCGATAG	Sequencing primer reverse, binds in <i>DHCR7</i>
SSP110	CCGAATGGGATGATGTCTTG	Sequencing primer reverse, binds in <i>DHCR24</i>
SSP111	ATTACCTTCGCCGCTTTGTTGTTTTAGAGCTAG AAATAGCAAGTTAAAATAAGG	Amplification of the CrispR pRCC plasmid and insertion of the target RNA for <i>ERG5</i> locus, forward
SSP112	CAACAAAGCGGCCGAAGGTAATGATCATTATCT TTCAGTGCAGGAG	Amplification of the CrispR pRCC plasmid and insertion of the target RNA for <i>ERG5</i> locus, reverse
SSP117	TTATTTCCGCGGCGCGGTTG	Primer binds upstream of <i>ERG5</i> , used to test if <i>ERG5</i> deletion was successful
SSP118	CTGGCAGGGTGAGTATTTG	Primer binds downstream of <i>ERG5</i> , used to test if <i>ERG5</i> deletion was successful
SSP128	CTCGCCATCACGTGTACCAG	Primer binds upstream of <i>ERG6</i> , used to test if <i>ERG6</i> deletion was successful
SSP129	CGTTAGCGGAATTTCTTTCCG	Primer binds downstream of <i>ERG6</i> , used to test if <i>ERG6</i> deletion was successful
MOP298	CCCATTATACCCATATAAATCAGC	Primer (reverse) binds in <i>KanMX</i> cassette, used to

Additional results

		verify successful integration of cassette
MOP300	GATAATCCTGATATGAATAAATTGC	Primer (forward) binds in <i>KanMX</i> cassette, used to verify successful integration of cassette
SSP86	ATTTTGCTATTCCAATAGACAATAAATACCTTTT AACAAATGGGGAAAAACAGAAGCTTTGTCCAGAC AATAAATCATATT	Donor DNA for integration into <i>ERG5</i> locus
SSP87	AATATGATTTATTGTCTGGACAAAGTTCTGTTTT TCCCCATTTGTTAAAAGGTATTTATTGTCTATTG GAATAGCAAAAT	Donor DNA for integration into <i>ERG5</i> locus
SSP57_SFK1d eltaCrev.	GAATGTAAGCGTGACATAACTAATTACATGATC ATCTTCCACCTAAATAAAAGTC	Truncation of 64 amino acids of the C-Terminus of Sfk1
SSP78	TGTTCCATGTGCGACGTGGCTGTTTTAGAGCTAG AAATAGCAAGTTAAAATAAGG	Amplification of the CrispR pRCC plasmid and insertion of the target RNA for <i>ERG6</i> locus, forward
SSP79	CAGCCACGTCGACATGGAACAGATCATTTATCT TTCAGTCCGGAG	Amplification of the CrispR pRCC plasmid and insertion of the target RNA for <i>ERG6</i> locus, reverse
WGP243	TCTTCTTGAAGTAGTCTTCC	Amplification of the CrispR pRCC plasmid, forward
WGP245	GGCTATTGTTGACTTGTTG	Amplification of the CrispR pRCC plasmid, reverse
JHeP5	TAGATACAATTCTATTACCCCCATCCATACATGA CAGGTCCAATA GTGTAC	Amplification of <i>SAC1</i> , overhang to <i>MET25</i> promotor, forward
JHeP6	GAATGTAAGCGTGACATAACTAATTACATGATTA ATCTCTTTTTAA AGGATCTGG	Amplification of <i>SAC1</i> , overhang to <i>CYC1</i> terminator, reverse
JHeP7	ATACAATTCTATTACCCCCATCCATACATGAGAT TTACCAGAGGA TTGAAAGCCTC	Amplification of <i>STT4</i> , overhang to <i>MET25</i> promotor, forward
JHeP8	GAATGTAAGCGTGACATAACTAATTACATGATC AGTACGGAATGC CATTG	Amplification of <i>STT4</i> , overhang to <i>CYC1</i> terminator, reverse
JHeP9	CATAGATACAATTCTATTACCCCCATCCATACAT GAGTAACGAAG CTTACCAGC	Amplification of <i>LSB6</i> , overhang to <i>MET25</i> promotor, forward

JHeP10	GAATGTAAGCGTGACATAACTAATTACATGATC AACACCAGGTGA ATACG	Amplification of <i>LSB6</i> , overhang to <i>CYC1</i> terminator, reverse
JHeP11	TAGATACAATTCTATTACCCCATCCATACATGA TTCAATTTAAAA GTCCAGG	Amplification of <i>SFK1</i> , overhang to <i>MET25</i> promotor, forward
JHeP12	GAATGTAAGCGTGACATAACTAATTACATGATC ATACGACTACTT GAATAGATTC	Amplification of <i>SFK1</i> , overhang to <i>CYC1</i> terminator, reverse
JHeP77	AGATACAATTCTATTACCCCATCCATACATGTC AGTCTTGCGAT CACAACCTCCTTCAG	Amplification of <i>MSS4</i> , overhang to <i>MET25</i> promotor, forward
JHeP78	AATGTAAGCGTGACATAACTAATTACATGATCA GTCTTTATAATTT TTCTGGTTAGGGTC	Amplification of <i>MSS4</i> , overhang to <i>CYC1</i> terminator, reverse
JHeP79	TAGATACAATTCTATTACCCCATCCATACATGT GGACAAACACT TTCAAATGGTGCAGC	Amplification of <i>ICT1</i> , overhang to <i>MET25</i> promotor, forward
JHeP80	GAATGTAAGCGTGACATAACTAATTACATGATTA CTTTGACAGGA ACGAGACTAAAGAAG	Amplification of <i>ICT1</i> , overhang to <i>CYC1</i> terminator, reverse
JHeP81	CTGCCCAATATTCCCTTTC	Sequencing primer forward, binds in <i>MSS4</i>

5.3.2 Strain construction

S. cerevisiae strains that were used in the additional results are listed in Table 2. For the integration of *DHCR7* or *DHCR24*, respectively, SSV80 or SSV101 were digested with Not1, by adding 1 µl of the restriction enzyme to the Cut Smart reaction (New England Biolabs GmbH) containing 1 µg of the plasmid (total volume of 12 µl) and incubating the mix at 37°C for at least two hours. The reaction was stopped by a 20 min incubation at 65°C. The respective strain was then transformed with the digested DNA (~1 µg). When the plasmid SSV80 was used (ALV1_TDH3p-DHCR7-CYC1t), 50 ng of the CRISPR/Cas9 plasmid SSV67 was applied as well, which cuts in the *URA3* locus. In this case, the transformants were regenerated for four hours at 30°C with shaking (180 rpm) in liquid YP medium with maltose (1% (w/v)) and plated on solid YP M (1% (w/v)) medium with 200 µg/ml G-418 to select for *KanMX*. For SSV101 (SiHV111_TDH3p-DHCR24-CYC1t), no additional CRISPR/Cas9 plasmid was added, and cells were plated directly

(without a regeneration phase) on SC-LEU M (1% (w/v)) medium. After 3-6 days, colonies appeared that were picked and cultured in liquid YP M (1% (w/v)) (SSV80) or SC-LEU M (1% (w/v)) (SSV101) medium. DNA was extracted and sequenced with appropriate primers (see Table 5), according to standard procedures, to check for the success of the integration. Deletions of *ERG5* and *ERG6* were performed utilizing the CRISPR/Cas9 system (Generoso et al., 2016) and pRCC-K plasmids SSV100 (for *ERG5*) or SSV98 (for *ERG6*). Oligonucleotides (80 bp) connecting the regions up- and downstream of *ERG5* were ordered (Microsynth AG, Balgach, Switzerland), annealed, and used as donor DNA for insertion in the *ERG5* locus. For *ERG6* deletion, the strain BY4741 with a *KanMX* cassette in its *ERG6* locus (Euroscarf strain Y00568) was ordered. The cassette and 500 bp up- and downstream of it was amplified from extracted gDNA and the PCR product was used as donor DNA. After a 4h regeneration phase (incubation at 30°C with shaking (180 rpm), in liquid YP M (1% (w/v)) medium with ergosterol (10 µg/ml)), transformants were plated on solid YP M (1% (w/v)) with G-418 (200 µg/ml) and ergosterol (10 µg/ml). After ~6-7 days, colonies appeared that were picked and cultured in liquid YP M (1% (w/v)) medium with ergosterol (10 µg/ml) but without any selection pressure to cure cells from plasmids. DNA was extracted and sequenced with appropriate primers (see Table 5), according to standard procedures, to check if the deletion was successful. The yeast transformations were performed according to Gietz and Schiestl (2007).

5.3.3 Media and growth conditions

For maintenance and preparation of competent cells, plasmid-free cells were grown in standard YP media (1% (w/v) yeast extract, 2% (w/v) peptone) supplemented with 1% (w/v) maltose (M). If pRCC-K plasmids were applied to modify the genome of the yeast, cells were streaked out on YP M (1% (w/v)) with 200 µl/ml G-418 for the selection pressure. For mutants that were expected to have a modified sterol composition (e.g., in $\Delta erg5$ or $\Delta erg6$ mutants), 10 µg/ml ergosterol was added to the plates (and liquid medium for regeneration). Transformants with one or more plasmids were plated on solid, selective synthetic complete (SC) medium with 1% (w/v) maltose (M) and amino acids as stated in Bruder et al. (2016) in which the respective amino acid(s) was or were omitted to maintain

selection pressure. For experiments with the biosensor pHluorin, cells were grown in filter-sterilized, low fluorescent, synthetic complete medium (lf-SC) containing 6.9 g/l YNB with ammonium sulfate, without amino acids, without folic acid and without riboflavin (MP Biomedicals), containing 1% (w/v) maltose and amino acids as stated in Bruder et al. (2016), in which uracil and leucine were omitted. For subcloning, electrocompetent *E. coli* DH10 β (Gibco BRL, Gaithersburg, MD) were used that were cultured in lysogeny broth (LB) medium with 100 μ g/mL carbenicillin (Sambrook et al., 1989).

5.3.4 Growth tests

For growth tests on solid medium, drop tests were performed on minimal SC medium with the respective sugar and amino acids as stated in Bruder et al. (2016) in which uracil was omitted (for cells containing the p426H7 plasmid with the respective transporter), or the three amino acids uracil, histidine, and methionine were omitted (for cells expressing two plasmids; p426H7 and p423MET25, methionine was omitted for a strong promoter activity). Pre-cultures were grown overnight in 10 ml SC M (1% (w/v)) -URA or SC M (1% (w/v)) -URA -HIS -MET medium at 30°C and 180 rpm, centrifuged (3,000 g, 3 min, 20°C) and washed twice in double-distilled, sterile water (ddH₂O). Cells were resuspended in ddH₂O and OD_{600nm} was adjusted to 1. Dilutions (10⁻¹, 10⁻², 10⁻³) were prepared and 4 μ l of each dilution was dropped onto the agar plate. Plates were incubated at 30°C for five or six days.

Cell growth in liquid SC -URA -HIS -MET medium (with the respective sugar) was measured with the Cell Growth Quantifier (Aquila Biolabs) (Bruder et al., 2016), for which pre-cultures were grown overnight in the same medium with 1 % (w/v) maltose, harvested and washed twice in ddH₂O. These cells were used to inoculate 30 ml medium to an OD_{600nm} of 0.2 in 300 ml Erlenmeyer flasks which were mounted onto the sensor plate. Quantification of cell growth and calculation of apparent maximal growth rates (h⁻¹) were performed with the CGQuant software (Aquila Biolabs) as previously described (Bruder et al., 2016).

To measure cell growth in the presence of HIV integrase inhibitors, 24 well-plates (clear, with flat bottom, Greiner Bio One) were utilized. Pre-cultures of SDY.022

cells expressing GLUT4 from the multicopy plasmid p426H7, were grown, in biological duplicates, in SC -URA M (1% (w/v)) medium, harvested (3000 g, 3 min, 20°C), washed twice in ddH₂O, and adjusted in SC -URA medium with the respective sugar to an OD_{600nm} of 0.4. 475 µl of the cell suspensions (duplicates) were distributed in each well of the 24-well plate, except for four wells, that contained cell-free medium as a blank. 25 µl of the 20x stock solution of integrase inhibitors (dolutegravir, bictegravir, or raltegravir, respectively; final concentration: 10 µM) or DMSO as a control were then added in a previously defined pattern to the cells leading to a randomized distribution in which each sample was represented four times (two biological replicates and two technical replicates) with varying location of each replicate (e.g., of each sample at least one replicate was located in the center, where liquid evaporation was assumed to be lower than at the border). Cells were fixated in a bigger plastic box and incubated at 30°C with shaking (180 rpm) for one week. The OD_{600nm} was measured at indicated time points with the platereader (CLARIOstar®, BMG Labtech, Ortenberg, Germany), for which the lid was removed. The blank value was subtracted from the final absorbance. Mean values and standard deviations of the four replicates were calculated with Microsoft Excel 2016.

5.3.5 C¹⁴ glucose uptake assay

To measure the uptake of radiolabeled C¹⁴ glucose in p426H7_Glut4 expressing SDY.022 cells, cultures were grown over night in SC -URA M (1% (w/v)) medium and harvested at an early exponential phase (OD_{600nm}=0.8). Pellets were washed twice in ice-cold 0.1 M potassium phosphate buffer (KH₂PO₄, pH 6.5, adjusted with KOH) and resuspended in the same buffer to a wet weight of 60 mg/ml. Aliquots of 110 µl were prepared and kept on ice. The integrase inhibitors (final concentration: 10 µM) or DMSO as a control were added, respectively, and incubated for 35 s, before 100 µl of these cells were mixed with 50 mM C¹⁴ labeled glucose. After 5 s, the reaction was terminated by quenching with ice-cold quenching buffer (500 mM glucose, 0.1 M K₂PO₄, pH 6.5, adjusted with KOH). The uptake assay was described in detail by Boles and Oreb (2018). Diagrams were prepared from technical triplicates and t-tests were conducted (p-value=0.168, significance level: 0.05) with GraphPad Prism 5.

5.3.6 Platerreader-assisted inhibitor screening with the pHluorin-based assay

To test if the pHluorin-based assay could be employed to assess inhibitory effects of compounds on GLUTs, EBY.VW4000 cells were transformed with pHluorin and the respective transporter (or empty vector, as a negative control) on separate plasmids. Cells were grown over night in low fluorescent SC -URA -LEU medium with maltose (1% (w/v)), harvested at an early exponential phase ($OD_{600nm}=0.5 - 1.5$), and starved for 3-4 hours in medium without sugar, while shaking (180 rpm) at 30°C. An OD_{600nm} of 1 was adjusted in the same medium (If SC -URA -LEU without sugar) and 180 μ l of the cell suspension (biological and technical triplicates) was aliquoted in a 96-well microtiter plate (black polystyrene, with flat micro-clear bottom, Greiner Bio One). The ratio of the emission intensities (at 512 nm) at the two different excitation wavelengths 390 nm and 470 nm ($R_{390/470}$) was measured after 30 s of double orbital shaking (700 rpm) with the platerreader (CLARIOstar®, BMG Labtech, Ortenberg, Germany) that was previously set to 30°C (time point=-5). A mix (volume of 20 μ l) of 10% (w/v) glucose (final concentration 1% (w/v)) and different concentrations of the GLUT1 inhibitor phloretin (final concentrations: 0 μ M, 20 μ M, 50 μ M and 100 μ M) were then added with a multichannel pipette (Kinesis, Wertheim, Germany), mixed by pipetting up and down, before the plate was quickly mounted again into the platerreader. $R_{390/470}$ was measured again (time point=0) and every ~5.7 min for the next ~17 min, with 30 s double orbital shaking (700 rpm) between the measurements. The raw data was analyzed with the MARS data analysis software (BMG Labtech) and Microsoft Excel 2016.

The pH_{cyt} was determined with the help of a calibration curve. For this, EBY.VW4000 cells expressing pHluorin and the empty p426H7 vector were grown over night in biological triplicates in If SC -URA -LEU M (1% (w/v)) medium to an $OD_{600nm}=0.5-1.5$ and harvested by centrifugation (3000 g, 5 min). Pellets were washed once in ddH₂O and resuspended in PBS buffer containing 100 μ g/ml digitonin. After 10 min of incubation at room temperature, cells were centrifuged, washed once with PBS buffer, adjusted to an OD_{600nm} of 10 in PBS buffer, and put on ice. 180 μ l of citric acid/ Na₂HPO₄ buffers with pH values ranging from 5.0 – 9.0 (in steps of 0.5) were prepared in the wells of a 96-well plate (black polystyrene, with flat micro-clear bottom, Greiner Bio One) and 20 μ l of the cell suspension was

added (final OD_{600nm}=1). After 30 s of double orbital shaking (700 rpm), R_{390/470} values were determined. The data was analyzed with the MARS data analysis software (BMG Labtech) and the calibration curve was generated by GraphPad Prism 5 with a sigmoidal dose response fit.

5.4 References for the additional results

- Audhya, A., and Emr, S. D. (2002). Stt4 PI 4-Kinase localizes to the plasma membrane and functions in the Pkc1-mediated MAP kinase cascade. *Dev Cell* 2, 593–605. doi: 10.1016/s1534-5807(02)00168-5
- Baird, D., Stefan, C., Audhya, A., Weys, S., and Emr, S. D. (2008). Assembly of the PtdIns 4-kinase Stt4 complex at the plasma membrane requires Ypp1 and Efr3. *J Cell Biol* 183, 1061–1074. doi: 10.1083/jcb.200804003
- Becker, J., and Boles, E. (2003). A modified *Saccharomyces cerevisiae* strain that consumes L-Arabinose and produces ethanol. *Appl Environ Microbiol* 69, 4144–4150. doi: 10.1128/AEM.69.7.4144-4150.2003
- Boles, E., Dlugai, S., Mueller, G., and Voss, D. (2004). Use of *Saccharomyces cerevisiae* *ERG4* mutants for the expression of glucose transporters from mammals. Geneva, Switzerland: World Intellectual Property Organisation. WO002004026907A3.
- Boles, E., Oreb, M. (2018). A growth-based screening system for hexose transporters in yeast. *Methods Mol Biol* 1713, 123-135. doi: 10.1007/978-1-4939-7507-5_10
- Bruder, S., Reifenrath, M., Thomik, T., Boles, E., and Herzog, K. (2016). Parallelised online biomass monitoring in shake flasks enables efficient strain and carbon source dependent growth characterisation of *Saccharomyces cerevisiae*. *Microb Cell Fact* 15, 127. doi: 10.1186/s12934-016-0526-3
- Fraenkel, D. G. (2011). Yeast Intermediary Metabolism. *Cold Spring Harb Lab Press. New York*.
- Generoso, W. C., Gottardi, M., Oreb, M., and Boles, E. (2016). Simplified CRISPR-Cas genome editing for *Saccharomyces cerevisiae*. *J Microbiol Methods* 127, 203–205. doi: 10.1016/j.mimet.2016.06.020
- Gibson, D. G., Glass, J. I., Lartigue, C., Noskov, V. N., Chuang, R.-Y., Algire, M. A., et al. (2010). Creation of a bacterial cell controlled by a chemically synthesized genome. *Science* 329, 52–56. doi: 10.1126/science.1190719
- Gietz, R. D., and Schiestl, R. H. (2007). Frozen competent yeast cells that can be transformed with high efficiency using the LiAc/SS carrier DNA/PEG method. *Nat Protoc* 2, 1–4. doi: 10.1038/nprot.2007.17

- Grote, A., Hiller, K., Scheer, M., Münch, R., Nörtemann, B., Hempel, D. C., et al. (2005). JCat: a novel tool to adapt codon usage of a target gene to its potential expression host. *Nucleic Acids Res* 33, W526-W531. doi: 10.1093/nar/gki376
- Hresko, R. C., and Hruz, P. W. (2011). HIV protease inhibitors act as competitive inhibitors of the cytoplasmic glucose binding site of GLUTs with differing affinities for GLUT1 and GLUT4. *PLoS ONE* 6, e25237. doi: 10.1371/journal.pone.0025237
- Kintu, K., Malaba, T. R., Nakibuka, J., Papamichael, C., Colbers, A., Byrne, K., et al. (2020). Dolutegravir versus efavirenz in women starting HIV therapy in late pregnancy (DoIPHIN-2): an open-label, randomised controlled trial. *Lancet HIV* 7, e332-e339. doi: 10.1016/S2352-3018(20)30050-3
- Kouanfack, C., Mpoudi-Etame, M., Omgba Bassega, P., Eymard-Duvernay, S., Leroy, S., Boyer, S., et al. (2019). Dolutegravir-based or low-dose efavirenz-based regimen for the treatment of HIV-1. *N Engl J Med* 381, 816–826. doi: 10.1056/NEJMoa1904340
- Lee, M. E., DeLoache, W. C., Cervantes, B., and Dueber, J. E. (2015). A highly characterized yeast toolkit for modular, multipart assembly. *ACS Synth Biol* 4, 975–986. doi: 10.1021/sb500366v
- Mesmin, B., and Antony, B. (2016). The counterflow transport of sterols and PI4P. *Biochim Biophys Acta* 1861, 940–951. doi: 10.1016/j.bbali.2016.02.024
- Mioka, T., Fujimura-Kamada, K., Mizugaki, N., Kishimoto, T., Sano, T., Nunome, H., et al. (2018). Phospholipid flippases and Sfk1p, a novel regulator of phospholipid asymmetry, contribute to low permeability of the plasma membrane. *Mol Biol Cell* 29, 1203–1218. doi: 10.1091/mbc.E17-04-0217
- Oldenburg, K., Vo, K. T., Michaelis, S., and Paddon, C. (1997). Recombination-mediated PCR-directed plasmid construction *in vivo* in yeast. *Nucleic Acids Res* 25, 451–452. doi: 10.1093/nar/25.2.451
- Orij, R., Postmus, J., Ter Beek, A., Brul, S., and Smits, G. J. (2009). *In vivo* measurement of cytosolic and mitochondrial pH using a pH-sensitive GFP derivative *in Saccharomyces cerevisiae* reveals a relation between intracellular pH and growth. *Microbiology* 155, 268–278. doi: 10.1099/mic.0.022038-0
- Sambrook, J., Fritsch, E. F., and Maniatis, T. (1989). Molecular cloning: A laboratory manual. Second edition. *Cold Spring Harb Lab Press. New York.*
- Schmidl, S., Iancu, C. V., Reifenrath, M., Choe, J., and Oreb, M. (2021a). A label-free real-time method for measuring glucose uptake kinetics in yeast. *FEMS Yeast Res* 21, foaa069. doi: 10.1093/femsyr/foaa069
- Schmidl, S., Tamayo Rojas, S. A., Iancu, C. V., Choe, J., and Oreb, M. (2021b). Functional expression of the human glucose transporters GLUT2 and GLUT3 in yeast offers novel screening systems for GLUT-targeting drugs. *Front Mol Biosci* 7, 598419. doi: 10.3389/fmolb.2020.598419
- Souza, C. M., Schwabe, T. M. E., Pichler, H., Ploier, B., Leitner, E., Guan, X. L., et al. (2011). A stable yeast strain efficiently producing cholesterol instead of ergosterol is

functional for tryptophan uptake, but not weak organic acid resistance. *Metab Eng* 13, 555–569. doi: 10.1016/j.ymben.2011.06.006

Tsujihara, K., Hongu, M., Saito, K., Inamasu, M., Arakawa, K., Oku, A., et al. (1996). Na⁺-glucose cotransporter inhibitors as antidiabetics. I. synthesis and pharmacological properties of 4'-dehydroxyphlorizin derivatives based on a new concept. *Chem Pharm Bull* 44, 1174–1180. doi: 10.1248/cpb.44.1174

van 't Klooster, J. S., Cheng, T.-Y., Sikkema, H. R., Jeucken, A., Moody, B., and Poolman, B. (2020a). Periprotein lipidomes of *Saccharomyces cerevisiae* provide a flexible environment for conformational changes of membrane proteins. *Elife* 9, e57003. doi: 10.7554/eLife.57003

van 't Klooster, J. S., Cheng, T.-Y., Sikkema, H. R., Jeucken, A., Moody, D. B., and Poolman, B. (2020b). Membrane lipid requirements of the lysine transporter Lyp1 from *Saccharomyces cerevisiae*. *J Mol Biol* 432, 4023–4031. doi: 10.1016/j.jmb.2020.04.029

Wieczorke, R. (2001). Molekulargenetische und physiologische Untersuchungen zur Funktion von FGY1 bei der heterologen Expression von Glukosetransportern in der Hefe *Saccharomyces cerevisiae*. Dissertation, Heinrich-Heine-Universität Düsseldorf.

Wieczorke, R., Dlugai, S., Krampe, S., and Boles, E. (2002). Characterisation of mammalian GLUT glucose transporters in a heterologous yeast expression system. *Cell Physiol Biochem* 13, 123–134. doi: 10.1159/000071863

Wieczorke, R., Krampe, S., Weierstall, T., Freidel, K., Hollenberg, C. P., and Boles, E. (1999). Concurrent knock-out of at least 20 transporter genes is required to block uptake of hexoses in *Saccharomyces cerevisiae*. *FEBS Letters* 464, 123–128. doi: 10.1016/S0014-5793(99)01698-1

6 Publications

6.1 Ligand screening systems for human glucose transporters as tools in drug discovery

Declaration of author contributions to the publication:

Ligand screening systems for human glucose transporters as tools in drug discovery
[mini review]

Status: published, May 2018

Journal: Frontiers in Chemistry

Type of manuscript: review article

Contributing authors: Sina Schmidl (SS), Cristina V. Iancu (CVI), Jun-yong Choe (JYC) & Mislav Oreb (MO)

Contributions of doctoral candidate and co-authors

(1) Concept and design

Doctoral candidate SS: 35%

Co-authors CVI, JYC, MO: 20%, 20%, 25%

(2) Conducting tests and experiments

n/a

(3) Literature collection

Doctoral candidate SS: 35%

Co-authors CVI, JYC, MO: 20%, 20%, 25%

(4) Analysis and interpretation of data

Doctoral candidate SS: 30%

Co-authors CVI, JYC, MO: 20%, 20%, 30%

(5) Drafting of manuscript

Doctoral candidate SS: 35%

Co-authors CVI, JYC, MO: 20%, 20%, 25%



Ligand Screening Systems for Human Glucose Transporters as Tools in Drug Discovery

Sina Schmidl¹, Cristina V. Iancu², Jun-yong Choe^{2*} and Mislav Oreb^{1*}

¹ Institute of Molecular Biosciences, Goethe University Frankfurt, Frankfurt am Main, Germany, ² Department of Biochemistry and Molecular Biology, Rosalind Franklin University of Medicine and Science, North Chicago, IL, United States

Hexoses are the major source of energy and carbon skeletons for biosynthetic processes in all kingdoms of life. Their cellular uptake is mediated by specialized transporters, including glucose transporters (GLUT, SLC2 gene family). Malfunction or altered expression pattern of GLUTs in humans is associated with several widespread diseases including cancer, diabetes and severe metabolic disorders. Their high relevance in the medical area makes these transporters valuable drug targets and potential biomarkers. Nevertheless, the lack of a suitable high-throughput screening system has impeded the determination of compounds that would enable specific manipulation of GLUTs so far. Availability of structural data on several GLUTs enabled *in silico* ligand screening, though limited by the fact that only two major conformations of the transporters can be tested. Recently, convenient high-throughput microbial and cell-free screening systems have been developed. These remarkable achievements set the foundation for further and detailed elucidation of the molecular mechanisms of glucose transport and will also lead to great progress in the discovery of GLUT effectors as therapeutic agents. In this mini-review, we focus on recent efforts to identify potential GLUT-targeting drugs, based on a combination of structural biology and different assay systems.

Keywords: glucose transport, sugar transport inhibitors, screening system, sugar transport assays, drug discovery, hxt⁰ strain

OPEN ACCESS

Edited by:

Cesare Indiveri,
University of Calabria, Italy

Reviewed by:

Ali Mobasher,
University of Surrey, United Kingdom
Ivano Eberini,
Università degli Studi di Milano, Italy

*Correspondence:

Jun-yong Choe
junyong.choe@rosalindfranklin.edu
Mislav Oreb
m.oreb@bio.uni-frankfurt.de

Specialty section:

This article was submitted to
Chemical Biology,
a section of the journal
Frontiers in Chemistry

Received: 05 March 2018

Accepted: 07 May 2018

Published: 25 May 2018

Citation:

Schmidl S, Iancu CV, Choe J and Oreb M (2018) Ligand Screening Systems for Human Glucose Transporters as Tools in Drug Discovery. *Front. Chem.* 6:183. doi: 10.3389/fchem.2018.00183

INTRODUCTION

In human cell membranes, glucose transporter family members (GLUT, gene family SLC2) facilitate the diffusion of glucose and related monosaccharides along the concentration gradient. The 14 GLUTs are grouped according to phylogenetic homology into 3 classes: class I with GLUT1-4 (all transport glucose, GLUT2 also transports fructose), class II with GLUT5, 7, 9, and 11 (all transport fructose and glucose except for GLUT5—a fructose-only transporter; GLUT9 also transports uric acid), and class III with GLUT6, 8, 10, 12, and 13 (all transport glucose, except for GLUT13, which is a myo-inositol/proton symporter) (Thorens and Mueckler, 2010; Mueckler and Thorens, 2013). Other GLUT substrates are galactose, mannose, glucosamine, and dehydroascorbic acid. GLUTs differ in transport capacity, substrate affinity and specificity, and tissue distribution; the latter reflects local physiological needs. Alterations in the function, localization or expression of GLUTs are associated with Mendelian disorders (Santer et al., 1997; Seidner et al., 1998), cancer (Thorens and Mueckler, 2010; Barron et al., 2016), diabetes (Elsas and Longo, 1992), obesity (Song and Wolfe, 2007), gout (George and Keenan, 2013), non-alcoholic

fatty liver disease (Douard and Ferraris, 2013), and renal disease (Kawamura et al., 2011). Thus GLUTs are important subjects for medical research and show great potential as drug targets for the treatment of a number of these diseases for instance in cancer therapy. It is known that cancer cells show an increased expression of glucose transporters to meet their need for higher energy demand due to uncontrolled proliferation (Warburg, 1956; Cairns et al., 2011). A higher expression rate of several GLUTs has already been identified in various kinds of tumors (Szablewski, 2013). Most prominently, higher expression rates of GLUT1 have been found in most cancer tissues (Godoy et al., 2006) and studies indicate that this overexpression is an early event in the course of the disease (Rudlowski et al., 2003; Macheda et al., 2005). Various studies also related abnormal expression of other transporters, including GLUT4, GLUT6, GLUT7, GLUT8, GLUT11, and GLUT12, with the fast proliferation of cancer cells (Rogers et al., 2002; Godoy et al., 2006; McBrayer et al., 2012); GLUT5 was found in breast cancer tissue but was absent in normal breast tissue (Zamora-León et al., 1996). Metabolites which specifically modify the activity of certain GLUT isoforms would therefore be very valuable for cancer therapy which is furthermore encouraged by studies showing that cancer cells die faster than normal cells under glucose-limiting conditions (Liu et al., 2010).

Diabetes mellitus type 2 is another prominent example of a GLUT-related disease whereas GLUT4 is considered a key player in the pathogenesis of this disease. This transporter is predominantly expressed in adipose tissue, heart, and skeletal muscle and is stored in small vesicles in the cytoplasm until insulin triggers its translocation to the plasma membrane, where it mediates glucose uptake (Hajiaghaalipour et al., 2015). Diabetic type 2 cells show diminished expression of GLUT4 as well as impaired trafficking to the plasma membrane (Patel et al., 2006). Furthermore, a proper anchoring of GLUT2 at the surface of β -cells seems to be crucial for the physiological glucose-uptake in these cells which is in turn required for normal glucose-stimulated insulin secretion (Ohtsubo et al., 2005). Reduced stability of GLUT2 in the plasma membrane disrupts insulin secretion and therefore favors the development of type 2 diabetes (Ohtsubo et al., 2005). Substrates with the ability to modulate altered functions of GLUTs involved in the pathogenesis of diabetes might contribute to the therapy and diminish symptoms of diabetes type 2 patients.

Given the complex role that GLUTs play in different diseases the discovery of GLUT-selective is highly desirable. Recent advances in three-dimensional structure determination of GLUTs and their homologs (Sun et al., 2012; Iancu et al., 2013; Deng et al., 2014; Nomura et al., 2015) finally make structure-based drug design possible, as exemplified by two HIV integrase inhibitors Raltegravir and Elvitegravir (Williamson et al., 2012). In particular, *in silico* ligand screening studies have uncovered GLUT-specific inhibitors for the first time. In this mini-review article, we will summarize the current efforts to identify potential GLUT-targeting drugs, based on a combination of structural biology and different assay systems.

STRUCTURE-BASED DISCOVERY OF COMPOUNDS TARGETING GLUTs

GLUTs belong to the sugar porter family of the Major Facilitator Superfamily (MFS) proteins (Saier et al., 1999; www.tcdb.org), one of the largest and most ubiquitous protein families. As other MFS proteins, GLUTs have 12 transmembrane helices organized into two 6-helices domains (the N- and C-halves); a central polar cavity formed between the N- and C-domains contains the substrate binding site. GLUTs have an alternating access transport mechanism whereby the substrate cavity presents in turn to either the lumen (outward-facing conformation) or cytoplasm (inward-facing conformation). Crystal structures of GLUTs and their homologs have captured outward- and inward-facing conformations, in different ligation states (apo, with substrate or inhibitors), with the substrate cavity open (open conformation) to or partially shielded (occluded conformation) from solvent (Sun et al., 2012; Iancu et al., 2013; Deng et al., 2014; Nomura et al., 2015; Kapoor et al., 2016; see **Table 1**). Comparison of the crystal structures of GLUT1 inward-open conformation and GLUT3 outward-facing conformations (outward-occluded and -open), suggest that the alternating access mechanism involves a rigid-body rotation of the N-terminal half relative to the C-terminal half and rearrangements in the substrate interactions with residues mostly from the C-terminal domain (Deng et al., 2015). Ligand docking studies of substrate and inhibitors to different conformations of GLUT1, based on crystal structures of GLUT1, GLUT3 and the bacterial homolog Xyle, show conformation-dependent variation in the number and location of the ligand binding sites: several potential glucose binding sites (three for the outward-open conformation, two for the outward-occluded conformation and one each for the inward-occluded and inward-open conformations) and, in the case of GLUT1 inhibitors, two maltose binding sites in the outward-facing conformation, and two sites for cytochalasin B in the outward-facing conformation (Lloyd et al., 2017). Obviously, structure-based ligand screening for GLUTs will need to employ all available conformations of a transporter.

Structure-based drug discovery relies on reliable 3D structures of a target protein, *in silico* ligand screening with libraries of small compounds, and assay systems to validate and characterize the ligand candidates. Subsequent rounds of chemical optimization, informed by structure-based design, may further increase the potency and specificity of the identified ligands (Sliwoski et al., 2014; Schreiber et al., 2015).

So far, *in silico* ligand screening has been reported for GLUT1, GLUT4, and GLUT5 (Mishra et al., 2015; George Thompson et al., 2016; Ung et al., 2016). This is a high-throughput ligand screening method in which millions of small compounds are assessed computationally for their ability to bind to a target structure (Colas et al., 2016). **Table 2** lists GLUT inhibitors with IC₅₀ under 20 μ M uncovered through *in silico* ligand screening studies. Human GLUT crystal structures were unavailable at the time of the initial virtual screening, so structural models were based on the crystal structures of bacterial GLUT homologs or

TABLE 1 | Crystal structures of GLUTs and their homologs.

Protein	Source	Conformation	PDB ID	References
Xylose/H ⁺ symporter	<i>Escherichia coli</i>	Outward-occluded	4GBY 4GBZ 4GCO	Sun et al., 2012
		Inward-open	4JA4 4JA3	Quistgaard et al., 2013
		Inward-open	4QIQ	Wisedchaisri et al., 2014
Glucose/H ⁺ symporter GLUT1	<i>Staphylococcus epidermidis</i> <i>Homo sapiens</i>	Inward-open	4LDS	Iancu et al., 2013
		Inward-open	4PYP	Deng et al., 2014
		Inward-open	5EQI 5EQG 5EGH	Kapoor et al., 2016
GLUT3	<i>Homo sapiens</i>	Outward-occluded	4ZW9	Deng et al., 2015
		Outward-occluded	4ZWB	
		Outward-open	4ZWC	
		Outward-occluded	5C65	Pike et al., 2015
GLUT5	<i>Rattus</i> <i>Bos taurus</i>	Outward-facing	4YBQ	Nomura et al., 2015
		Inward-open	4YB9	

other MFS proteins (Table 2) and represented either the inward-facing conformation (GLUT4 and GLUT5) or the outward-facing conformation (GLUT1). The number of molecules in the screen library varied: ~550,000 (Fragment Now and NCI-2007) for GLUT1, ~6 million (Chemnavigator) for GLUT5, and ~10 million (ZINC) for GLUT4. The number of resulting ligand candidates purchased and checked for activity against GLUTs was 17, 19, and 175, respectively, for GLUT4, GLUT1, and GLUT5. The transport assay systems were: GLUT1-expressing CHO cells, GLUT4-expressing HEK293 cells or multiple myeloma cell lines, and GLUT5 proteoliposomes. The studies identified eight GLUT1 inhibitors (including compounds A and B in Table 2), two GLUT4 inhibitors (compound E is a structural derivative of compound C, Table 2) and one GLUT5 inhibitor. Inhibitor selectivity was not established for GLUT1, but was determined at different extents for GLUT4 and GLUT5 inhibitors. Thus, compounds C and D (Table 2), seemed selective for GLUT4, compared to GLUT1, which is impressive given the extensive amino acid sequence conservation in the substrate binding cavity between these class I GLUTs. Compound F, did not affect the glucose transport of GLUT1, 2, 3 or 4, or the fructose transport of GLUT2, in proteoliposomes, proving to be a GLUT5-specific inhibitor. Mutagenesis studies on GLUT1, 5 and the bacterial GLUT homolog GlcP_{Se} confirmed the predicted binding site of compound F in GLUT5 and identified His 387 of GLUT5 as a residue important in inhibitor selectivity. Nevertheless, whether compound F remains GLUT5-selective, compared to other class II GLUTs, in particular GLUT7, which has the equivalent of His 387, remains to be established. Subsequent chemical optimization has been done only for GLUT4 inhibitors so far. Based on compound E, Wei et al. performed SAR (structure-activity relationship) analysis and antagonist synthesis and found that

compound E analogs decreased proliferation of the plasma cell malignancy multiple myeloma (Wei et al., 2017).

All the described *in silico* studies are a promising start for drug discovery efforts targeting GLUTs. Now that crystal structures for several human GLUTs are available, *in silico* studies for all GLUTs are possible. Furthermore, for the same GLUTs, inhibitors for the outward-facing and inward-facing conformations can be identified. To further establish the selectivity of the new inhibitors, GLUT-specific assay systems are required.

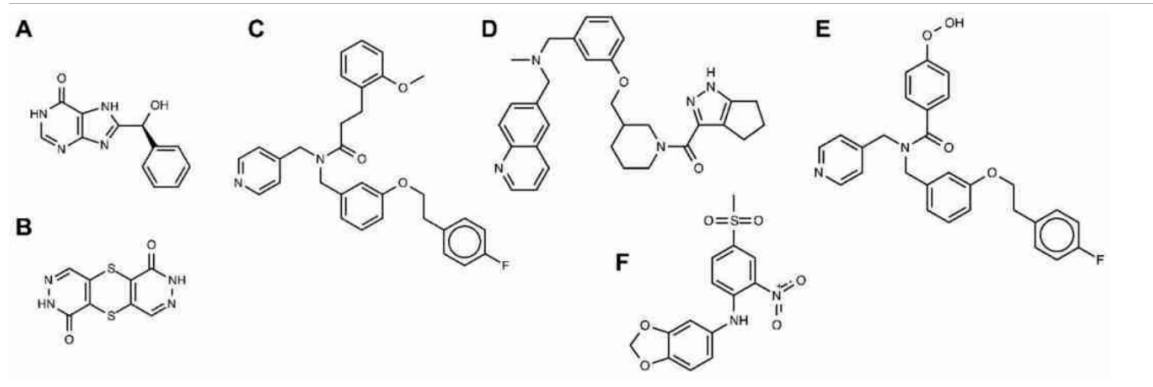
ASSAYS AND SCREENING SYSTEMS FOR GLUT ACTIVITY

In silico approaches usually yield a large number of compounds that need to be evaluated for their effect on hexose transport by GLUTs to select the best candidates for possible (pre)clinical trials. Thereby, an ideal assay system should be quick and inexpensive, but at the same time it must preserve the transporter's properties, e.g., in terms of transport kinetics.

In vitro (cell-free) systems offer the advantage of a strictly defined composition, which minimizes the risk of non-controllable interferences as often encountered in a complex cellular context. Thereby, studies of membrane proteins require the simulation of their native lipid environment. Different approaches have been tested with purified GLUTs to fulfill this task. Kraft et al. (2015) succeeded in producing milligram amounts of rat GLUT4 in mammalian HEK293 cells and were able to reconstitute correctly folded protein into detergent micelles, amphipols, nanodiscs and proteoliposomes. The latter are suitable for transport assays by constituting a two-compartment (outside/inside) system (Saier et al., 1999;

TABLE 2 | Leading probes for GLUTs from *in silico* ligand screening.

	Target protein	Template PDB ID	Screen library	Chemical IDs	Smiles	Synonyms	IC50 (μ M)	References
A	GLUT1 Outward	4CGO (XylE)	Fragment Now, NCI-2007	PubChem CID: 417049	<chem>C1=CC=C(C=C1)C(C2=NC3C(=NC=NC3=O)N2)O</chem>	8-[hydroxy(phenyl)methyl]-5,9-dihydropurin-6-one	0.45	1
B	GLUT1 Outward	4CGO (XylE)	Fragment Now, NCI-2007	ZINC 17003013, PubChem CID: 250016, CAS: 13617-04-4	<chem>c1c2c(c(=O)[nH]n1)Sc3cn[nH]c(=O)c3S2</chem>	[1,4]dithiino[2,3-d:5,6-d']dipyridazine-1,6-diol	11.8	1
C	GLUT4 Inward	1PW4 (GlpT), 1PV6 (LacY), 2GFP (EmrD)	ZINC	ZINC 14974263, ChemBridge: 59900452	<chem>COc1cccc1CCC(=O)N(Cc2ccccc2)Cc3cccc(c3)OCCc4ccc(cc4)F</chem>	N-{3-[2-(4-fluorophenyl)ethoxy]benzyl}-3-(2-methoxyphenyl)-N-(4-pyridinyl)methyl)propanamide	18.9	2
D	GLUT4 Inward	1PW4 (GlpT), 1PV6 (LacY), 2GFP (EmrD)	ZINC	ZINC 11785066, ChemBridge: 27190707	<chem>C[NH+](C1cccc(c1)OC[C@@H]2C(CCN(C2)C(=O)c3c4c([nH]n3)CCC4)Cc5ccc6c(c5)ccn6</chem>	N-methyl-1-(6-quinolyl)-N-(3-[[1-(1,4,5,6-tetrahydrocyclopenta[c]pyrazol-3-ylcarbonyl)-3-piperidinyl]methoxy]benzyl)methanamine	10.8	2
E	GLUT4 Inward	1PW4 1PV6, 2GFP	ZINC	ZINC 12152508, ChemBridge: 55751832	<chem>COc1ccc(cc1)C(=O)N(Cc2ccccc2)Cc3cccc(c3)OCCc4ccc(cc4)F</chem>	N-[[3-[2-(4-fluorophenyl)ethoxy]phenyl]methyl]-4-methoxy-N-(4-pyridyl)methyl)benzamide	6.67	2
F	GLUT5 Inward	4LDS (GlcP _{Sa})	Chem Navigator	Structure_ID: 32283234, Enamine: Z31191163	<chem>[S](=O)(=O)C1cc(c(cc1)Nc2cc3c(cc2)OCO3)[N+](=O)[O-]</chem>	N-[4-(methylsulfonyl)-2-nitrophenyl]-1,3-benzodioxol-5-amine, MSNBA	5.8	3



References: 1. Ung et al. (2016); 2. Mishra et al. (2015); 3. George Thompson et al. (2016).

Geertsma et al., 2008). By allowing lateral diffusion and the generation of a membrane curvature, this system best mimics the native surroundings of GLUTs compared to other *in vitro* systems (Kraft et al., 2015). A noteworthy advantage of proteoliposomes is the fact that parameters like the lipid composition or the degree of membrane curvature can be varied systematically. For instance, Hresko et al. (2016) could show that presence of anionic phospholipids in the proteoliposomes stabilized reconstituted GLUT3 and GLUT4 while conical

lipids enhanced the transport rate. Besides considerable advantages, the liposome reconstitution approach also bears some drawbacks. First, for membrane reconstitution, a sufficient amount of purified protein is necessary. A general instability of membrane proteins outside of their native lipid environment and the shortcomings of most purification methods, concerning the purity or the yield of the target protein, makes the heterologous expression and purification of structurally and functionally stable protein time-, labor- and cost-intensive

(Geertsma et al., 2008; Kraft et al., 2015). Furthermore, many factors have to be taken into account and optimized for a successful membrane reconstitution, such as the application of a suitable (mild or harsh) detergent, its concentration as well as the protein-to-lipid ratio, protein-orientation and the choice for either synthetic lipids or lipid extracts (Geertsma et al., 2008) resulting in a complex handling. Nevertheless, progress has been made in the various fields of protein purification and stability (Kraft et al., 2015), improving the utility of proteoliposomes for transport assays. For instance, proteoliposomes were successfully used to assess the effect of inhibitors of GLUT1 (George Thompson et al., 2015) and GLUT5 (George Thompson et al., 2015, 2016).

As a complementary approach that avoids laborious protein purification and reconstitution procedures, different cell-based systems for assaying GLUTs have been employed.

Functional expression of membrane proteins in *Xenopus laevis* oocytes opened the gate for closer molecular characterization (Hediger et al., 1987). Early experiments on GLUT1-5 in this expression system already yielded valuable information about the kinetic properties, substrate selectivity and effective inhibitors of the transporters (Birnbaum, 1989; Gould and Lienhard, 1989; Keller et al., 1989; Kayano et al., 1990; Gould et al., 1991). The system was proven to be suitable for investigating GLUT functions, due to a low endogenous GLUT expression in frog oocytes (Gould and Lienhard, 1989). Additionally, the large size of these cells facilitates handling and allows their application for electrophysiological experiments (Long et al., 2018). However, not all GLUT isoforms integrate properly into the oocyte plasma membrane and calculating their abundance in membrane is not trivial (Gould and Lienhard, 1989; Keller et al., 1989). Furthermore, *Xenopus laevis* oocytes might be too unstable for the application in high-throughput screening assays (César-Razquin et al., 2015).

Investigations on GLUTs can also be performed by expression in human cell lines such as MCF-7 or Caco-2 cells as it has been shown for GLUT2 and GLUT5 (Mahraoui et al., 1994; Zamora-León et al., 1996; Lee et al., 2015). In these systems, parameters such as lipid composition, posttranslational modifications and protein trafficking are most likely identical to the native conditions, although some alterations in cultured cells are, at least principally, possible. However, mammalian cell lines endogenously express several GLUT isoforms with overlapping activity, making it difficult to establish unambiguously the GLUT member(s) targeted by a compound (Lee et al., 2015; Tripp et al., 2017).

More recently, efforts have concentrated on establishing a microbial system amenable to high-throughput screening of GLUT inhibitors. Due to the easy manipulation and short generation time, the yeast *Saccharomyces cerevisiae* provides a time-efficient, low-cost and versatile platform for this purpose (Tripp et al., 2017; Boles and Oreb, 2018). For exclusive uptake of hexoses via heterologously expressed GLUTs, all genes encoding endogenous transporters capable of hexose transport (*HXT1-17*, *GAL2* as well as the maltose transporter genes *AGT1*, *MPH2*, and *MPH3*) were deleted in the yeast strain background CEN.PK2-1C using the loxP-Cre recombinase system (Wieczorke et al., 1999). The resulting strain was named EBY.VW4000 and is unable to

take up and grow on glucose or related hexoses as sole carbon source. The functional expression of human GLUTs in this hexose transporter deficient (*hxt⁰*) yeast strain restores its ability to grow on glucose or fructose enabling compound screening for the particular human GLUT via simple cell growth assays (Wieczorke et al., 2002). Even though cell growth is the simplest parameter to determine the functionality of the transporters or potency of the inhibitors, compound screening is not limited to this method. For instance, yeast cells can be conveniently used for uptake assays of radiolabeled sugars, which allows for the determination of kinetic parameters of the transporters, including inhibitor constants (Maier et al., 2002; Tripp et al., 2017; Boles and Oreb, 2018).

However, the functional expression of human GLUTs in yeast cells require additional modifications either within the transporter or in the genome of the yeast strain. Whereas wildtype GLUT1, GLUT4 and GLUT5 (Kasahara and Kasahara, 1996, 1997; Wieczorke et al., 2002; Tripp et al., 2017) were not active in the *hxt⁰* strain, single point mutations in the transmembrane region 2 of GLUT1 and GLUT5 mediated their functional expression (Wieczorke et al., 2002; Tripp et al., 2017). Wild-type GLUT1 was active only in the *hxt⁰* strain that additionally acquired the *fgy1* (for functional expression of GLUT1 in yeast) mutation (Wieczorke et al., 2002). The affected gene encodes the Efr3 protein (Wieczorke and Boles, personal communication) that was later described as a scaffold for recruiting the Stt4 phosphatidylinositol-4-kinase to the plasma membrane and therefore necessary for normal phosphatidylinositol-4-phosphate levels in this compartment (Wu et al., 2014). The functional expression of GLUT4 required, in addition to *fgy1*, the *fgy4* mutation, that was later found to affect the *ERG4* gene (Boles et al., 2004), which encodes an enzyme involved in the last step of ergosterol biosynthesis. These observations suggest that the lipid composition of yeast membranes interferes with the functionality of GLUTs. Nevertheless, GLUT1, GLUT4 (Wieczorke et al., 2002), and GLUT5 (Tripp et al., 2017) expressed in yeast exhibited transport kinetic parameters comparable to those determined in liposomes or human cell lines and were responsive to established inhibitors of these transporters. Therefore, *hxt⁰* strains represent a convenient platform for screening approaches and characterization of human GLUTs in a high throughput manner. The discovery of specific effectors for one certain GLUT, which do not influence homologs of the same protein family, is challenging due to the high protein sequence similarity shared by the members of this family (George Thompson et al., 2015). Among existing screening systems, the microbial, high-throughput screening system is the most effective method to face this challenge. Its usage and expansion to other disease-relevant GLUTs will likely reveal new GLUT-specific effectors which might be of fundamental importance for clinical applications in the battle against widespread diseases like cancer or diabetes.

AUTHOR CONTRIBUTIONS

All authors listed have made a substantial, direct and intellectual contribution to the work, and approved it for publication.

FUNDING

This work was supported by the National Institutes of Health, Grant number R01-GM123103 (to JC and MO).

REFERENCES

- Barron, C. C., Bilan, P. J., Tsakiridis, T., and Tsiani, E. (2016). Facilitative glucose transporters. Implications for cancer detection, prognosis and treatment. *Metabolism* 65, 124–139. doi: 10.1016/j.metabol.2015.10.007
- Birnbaum, M. J. (1989). Identification of a novel gene encoding an insulin-responsive glucose transporter protein. *Cell* 57, 305–315. doi: 10.1016/0092-8674(89)90968-9
- Boles, E., Dlugai, S., Mueller, G., and Voss, D. (2004). *Use of Saccharomyces Cerevisiae ERG4 Mutants for the Expression of Glucose Transporters From Mammals*. WO002004026907A3. Geneva: World Intellectual Property Organization.
- Boles, E., and Oreb, M. (2018). A growth-based screening system for hexose transporters in yeast. *Methods Mol. Biol.* 1713, 123–135. doi: 10.1007/978-1-4939-7507-5_10
- Cairns, R. A., Harris, I. S., and Mak, T. W. (2011). Regulation of cancer cell metabolism. *Nat. Rev. Cancer* 11, 85–95. doi: 10.1038/nrc2981
- César-Razquin, A., Snijder, B., Frappier-Brinton, T., Isserlin, R., Gyimesi, G., Bai, X., et al. (2015). A call for systematic research on solute carriers. *Cell* 162, 478–487. doi: 10.1016/j.cell.2015.07.022
- Colas, C., Ung, P. M.-U., and Schlessinger, A. (2016). SLC transporters. structure, function, and drug discovery. *Med. Chem. Comm.* 7, 1069–1081. doi: 10.1039/C6MD00005C
- Deng, D., Xu, C., Sun, P., Wu, J., Yan, C., Hu, M., et al. (2014). Crystal structure of the human glucose transporter GLUT1. *Nature* 510, 121–125. doi: 10.1038/nature13306
- Deng, D., Sun, P., Yan, C., Ke, M., Jiang, X., Xiong, L., et al. (2015). Molecular basis of ligand recognition and transport by glucose transporters. *Nature* 526, 391–396. doi: 10.1038/nature14655
- Douard, V., and Ferraris, R. P. (2013). The role of fructose transporters in diseases linked to excessive fructose intake. *J. Physiol. (Lond.)* 591, 401–414. doi: 10.1113/jphysiol.2011.215731
- Elsas, L. J., and Longo, N. (1992). Glucose transporters. *Annu. Rev. Med.* 43, 377–393. doi: 10.1146/annurev.me.43.020192.002113
- Geertsma, E. R., Nik Mahmood, N. A., Schuurman-Wolters, G. K., and Poolman, B. (2008). Membrane reconstitution of ABC transporters and assays of translocator function. *Nat. Protoc.* 3, 256–266. doi: 10.1038/nprot.2007.519
- George, R. L., and Keenan, R. T. (2013). Genetics of hyperuricemia and gout. Implications for the present and future. *Curr. Rheumatol. Rep.* 15:309. doi: 10.1007/s11926-012-0309-8
- George Thompson, A. M., Iancu, C. V., Nguyen, T. T., Kim, D., and Choe, J. Y. (2015). Inhibition of human GLUT1 and GLUT5 by plant carbohydrate products; insights into transport specificity. *Sci. Rep.* 5:12804. doi: 10.1038/srep12804
- George Thompson, A. M., Ursu, O., Babkin, P., Iancu, C. V., Whang, A., Oprea, T. I., et al. (2016). Discovery of a specific inhibitor of human GLUT5 by virtual screening and *in vitro* transport evaluation. *Sci. Rep.* 6:160. doi: 10.1038/srep24240
- Gould, G. W., Thomas, H. M., Jess, T. J., and Bell, G. I. (1991). Expression of human glucose transporters in *Xenopus* oocytes: kinetic characterization and substrate specificities of the erythrocyte, liver, and brain isoforms. *Biochemistry* 30, 5139–5145. doi: 10.1021/bi00235a004
- Gould, G. W., and Lienhard, G. E. (1989). Expression of a functional glucose transporter in *Xenopus* oocytes. *Biochemistry* 28, 9447–9452. doi: 10.1021/bi00450a030
- Godoy, A., Ulloa, V., Rodriguez, F., Reinicke, K., Yañez, A. J., GarcíaMde, L. et al. (2006). Differential subcellular distribution of glucose transporters GLUT1-6 and GLUT9 in human cancer. ultrastructural localization of GLUT1 and GLUT5 in breast tumor tissues. *J. Cell. Physiol.* 207, 614–627. doi: 10.1002/jcp.20606
- Hajiaghaalipour, F., Khalilpourfarshbafi, M., and Arya, A. (2015). Modulation of glucose transporter protein by dietary flavonoids in type 2 diabetes mellitus. *Int. J. Biol. Sci.* 11, 508–524. doi: 10.7150/ijbs.11241
- Hediger, M. A., Coady, M. J., Ikeda, T. S., and Wright, E. M. (1987). Expression cloning and cDNA sequencing of the Na⁺/glucose co-transporter. *Nature* 330, 379–381. doi: 10.1038/330379a0
- Hresko, R. C., Kraft, T. E., Quigley, A., Carpenter, E. P., and Hruz, P. W. (2016). Mammalian glucose transporter activity is dependent upon anionic and conical phospholipids. *J. Biol. Chem.* 291, 17271–17282. doi: 10.1074/jbc.M116.730168
- Iancu, C. V., Zamoan, J., Woo, S. B., Aleshin, A., and Choe, J. Y. (2013). Crystal structure of a glucose/H⁺ symporter and its mechanism of action. *Proc. Natl. Acad. Sci. U.S.A.* 110, 17862–17867. doi: 10.1073/pnas.1311485110
- Kapoor, K., Finer-Moore, J. S., Pedersen, B. P., Caboni, L., Waight, A., Hillig, R. C., et al. (2016). Mechanism of inhibition of human glucose transporter GLUT1 is conserved between cytochalasin B and phenylalanine amides. *Proc. Natl. Acad. Sci. U.S.A.* 113, 4711–4716. doi: 10.1073/pnas.1603735113
- Kasahara, T., and Kasahara, M. (1996). Expression of the rat GLUT1 glucose transporter in the yeast *Saccharomyces cerevisiae*. *Biochem. J.* 315, 177–182. doi: 10.1042/bj3150177
- Kasahara, T., and Kasahara, M. (1997). Characterization of rat Glut4 glucose transporter expressed in the yeast *Saccharomyces cerevisiae*: comparison with Glut1 glucose transporter. *Biochim. Biophys. Acta* 1324, 111–119. doi: 10.1016/S0005-2736(96)00217-9
- Kawamura, Y., Matsuo, H., Chiba, T., Nagamori, S., Nakayama, A., Inoue, H., et al. (2011). Pathogenic GLUT9 mutations causing renal hypouricemia type 2 (RHUC2). *Nucleos. Nucleot. Nucl.* 30, 1105–1111. doi: 10.1080/15257770.2011.623685
- Kayano, T., Burant, C. F., Fukumoto, H., Gould, G. W., Fan, Y. S., Eddy, R. L., et al. (1990). Human facilitative glucose transporters. *J. Biol. Chem.* 265, 13276–13282.
- Keller, K., Strube, M., and Mueckler, M. (1989). Functional expression of the human HepG2 and rat adipocyte glucose transporters in *Xenopus* Oocytes. *J. Biol. Chem.* 264, 18884–18889.
- Kraft, T. E., Hresko, R. C., and Hruz, P. W. (2015). Expression, purification, and functional characterization of the insulin-responsive facilitative glucose transporter GLUT4. *Prot. Sci.* 24, 2008–2019. doi: 10.1002/pro.2812
- Lee, Y., Lim, Y., and Kwon, O. (2015). Selected phytochemicals and culinary plant extracts inhibit fructose uptake in Caco-2 Cells. *Molecules* 20, 17393–17404. doi: 10.3390/molecules200917393
- Liu, Y., Zhang, W., Cao, Y., Liu, Y., Bergmeier, S., and Chen, X. (2010). Small compound inhibitors of basal glucose transport inhibit cell proliferation and induce apoptosis in cancer cells via glucose-deprivation-like mechanisms. *Cancer Lett.* 298, 176–185. doi: 10.1016/j.canlet.2010.07.002
- Lloyd, K. P., Ojelabi, O. A., De Zutter, J. K., and Carruthers, A. (2017). Reconciling contradictory findings: Glucose transporter 1 (GLUT1) functions as an oligomer of allosteric, alternating access transporters. *J. Biol. Chem.* 292, 21035–21046. doi: 10.1074/jbc.M117.815589
- Long, W., O'Neill, D., and Cheeseman, C. I. (2018). GLUT characterization using frog *Xenopus laevis* Oocytes. *Methods Mol. Biol.* 1713, 45–55. doi: 10.1007/978-1-4939-7507-5_4
- Macheda, M. L., Rogers, S., and Best, J. D. (2005). Molecular and cellular regulation of glucose transporter (GLUT) proteins in cancer. *J. Cell. Physiol.* 202, 654–662. doi: 10.1002/jcp.20166
- Mahraoui, L., Takeda, J., Mesonero, J., Chantret, I., Dussaulx, E., Bell, G. I., et al. (1994). Regulation of expression of the human fructose transporter (GLUT5) by cyclic AMP. *Biochem. J.* 301, 169–175. doi: 10.1042/bj3010169
- Maier, A., Völker, B., Boles, E., and Fuhrmann, G. F. (2002). Characterisation of glucose transport in *Saccharomyces cerevisiae* with plasma membrane vesicles (countertransport) and intact cells (initial uptake) with single Hxt1, Hxt2, Hxt3, Hxt4, Hxt6, Hxt7 or Gal2 transporters. *FEMS Yeast Res.* 2, 539–550. doi: 10.1111/j.1567-1364.2002.tb00121.x

- McBrayer, S. K., Cheng, J. C., Singhal, S., Krett, N. L., Rosen, S. T., and Shanmugam, M. (2012). Multiple myeloma exhibits novel dependence on GLUT4, GLUT8, and GLUT11. Implications for glucose transporter-directed therapy. *Blood* 119, 4686–4697. doi: 10.1182/blood-2011-09-377846
- Mishra, R. K., Wei, C., Hresko, R. C., Bajpai, R., Heitmeier, M., Matulis, S. M., et al. (2015). *In silico* modeling-based identification of glucose transporter 4 (GLUT4)-selective inhibitors for cancer therapy. *J. Biol. Chem.* 290, 14441–14453. doi: 10.1074/jbc.M114.628826
- Mueckler, M., and Thorens, B. (2013). The SLC2 (GLUT) family of membrane transporters. *Mol. Aspects Med.* 34, 121–138. doi: 10.1016/j.mam.2012.07.001
- Nomura, N., Verdon, G., Kang, H. J., Shimamura, T., Nomura, Y., Sonoda, Y., et al. (2015). Structure and mechanism of the mammalian fructose transporter GLUT5. *Nature* 526, 397–401. doi: 10.1038/nature14909
- Ohtsubo, K., Takamatsu, S., Minowa, M. T., Yoshida, A., Takeuchi, M., and Marth, J. D. (2005). Dietary and genetic control of glucose transporter 2 glycosylation promotes insulin secretion in suppressing diabetes. *Cell* 123, 1307–1321. doi: 10.1016/j.cell.2005.09.041
- Patel, N., Huang, C., and Klip, A. (2006). Cellular location of insulin-triggered signals and implications for glucose uptake. *Pflugers Arch.* 451, 499–510. doi: 10.1007/s00424-005-1475-6
- Pike, A. C. W., Quigley, A., Chu, A., Tessitore, A., Xia, X., Mukhopadhyay, S., et al. (2015). Structure of the Human Glucose Transporter GLUT3/SLC2A3. Available online at: <http://www.rcsb.org/structure/5C65>
- Quistgaard, E. M., Löw, C., Moberg, P., Trésaugues, L., and Nordlund, P. (2013). Structural basis for substrate transport in the GLUT-homology family of monosaccharide transporters. *Nat. Struct. Mol. Biol.* 20, 766–768. doi: 10.1038/nsmb.2569
- Rogers, S., Macheda, M. L., Docherty, S. E., Carty, M. D., Henderson, M. A., Soeller, W. C., et al. (2002). Identification of a novel glucose transporter-like protein-GLUT-12. *Am. J. Physiol.* 282, 733–738. doi: 10.1152/ajpendo.2002.282.3.E733
- Rudlowski, C., Becker, A. J., Schroder, W., Rath, W., Büttner, R., and Moser, M. (2003). GLUT1 messenger RNA and protein induction relates to the malignant transformation of cervical cancer. *Am. J. Clin. Pathol.* 120, 691–698. doi: 10.1309/4KYNQM5862JW2GD7
- Saier, M. H., Beatty, J. T., Goffeau, A., Harley, K. T., Heijne, W. H., Huang, S. C., et al. (1999). The major facilitator superfamily. *J. Mol. Microbiol. Biotechnol.* 1, 257–279.
- Santer, R., Schneppenheim, R., Dombrowski, A., Götze, H., Steinmann, B., and Schaub, J. (1997). Mutations in GLUT2, the gene for the liver-type glucose transporter, in patients with Fanconi-Bickel syndrome. *Nat. Genet.* 17, 324–326. doi: 10.1038/ng1197-324
- Schreiber, S. L., Kotz, J. D., Li, M., Aubé, J., Austin, C. P., Reed, J. C., et al. (2015). Advancing biological understanding and therapeutics discovery with small-molecule probes. *Cell* 161, 1252–1265. doi: 10.1016/j.cell.2015.05.023
- Seidner, G., Alvarez, M. G., Yeh, J. I., O'Driscoll, K. R., Klepper, J., Stump, T. S., et al. (1998). GLUT-1 deficiency syndrome caused by haploinsufficiency of the blood-brain barrier hexose carrier. *Nat. Genet.* 18, 188–191. doi: 10.1038/ng0298-188
- Sliwoski, G., Kothiwale, S., Meiler, J., and Lowe, E. W. (2014). Computational methods in drug discovery. *Pharmacol. Rev.* 66, 334–395. doi: 10.1124/pr.112.007336
- Song, D. H., and Wolfe, M. M. (2007). Glucose-dependent insulinotropic polypeptide and its role in obesity. *Curr. Opin. Endocrinol.* 14, 46–51. doi: 10.1097/MED.0b013e328011aa88
- Sun, L., Zeng, X., Yan, C., Sun, X., Gong, X., Rao, Y., et al. (2012). Crystal structure of a bacterial homologue of glucose transporters GLUT1-4. *Nature* 490, 361–366. doi: 10.1038/nature11524
- Szablewski, L. (2013). Expression of glucose transporters in cancers. *Biochim. Biophys. Acta* 1835, 164–169. doi: 10.1016/j.bbcan.2012.12.004
- Thorens, B., and Mueckler, M. (2010). Glucose transporters in the 21st Century. *Am. J. Physiol. Endocrinol.* 298, E141–E145. doi: 10.1152/ajpendo.00712.2009
- Tripp, J., Essl, C., Iancu, C. V., Boles, E., Choe, J. Y., and Oreb, M. (2017). Establishing a yeast-based screening system for discovery of human GLUT5 inhibitors and activators. *Sci. Rep.* 7:124. doi: 10.1038/s41598-017-06262-4
- Ung, P. M., Song, W., Cheng, L., Zhao, X., Hu, H., Chen, L., et al. (2016). Inhibitor discovery for the human GLUT1 from homology modeling and virtual screening. *ACS Chem. Biol.* 11, 1908–1916. doi: 10.1021/acscchembio.6b00304
- Warburg, O. (1956). On the origin of cancer cells. *Science* 3191, 309–314. doi: 10.1126/science.123.3191.309
- Wei, C., Bajpai, R., Sharma, H., Heitmeier, M., Jain, A. D., Matulis, S. M., et al. (2017). Development of GLUT4-selective antagonists for multiple myeloma therapy. *Eur. J. Med. Chem.* 139, 573–586. doi: 10.1016/j.ejmech.2017.08.029
- Wieczorko, R., Dlugai, S., Krampe, S., and Boles, E. (2002). Characterisation of mammalian GLUT glucose transporters in a heterologous yeast Expression system. *Cell. Physiol. Biochem.* 13, 123–134. doi: 10.1159/000071863
- Wieczorko, R., Krampe, S., Weierstall, T., Freidel, K., Hollenberg, C. P., and Boles, E. (1999). Concurrent knock-out of at least 20 transporter genes is required to block uptake of hexoses in *Saccharomyces cerevisiae*. *FEBS Lett.* 464, 123–128. doi: 10.1016/S0014-5793(99)01698-1
- Williamson, E. A., Damiani, L., Leitao, A., Hu, C., Hathaway, H., Oprea, T., et al. (2012). Targeting the transposase domain of the DNA repair component Metnase to enhance chemotherapy. *Cancer Res.* 72, 6200–6208. doi: 10.1158/0008-5472.CAN-12-0313
- Wisredchaisri, G., Park, M. S., Iadanza, M. G., Zheng, H., and Gonen, T. (2014). Proton-coupled sugar transport in the prototypical major facilitator superfamily protein XylE. *Nat. Comm.* 5:4521. doi: 10.1038/ncomms5521
- Wu, X., Chi, R. J., Baskin, J. M., Lucast, L., Burd, C. G., De Camilli, P., et al. (2014). Structural insights into assembly and regulation of the plasma membrane phosphatidylinositol 4-Kinase Complex. *Dev. Cell* 28, 19–29. doi: 10.1016/j.devcel.2013.11.012
- Zamora-León, S. P., Golde, D. W., Concha, II., Rivas, C. I., Delgado-López, F., Baselga, J., et al. (1996). Expression of the fructose transporter GLUT5 in human breast cancer. *Proc. Natl. Acad. Sci. U.S.A.* 93, 1847–1852. doi: 10.1073/pnas.93.5.1847

Conflict of Interest Statement: The authors declare that the research was conducted in the absence of any commercial or financial relationships that could be construed as a potential conflict of interest.

Copyright © 2018 Schmidl, Iancu, Choe and Oreb. This is an open-access article distributed under the terms of the Creative Commons Attribution License (CC BY). The use, distribution or reproduction in other forums is permitted, provided the original author(s) and the copyright owner are credited and that the original publication in this journal is cited, in accordance with accepted academic practice. No use, distribution or reproduction is permitted which does not comply with these terms.

6.2 A label-free real-time method for measuring glucose uptake kinetics in yeast

Declaration of author contributions to the publication:

A label-free real-time method for measuring glucose uptake kinetics in yeast

Status: published, December 2020

Journal: FEMS Yeast Research

Type of manuscript: research article

Contributing authors: Sina Schmidl (SS), Cristina V. Iancu (CVI), Mara Reifenrath (MR), Jun-yong Choe (JYC) & Mislav Oreb (MO)

Contributions of doctoral candidate and co-authors

(1) Concept and design

Doctoral candidate SS: 40%

Co-authors MR, JYC, MO: 10%, 10%, 40%

(2) Conducting tests and experiments

Doctoral candidate SS: 95%, yeast molecular biology, pHluorin-based assays, C¹⁴ glucose uptake assays, enzyme activity assay

Co-author CVI: 5%, pHluorin-based assay

(3) Compilation of data sets and figures

Doctoral candidate SS: 100%, Michaelis Menten curves, pH profiles, correlation of transport velocities

(4) Analysis and interpretation of data

Doctoral candidate SS: 70%, Michaelis Menten curves, K_M values

Co-authors MO, MR: 25%, 5%

(5) Drafting of manuscript

Doctoral candidate SS: 65%

Co-authors MO, CVI, JYC, MR: 20%, 5%, 5%, 5%



RESEARCH ARTICLE

A label-free real-time method for measuring glucose uptake kinetics in yeast

Sina Schmidl^{1,†}, Cristina V. Iancu², Mara Reifenrath¹, Jun-yong Choe^{2,*} and Mislav Oreb^{1,*‡}¹Institute of Molecular Biosciences, Faculty of Biological Sciences, Goethe University Frankfurt, 60438 Frankfurt am Main, Germany and ²Department of Chemistry, East Carolina Diabetes and Obesity Institute, East Carolina University, Greenville, NC27834, USA

*Corresponding authors: Goethe University Frankfurt, Institute of Molecular Biosciences, Max-von-Laue Straße 9, 60438 Frankfurt, Germany. Tel: +49 (0)69-798-29331; Fax: +49 (0)69-798-29527; E-Mail m.oreb@bio.uni-frankfurt.de; East Carolina Diabetes and Obesity Institute, 115 Heart Drive ECHI Rm 4114, Greenville NC27834, USA. Tel: 1-252-744-3368; E-Mail: Choej18@ecu.edu

One sentence summary: A novel method for the kinetic characterization of transporters that avoids the usage of radiolabeled sugars and is safer, cheaper and faster than the conventional sugar uptake assay.

Editor: John Morrissey

[†]Sina Schmidl, <http://orcid.org/0000-0002-4643-0722>

[‡]Mislav Oreb, <http://orcid.org/0000-0002-6118-1517>

ABSTRACT

Glucose uptake assays commonly rely on the isotope-labeled sugar, which is associated with radioactive waste and exposure of the experimenter to radiation. Here, we show that the rapid decrease of the cytosolic pH after a glucose pulse to starved *Saccharomyces cerevisiae* cells is dependent on the rate of sugar uptake and can be used to determine the kinetic parameters of sugar transporters. The pH-sensitive green fluorescent protein variant pHluorin is employed as a genetically encoded biosensor to measure the rate of acidification as a proxy of transport velocity in real time. The measurements are performed in the hexose transporter-deficient (hxt⁰) strain EBY.VW4000 that has been previously used to characterize a plethora of sugar transporters from various organisms. Therefore, this method provides an isotope-free, fluorometric approach for kinetic characterization of hexose transporters in a well-established yeast expression system.

Keywords: glucose uptake assay; radiolabeled glucose; Michaelis–Menten constant; pHluorin; hexose transporters; hxt⁰ yeast

INTRODUCTION

As the entry point of central carbon metabolism, the transfer of sugars (mainly glucose) across cellular membranes is essential for cell survival in most life forms. Based on this premise, sugar transporters are regarded as promising drug targets to combat serious human diseases, including cancer and diabetes (Schmidl et al. 2018), or pathogens such as the malaria causative *Plasmodium falciparum* (Qureshi et al. 2020). Therefore, mechanisms and kinetics of sugar transporters are an object of intensive research. Current methods for measuring glucose uptake, mainly relying

on isotope labeling, are cost intensive and necessitate specialized laboratories (Walsh et al. 1994a,b; Yamamoto et al. 2011). Furthermore, these experiments contribute to radioactive waste accumulation, a threat to human and environmental health that requires complex waste management strategies of governments and institutions (Poškas et al. 2019).

Isotope-free assays have also been described, employing the non-metabolizable glucose analog 2-deoxyglucose and externally added fluorogenic (Yamamoto et al. 2011) or bioluminescent (Valley et al. 2016) substrates. By using sugar analogs,

Received: 19 October 2020; Accepted: 16 December 2020

© The Author(s) 2020. Published by Oxford University Press on behalf of FEMS. All rights reserved. For permissions, please e-mail: journals.permissions@oup.com

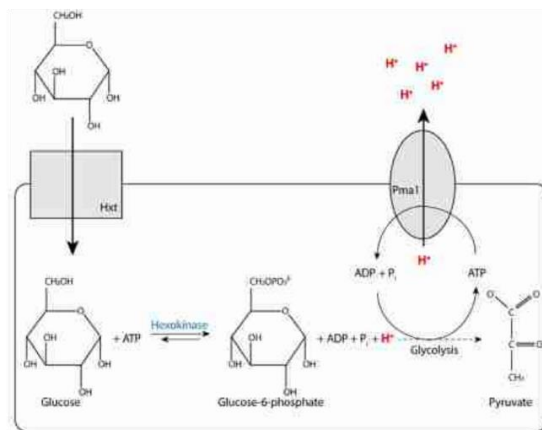


Figure 1. Mechanism of cytosol acidification in yeast cells after a glucose pulse. Glucose is transported into the cell through a hexose transporter (Hxt) and immediately phosphorylated by the hexokinase. In this process, one molecule ATP per molecule glucose is hydrolyzed, releasing one proton and causing the drop of the pH_{Cyt} (see Fig. 2A; Figure S2, Supporting Information). With the progress of glycolysis, ATP is regenerated, fueling the plasma membrane ATPase Pma1, which actively transports protons out of the cell and thereby recovers the pH_{Cyt} . For simplicity, multiple glycolytic steps between glucose-6-phosphate and pyruvate are indicated by the dashed arrow and the stoichiometry is neglected.

the latter methods are not suitable for determining the kinetic parameters of the transporters. Here, we describe an alternative method, based on the intracellular pH change upon glucose uptake. The acidification of the yeast cytosol in response to a glucose pulse to glucose-starved cells is a well-known phenomenon (Ramos et al. 1989; Orij et al. 2009). During glucose starvation, the cytosolic pH (pH_{Cyt}) of yeast cells drops to ~ 6 (Orij, Brul and Smits 2011). Under these conditions, the lack of glycolysis substrates diminishes ATP production, which leads to lower activities of the plasma membrane ATPase and the vacuolar V-ATPase, both of which consume ATP to translocate protons out of the cytosol (Orij, Brul and Smits 2011). When glucose is provided, it is transported across the plasma membrane and phosphorylated by the hexokinase as the first step of glycolysis. In this step, one molecule of ATP is hydrolyzed, and one proton is released (Fig. 1), causing the observed rapid additional acidification shortly after the glucose pulse (Ramos et al. 1989; Orij et al. 2009). Subsequently, a recovery of the neutral pH_{Cyt} up to pre-starvation conditions ($pH = 7$) (Reifenrath and Boles 2018) occurs, as glucose metabolism yields sufficient ATP to fuel the export of protons by the plasma membrane ATPase.

Since the initial acidification is a direct consequence of glucose uptake, we reasoned that kinetics of both processes should be strongly correlated. For real-time measurements of the fast changes of pH_{Cyt} , we use the pH-sensitive green fluorescent protein (GFP) variant, the ratiometric pHluorin, which allows accurate and fast measurements in the pH range from 5.5 to 8 that were derived from emission intensity ratios from two different excitation wavelengths—390 and 470 nm (Miesenböck, Angelis and Rothman 1998; Orij et al. 2009). Importantly, overexpression of pHluorin in *Saccharomyces cerevisiae* cells does not affect the cellular metabolism (Orij et al. 2009) and a tuning of pHluorin expression levels can be neglected because of its ratiometric character (Kuhn, Rohrbach and Lanzer 2007), qualifying it as an ideal biosensor for our approach. Fluorescent dyes like fluorescein (Ramos et al. 1989), 2',7'-bis-2-carboxyethyl-5- (and -6)-carboxyfluorescein (BCECF) (Ozkan and Mutharasan

2002) or semi-naphthorhodafluor (SNARF) (Blank et al. 1992) are also often used to estimate intracellular pH but exhibit certain deficits like leakage of the dyes (Ozkan and Mutharasan 2002), the compartmentalization in particular cell types (Blank et al. 1992) or a loss of pH sensitivity over time (Weiner and Hamm 1989), in addition to considerable costs of these dyes. We developed the pHluorin-based assay in the well-established EB.Y.VW4000 *hxt⁰* yeast strain, which lacks all endogenous transporters capable of hexose transport (i.e. Gal2, Hxt1-Hxt17, Agt1) (Wieczorke et al. 1999; Boles and Oreb 2018). Therefore, this strain is practically free of residual hexose uptake and has been used to express and characterize heterologous sugar transporters, including human Gluts (Boles and Oreb 2018).

RESULTS

Using pHluorin as a biosensor for time-resolved measurements of glucose uptake

With ratiometric pHluorin, the decrease of pH_{Cyt} is represented by a drop in the emission intensities ratio at 512 nm at the two excitation wavelengths 390 and 470 nm ($R_{390/470}$) (Orij et al. 2009). For the purposes described in this study, we consider the time-dependent $R_{390/470}$ decrease as an adequate kinetic parameter and its translation to pH_{Cyt} is therefore not necessary. Nevertheless, in initial experiments, we generated a calibration curve as described previously (Reifenrath and Boles 2018) for $R_{390/470}$ values in the range from pH 5 to pH 9 (Figure S1, Supporting Information). The formula (indicated within the graph, see Figure S1, Supporting Information) confirmed the correlation between the $R_{390/470}$ and pH_{Cyt} as published in previous studies (Orij et al. 2009; Reifenrath and Boles 2018) under our experimental conditions and it can therefore be used to estimate the pH range variation in the measurements shown below. We then demonstrated that the rapid changes of $R_{390/470}$ can be measured in a time-resolved manner using the high-performance spectrofluorometer PTI QuantaMasterTM 8000 (HORIBA Scientific, Kyoto, Japan). We expressed pHluorin and the endogenous transporter Hxt5 (each from a separate multicopy plasmid) in the *hxt⁰* yeast system EB.Y.VW4000 to avoid any interferences of the measurement with other hexose transporters. The use of multicopy plasmids for pHluorin expression has been established before (Orij et al. 2009; Reifenrath and Boles 2018), but expression levels of both, transporters and pHluorin, might vary under these circumstances (Lee et al. 2015). To take into account any putative variances due to expression levels or the physiological conditions of the cells, the average of biological triplicates was calculated for all experiments. The cells were grown on selective, low fluorescent maltose medium (see the 'Methods' section), and harvested and starved for 3.5 h. One minute after starting the fluorescence measurement, the cells were pulsed with 10 mM glucose, leading to the expected cytoplasm acidification. Within ~ 10 s, a nearly linear decrease of $R_{390/470}$ was observed (Fig. 2A), followed by a slower recovery phase. Moreover, the acidification rate was dependent on the glucose concentration (Fig. 2B), supporting the idea that it mirrors the velocity of glucose uptake.

To validate the hypothesis that the initial acidification after the glucose pulse is caused by the hexokinase-catalyzed phosphorylation of glucose (Ramos et al. 1989) under our experimental conditions, we tested pHluorin-expressing cells of the *S. cerevisiae* strain TSY11, which is devoid of all three yeast hexokinases (Subtil and Boles 2012). Indeed, the rapid, intense drop of pH_{Cyt} after the glucose pulse is absent in these cells but is recovered when HXX2, the predominant yeast hexokinase (Rodríguez

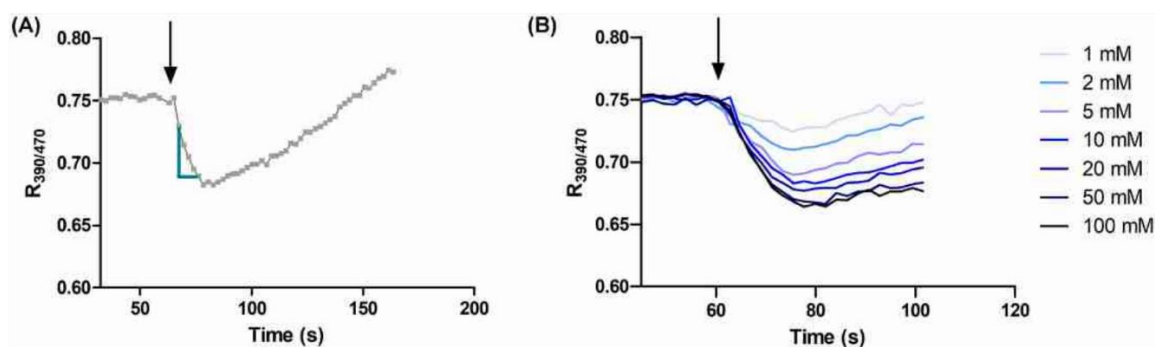


Figure 2. pHluorin-based measurement of acidification rate following a glucose pulse. The arrow indicates the time point of the glucose addition. (A) A fluorometric measurement of pH_{cyt} changes after a glucose pulse to glucose-starved yeast cells. The change in the emission ratios (512 nm) at the two excitation wavelengths 390 and 470 nm ($R_{390/470}$) of pHluorin serves as a proxy for the pH_{cyt} change. The blue lines indicate the acidification phase in which the slope decreases linearly. Values from this phase were used to calculate the reciprocal $R_{390/470}$ slope as a parameter of velocity. After the acidification phase, the $R_{390/470}$ values rise gradually to the pre-starving state. The average from biological triplicates (EBY.VW4000 cells harboring the Hxt5 transporter, pulsed with 10 mM glucose) is shown exemplarily. Error bars are omitted for clarity. According to the calibration curve shown in Figure S1 (Supporting Information), the pH_{cyt} decrease spans the range from 6.6 to 6.4 in these measurements. (B) The dependence of acidification velocity on glucose concentration. Indicated glucose concentrations were added to glucose-starved hxt^0 yeast cells, expressing pHluorin and the transporter of interest (here Hxt5). The acidification velocity increases until reaching saturation.

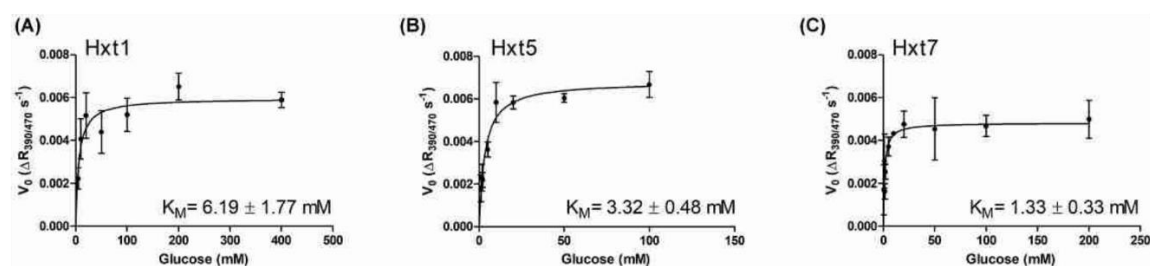


Figure 3. Glucose transport kinetics determined by the pHluorin-based assay. Michaelis-Menten constants (K_M) of three prominent yeast hexose transporters Hxt1 (A), Hxt5 (B) and Hxt7 (C) were determined in the hxt^0 strain background. Reciprocal values of the acidification slopes were plotted against the glucose concentration. Mean values and standard deviations were calculated from biological triplicates. The lines represent a least-square fit to the Michaelis-Menten equation. Determined K_M values are indicated within the graphs.

et al. 2001), is reintroduced on a plasmid (Figure S2, Supporting Information). However, we observed a small residual decrease of $R_{390/470}$ for hexokinase devoid cells (hxx^0 , TSY11; Subtil and Boles 2012), especially when pulsed with the higher concentration of 200 mM glucose. The same was also true for the hexose transporter devoid cells (hxt^0 , EBY.VW4000; Wieczorke et al. 1999) and even for cells that contain neither transporters nor kinases ($\text{hxt}^0/\text{hxx}^0$, AFY10; Farwick et al. 2014) (Figure S3A, Supporting Information). Also, the non-metabolizable sugar lactose induces this residual decrease of $R_{390/470}$ (Figure S3B, Supporting Information), indicating that neither the sugar metabolism nor transport-related processes are the cause of this effect. More likely, the osmotic pressure that increases due to the addition of a sugar drives water out of the cell affecting the pH_{cyt} in a concentration-dependent manner. Overall, this 'background' changes of pH_{cyt} were low compared to those caused by glucose transport and—since they were dependent on the sugar concentration—we corrected the slopes measured in the presence of hexose transporters by subtracting the values measured for each glucose concentration in the absence of a transporter (i.e. the empty vector control) in subsequent analyses.

Suitability of the pHluorin-based method for determination of kinetic constants of glucose transporters

To evaluate the method as a tool for kinetic characterization of transporters, we selected three well-described yeast hexose

transporters with glucose affinities differing within two orders of magnitude—Hxt1 ($K_M = 100$ mM; Reifemberger, Boles and Ciriacy 1997; Roy et al. 2015), Hxt5 ($K_M = 6$ –10 mM; Diderich et al. 2001; Buziol et al. 2002) and Hxt7 ($K_M = 1$ –2 mM; Reifemberger, Boles and Ciriacy 1997). All three transporters were expressed from multicopy plasmids in EBY.VW4000 and the measurements were performed as described above. The slopes of the first time points after the pulse (as exemplified in Fig. 2A) at different glucose concentrations were determined, corrected as described above, and their reciprocal values (to avoid negative values) were plotted against respective glucose concentrations, revealing saturable kinetics (Fig. 3A–C). Fitting to the Michaelis-Menten equation produced the following apparent K_M values for the transporters tested: 6.2 mM (Hxt1, Fig. 3A), 3.3 mM (Hxt5, Fig. 3B) and 1.3 mM (Hxt7, Fig. 3C).

For Hxt7, the determined K_M of 1.3 mM with this method is in agreement with the K_M of 1–2 mM as determined by Reifemberger, Boles and Ciriacy (1997). However, the discrepancy between previously published data and the K_M values of Hxt5 and (especially) Hxt1 determined by our method prompted us to re-determine the kinetics of these transporters using radiolabeled glucose but under conditions otherwise equal to those of the pHluorin-based assay (Figure S4A and B, Supporting Information). The results for Hxt1 ($K_M = 111.3$ mM) confirmed those of Reifemberger, Boles and Ciriacy (1997) ($K_M = 100$ mM) within the error range of the measurement. For Hxt5, we determined a slightly lower K_M of 3.1 mM compared with the published values of 6.1 mM (Buziol et al. 2002) and 10 mM (Diderich et al.

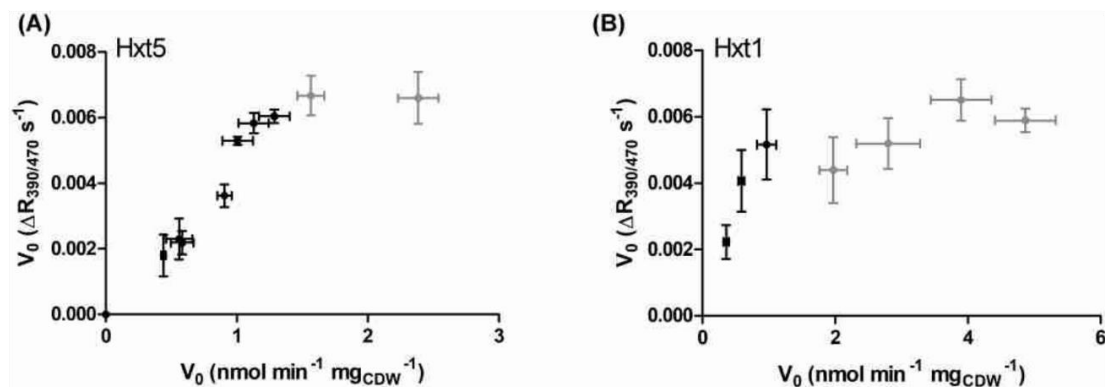


Figure 4. Correlation of initial transport velocity (V_0) values measured with the pFluorin-based and radiolabeled glucose assays. V_0 values measured by the radiolabeled glucose method are shown on the x-axes and those measured by the pFluorin-based assay on the y-axes, for the medium capacity transporter Hxt5 (A) and the high-capacity transporter Hxt1 (B). Error bars (standard deviation) of three replicates are shown. Correlation was calculated only for values below a threshold of $0.006 R_{390/470} s^{-1}$ or $1.5 \text{ nmol min}^{-1} \text{ mg}_{\text{CDW}}^{-1}$ (excluding the data points that are colored grey).

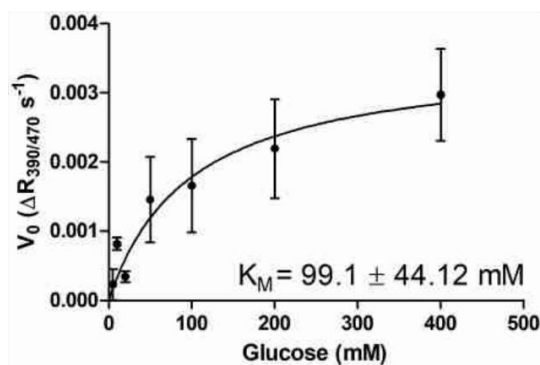


Figure 5. Glucose transport kinetics of the yeast hexose transporter Hxt1. The Michaelis-Menten constant (K_M) was determined by the pFluorin-based assay with Hxt1 expressed on a low-copy CEN.ARS (pUCPY1) plasmid in the hxt^{Δ} strain background, and its value is indicated within the graph. Mean values and standard deviations of two (for 5, 50 and 100 mM) or three (for 10, 20, 200 and 400 mM) biological replicates are shown. The line represents a least-square fit to the Michaelis-Menten equation.

2001). Strikingly, the K_M values determined for Hxt5 with the pFluorin-based assay were in agreement with our results from the C^{14} -glucose uptake assay, thereby, like the results for Hxt7, validating the new method. However, the measured K_M values for Hxt1 obtained from the two methods still showed severe discrepancies. We, therefore, analyzed the correlation of V_0 values measured by the pFluorin-based versus the radiolabeled glucose assay (Fig. 4).

A linear correlation is observed for both Hxt5 ($r = 0.98$) and Hxt1 ($r = 0.96$) up to a threshold at $\sim 0.006 R_{390/470} s^{-1}$ and $1.5 \text{ nmol min}^{-1} \text{ mg}_{\text{CDW}}^{-1}$ (Fig. 4A and B), which apparently marks the upper limit of the acidification slope. We reasoned that the intrinsically high transport capacity of Hxt1 (Reifenberger, Boles and Ciriacy 1997), in combination with the expression from a strong promoter and a multicopy plasmid, could lead to approaching this threshold already at lower glucose concentration and, consequently, to an underestimation of the K_M value. To test this hypothesis, we expressed Hxt1 on a low-copy plasmid (the CEN.ARS plasmid pUCPY1) and repeated the

measurement of its glucose uptake kinetics (Fig. 5). By lowering its expression and, consequently, the number of transporters present at the plasma membrane, the transport capacity is diminished, reflected by lower $R_{390/470} s^{-1}$ values (compare Figs 3A and 5).

This experiment revealed a K_M of 99.1 mM for the tested transporter (Fig. 5), matching both the published data (Reifenberger, Boles and Ciriacy 1997) and those from our radiolabeled glucose uptake assay (Figure S4A, Supporting Information) very well. It demonstrates that a very high V_{max} value imposes an upper limit to the pFluorin-based method, likely since other factors than the transport might become rate-limiting and lead to underestimating transporter-saturating glucose concentrations. To test if hexokinase activity is a possible limiting factor, we overexpressed HXK2 along with HXT1 and pFluorin. However, despite a 3.6-fold increase in hexokinase activity (Figure S5A, Supporting Information), the apparent K_M value of Hxt1 expressed from a multicopy plasmid was still underestimated (Figure S5B and C, Supporting Information). Hence, as the phosphorylation of glucose is ATP dependent, rapid ATP depletion is a likely explanation for our observation. However, we cannot rule out other bottlenecks, e.g. in the downstream glycolytic reactions.

DISCUSSION

The most commonly used method for determining glucose uptake in yeast (Boles and Oreb 2018) requires radiolabeled (^{14}C) sugar and includes the following steps: (i) incubation of the cells with the sugar solution; (ii) quenching with an excess of unlabeled sugar; (iii) collecting the cells by filtering; (iv) washing (twice) the filter; (v) inserting the filter into a scintillation vial and (vi) measurement using a scintillation counter. The hands-on time requirement for steps (i)–(v) is considerable (~ 2 – 3 min per sample), adding up to 60–90 min of work necessary for a typical determination of the K_M value for each transporter. Moreover, scintillation counting requires 10 min per sample, and obtaining the raw data for the complete dataset is only possible after several hours (e.g. 5 h for a typical K_M determination/30 samples). Our new method reduces the handling time and raw data collection to ~ 90 min for the same number of samples. Importantly, signal acquisition can be monitored in real-time,

enabling data quality control during the measurement, in contrast to ^{14}C assays that can be evaluated only *a posteriori*. Also, the pHluorin assay substantially reduces the costs for consumables, as no radiochemicals, filters, scintillation liquid and scintillation vials are necessary. Radiochemicals are not only expensive themselves, but their handling, storage and disposal requires specialized laboratories and spaces, associated with substantial costs and administrative effort. Most importantly, the pHluorin-based method avoids the exposure of the experimenter to radiation and radioactive waste production.

It should be noted that the hexokinase-dependence cannot be regarded as a particular disadvantage of the pHluorin-based assay; previous work by others has shown that the uptake of (^{14}C -labeled) phosphorylatable sugars is dependent on intracellular ATP concentration (Walsh, Smits and van Dam 1994c) and hexokinase activity (Smits et al. 1996), when the assays are performed on the 5-s timescale, according to the common protocol (Boles and Oreb 2018). In fact, hexose phosphorylation prevents the accumulation of intracellular sugar, which would—due to the breakdown of the concentration gradient across the membrane—cause an underestimation of the transport rates, especially for facilitative transporters, as it has been observed in hexokinase-deficient cells (Smits et al. 1996). The authors demonstrated that for determination of the ‘true’ initial velocity of sugar uptake, which is not dependent on the events downstream of the transport, the assays must be performed on the 200-ms timescale using the so-called quench-flow technique (Walsh, Smits and van Dam 1994c). Nevertheless, the kinetic constants of sugar uptake measured in wild-type (hexokinase expressing) cells were comparable on both timescales (Smits et al. 1996), demonstrating that a fairly good approximation of the transport kinetics can be obtained even on the 5-s timescale, if the sugar transport does not exceed the capacity of sugar phosphorylation. This is consistent with our observation that the upper limit of the accuracy of the pHluorin assay is determined by the capacity (V_{max}) of the transporter, since a very high uptake rate leads to a saturation of the system and underestimation of the K_M value, as shown here for Hxt1 when expressed from a multicopy plasmid. Based on correlation analyses (Fig. 4), we determined a threshold value of $0.006 \text{ R}_{390/470} \text{ s}^{-1}$ (corresponding to $1.5 \text{ nmol min}^{-1} \text{ mg}_{\text{CDW}}^{-1}$ with the radiolabeled glucose uptake assay), after which the pHluorin-based assay becomes inaccurate for determination of kinetic constants in EBY.VW4000 cells. By defining the threshold value within the method itself, no *a priori* knowledge about the transport capacity for a particular transporter is necessary. If the upper limit is reached, low copy plasmids (as shown for Hxt1, Fig. 5), a genomic integration, weak or regulatable promoters can be applied to reduce the expression and, thereby, allow for an accurate measurement. However, if the determination of transport rates of, for example, wild-type strains (and not plasmid-expressed transporters in the hxt_0 strain) is desired, transport capacities cannot be altered, which restricts the applicability of our method. Also, the prerequisite of using starved cells precludes the possibility to measure transport rates in growing cells. However, in this context it is noteworthy that all available sugar uptake assays require washing of the cells and storing them in a sugar-free solution prior to the measurement, which also likely induces starvation-like changes of cellular physiology.

In starved EBY.VW4000 cells, we have shown for three model transporters that the K_M values (spanning the range from 1 to 100 mM) can be accurately determined with the pHluorin-based method. Whereas the K_M value is an intrinsic property (a kinetic constant) of each transporter, the V_{max} is variable, as

it depends on the protein abundance (i.e. the expression level) of the transporter. Nevertheless, in some circumstances, it is desirable to determine the V_{max} , e.g. for comparative purposes. Based on the strong correlation shown in Fig. 4, linear regression (Formula: $[\text{nmol min}^{-1} \text{ mg}_{\text{CDW}}^{-1}] = [\text{R}_{390/470} \text{ s}^{-1}]/0.00466$) can be used to interconvert the values, at least under experimental conditions comparable to those applied here (i.e. regarding strain background, hexokinase levels and preculture conditions). For validation of the assay conditions in other laboratories, we recommend including at least one transporter plasmid used in this study as a control. While adapting the expression levels of transporters must be considered due to the above-mentioned reasons, the signal sensitivity of measurements should not be influenced by the expression level of pHluorin. Due to their ratiometric character, pHluorin-based measurements are independent of the biosensor concentration and not affected by artefacts such as bleaching (Kuhn, Rohrbach and Lanzer 2007). In previous studies, a super-folder pHluorin was expressed in *S. cerevisiae* cells under the control of the repressible promoter *MET25* and pH calibration was performed (as in this study, see the ‘Methods’ section) for cells grown under fully inducible conditions (no methionine) and partly repressible conditions (0.1 mM methionine) (Reifenrath and Boles 2018). The sigmoidal-dose response fits of both experiments were in agreement within the error range (Reifenrath and Boles 2018), further indicating that the quantity of pHluorin molecules is not a relevant factor. In summary, the pHluorin-based method provides a comparably accurate, but simpler, faster, cheaper and safer alternative to the common ^{14}C -based method for measuring uptake of glucose and other phosphorylatable sugars, which account for the preferred and largest fraction of carbohydrates used by living organisms, including humans and most human pathogens. In combination with the widely used hxt^0 background, this approach can be applied to characterize all heterologous transporters that can be functionally expressed in yeast.

METHODS

Strains and media

The construction of *S. cerevisiae* strains EBY.VW4000 (hxt^0), TSY11 (hxx^0) and AFY10 ($\text{hxt}^0/\text{hxx}^0$) was reported previously (Wieczorke et al. 1999; Subtil and Boles 2012; Farwick et al. 2014). Plasmid-free cells were grown in standard YEP-media (1% (w/v) yeast extract, 2% (w/v) peptone) supplemented with 1% (w/v) maltose (for EBY.VW4000 cells) or 2% (v/v) ethanol (for TSY11 and AFY10 cells) for maintenance and preparation of competent cells. Frozen competent cells were prepared and transformed according to Gietz and Schiestl (2007). The transformants were plated on solid, selective synthetic complete (SC) medium (Bruder et al. 2016) with 1% (w/v) maltose (SCM) or 2% (v/v) ethanol (SCeOH), where leucine, uracil or histidine were omitted as required for the selection of the plasmids. Filter-sterilized, low fluorescent, synthetic complete medium (lf-SC) containing 6.9 g/L YNB with ammonium sulfate, without amino acids, without folic acid and without riboflavin (MP Biomedicals), containing 1% (w/v) maltose or 2% (v/v) ethanol and amino acids as stated in Bruder et al. (2016), in which the respective amino acid(s) were omitted, was used for cultivation of cultures for the pHluorin measurements. For subcloning of plasmids, *E. coli* strain DH10B (Gibco BRL, Gaithersburg, MD) was used.

Plasmid construction

For plasmid assembly, the vector backbone p425H7 (for p_{Hluorin}), p426H7 (for all applied transporters or HXK2), pUCPY1 (to express Hxt1 with lower capacity) and p423H7 (for HXT1 in the HXK2 overexpression experiment) were linearized with restriction enzymes BamH1 and EcoR1 (New England Biolabs GmbH). The backbones were transformed together with the corresponding PCR fragment in EBY.VW4000 for homologous recombination, according to Oldenburg *et al.* (1997). All genes applied in this study were under the control of the strong, constitutive, truncated HXT7⁻¹⁻³⁹² promoter and the CYC1 terminator. PCRs were performed with Phusion polymerase (New England Biolabs GmbH) and primers listed in Table S1 (Supporting Information). The plasmids are listed in Table S2 (Supporting Information).

Calibration of p_{Hluorin}

EBY.VW4000 cells expressing p_{Hluorin} on the multicopy p425H7 plasmid were grown overnight in 15 mL If-SC-LEU medium containing maltose (1%, w/v) and harvested the next day in the exponential growth phase at an OD_{600nm} of 0.5–1.5. The pellets were resuspended in PBS buffer (137 mM NaCl, 2.7 mM KCl, 10 mM Na₂HPO₄, 1.8 mM KH₂PO₄, pH 7.4) containing 100 µg/mL digitonin and incubated 10 min on ice to permeabilize the cell wall as described by Orij *et al.* (2009). Thereafter, cells were washed twice and resuspended in PBS. pH calibration was performed as described in Reifemath and Boles (2018), where the cells were added (to a final OD_{600nm} = 0.5) to citric acid/Na₂HPO₄ buffer solutions, with different pH values ranging from 5.0 to 9.0. The cell/buffer suspensions were transferred into a black polystyrene clear-bottom 96-well microtitre plate (Greiner Bio One, article Nr. 655 097) and mounted onto the CLARIOstar microplate reader (BMG LABTECH GmbH) (set at 30°C) to measure the emission intensities at 512 nm when excited at 390 nm or 470 nm, respectively, to calculate the ratio R_{390/470}. Data from biological triplicates was analyzed with the sigmoidal dose-response fit in GraphPad Prism 5.

The p_{Hluorin}-based assay and data analysis

To test the response of a sugar-pulse to sugar-starved cells, 15 mL of selective If-SCM (or If-SC-EtOH) medium was inoculated with the transformed cells in biological triplicates, and grown overnight in 100-mL Erlenmeyer flasks at 30°C and 180 rpm. On the next day, the cultures were harvested in the exponential growth phase (at an OD_{600nm} between 0.5 and 1.5). Cells were washed twice with double-distilled water and resuspended in the If-SC medium without any carbon source to a final OD_{600nm} of 1. These suspensions were incubated at 30°C and 180 rpm in Erlenmeyer flasks for 3.5–4 h to induce starvation.

To monitor the effect of a sugar pulse to sugar-starved cells on the intracellular pH, we used a PTI QuantaMaster 8000 Spectrofluorometer (Model QM-8075-11-C, HORIBA Scientific). After starvation, 1800 µL of the cell suspension was transferred into a macro cell quartz-glass cuvette (type 100-QS, layer thickness 10 mm, volume 3.5 mL, Hellma Analytics) together with a magnetic stirring bar (3 mm × 6 mm, Sigma-Aldrich). Cells were kept in a water bath at 30°C until just before the measurement, and the temperature in the fluorometer was set to 30°C. The cuvette was mounted into the sample compartment, and the lid, which contained a sample port, was closed. The magnetic stirring function was switched on and adjusted to medium velocity. Integration time was set to 0.5 s, and slit widths were set to 3 nm. The

measurement was performed by exciting the samples successively at the two excitation wavelengths 390 and 470 nm and recording the emission intensity at 512 nm. The ratio of these intensities (R_{390/470}) was calculated and plotted on-line during the measurement, presenting one R_{390/470} value every 2.2 s. After 60 s, 200 µL of the 10× sugar solution was injected through the port into the cuvette with a Hamilton syringe (500 µL, Sigma-Aldrich) and the R_{390/470} value was recorded for another 3 min. After a total time of 4 min, the cuvette was removed from the device. For the determination of transport kinetics, this measurement was performed in biological triplicates for the following final glucose concentrations: 5, 10, 20, 50, 100, 200 and 400 mM (for Hxt1, for HXK2 overexpression experiments, 400 mM was omitted); 1, 1.5, 2, 5, 10, 20, 50 and 100 mM (for Hxt5); and 0.5, 1, 1.5, 2, 5, 10, 20, 50, 100 and 200 mM (for Hxt7).

For each derived data set, the time frame after the glucose pulse, in which R_{390/470} decreased linearly, was identified. In this time frame, the slope ($\Delta R_{390/470}/\Delta t$) was calculated and multiplied by -1 to obtain positive values (for plotting over glucose concentrations for Michaelis–Menten analysis). The same was done with the data sets derived from the empty vector control (p_{Hluorin}-expressing EBY.VW4000 cells without any transporter), pulsed with the corresponding glucose concentration, and the average from triplicates was calculated. The corresponding empty vector control average values were subtracted for each glucose concentration from slopes obtained in transporter measurements to correct for the background change of R_{390/470} (see Figure S3, Supporting Information). The values were plotted against glucose concentrations and analyzed by non-linear regression using GraphPad Prism 5 to calculate the K_M parameter.

Radiolabeled glucose uptake assay

K_M values for Hxt1 and Hxt5 were also determined by the conventional uptake assay using radiolabeled glucose to compare the results with the K_M values derived from the p_{Hluorin}-based assay. Precultures expressing p_{Hluorin} and concomitantly either HXT1 or HXT5 on a multicopy plasmid were grown for 6 h in 30 mL If-SCM medium, in which leucine and uracil were omitted, in a 300-mL Erlenmeyer flask. Pre-grown cells were transferred to pre-warmed If-SCM medium, without leucine or uracil, to a total volume of 200 mL, in 2-L Erlenmeyer flasks. Despite the larger volume of the culture, cells were grown overnight under the same conditions as applied for the p_{Hluorin}-based assay (30°C, 180 rpm) and harvested on the next day in the early exponential growth phase (at an OD_{600nm} between 0.5 and 1.5). Cells were washed twice with double-distilled water and resuspended in selective If-SC medium without any carbon source to a final OD_{600nm} = 1. Cell suspensions were incubated at 30°C and 180 rpm in 1-L Erlenmeyer flasks for 3.5–4 h to induce starvation. After this time, cells were transferred to 50-mL Falcon tubes, of which the empty weight has been determined before to later calculate the cell fresh and dry weight, and centrifuged (4000 × g, 5 min, 20°C). Pellets were washed once in ice-cold 0.1 M potassium phosphate buffer (KH₂PO₄, pH 6.5, adjusted with KOH). After another centrifugation (4000 × g, 5 min, 4°C), the supernatant was discarded; the pellet was weighed and resuspended in 0.1 M potassium phosphate buffer to a wet-weight concentration of 60 mg/mL. One hundred ten microlitre aliquots of these cell suspensions were prepared and kept on ice. The volume of the leftover cell suspension was determined, and cells were centrifuged (4000 × g, 5 min, 4°C). The pellet was frozen at -80°C overnight or longer to prepare for freeze drying. The procedure

of the uptake assay, the freeze drying and the calculation of data have been described previously in detail by Boles and Oreb (Boles and Oreb 2018). The measured uptake velocity was expressed as nmol C^{14} glucose taken up per minute per milligram cell dry weight ($\text{nmol min}^{-1} \text{mg}_{\text{CDW}}^{-1}$). The cell suspension–radiolabeled glucose mixture was incubated for only 5 s before application to the membrane filter. Uptake was measured at glucose concentrations 5, 10, 20, 50, 100, 200 and 400 mM (for Hxt1) and 1, 1.5, 2, 5, 10, 20, 50, 100 and 200 mM (for Hxt5).

Calculation of the K_M and the V_{max} was done by nonlinear regression analysis and global curve fitting in Prism 5 (GraphPad Software) with values from technical triplicates.

Preparation of protein crude extracts

To produce crude extracts, EBY.VW4000 cells expressing HXK2 on the high-copy p426H7 plasmid as well as EBY.VW4000 and TSY11 cells containing an empty p426H7 plasmid as controls were grown overnight in 30 mL SC medium without uracil and with 1% (w/v) maltose (for EBY.VW4000 cells) or 2% (w/v) galactose (for TSY11 cells). Cells were harvested at the exponential phase (at an $\text{OD}_{600\text{nm}}$ between 2 and 3), transferred in 50-mL Falcon tubes and centrifuged ($4000 \times g$, 10 min, 20°C). Pellets were washed twice in double-distilled water and transferred to 2-mL Eppendorf reaction tubes during the second washing step. The pellets were suspended in $1 \times$ pellet volume of 50-mM HEPES buffer (pH 7.6, adjusted with KOH), containing $1 \times$ Halt Protease Inhibitor Cocktail (Thermo Fisher) and 1 mM PMSF (Sigma-Aldrich) to prevent proteolytic degradation. The same volume glass beads (0.25–0.5 mm, Roth) were added, and cells were disrupted by vortexing on the vibrax for 10 min at 4°C . After centrifugation ($13000 \times g$, 5 min, 4°C), the supernatant was transferred to a fresh Eppendorf reaction tube and kept on ice. Protein concentration was determined by Bradford assay (Bradford 1976).

Enzyme activity assay

Hexokinase activity was assayed, in technical triplicates, based on the coupled reaction of the hexokinase and the glucose-6-phosphate dehydrogenase (G6P-DH), releasing $\text{NADPH} + \text{H}^+$. The accumulation of $\text{NADPH} + \text{H}^+$ can be quantified photometrically as an increase of the absorption at 340 nm (Bergmeyer 1974).

The following components of the assay were pre-mixed in cold 50-mM HEPES buffer (pH 7.6, adjusted with KOH) and stored on ice: glucose (217 mM), MgCl_2 (8 mM), NADP (1.027 mM), ATP (0.71 mM) and G6P-DH (0.11 units/reaction). One hundred ninety microlitres of the mix was dispensed in a cuvette (UV-Cuvette micro, Brand) and incubated in the photometer (Ultrospec 2100 pro, Amersham Biosciences), which was pre-warmed to 30°C , for 2 min. Ten microlitres of the crude extract was added, and the sample was mixed thoroughly by pipetting up and down. A continuous measurement of the absorption at $\text{OD}_{340\text{nm}}$ was started and stopped after ~ 10 min, when no increase of $\text{OD}_{340\text{nm}}$ was observed anymore. Specific activity was calculated from the slope ($\Delta\text{OD}_{340\text{nm}}/\Delta t$) (Bergmeyer 1974), taking into account the determined protein concentration.

ACKNOWLEDGMENTS

We thank Eckhard Boles and Sebastian Tamayo Rojas for support and stimulating discussions.

SUPPLEMENTARY DATA

Supplementary data are available at [FEMSYR](https://www.femsyr.com) online.

FUNDING

Financial support by the NIH (grant number R01-GM123103 to JC and MO) and the Boehringer Ingelheim Fonds (travel grant to SS) is gratefully acknowledged.

AUTHOR CONTRIBUTIONS

SS performed the experiments, analyzed the data and drafted the manuscript. CVI helped with the experiments. MR suggested using pHluorin as a sensor for glucose uptake. JC provided advice and resources. MO conceived the kinetic analysis approach and guided the project. All authors edited and approved the manuscript.

Conflict of Interest. None declared.

REFERENCES

- Bergmeyer HU. *Methoden der enzymatischen Analyse*. Ch 4, 3rd edn. Weinheim: Verlag Chemie GmbH, 1974.
- Blank PS, Silverman HS, Chung OY et al. Cytosolic pH measurements in single cardiac myocytes using carboxy-seminaphthorhodafluor-1. *Am J Physiol* 1992;**263**:H276–84.
- Boles E, Oreb M. A growth-based screening system for hexose transporters in yeast. *Methods Mol Biol* 2018;**1713**:123–35.
- Bradford MM. A rapid and sensitive method for the quantitation of microgram quantities of protein utilizing the principle of protein–dye binding. *Anal Chem* 1976;**72**:248–54.
- Bruder S, Reifernath M, Thomik T et al. Parallelised online biomass monitoring in shake flasks enables efficient strain and carbon source dependent growth characterisation of *Saccharomyces cerevisiae*. *Microb Cell Fact* 2016;**15**:127.
- Buziol S, Becker J, Baumeister A. et al. Determination of in vivo kinetics of the starvation-induced Hxt5 glucose transporter of *Saccharomyces cerevisiae*. *FEMS Yeast Res* 2002;**2**:283–91.
- Diderich JA, Schuurmans JM, van Gaalen MC et al. Functional analysis of the hexose transporter homologue HXT5 in *Saccharomyces cerevisiae*. *Yeast* 2001;**18**:1515–24.
- Farwick A, Bruder S, Schadeweg V et al. Engineering of yeast hexose transporters to transport D-xylose without inhibition by D-glucose. *Proc Natl Acad Sci USA* 2014;**111**:5159–64.
- Gietz RD, Schiestl RH. Frozen competent yeast cells that can be transformed with high efficiency using the LiAc/SS carrier DNA/PEG method. *Nat Protoc* 2007;**2**:1–4.
- Kuhn Y, Rohrbach P, Lanzer M. Quantitative pH measurements in *Plasmodium falciparum*-infected erythrocytes using pHluorin. *Cell Microbiol* 2007;**9**:1004–13.
- Lee ME, DeLoache WC, Cervantes B et al. A highly characterized yeast toolkit for modular, multipart assembly. *ACS Synth Biol* 2015;**9**:975–86.
- Miesenböck G, Angelis DA, Rothman JE. Visualizing secretion and synaptic transmission with pH-sensitive green fluorescent proteins. *Nature* 1998;**394**:192–5.
- Oldenburg K, Vo KT, Michaelis S et al. Recombination-mediated PCR-directed plasmid construction in vivo in yeast. *Nucleic Acids Res* 1997;**25**:451–2.
- Orij R, Brul S, Smits GJ. Intracellular pH is a tightly controlled signal in yeast. *Biochim Biophys Acta* 2011;**1810**:933–44.

- Orij R, Postmus J, Ter Beek A et al. *In vivo* measurement of cytosolic and mitochondrial pH using a pH-sensitive GFP derivative in *Saccharomyces cerevisiae* reveals a relation between intracellular pH and growth. *Microbiology* 2009;155:268–78.
- Ozkan P, Mutharasan R. A rapid method for measuring intracellular pH using BCECF-AM. *Biochim Biophys Acta* 2002;1572:143–8.
- Poškaskas P, Kilda R, Šimonis A et al. Disposal of very low-level radioactive waste: Lithuanian case on the approach and long-term safety aspects. *Sci Total Environ* 2019;667:464–74.
- Qureshi AA, Suades A, Matsuoka R et al. The molecular basis for sugar import in malaria parasites. *Nature* 2020;578:321–32.
- Ramos S, Balbin M, Raposo M et al. The mechanism of intracellular acidification induced by glucose in *Saccharomyces cerevisiae*. *J Gen Microbiol* 1989;135:2413–22.
- Reifenberger E, Boles E, Ciriacy M. Kinetic characterization of individual hexose transporters of *Saccharomyces cerevisiae* and their relation to the triggering mechanisms of glucose repression. *Eur J Biochem* 1997;245:324–33.
- Reifenrath M, Boles E. A superfolder variant of pH-sensitive pHluorin for *in vivo* pH measurements in the endoplasmic reticulum. *Sci Rep* 2018;8:11985.
- Rodríguez A, Cera T de La, Herrero P et al. The hexokinase 2 protein regulates the expression of the *GLK1*, *HXK1* and *HXK2* genes of *Saccharomyces cerevisiae*. *Biochem J* 2001;355:625–31.
- Roy A, Dement AD, Cho KH et al. Assessing glucose uptake through the yeast hexose transporter 1 (Hxt1). *PLoS One* 2015, DOI: 10.1371/journal.pone.0121985.
- Schmidl S, Iancu CV, Choe J-y et al. Ligand screening systems for human glucose transporters as tools in drug discovery. *Front Chem* 2018;6:183.
- Smits HP, Smits GJ, Postma PW et al. High-affinity glucose uptake in *Saccharomyces cerevisiae* is not dependent on the presence of glucose-phosphorylating enzymes. *Yeast* 1996;12:439–47.
- Subtil T, Boles E. Competition between pentoses and glucose during uptake and catabolism in recombinant *Saccharomyces cerevisiae*. *Biotechnol Biofuels* 2012;5:14.
- Valley MP, Karassina N, Aoyama N et al. A bioluminescent assay for measuring glucose uptake. *Anal Biochem* 2016;505:43–50.
- Walsh MC, Smits HP, Scholte M et al. Affinity of glucose transport in *Saccharomyces cerevisiae* is modulated during growth on glucose. *J Bacteriol* 1994a;176:953–8.
- Walsh MC, Smits HP, Scholte M et al. Rapid kinetics of glucose uptake in *Saccharomyces cerevisiae*. *Folia Microbiol* 1994b;39:557–9.
- Walsh MC, Smits HP, van Dam K. Respiratory inhibitors affect incorporation of glucose into *Saccharomyces cerevisiae* cells, but not the activity of glucose transport. *Yeast* 1994c;10:1553–8.
- Weiner ID, Hamm LL. Use of fluorescent dye BCECF to measure intracellular pH in cortical collecting tubule. *Am J Physiol* 1989;256:F957–64.
- Wieczorke R, Krampe S, Weierstall T et al. Concurrent knock-out of at least 20 transporter genes is required to block uptake of hexoses in *Saccharomyces cerevisiae*. *FEBS Lett* 1999;464:123–8.
- Yamamoto N, Ueda M, Sato T et al. Measurement of glucose uptake in cultured cells. *Curr Protoc Pharmacol* 2011, DOI: 10.1002/0471141755.ph1214s55.

SUPPLEMENTARY INFORMATION

A label-free real-time method for measuring glucose uptake kinetics in yeast

Sina Schmidl¹, Cristina V. Iancu², Mara Reifenrath¹, Jun-yong Choe^{2*} and Mislav Oreb^{1*}

¹Institute of Molecular Biosciences, Faculty of Biological Sciences, Goethe University
Frankfurt, Frankfurt am Main, Germany

²Department of Chemistry, East Carolina Diabetes and Obesity Institute, East Carolina
University, Greenville, NC, USA

*Corresponding authors

Dr. Mislav Oreb

Institute of Molecular Biosciences

Max-von-Laue Straße 9

60438 Frankfurt

Germany

Telephone +49 (0)69 798 29331

Telefax +49 (0)69 798 29527

E-Mail m.oreb@bio.uni-frankfurt.de

Jun-yong Choe

East Carolina University

Department of Chemistry

East Carolina Diabetes and Obesity Institute

115 Heart Drive

ECHI Rm 4114

Greenville, NC27834

USA

Telephone 1-252-744-3368

E-Mail Choej18@ecu.edu

Supplementary Tables

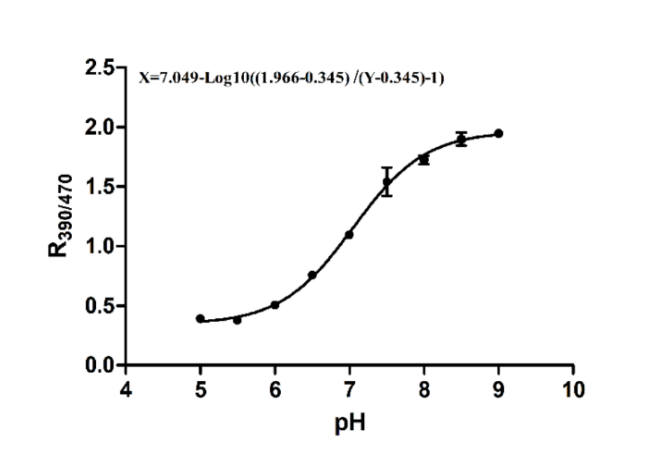
Supplementary Table S1 | Primers used in this study.

Primer name	Sequence 5'-3'	Application
MOP289	CAAGAACAAACAAGCTCAAC	Sequencing primer forward, binds in <i>HXT7</i> promotor region
MOP290	ACCTAGACTTCAGGTTGTC	Sequencing primer reverse, binds in <i>CYC1</i> terminator region
SSP36	ACAAAAAGTTTTTTAATTTAATCAAAAAATGAGTAAAGGAGA AGAACTTTTCAC	Amplification of pHluorin, overhang to <i>HXT7</i> promotor, forward
SSP37	ATGTAAGCGTGACATAACTAATTACATGACTCGAGTTATTTGTA TAGTTCATCCATGCC	Amplification of pHluorin, overhang to <i>CYC1</i> terminator, reverse
MOP160	CAAAAAGTTTTTTAATTTAATCAAAAAGTTAACATGAATTCA ACTCCCGATCTAATATCTC	Amplification of <i>HXT1</i> , overhang to <i>HXT7</i> promotor, forward
SSP77	GAATGTAAGCGTGACATAACTAATTACATGATTATTTCTGCTA AACAAACTC	Amplification of <i>HXT1</i> , overhang to <i>CYC1</i> terminator, reverse
MOP161	CAAAAAGTTTTTTAATTTAATCAAAAAGTTAACATGTCGGAA CTTGAAAACGCTC	Amplification of <i>HXT5</i> , overhang to <i>HXT7</i> promotor, forward
MOP153	GCGTGACATAACTAATTACATGACTCGAGTTATTTTTCTTTAGT GAACATCCTTTTAT	Amplification of <i>HXT5</i> , overhang to <i>CYC1</i> terminator, reverse
AFxp07	ATAAACACAAAAACAAAAAGTTTTTTAATTTAATCAAAAAAT GTCACAAGACGCTGCTATTG	Amplification of <i>HXT7</i> , overhang to <i>HXT7</i> promotor, forward
AFxp08	GGAGGGCGTGAATGTAAGCGTGACATAACTAATTACATGACTC GAGTTATTTGGTGCTGAACATTCTC	Amplification of <i>HXT7</i> , overhang to <i>CYC1</i> terminator, reverse
MBP67	GGGATCGCCAACAATACTACC	Sequencing primer, reverse, binds in CEN6/ARS4 region

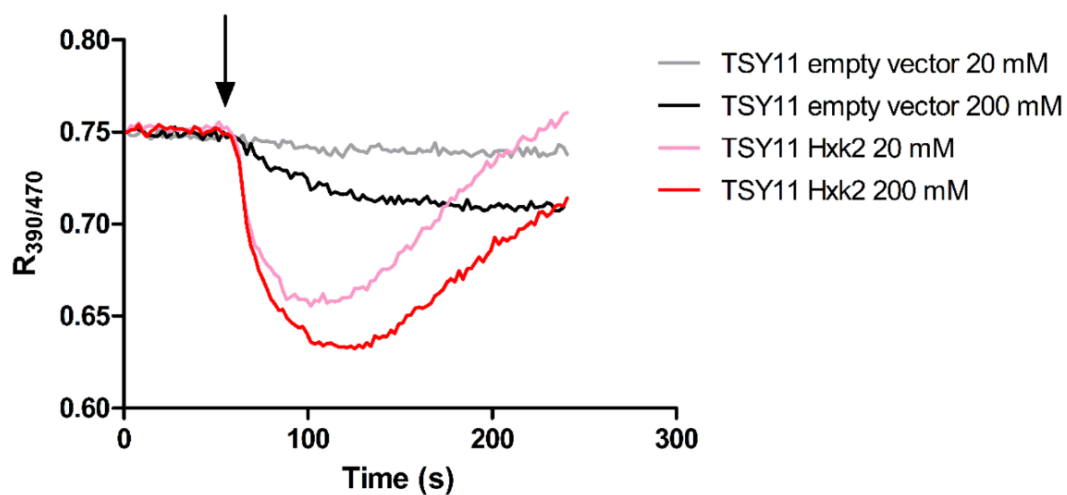
Supplementary Table S2 | Plasmids used in this study.

Plasmid names	Relevant properties	Reference
p426H7	2 μ , <i>URA3</i> , <i>Amp^r</i> , <i>HXT7p¹⁻³⁹²</i> , <i>CYC1t</i>	Hamacher et al., 2002
p425H7	2 μ , <i>LEU2</i> , <i>Amp^r</i> , <i>HXT7p¹⁻³⁹²</i> , <i>CYC1t</i>	Hamacher et al., 2002
p423H7	2 μ , <i>HIS3</i> , <i>Amp^r</i> , <i>HXT7p¹⁻³⁹²</i> , <i>CYC1t</i>	Hamacher et al., 2002
pUCPY1	CEN6/ARS4, <i>URA3</i> , <i>Amp^r</i> , <i>HXT7p¹⁻³⁹²</i> , <i>CYC1t</i>	Fernando Garces Daza, Goethe Universität Frankfurt
SSV20	p426H7_Hxt1	This study
SSV64	p426H7_Hxt5	This study
SSV17	p426H7_Hxt7	This study
MOV51	p423H7_Hxt1	This study
SSV68	p426H7_Hxk2	This study
SSV61	p425H7_pHluorin	This study
SSV73	pUCPY1_Hxt1	This study

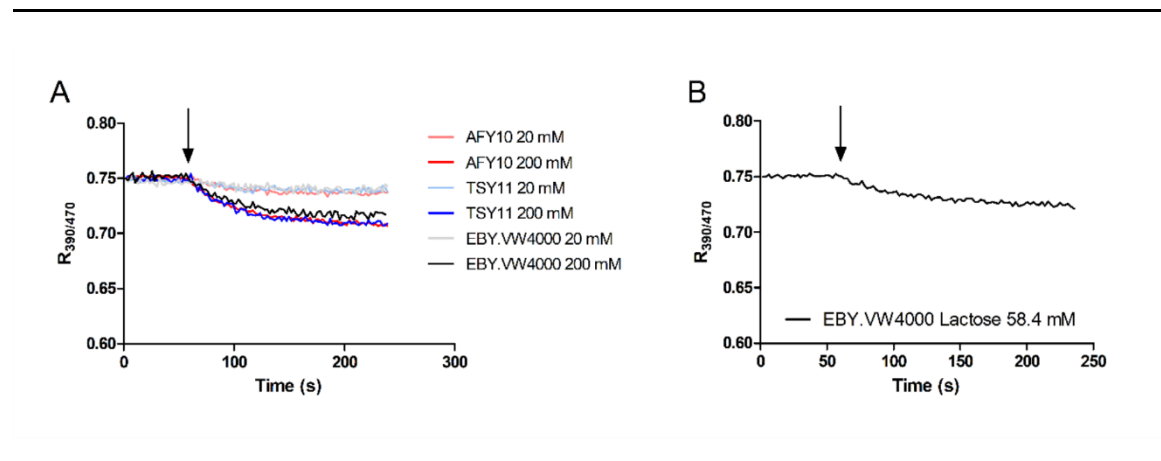
Supplementary Figures

**Supplementary Figure S1 | pH calibration of pHluorin.**

EBY.VW4000 cells expressing pHluorin on a p425H7 plasmid were permeabilized and resuspended in citric acid/ Na_2HPO_4 buffer solutions ranging from pH 5.0 to 9.0. $R_{390/470}$ values were determined with the Clariostar microplate reader (BMG LABTECH GmbH) and analyzed with the sigmoidal dose-response fit in GraphPad Prism 5. The formula indicated within the graph can be used to convert $R_{390/470}$ (y) to pH (x).

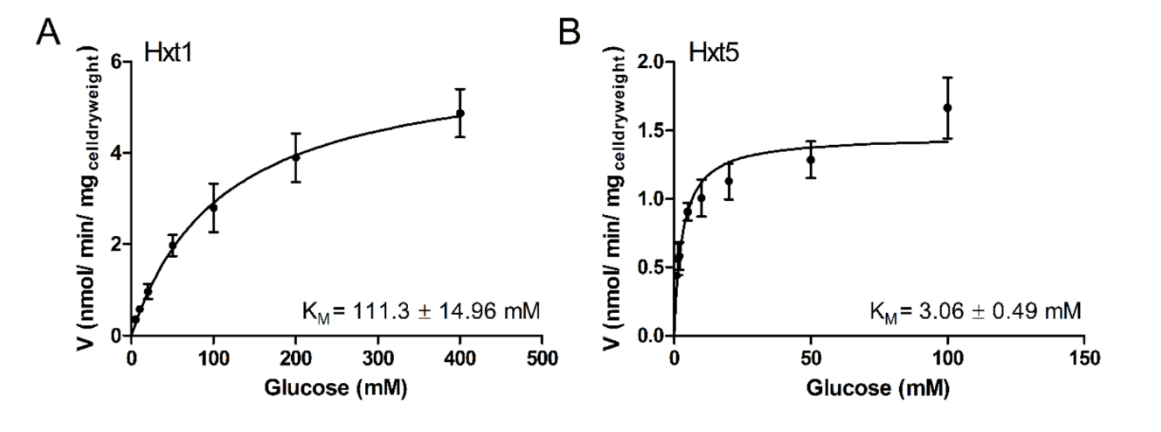
**Supplementary Figure S2 | Hexokinase-dependence of the initial acidification after a glucose pulse to glucose-starved yeast cells, monitored with the pHluorin-based method.**

Starved TSY11 (*hxx⁰*) cells transformed either with a *HXX2* plasmid or with an empty vector as a negative control were pulsed (time point indicated by the arrow) with 20 mM or 200 mM glucose.



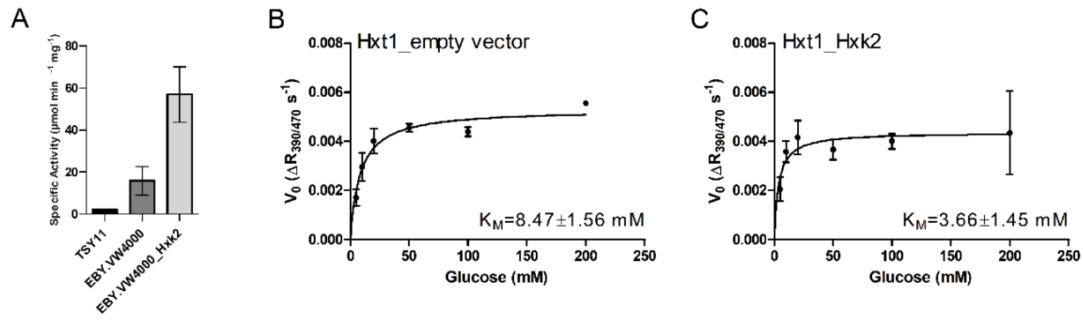
Supplementary Figure S3 | Assessment of the unspecific acidification of the yeast cytosol.

Starved TSY11 (*hxt⁰*), EB.Y.VW4000 (*hxt⁰*), and AFY10 (*hxt⁰/hxt⁰*) cells were pulsed (time point indicated by the arrow) with 20 mM or 200 mM glucose (A). A residual decrease of $R_{390/470}$ also occurs when the non-metabolizable sugar lactose (here 58.4 mM) is used for the sugar pulse (B).



Supplementary Figure S4 | Glucose transport kinetics determined with the radiolabeled glucose uptake assay.

Michaelis Menten constants (K_{MS}) were determined by the conventional radiolabeled glucose uptake assay for Hxt1 (A) and Hxt5 (B), expressed on a 2μ plasmid in *hxt⁰* EB.Y.VW4000 cells in which pHluorin was also expressed on a separate plasmid.

**Supplementary Figure S5 | Influence of the *HXK2* overexpression on the pFluorin based assay.**

An enzyme assay was performed with crude protein extracts from *hxt⁰* cells overexpressing *HXK2* from a plasmid (EBY.VW4000_Hxk2) in comparison to *hxt⁰* cells that contain only the native *HXK2* copy in their genome (EBY.VW4000). *hxt⁰* (TSY11) cells were used as a negative control (A). The apparent K_M values of EBY.VW4000 (*hxt⁰*) yeast cells expressing *HXT1* and *pFluorin* and additionally an empty vector (B) or a *HXK2* plasmid (C) were determined with the pFluorin-based assay as described in the main manuscript and are indicated within the graphs.

6.3 Functional expression of the human glucose transporters GLUT2 and GLUT3 in yeast offers novel screening systems for GLUT-targeting drugs

Declaration of author contributions to the publication:

Functional expression of the human glucose transporters GLUT2 and GLUT3 in yeast offers novel screening systems for GLUT-targeting drugs

Status: published, February 2021

Journal: Frontiers in Molecular Biosciences

Type of manuscript: research article

Contributing authors: Sina Schmidl (SS), Sebastian A. Tamayo Rojas (STR), Cristina V. Iancu (CVI), Jun-yong Choe (JYC) & Mislav Oreb (MO)

Contributions of doctoral candidate and co-authors

(1) Concept and design

Doctoral candidate SS: 40%

Co-authors MO, JCY, CVI, STR: 30%, 20%, 5%, 5%

(2) Conducting tests and experiments

Doctoral candidate SS: 80%, yeast molecular biology, site-directed mutagenesis, screening for functional candidates, growth tests, fluorescence microscopy

Co-authors STR, CVI, JYC: 10%, 5%, 5%, help with fluorescence microscopy, advice, structural modeling

(3) Compilation of data sets and figures

Doctoral candidate SS: 80%, generation of modified transporters, growth tests, fluorescence microscopy

Co-author JYC, CVI: 10%, 10%, structural models, inhibition studies

(4) Analysis and interpretation of data

Doctoral candidate SS: 55%

Co-authors MO, JYC, CVI: 25%, 10%, 10%

(5) Drafting of manuscript

Doctoral candidate SS: 75%

Co-authors MO, CVI, JYC: 10%, 10%, 5%



Functional Expression of the Human Glucose Transporters GLUT2 and GLUT3 in Yeast Offers Novel Screening Systems for GLUT-Targeting Drugs

Sina Schmid¹, Sebastian A. Tamayo Rojas¹, Cristina V. Iancu², Jun-Yong Choe^{2,3*} and Mislav Oreb^{1*}

OPEN ACCESS

Edited by:

Cesare Indiveri,
University of Calabria, Italy

Reviewed by:

Sergi Puig,
Institute of Agrochemistry and Food
Technology (IATA), Spain
Mariafrancesca Scalise,
University of Calabria, Italy

*Correspondence:

Mislav Oreb
m.oreb@bio.uni-frankfurt.de
Jun-Yong Choe
Choej18@ecu.edu

Specialty section:

This article was submitted to
Cellular Biochemistry,
a section of the journal
Frontiers in Molecular Biosciences

Received: 24 August 2020

Accepted: 23 December 2020

Published: 18 February 2021

Citation:

Schmid S, Tamayo Rojas SA,
Iancu CV, Choe J-Y and Oreb M (2021)
Functional Expression of the Human
Glucose Transporters GLUT2 and
GLUT3 in Yeast Offers Novel
Screening Systems for GLUT-
Targeting Drugs.
Front. Mol. Biosci. 7:598419.
doi: 10.3389/fmolb.2020.598419

¹Institute of Molecular Biosciences, Faculty of Biological Sciences, Goethe University Frankfurt, Frankfurt am Main, Germany, ²Department of Chemistry, East Carolina Diabetes and Obesity Institute, East Carolina University, Greenville, NC, United States, ³Department of Biochemistry and Molecular Biology, The Chicago Medical School, Rosalind Franklin University of Medicine and Science, North Chicago, IL, United States

Human GLUT2 and GLUT3, members of the GLUT/SLC2 gene family, facilitate glucose transport in specific tissues. Their malfunction or misregulation is associated with serious diseases, including diabetes, metabolic syndrome, and cancer. Despite being promising drug targets, GLUTs have only a few specific inhibitors. To identify and characterize potential GLUT2 and GLUT3 ligands, we developed a whole-cell system based on a yeast strain deficient in hexose uptake, whose growth defect on glucose can be rescued by the functional expression of human transporters. The simplicity of handling yeast cells makes this platform convenient for screening potential GLUT2 and GLUT3 inhibitors in a growth-based manner, amenable to high-throughput approaches. Moreover, our expression system is less laborious for detailed kinetic characterization of inhibitors than alternative methods such as the preparation of proteoliposomes or uptake assays in *Xenopus* oocytes. We show that functional expression of GLUT2 in yeast requires the deletion of the extended extracellular loop connecting transmembrane domains TM1 and TM2, which appears to negatively affect the trafficking of the transporter in the heterologous expression system. Furthermore, single amino acid substitutions at specific positions of the transporter sequence appear to positively affect the functionality of both GLUT2 and GLUT3 in yeast. We show that these variants are sensitive to known inhibitors phloretin and quercetin, demonstrating the potential of our expression systems to significantly accelerate the discovery of compounds that modulate the hexose transport activity of GLUT2 and GLUT3.

Keywords: GLUT2, GLUT3, Glucose transport inhibitor, drug screening system, hxt⁰ yeast strain

INTRODUCTION

Transport of hexoses across plasma membranes marks the first and rate-limiting step of energy metabolism in cells of all domains of life. In humans, 14 glucose transporter family members (GLUTs, SLC2 gene family), with differing tissue distributions, mediate the facilitative diffusion of sugar along a concentration gradient. Despite a high sequence similarity, GLUTs differ in substrate specificity and affinity (Mueckler and Thorens, 2013), matching the demands for complex, tissue-dependent hexose uptake. Abnormal expression, localization or function of GLUTs are related to the pathogenesis of several diseases including cancer (Barron et al., 2016), diabetes (Ohtsubo et al., 2005; Hajiaghaalipour et al., 2015), and other severe metabolic disorders (Santer et al., 1997; Brockmann, 2009), making these transporters important drug targets.

GLUT2 is the primary GLUT isoform found in the liver. It also mediates glucose transport in the kidney, intestine, pancreatic β -cells and the central nervous system (Fukumoto et al., 1988; Thorens, 2015). It exhibits a low affinity for glucose ($K_M = \sim 17$ mM (Uldry et al., 2002)) and even lower for fructose, galactose, and mannose ($K_M = \sim 76$, ~ 92 , and ~ 125 mM, respectively (Mueckler and Thorens, 2013)). For glucosamine, however, GLUT2 shows a very high substrate affinity ($K_M = \sim 0.8$ mM) (Uldry et al., 2002). Under normal physiological conditions, the glucose concentration in human blood is ~ 5.5 mM (Jung et al., 2013); the glucose uptake by GLUT2 would be inefficient, indicating that it is not the primary function of this transporter. More likely, glucose sensing (Ohtsubo et al., 2005) and/or signaling (Guillemain et al., 2000) are the main functions of GLUT2, consistent with its expression in tissues with high glucose fluxes. In murine pancreatic β -cells, GLUT2 mediates glucose stimulated insulin secretion, thereby regulating blood glucose levels. The absence of this function impairs glucose homeostasis leading to diabetes (Ohtsubo et al., 2005). Furthermore, GLUT2 may also be involved in mediating transcriptional glucose signaling (Guillemain et al., 2000). Loss of GLUT2 function causes the Fanconi Bickel Syndrome (Santer et al., 1997), a rare autosomal disease with various symptoms like hepatomegaly, tubular nephropathy, glucose and galactose intolerance, fasting hypoglycemia, rickets, and retarded growth (Santer et al., 2002).

In contrast to GLUT2, GLUT3 exhibits a high affinity for glucose ($K_M = 1.4$ mM (Colville et al., 1993)). Other substrates of GLUT3 are mannose, galactose, and xylose (Simpson et al., 2008). GLUT3 shares a high sequence identity (66%) with GLUT1 (Deng et al., 2015), and together they are predominantly responsible for glucose uptake in the brain - GLUT1 in the blood-brain barrier and GLUT3 in neurons (Simpson et al., 2007). Accordant with its high affinity for glucose, GLUT3 plays a pivotal role in the glucose uptake of cell types with a high demand for energy, such as sperm, circulating white blood cells, and preimplantation embryos (Simpson et al., 2007). Consistently, as tumor tissues have an increased need for carbon sources to sustain uncontrolled proliferation, GLUT3 is upregulated in many cancers, including gliomas, lung, laryngeal and bladder tumors (Ancy et al., 2018; Barron et al., 2016). In

general, high expression of GLUT3 (and GLUT1) is associated with severe pathogenesis and poor survival in most cancer tissues (Ancy et al., 2018). Recently, an association between diverse diseases and variations of copy numbers of the GLUT3 gene has been hypothesized (Ziegler et al., 2020). Hence, the discovery of activating or inhibiting drugs specific for GLUT2 or GLUT3 is highly desirable.

Both transporters GLUT2 and GLUT3 belong to the Class I GLUT family, therefore sharing certain structure similarities as, for example, the position of the glycosylation site in the extracellular loop between the transmembrane helices (TM) 1 and 2 (Joost and Thorens, 2009). For GLUT2, it has been proposed that its glycosylation is essential for proper anchoring of the transporter to the plasma membrane of β -cells and its stability in these cells (Ohtsubo et al., 2005). However, the loop itself differs in the two transporters, with GLUT2 exhibiting a significantly larger loop size than GLUT3. The role of the cytoplasmic and extracellular loops between transmembrane domains of GLUTs is still dramatically understudied and putatively underestimated. The C-terminal intracellular domain of GLUT2 has been implicated in the low glucose affinity of this transporter (Katagiri et al., 1992). Furthermore, it has been shown that conformational changes in facilitators like GLUTs, during the rocker switch mechanism, are the primary force for the translocation of sugar (Qureshi et al., 2020). Therefore, residues distant from the sugar-binding sites likely influence transport dynamics significantly, including the role of hydrophilic regions. Investigation of the extra-membrane domains will further elucidate the origins of the transporter's different properties.

The need for a convenient platform to investigate GLUTs has been recognized, and among different systems (Gould and Lienhard, 1989; Zamora-Leon et al., 1996; Kraft et al., 2015), the yeast cell-based investigation system has many benefits (Schmidl et al., 2018). The yeast *Saccharomyces cerevisiae* is a widely used GRAS organism and a model organism for diverse research applications. Cells are easily manipulated and maintained and exhibit a short generation time. By deleting all endogenous hexose transporter genes (*HXT1-17*, *GAL2*) and the genes of hexose transporting maltose transporters (*AGT1*, *MPH2*, *MPH3*) with the loxP-Cre recombinase system in a CEN.PK2-1C strain background (Entian and Kötter, 2007), a hexose transporter-deficient (*hxt⁰*) strain, incapable of growing on glucose or related monosaccharides, was constructed and named EBY.VW4000 (Wieczorke et al., 1999; Solis-Escalante et al., 2015). The strain is maintained on maltose, a disaccharide taken up by specialized maltose symporters (Chow et al., 1989), and cleaved inside the cell into two glucose molecules. The selective uptake of the respective monosaccharide by a heterologously expressed transporter can, therefore, be examined by simple growth tests or uptake assays with the radiolabeled sugar (Boles and Oreb, 2018; Schmidl et al., 2018). Moreover, a radiolabel-free assay to determine transport kinetics in the *hxt⁰* yeast system has been recently developed (Schmidl et al., 2021).

However, the functional, heterologous expression of GLUTs in this strain is a challenging task. In previous studies, the

transformation of EBY.VW4000 cells with native rat GLUTs did not yield cell growth on glucose (for GLUT1 and GLUT4) (Kasahara and Kasahara, 1996; Kasahara and Kasahara, 1997) or fructose (for GLUT5) (Tripp et al., 2017). Nevertheless, single point mutations in the TM2 of GLUT1 and GLUT5 enabled their activity in EBY.VW4000 (Wieczorke et al., 2002; Tripp et al., 2017). Also, wild-type GLUT1 was functionally expressed in a *hxt*⁰ strain harboring the additional *fgy1* (“functional expression of GLUT1 in yeast”) mutation (Wieczorke et al., 2002) that affects the scaffold protein Efr3 (Wieczorke and Boles, personal communication). Efr3 is essential for recruiting the Stt4 phosphatidylinositol-4-kinase to the plasma membrane and, consequently, builds a prerequisite for normal membrane phosphatidylinositol-4-phosphate levels (Wu et al., 2014). The corresponding strain was named EBY.S7 (Wieczorke et al., 2002). Murine GLUT4 was only active in a strain named SDY.022 that, besides the *fgy1* mutation, had a mutation in the *ERG4* gene, coding for the terminal enzyme of the ergosterol biosynthesis pathway (Boles et al., 2004). The latter mutation putatively leads to a different sterol composition in the yeast plasma membrane, which seems beneficial for GLUT4 activity.

Here, we report the functional expression of human GLUT2 and GLUT3 in the *hxt*⁰ yeast system. Thereby, we complete the accessibility of the well-characterized Class I GLUTs (GLUTs1-4, categorized according to their sequence similarities (Joost and Thorens, 2009)) in a convenient system that enables detailed characterizations of these transporters and the screening for small molecules affecting their activity in a high-throughput manner. These new platforms facilitate the rapid discovery of drugs addressing severe diseases associated with these essential human transporters.

MATERIALS AND METHODS

Strains and Media

The construction of the strains CEN.PK2-1C (Entian and Kötter, 2007), EBY.VW4000 (Wieczorke et al., 1999), EBY.S7 (Wieczorke et al., 2002) and SDY.022 (Boles et al., 2004) used in this study was reported previously and their genotypes are listed in **Supplementary Table S1**. For maintenance and preparation of competent cells, plasmid-free cells were grown in standard YEP-media (1% (w/v) yeast extract, 2% (w/v) peptone) supplemented with 1% (w/v) maltose. Frozen competent cells were prepared and transformed according to Gietz and Schiestl (Gietz and Schiestl, 2007). The transformants were plated on solid, selective synthetic complete (SC) medium with 1% (w/v) maltose (M) in which uracil was omitted (-URA) to maintain the selection pressure. For experiments with *envyGFP* constructs at the microscope, EBY.S7 or CEN.PK2-1C cells were grown in filter-sterilized, low fluorescent, synthetic complete medium (lf-SC) containing 6.9 g/l YNB with ammonium sulfate, without amino acids, without folic acid and without riboflavin (MP Biomedicals), containing 1% (w/v) maltose (for EBY.S7) or 2% (w/v) glucose (for CEN.PK2-1C) and amino acids as stated in Bruder et al. (Bruder et al., 2016), in which uracil was

omitted. For subcloning of plasmids, *E. coli* strain DH10B (Gibco BRL, Gaithersburg, MD) was used.

PCR and Plasmid Construction

DNA Sequences of GLUT2 and GLUT3 are listed in **Supplementary Table S2**. PCRs were performed with Phusion polymerase (New England Biolabs GmbH) and the respective primers, according to the intended modifications, which are listed in **Supplementary Table S3**. The resulting fragments were transformed together with the EcoR1/BamH1 linearized p426H7 vector into EBY.VW4000, EBY.S7 or SDY.022 frozen competent cells, respectively, to allow for plasmid assembly via homologous recombination (Oldenburg et al., 1997). Cells were plated on SCM (1% (w/v)) -URA agar plates and incubated for 3 days at 30°C. The grown colonies were then replica plated onto solid SC -URA medium with 0.2% (w/v) glucose (SCD (0.2% (w/v))). If growth occurred on glucose medium, single colonies from these plates were picked, sub-cultivated and plasmids were recovered by the standard alkaline lysis protocol. If no growth on glucose was observed, colonies from the maltose plates were picked and treated accordingly. For propagation and amplification, plasmids were transformed via electroporation in *E. coli*. Plasmid isolation from overnight *E. coli* cultures was carried out using a GeneJET Plasmid Miniprep Kit (Thermo Scientific) according to the manufacturer's instructions and sequenced at GATC Biotech (Konstanz, Germany). For subcloning into a vector with a dominant marker, the respective transporter sequences were amplified from the p426H7 plasmids as described, with primers exhibiting overhangs to the *HXT7* promoter or *CYC1* terminator, respectively, and PCR products were transformed together with the linearized pRS62K plasmid, which contains the same promoter and terminator regions, into EBY.VW4000 cells to allow for homologous recombination. To check the *in vivo* localization, *envyGFP* (Slubowski et al., 2015) was fused to the C-terminus of transporter constructs via homologous recombination of PCR fragments presenting the specific overhangs, and the whole construct which was flanked by the *HXT7* promoter and the *CYC1* terminator was inserted into the low-copy CEN6/ARS4 vector pUCPY1. All plasmids used in this study are listed in **Supplementary Table S4**.

Growth Tests

For growth tests on solid medium, drop tests were performed on minimal SC -URA medium, containing the respective sugar, with cells expressing transporter constructs in the p426H7 vector backbone. Pre-cultures were grown overnight in 10 ml SCM (1% (w/v)) -URA medium at 30°C and 180 rpm, centrifuged (3,000 g, 3 min, 20°C) and washed twice in double-distilled, sterile water (ddH₂O). Cells were resuspended in ddH₂O and OD_{600nm} was adjusted to 1. Dilutions of OD_{600nm} 0.1, 0.01 and 0.001 were prepared and 4 µl of each dilution was dropped onto the agar plate. Plates were incubated at 30°C for 5 days.

Cell growth in liquid YEP medium was measured with the Cell Growth Quantifier (Aquila Biolabs) (Bruder et al., 2016). Pre-cultures of cells expressing the transporter constructs in the pRS62K vector backbone were grown overnight in 10 ml

YEPM (1% (w/v)) medium with 200 µg/ml G418 for plasmid selection, harvested by centrifugation (3,000 g, 3 min, 20°C) and washed twice with ddH₂O. Washed cells were used to inoculate 30 ml YEP G418 (200 µg/ml) medium with the indicated sugar to an OD_{600nm} of 0.2 in 300 ml Erlenmeyer flasks, which were mounted onto the sensor plate. Quantification of cell growth and calculation of apparent maximal growth rates were performed with the CGQuant software (Aquila Biolabs) as previously described (Bruder et al., 2016).

Fluorescence Microscopy

To investigate the *in vivo* localization of the (modified) transporters, CEN.PK2-1C and EB.Y.S7 cells expressing the envyGFP-tagged constructs on the low-copy CEN.ARS plasmid pUCPY1 were grown overnight in filter-sterilized, low fluorescent SC medium in which uracil was omitted (If-SC -URA) and 1% (w/v) maltose (for EB.Y.S7 cells) or 2% (w/v) glucose (for CEN.PK2-1C) was added. 500 µl cell suspension of an OD_{600nm} between 1.5 and 3 was mixed with 500 µl If-SC -URA medium with the respective sugar containing 1.2% (w/v) low melting agarose (Roth) to reach a suspension with 0.6% (w/v) low melting agarose for immobilization. Six microliters were applied to an object plate, sealed with a cover slip and GFP fluorescence was located with the Confocal Laser Scanning Microscope (Zeiss LSM 780, Jena, Germany).

To confirm the activity of envyGFP-tagged transporter constructs, EB.Y.S7 cells expressing the respective construct were streaked out on solid SC -URA medium with 0.2% (w/v) glucose and growth was recorded after 5 days of incubation at 30°C.

Structural Modeling of GLUT2 and GLUT3

The crystal structure of GLUT2 is unknown and only the outward-facing GLUT3 structures are available. The homology models of the inward-facing GLUT2 and GLUT3 were generated with the 'Homology Model' function of the program package Molecular Operating Environment (MOE; Chemical Computing Group, <https://www.chemcomp.com>), using as a template the crystal structure of GLUT1 (PDB ID 4PYP). The homology models for the outward-facing GLUT2 were generated with MOE from the crystal structure of GLUT3 (PDB ID 5C65 or 4ZWC). The amino acid sequence identity and similarity between GLUT2 and GLUT3 are 50% and 68%, between GLUT1 and GLUT2 are 52% and 68%, and between GLUT1 and GLUT3 are 63% and 78%, respectively, as determined with the alignment function from MOE. The homology models generated were scored with GB/VI. The mutations were performed in MOE Protein Designing function and subject to energy minimization with the Forcefield Amber10.

Transport Assay for Inhibition Studies

The culturing of yeast cells was done at 30°C with shaking (180 rpm). EB.Y.S7 yeast cells expressing GLUT2_{ΔloopS_Q455R} were grown for a day in YEPM (1% (w/v)) media containing 200 µg/ml G418. Cells were washed once in YEP media containing 0.2% (w/v) glucose (YEPG) and 200 µg/ml G418 and transferred in the same media so that OD_{600nm} ~ 0.5 and

grown further for 1 to 2 days. GLUT3_{S66Y} expressed in EB.Y.S7 were grown for two days in SC-URA with 1% (w/v) maltose, then washed and transferred in SC-URA with 0.2% (w/v) glucose, followed by further growth for 1-2 days. For transport activity assay, cells were centrifuged (1000 g, 5 min), washed once with PBS solution (10 mM Na₂HPO₄, 1.8 mM KH₂PO₄, 2.7 mM KCl, 137 mM NaCl, pH 7.4), and resuspended in PBS buffer at an OD_{600nm} ~ 10; each assay determination contained 100 µl of this cell solution. Transport activity assay was started by adding C¹⁴-glucose (10 mM for GLUT2_{ΔloopS_Q455R} or 1 mM for GLUT3_{S66Y}). Transport activity assay was halted after 10 min by adding 3 ml ice-chilled Quench buffer (0.1 M KPi, 0.1 M LiCl, pH 5.5), followed by filtration through a glass fiber channel (GC50; Advantec, Tokyo, Japan) under vacuum, and another two washes with 3 ml Quench buffer and filtration. The filtration membranes were transferred into scintillation vials with 10 ml of Scintillation Solution (BioSafeII; Research Products International, Mount Prospect, IL, United States), and vortexed briefly. The radioactivity was determined with a scintillation counter (Tri-carb 2900TR, Perkin Elmer, Waltham, MA, USA). Phloretin and quercetin were dissolved in DMSO at 20 mM stock concentration, and inhibitor concentrations used for IC₅₀ determination were 100x stocks so that the final concentration of DMSO in the assay was 1%. Controls for determining the relative transport activity included 1% (v/v) DMSO to account for DMSO presence due to inhibitor, and the cells transformed with the empty vector. We found that the background activity with the empty vector was comparable to the transport activity of the transporters at 200 µM phloretin. Data were analyzed with the nonlinear fit analysis of GraphPad Prism (San Diego, CA, United States).

RESULTS

Generation of GLUT Constructs that Mediate Glucose Uptake into the hxt⁰ Yeast Strain

A GLUT3 Mutant Shows Enhanced Activity in the hxt⁰ Yeast System

A plasmid for the expression of GLUT3 in yeast was generated using either the native human coding sequence or a codon-optimized sequence for the expression in insect cells. Amplification of the open reading frame (ORF) with oligonucleotides having 30-40 base pair overhangs to the applied promoter (*HXT7*¹⁻³²⁹) or terminator (*CYCI*) region, respectively, and co-transformation with the linearized host plasmid (p426H7) in EB.Y.VW4000, EB.Y.S7, and SDY.022 cells allowed for the plasmid assembly via homologous recombination (Oldenburg et al., 1997; Boles and Oreb, 2018). The strong, truncated *HXT7* promoter region and the *CYCI* terminator were chosen to achieve high expression levels. Transformants were plated on selective SC -URA medium, containing 1% (w/v) maltose, and incubated for three days at 30°C, resulting in the growth of approximately 1000 colonies per plate. Subsequently, cells were replica plated on SC -URA

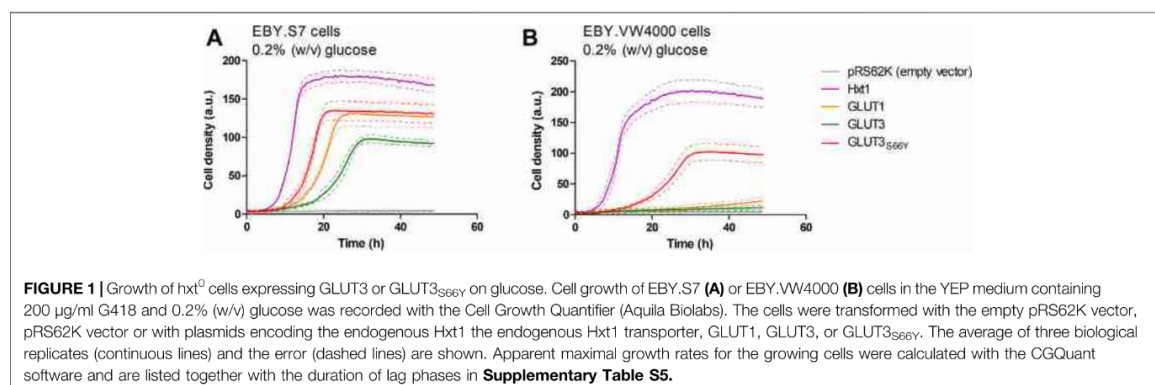
medium, containing 0.2% (w/v) glucose, to screen for cells that regained the ability to use glucose as a carbon source. EBY.VW4000 transformants did not show any growth on the solid glucose medium, even after a prolonged incubation of seven days. Most of the EBY.S7 and SDY.022 transformants grew after five days of incubation on glucose. To investigate if wild-type GLUT3 is active in these strain backgrounds, we isolated and sequenced plasmids of several colonies with various sizes. In bigger colonies, one single mutation (S66Y) was found, located in TM2. However, also unmodified GLUT3 mediated the growth of EBY.S7 and SDY.022 transformants on glucose. Re-transformation of the native GLUT3 and the modified GLUT3_{S66Y} construct in EBY.S7 cells resulted in growth on glucose medium, proving that no further mutations, except for the *fgy1* mutation, in the yeast strain were essential for this phenotype. However, while wild-type GLUT3 was incapable of mediating growth of EBY.VW4000 cells on solid glucose medium, slight growth was observed for GLUT3_{S66Y}-expressing EBY.VW4000 cells (**Supplementary Figure S7A**). Furthermore, the drop test of the EBY.S7 and SDY.022 cells expressing the different constructs (GLUT3 and GLUT3_{S66Y}) on a plasmid, revealed larger colonies for those expressing the mutated version (**Supplementary Figures S7B,C**), indicating that the S66Y mutation is beneficial for the functionality of the transporter in the heterologous system. Growth tests with *hxt*⁰ cells expressing GLUT3 or GLUT3_{S66Y} were performed in liquid YEP medium with 0.2% (w/v) glucose, for which the GLUT3 ORFs were transferred to pRS62K plasmid backbones. Consistent with the results observed in the drop tests, both constructs enabled the growth of EBY.S7 cells, but GLUT3-expressing cells showed a significantly longer lag phase and a 1.8 times lower apparent maximal growth rate than those expressing GLUT3_{S66Y} (**Figure 1A**; **Supplementary Table S5**). For EBY.VW4000 cells, only GLUT3_{S66Y} mediated growth, while the unmodified GLUT3 did not (**Figure 1B**). Positive controls were GLUT1, as a representative of a heterologous transporter active in EBY.S7 cells (Wieczorke et al., 2002), and Hxt1, an endogenous low-affinity transporter for glucose and fructose (Leandro et al., 2009).

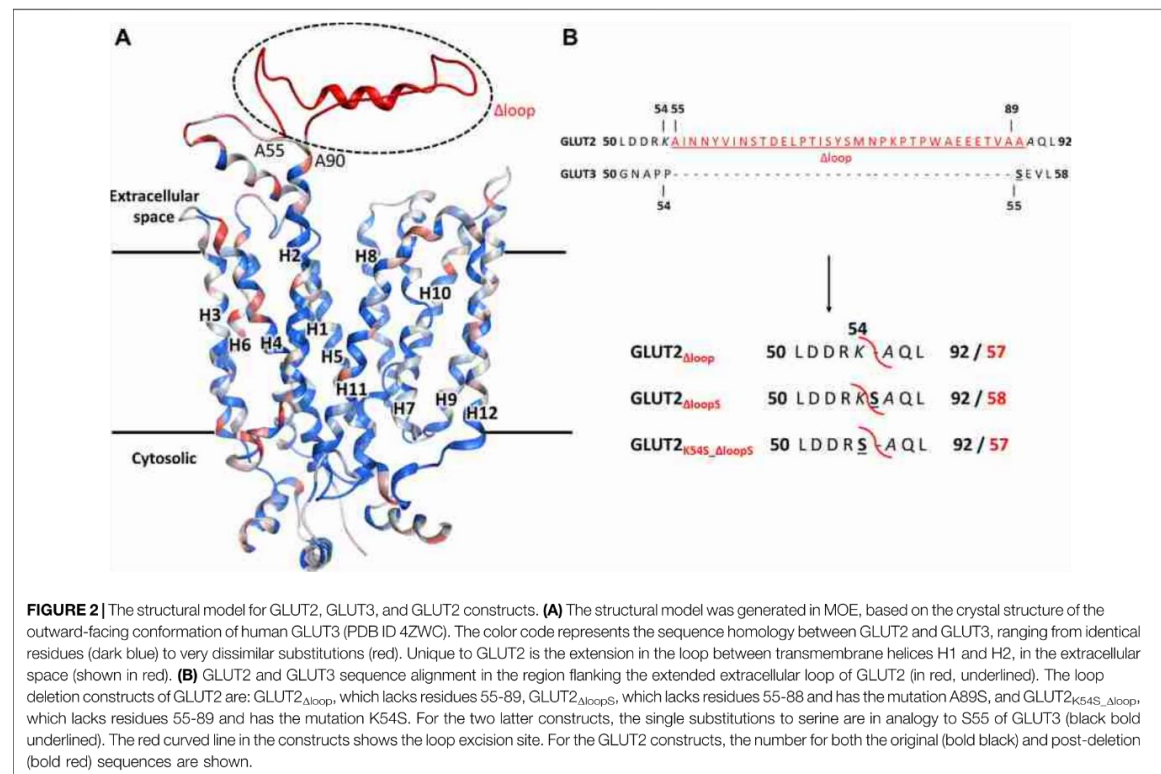
Site-Directed Mutagenesis Approaches to Enable GLUT2 Activity in Yeast

Expression plasmids carrying either the native or a codon-optimized (for insect cells) human GLUT2 sequence were generated as described above for GLUT3. However, after replica plating, EBY.VW4000, EBY.S7, or SDY.022 transformants, of which more than 1000 colonies grew on solid maltose medium, showed no growth on glucose-containing agar plates, even after prolonged incubation at 30°C for one week.

Like the S66Y mutation in GLUT3, previous studies found single point mutations in the second transmembrane region of GLUT1 (e.g., V69M) (Wieczorke et al., 2002) and GLUT5 (e.g., S72Y and S76I) (Tripp et al., 2017) that enabled or improved the functional expression of these GLUTs in yeast. Therefore, we focused on this critical region in GLUT2 as well. Comparison of the amino acids 96 – 104 in GLUT2 with the corresponding area in GLUT1, GLUT3, and GLUT5 (**Supplementary Figure S2**) revealed that GLUT2 primary sequence has two consecutive serines at positions 102-103 vs. hydrophobic amino acids in the other GLUTs successfully expressed in yeast (**Supplementary Figure S2**).

Interestingly, in GLUT3 and GLUT5, a single serine mutation to a more hydrophobic amino acid enabled or improved the functional expression of these two transporters in yeast (as shown in this study and by Tripp et al. (Tripp et al., 2017)). This observation prompted us to direct mutagenesis to the amino acids 101-103, including the valine at position 101, considering the effect of the V69M mutation in GLUT1 (Wieczorke et al., 2002). By using degenerate primers that allow for the introduction of different nucleotides at a particular position (Kwok et al., 1994) (see **Supplementary Table S3**), different codons were inserted to mutate the chosen amino acids. The following degenerate codons were used to insert the desired range of substitutions: at position 101, RTK (encoding Ile, Met and Val); at position 102, RYT (encoding Ala, Ile, Thr and Val); at position 103, ATK (encoding Ile and Met). Considering all permutations, a library encoding 24 different protein sequence variants of the critical region resulted from this approach. The sequencing of the isolated plasmids from random clones confirmed the successful introduction of the expected range of substitutions. Still, screening of more than 1000 colonies for growth on glucose-

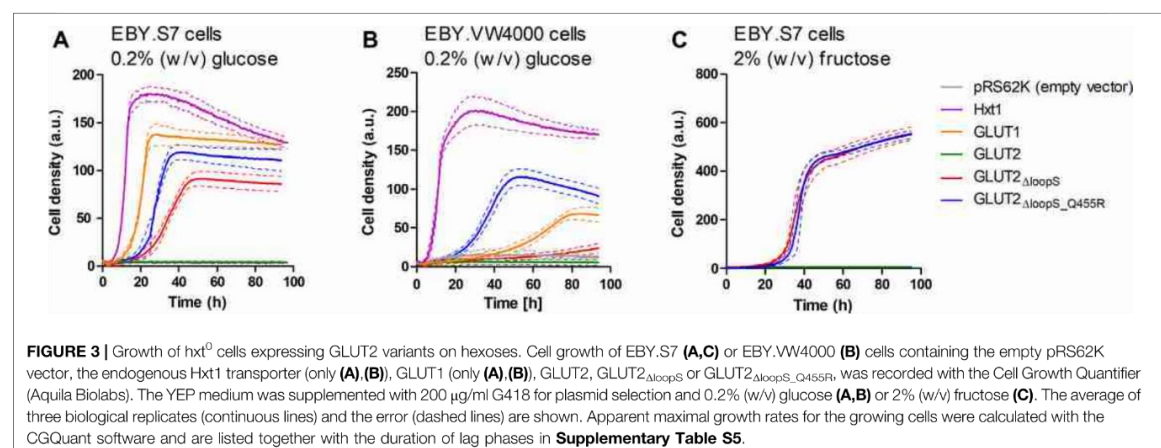




containing agar plates yielded no positive clones. In addition to these mutations in TM2, we mutated the N glycosylation site at position 62 (GLUT2 $_{N62Q}$) within the first extracellular loop, just in case the glycosylation disturbed the activity of the transporter in yeast cells. This modification also failed to restore *hxt*⁰ yeast cell growth on glucose.

Modification of the Extended Extracellular Loop of GLUT2

A conspicuous structural difference between GLUT2 and the other Class I GLUTs, which are active in yeast, is the extension of the extracellular loop connecting the TM helices H1 and H2 (Figure 2).

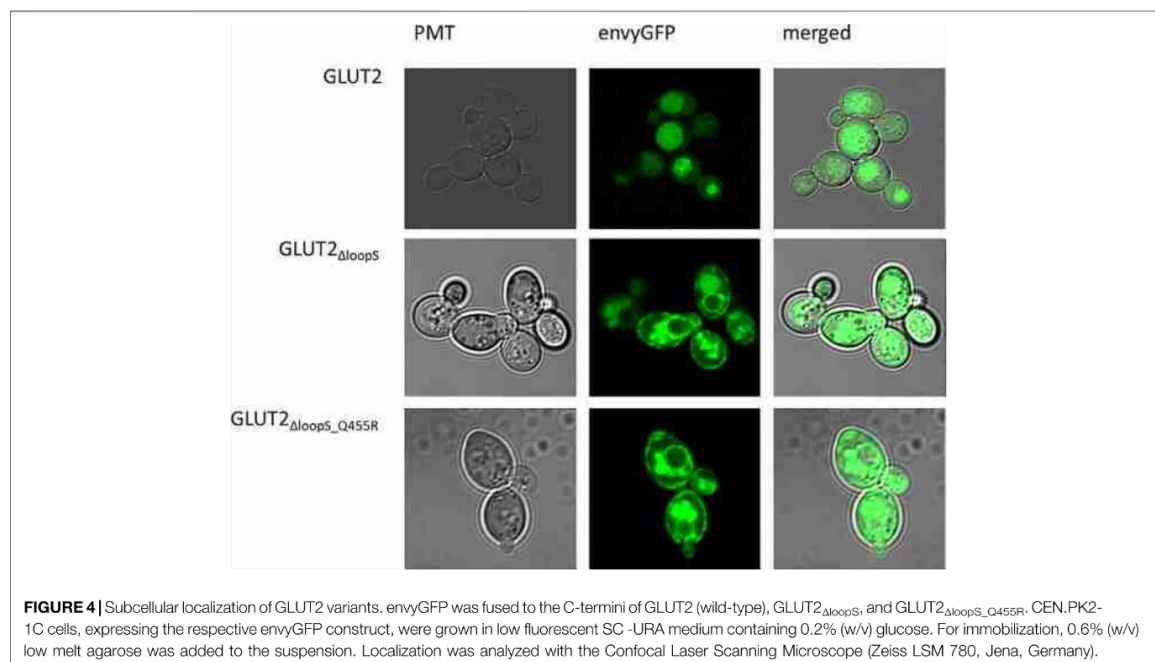


Since minor sequence modifications have not led to an active expression of GLUT2 in *hxt⁰* yeast strains, we reasoned that shortening the extension, thereby introducing a GLUT3-like-loop, could promote GLUT2 activity in the heterologous system.

In addition to just deleting the amino acids 55-89 (GLUT2 Δ loop), we also constructed one chimera in which those amino acids were replaced by one serine (GLUT2 Δ loopS) and one in which the lysine preceding the deleted region was mutated to serine (GLUT2 Δ loopS_{K54S}) (Figure 2B). Compared to GLUT3, the loop of GLUT2 Δ loop is one residue shorter, lacking the residue corresponding to S55 of GLUT3, while that of GLUT2 Δ loopS is the same length and includes a residue in analogy to S55 of GLUT3. GLUT2 Δ loopS_{K54S} contains the mutation corresponding to S55 of GLUT3 but at the beginning instead of the end of the deleted loop. The modifications were introduced into the ORFs via PCR (primers are listed in Supplementary Table S3), and the individual fragments were transformed together with a linearized p426H7 vector in EB.Y.VW4000, EB.Y.S7, or SDY.022 cells. Transformants that grew on solid maltose medium (more than 1000 colonies per plate) were then replica plated onto glucose containing plates. A substantial number (approximately 60%) of colonies expressing one of the three loop-modified constructs, respectively, grew on glucose. Multiple plasmids from each strain background and loop-construct combination were isolated and sequenced. Most of these plasmids did not show mutations other than those intentionally introduced. Strikingly, in 2 out of 3 sequenced plasmids harboring the GLUT2 Δ loopS construct that were isolated from EB.Y.VW4000 cells, a point mutation led to the substitution of the amino acid glutamine at position 455 with

either lysine (Q455K) or arginine (Q455R). Also, Q455R mutation was found in one out of three GLUT2 Δ loopS constructs isolated from SDY.022 cells, indicating an additional beneficial effect of this mutation on the glucose uptake via GLUT2. The isolated loop constructs GLUT2 Δ loop, GLUT2 Δ loopS_{K54S}, GLUT2 Δ loopS, and GLUT2 Δ loopS_{Q455R} were re-transformed in all three *hxt⁰* strains, and their growth was analyzed by a drop test on solid glucose medium (Supplementary Figure S9). The ability to grow on glucose was regained by EB.Y.S7 and SDY.022 cells with all loop constructs, whereas cells expressing GLUT2 Δ loopS and especially GLUT2 Δ loopS_{Q455R}, respectively, showed bigger colonies in comparison to GLUT2 Δ loop or GLUT2 Δ loopS_{K54S} expressing cells (Supplementary Figures S9B,C). EB.Y.VW4000 cells grew significantly only when expressing GLUT2 Δ loopS_{Q455R} (Supplementary Figure S9), providing further evidence for a crucial effect of this additional point mutation, when combined with the Δ loopS modification, on GLUT2 activity.

As with GLUT3, the ORFs of different GLUT2 variants were transferred into the pRS62K vector and tested for growth in liquid YEP media, using the Cell Growth Quantifier (Aquila Biolabs) (Bruder et al., 2016). In agreement with the results from the drop test, only GLUT2 Δ loopS and GLUT2 Δ loopS_{Q455R}, but not wild-type GLUT2, conferred growth of EB.Y.S7 cells on 0.2% (w/v) glucose (Figure 3A). For EB.Y.VW4000 cells, the additional point mutation in GLUT2 Δ loopS_{Q455R} was essential for growth in this medium (Figure 3B). Interestingly, no growth of EB.Y.S7 cells expressing either of the loop constructs was observed on 0.2% (w/v) fructose medium, while the positive controls expressing Hxt1 showed normal growth (data not shown).



This is likely due to the very low affinity of GLUT2 for fructose ($K_M = \sim 76$ mM) (Mueckler and Thorens, 2013). However, on 2% (w/v) fructose, both loop constructs conferred robust growth (Figure 3C). Analysis of the apparent maximal growth rates with the CGQuant Software (Bruder et al., 2016) showed a significantly faster doubling rate for EB.Y.S7 cells expressing GLUT2 $_{\Delta loopS_Q455R}$ compared to GLUT2 $_{\Delta loopS}$ -expressing cells on 0.2% (w/v) glucose medium (1.7 times) as well as on 2% (w/v) fructose medium (1.5 times) (Supplementary Table S5).

Subcellular Localization of Different GLUT2 Variants

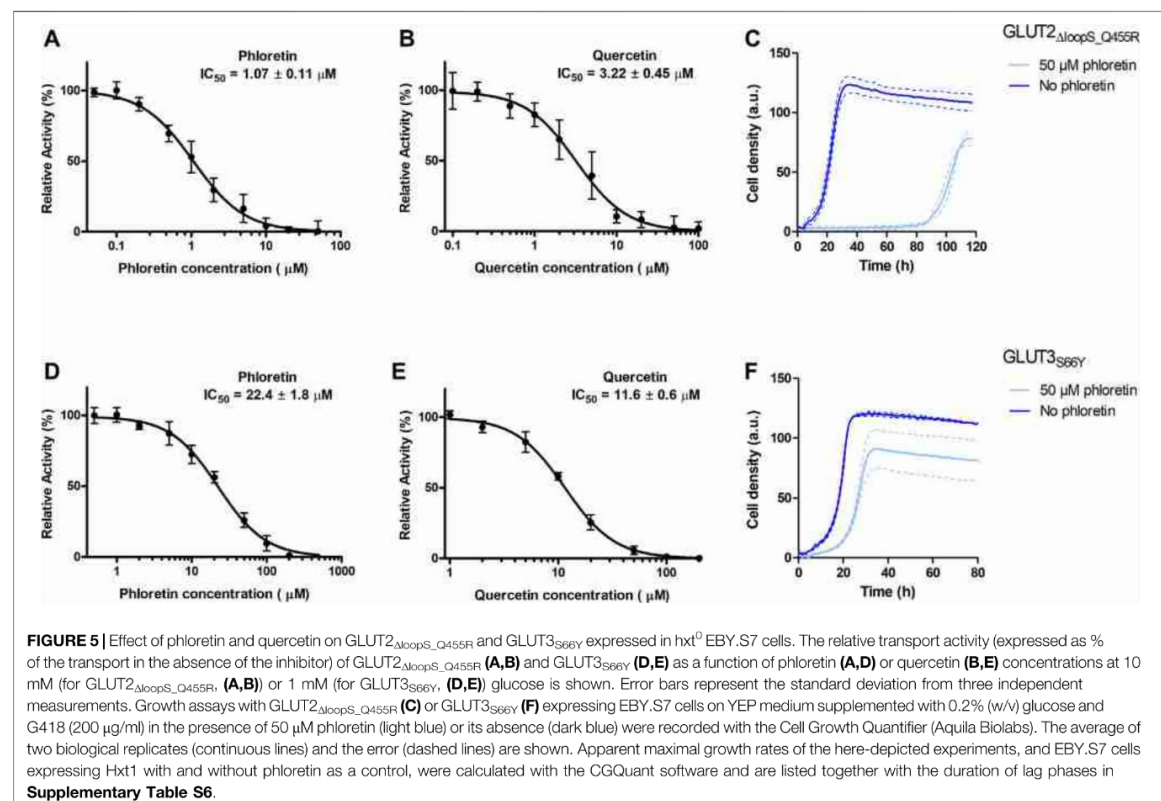
One hypothesis to explain the adverse effect of the extended loop on GLUT2 activity in yeast is possible interference with the transporter's targeting to the plasma membrane. To test if our loop modifications influence the transporter trafficking, we fused the strong GFP variant envyGFP (Slubowski et al., 2015) to the C-terminal ends of the two most active constructs GLUT2 $_{\Delta loopS}$ and GLUT2 $_{\Delta loopS_Q455R}$, and of the inactive wild-type GLUT2. The activity of these envyGFP-tagged transporters was confirmed by the growth of GLUT2 $_{\Delta loopS_Q455R}$ -envyGFP and GLUT2 $_{\Delta loopS}$ -envyGFP-expressing EB.Y.S7 cells on solid SC -URA 0.2% (w/v)

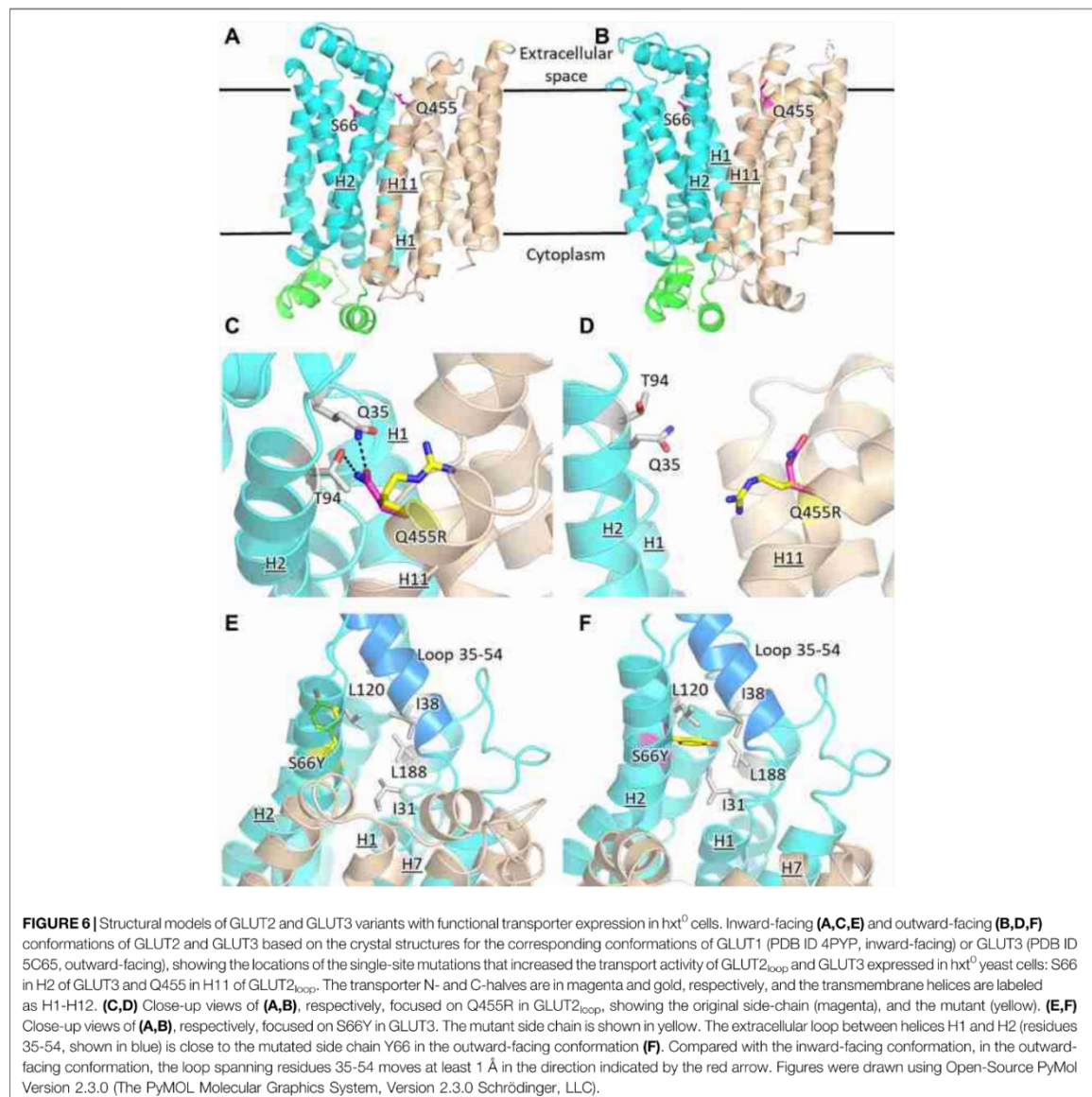
glucose medium (Supplementary Figure S11). Fluorescence microscopy of CEN.PK2-1C cells indeed revealed significant differences between the localization of the wild-type GLUT2 and the two truncated constructs. While cells expressing the latter showed a patchy distribution at the plasma membrane and partial retention in the endomembrane system, unmodified GLUT2 does not reach the plasma membrane and is located in vacuoles (Figure 4), thereby being destined for degradation.

The same pattern was observed in EB.Y.S7 cells (Supplementary Figure S10), demonstrating that the effect of the loop is not dependent on the strain background. Therefore, we conclude that the implemented loop modifications rescue the trafficking defect of GLUT2 in yeast cells. The additional point mutation appears not to influence the subcellular localization of the transporter and putatively improves the transporter's substrate-gating activity by other effects (see below).

The Yeast Platform is Suitable for Screening and Characterizing GLUT Inhibitors

Since the best activities of GLUT2 and GLUT3 constructs were observed in the EB.Y.S7 cells, this strain background was chosen to establish a yeast-based platform for screening and



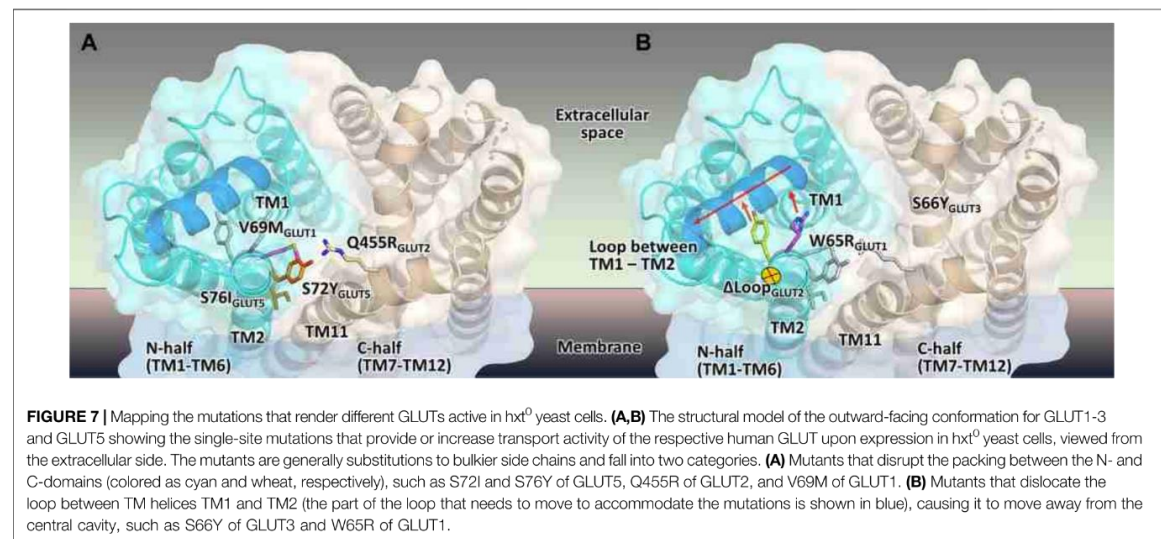


characterizing GLUT inhibitors. Phloretin (Kwon et al., 2007) and quercetin (Lee et al., 2015) are well-known inhibitors of GLUT2 and GLUT3 (Kwon et al., 2007; Augustin, 2010; Lee et al., 2015), and, therefore, we determined their half maximal inhibitory concentration (IC_{50} values) for GLUT2 $_{\Delta loopS_Q455R}$ expressed in EB.Y.S7 (Figures 5A,B).

The values obtained for GLUT2 $_{\Delta loopS_Q455R}$ (IC_{50} of 1.07 ± 0.11 and $3.22 \pm 0.45 \mu M$ for phloretin and quercetin, respectively) indicate a strong inhibition and confirm that yeast-expressed GLUT2 can be reliably used to identify and

characterize transport inhibitors despite the deletion of the extended extracellular loop. This is supported by growth tests in the presence of phloretin. We found that $50 \mu M$ phloretin inhibited the growth of EB.Y.S7 cells expressing GLUT2 $_{\Delta loopS_Q455R}$ significantly, leading to an extensive long lag phase of 87.4 hours, a diminished apparent maximal growth rate (Supplementary Table S6) and a lower maximal cell density (Figure 5C).

Inhibition of GLUT3 $_{S66Y}$ with phloretin and quercetin is less potent than for GLUT2 $_{\Delta loopS_Q455R}$ but still effective, as



demonstrated by the IC_{50} values ($22.4 \pm 1.8 \mu\text{M}$ for phloretin and $11.6 \pm 0.6 \mu\text{M}$ for quercetin) (Figures 5D,E). Moreover, the phloretin IC_{50} values are in the same range as those reported for the related GLUT1 and GLUT4 (Kasahara and Kasahara, 1997). Reflecting the higher IC_{50} values of phloretin compared to those measured with GLUT2 $_{\Delta\text{loopS}_Q455R}$, the growth delay of GLUT3 $_{S66Y}$ expressing EBYS7 cells in glucose containing medium in the presence of $50 \mu\text{M}$ phloretin is less pronounced but still significant (Figure 5F; Supplementary Table S6). In contrast, the apparent maximal growth rates of Hxt1-expressing EBYS7 cells do not show significant differences when grown in the absence or presence of $50 \mu\text{M}$ phloretin (Supplementary Table S6). As all tested transporters were expressed under the control of the truncated Hxt7 promoter, the Hxt1 control shows that the diminished growth phenotypes of GLUT2 $_{\Delta\text{loopS}_Q455R}$ and GLUT3 $_{S66Y}$ -expressing EBYS7 cells upon phloretin addition do not arise from lowered expression levels. Together, these data demonstrate that the yeast system can be conveniently used to screen large compound libraries for potential inhibitors of GLUT2 and GLUT3 in a simple, growth-based manner, amenable to high throughput screening.

Structural Analysis of GLUT2 and GLUT3 Constructs

The prevailing transport mechanism for the Major Facilitator Superfamily (MFS) proteins, including GLUTs, postulates that the substrate cavity of the transporter is alternately open to either side of the membrane with the transporter cycling between the so-called outward- and inward-facing conformations, through a relative rocking of the transporter N- and C- halves (domains) around the active site (Abramson et al., 2003; Yan, 2015). The structural models for GLUT2 $_{\Delta\text{loopS}}$, GLUT2 $_{\Delta\text{loopS}_Q455R}$, GLUT3, and GLUT3 $_{S66Y}$ were based on the crystal structures of the inward-

facing conformation for GLUT1 (PDB ID 4PYP) and the outward-facing conformation of GLUT3 (PDB ID 5C65 or 4ZWC) (Figure 6).

GLUT2 and GLUT3 share 50% and 68% amino acid sequence identity and homology, respectively (determined with MOE, Chemical Computing Group). Cell growth of GLUT-expressing EBYS7 cells showed that additional single mutations in GLUT2 $_{\Delta\text{loopS}}$ and GLUT3 improved the transport activities (Figures 1, 3): Q455R in GLUT2 $_{\Delta\text{loopS}}$ and S66Y in GLUT3. Q455 of GLUT2 is in the outward edge of the TM helix H11, close to the interface between the N- and C-domains (Figure 6A). Its substitution with arginine is inconsequential for the outward-facing conformation (Figures 6B,D), but disruptive for the inward-facing conformation of the transporter; the bulkier guanidinium moiety can no longer participate in the hydrogen bond interactions with Q35 of H1 and T94 of H2 (Figure 6C), sterically crowding its vicinity. In GLUT3, S66 is in the outer periphery of H2, part of a hydrophobic pocket composed of N-domain residues including, I31, I38, L120, and L188, close to the soluble loop linking H1 and H2 (Figures 6A,E,F). In the outward-facing conformation of GLUT3, S66 substitution with the larger side-chain of a tyrosine integrates well, as there is ample space around the loop connecting H1 and H2 (loop 35-54) (Figure 6F). Conversely, in the inward-facing

TABLE 1 | Mutations that enable the transport activity of human GLUTs expressed in *hxt⁰* cells.

Protein	Mutation	Reference
GLUT1	W65R	Wieczorke et al. (2002)
	V69M	
GLUT2 $_{\Delta\text{loopS}}$	Q455R	This study
GLUT3	S66Y	This study
GLUT	S72Y	Tripp et al. (2017)
	S76I	

conformation, loop 35-54 packs near H7, and the tyrosine side-chain is pushed away from the hydrophobic pocket (Figure 6E).

DISCUSSION

The work here completes the generation of GLUT-specific assay systems for class I GLUTs in the versatile and simple platform provided by the engineered yeast cells, *hxt*⁰. These systems enable high-throughput ligand screening for a particular GLUT and determination of the potency and selectivity of the ligand candidates relative to closely related GLUTs within class I, and also class II member, GLUT5. The co-existence of several GLUT isoforms within one tissue or cancer cell line complicates efforts to understand the role of a particular GLUT in the cell pathology or physiology. Thus, besides their medical importance as potential drugs, GLUT-selective inhibitors can also serve as investigative tools to unravel how healthy and abnormal cells adjust their energetic needs through GLUT expression, regulation or function (Carreño et al., 2019). Additionally, GLUT-specific substrate analogs can be optimized as diagnostic tools, especially in cancer detection (Barron et al., 2016; George Thompson et al., 2016; Wuest et al., 2018). Finally, discovery of GLUT-selective activators would be of particular interest in the case of GLUT4 or GLUT2, as strategies to ameliorate diabetes.

Having a GLUT2 assay system is particularly useful. The low affinity for glucose and fructose of this transporter makes it difficult to study its activity when other GLUT isoforms are present, even when GLUT2 is overexpressed. Deleting the loop extension between TM1 and TM2 helices was necessary for the functional expression of GLUT2, and the two transporters showed differences in their inhibition by phloretin and quercetin, with GLUT2 being significantly more sensitive than GLUT3 (Figure 5).

Besides their value for GLUT-specific ligand discovery and characterization, the GLUT expressing yeast systems point to intriguing clues regarding the regions important for transporters activity. As shown here for GLUT2 and GLUT3 and previously reported for GLUT1 (Wieczorke et al., 2002) and GLUT5 (Tripp et al., 2017), the functional expression of these transporters is facilitated or improved by single amino acid substitutions in the transporter sequence (summarized in Table 1, Figure 7). Although the elucidation of the underlying mechanism is complex and not in the scope of this study, structural modeling can help derive hypotheses to explain the observations.

Wild-type transporters and GLUT2_{ΔloopS}, although localized at the membrane, could not compensate for the absence of the endogenous hexose transporters when *EBY.VW4000* cells were grown in media with glucose or fructose as the carbon source. W65R and V69M of GLUT1 (Wieczorke et al., 2002), S66Y of GLUT3 (this study), S72Y and S76I of GLUT5 (Tripp et al., 2017) are all residues in the TM2, near the loop connecting TM helices 1 and 2, which in turn either packs closely to TM helices 7 and 11 (in the inward-facing conformation) or relaxes by moving at least 1 Å away from these helices (in the outward-facing conformation). Intriguingly, Q455R of GLUT2_{ΔloopS} is at the end of TM11, which also approaches the same region: TM1, TM2, and their connecting loop (residues 35-54) (Figures 6, 7). The convergence in the location of the mutations that functionalize the transporters (Figure 7), whether they are part of the Class I GLUTs (like GLUT1-3)

or Class II (like GLUT5), suggests that this region is critical for transport activity of human GLUTs in the yeast system. Consistent with the proposed role of the mutations in GLUT5 (Tripp et al., 2017), the ones described here for GLUT3 and GLUT2_{ΔloopS} (S66Y and Q455R, respectively) also seem to destabilize the inward-facing conformation while leaving the outward-facing one unaffected. More generally, the substitutions that functionalize GLUTs in yeast cells favor an open substrate cavity towards the extracellular space (i.e., outward-facing conformation), either by destabilizing the N- and C-domain interface of the inward-facing conformation (Figure 7A) or by pushing the TM1-TM2 extracellular loop away, leading to a more accessible substrate cavity from the extracellular side (Figure 7B).

Evidently, the lipid composition of the yeast's plasma membrane also impacts the heterologous expression of some human GLUTs (Wieczorke et al., 2002; Schmidl et al., 2018).

In *EBY.S7*, a strain in which the phosphatidylinositol-4-phosphate composition is putatively altered due to the *fyg1* mutation (Schmidl et al., 2018), wild-type GLUT1 and GLUT3, and GLUT2_{ΔloopS}, are actively expressed without any further point mutations. Conceivably, the cycling between the transporter conformations depends on the lipid environment; the relative stabilization of the outward-facing conformation vs. the inward-facing one may be a feature of functional expression of human GLUTs in yeast cells. Activating transport by stabilizing the outward-facing conformation has been documented for another classic MFS protein, LacY, for which interaction of the transporter periplasmic loops with a nanobody against the outward-facing conformation increased the substrate affinity 50-fold (Smirnova et al., 2014). Strikingly, the critical role of lipids in yeast for the functionality of transporters that undergo conformational changes during the transport cycle has been recently demonstrated, supporting our hypothesis (van't Klooster et al., 2020a; van't Klooster et al., 2020b).

For GLUT2, introducing point mutations or screening a combinatorial mini-library of 24 possible aminoacid combinations in the critical TM2 region was not sufficient for activating the transporter, even in strain backgrounds *EBY.S7* and *SDY.022* exhibiting an altered lipid composition. We demonstrated that truncating the large extension of the second extracellular loop, which is a distinctive property of GLUT2 compared to other GLUTs functionally expressed in yeast, was a successful strategy based on a rational approach. As shown by fluorescence microscopy, this modification promotes the trafficking of the transporter to the plasma membrane, whereas the full-length protein is largely retained in the vacuole. In general, the role of the soluble loops in MFS transporters is not well understood, but it is believed that they might affect the gating and conformational dynamics of the transporters (Qureshi et al., 2020). Our results suggest that the GLUT2-specific extension of the second loop is not essential for glucose transport per se. It might rather have a regulatory function, which is probably relevant only within its native environment in the human cells. Similar to our observations, the soluble loops were dispensable for the function of the human nucleoside transporters (belonging to the MFS superfamily) expressed in *Xenopus* oocytes (Aseervatham et al., 2015).

In summary, despite the necessary modifications of their sequence, our transporter variants retain their native function in facilitating glucose (GLUT2, GLUT3) and fructose (GLUT2) uptake. Importantly, they are sensitive to the known inhibitors phloretin and quercetin, which validates our system as a platform for screening and characterizing potential transport inhibitors.

DATA AVAILABILITY STATEMENT

The raw data supporting the conclusions of this article will be made available by the authors, without undue reservation.

AUTHOR CONTRIBUTIONS

Experimental work was performed by SS, SR, and CI. All authors contributed to experimental design and manuscript preparation. J-YC and MO guided the project.

REFERENCES

- Abramson, J., Smirnova, I., Kasho, V., Verner, G., Iwata, S., and Kaback, H.R. (2003). The lactose permease of *Escherichia coli*: overall structure, the sugar-binding site and the alternating access model for transport. *FEBS Lett.* 555, 96–101. doi:10.1016/s0014-5793(03)01087-1
- Ancey, P.-B., Contat, C., and Meylan, E. (2018). Glucose transporters in cancer—from tumor cells to the tumor microenvironment. *FEBS J.* 285, 2926–2943. doi:10.1111/febs.14577
- Aseervatham, J., Tran, L., Machaca, K., and Boudker, O. (2015). The role of flexible loops in folding, trafficking and activity of equilibrative nucleoside transporters. *PLoS One* 10, e0136779. doi:10.1371/journal.pone.0136779
- Augustin, R. (2010). The protein family of glucose transport facilitators: It's not only about glucose after all. *JUBMB life* 62, 315–333. doi:10.1002/iub.315
- Barron, C. C., Bilan, P. J., Tsakiridis, T., and Tsiani, E. (2016). Facilitative glucose transporters: Implications for cancer detection, prognosis and treatment. *Metabolism* 65, 124–139. doi:10.1016/j.metabol.2015.10.007
- Boles, E., Dlugai, S., Mueller, G., and Voss, D. (2004). Use of *Saccharomyces cerevisiae* ERG4 mutants for the expression of glucose transporters from mammals. Geneva, Switzerland: World Intellectual Property Organization. WO002004026907A3.
- Boles, E., and Oreb, M. (2018). A growth-based screening system for hexose transporters in yeast. *Methods Mol. Biol.* 1713, 123–135. doi:10.1007/978-1-4939-7507-5_10
- Brockmann, K. (2009). The expanding phenotype of GLUT1-deficiency syndrome. *Brain Dev.* 31, 545–552. doi:10.1016/j.braindev.2009.02.008
- Bruder, S., Reifenrath, M., Thomik, T., Boles, E., and Herzog, K. (2016). Parallelised online biomass monitoring in shake flasks enables efficient strain and carbon source dependent growth characterisation of *Saccharomyces cerevisiae*. *Microb. Cell Fact.* 15, 127. doi:10.1186/s12934-016-0526-3
- Carreño, D., Corro, N., Torres-Estay, V., Véliz, L. P., Jaimovich, R., Cisternas, P., et al. (2019). Fructose and prostate cancer: toward an integrated view of cancer cell metabolism. *Prostate Cancer Prostatic Dis.* 22, 49–58. doi:10.1038/s41391-018-0072-7
- Chow, T. H. C., Sollitti, P., and Marmur, J. (1989). Structure of the multigene family of MAL loci in *Saccharomyces*. *Mol. Gen. Genet.* 217, 60–69. doi:10.1007/BF00330943
- Colville, C. A., Seatter, M. J., Jess, T. J., Gould, G. W., and Thomas, H. M. (1993). Kinetic analysis of the liver-type (GLUT2) and brain-type (GLUT3) glucose transporters in *Xenopus* oocytes: substrate specificities and effects of transport inhibitors. *Biochem. J.* 290, 701–706. doi:10.1042/bj2900701
- Deng, D., Sun, P., Yan, C., Ke, M., Jiang, X., Xiong, L., et al. (2015). Molecular basis of ligand recognition and transport by glucose transporters. *Nature* 526, 391–396. doi:10.1038/nature14655

FUNDING

Financial support by NIH, grant number R01-GM123103 (to J-YC and MO) and the Boehringer Ingelheim Fonds (travel grant to SS) is gratefully acknowledged.

ACKNOWLEDGMENTS

We thank Christine Essl for assistance and Eckhard Boles for stimulating discussions.

SUPPLEMENTARY MATERIAL

The Supplementary Material for this article can be found online at: <https://www.frontiersin.org/articles/10.3389/fmolb.2020.598419/full#supplementary-material>.

- Entian, K.-D., and Kötter, P. (2007). 25 yeast genetic strain and plasmid collections. *Methods Microbiol.* 36, 629–666. doi:10.1016/S0580-9517(06)36025-4
- Fukumoto, H., Seino, S., Imura, H., Seino, Y., Eddy, R. L., Fukushima, Y., et al. (1988). Sequence, tissue distribution, and chromosomal localization of mRNA encoding a human glucose transporter-like protein. *Proc. Natl. Acad. Sci. U.S.A.* 85, 5434–5438. doi:10.1073/pnas.85.15.5434
- George Thompson, A. M., Ursu, O., Babkin, P., Iancu, C. V., Whang, A., Oprea, T. I., et al. (2016). Discovery of a specific inhibitor of human GLUT5 by virtual screening and *in vitro* transport evaluation. *Sci. Rep.* 6, 24240. doi:10.1038/srep24240
- Gietz, R. D., and Schiestl, R. H. (2007). Frozen competent yeast cells that can be transformed with high efficiency using the LiAc/SS carrier DNA/PEG method. *Nat. protoc.* 2, 1–4. doi:10.1038/nprot.2007.17
- Gould, G. W., and Lienhard, G. E. (1989). Expression of a functional glucose transporter in *Xenopus* oocytes. *Biochemistry* 28, 9447–9452. doi:10.1021/bi00450a030
- Guillemain, G., Loizeau, M., Pinnçon-Raymond, M., Girard, J., and Leturque, A. (2000). The large intracytoplasmic loop of the glucose transporter GLUT2 is involved in glucose signaling in hepatic cells. *J. Cell Sci.* 113, 841–847.
- Hajiaghaalipour, F., Khalilpourfarshbafi, M., and Arya, A. (2015). Modulation of glucose transporter protein by dietary flavonoids in type 2 diabetes mellitus. *Int. J. Biol. Sci.* 11, 508–524. doi:10.7150/ijbs.11241
- Joost, H.-G., and Thorens, B. (2009). The extended GLUT-family of sugar/polyol transport facilitators: Nomenclature, sequence characteristics, and potential function of its novel members. *Mol. Membr. Biol.* 18, 247–256. doi:10.1080/09687680110090456
- Jung, J. H., Wang, X. D., and Loeken, M. R. (2013). Mouse embryonic stem cells established in physiological-glucose media express the high Km Glut2 glucose transporter expressed by normal embryos. *Stem Cell Transl. Med.* 2, 929–934. doi:10.5966/sctm.2013-0093
- Kasahara, T., and Kasahara, M. (1996). Expression of the rat GLUT1 glucose transporter in the yeast *Saccharomyces cerevisiae*. *Biochem. J.* 315, 177–182. doi:10.1042/bj3150177
- Kasahara, T., and Kasahara, M. (1997). Characterization of rat Glut4 glucose transporter expressed in the yeast *Saccharomyces cerevisiae*: comparison with Glut1 glucose transporter. *Biochim. Biophys. Acta* 1324, 111–119. doi:10.1016/S0005-2736(96)00217-9
- Katagiri, H., Asano, T., Ishihara, H., Tsukuda, K., Lin, J.-L., Inukai, K., et al. (1992). Replacement of intracellular C-terminal domain of GLUT1 glucose transporter with that of GLUT2 increases V_{max} and K_m of transport activity. *J. Biol. Chem.* 267, 22550–22555.
- Kraft, T. E., Hresko, R. C., and Hruz, P. W. (2015). Expression, purification, and functional characterization of the insulin-responsive facilitative glucose transporter GLUT4. *Protein Sci.* 24, 2008. doi:10.1002/pro.2812

- Kwok, S., Chang, S.-Y., Sninsky, J. J., and Wang, A. (1994). A guide to the design and use of mismatched and degenerate primers. *PCR Meth. Appl.* 3, 39–47. doi:10.1101/gr.3.4.s39
- Kwon, O., Eck, P., Chen, S., Corpe, C. P., Lee, J.-H., Kruhlik, M., et al. (2007). Inhibition of the intestinal glucose transporter GLUT2 by flavonoids. *FASEB J.* 21, 366–377. doi:10.1096/fj.06-6620com
- Leandro, M. J., Fonseca, C., and Gonçalves, P. (2009). Hexose and pentose transport in ascomycetous yeasts: An overview. *FEMS Yeast Res.* 9, 511–525. doi:10.1111/j.1567-1364.2009.00509.x
- Lee, Y., Lim, Y., and Kwon, O. (2015). Selected phytochemicals and culinary plant extracts inhibit fructose uptake in Caco-2 cells. *Molecules* 20, 17393–17404. doi:10.3390/molecules200917393
- Mueckler, M., and Thorens, B. (2013). The SLC2 (GLUT) family of membrane transporters. *Mol. Aspects Med.* 34, 121–138. doi:10.1016/j.mam.2012.07.001
- Ohtsubo, K., Takamatsu, S., Minowa, M. T., Yoshida, A., Takeuchi, M., and Marth, J. D. (2005). Dietary and genetic control of glucose transporter 2 glycosylation promotes insulin secretion in suppressing diabetes. *Cell* 123, 1307–1321. doi:10.1016/j.cell.2005.09.041
- Oldenburg, K., Vo, K. T., Michaelis, S., and Paddon, C. (1997). Recombination-mediated PCR-directed plasmid construction *in vivo* in yeast. *Nucleic Acids Res.* 25, 451–452. doi:10.1093/nar/25.2.451
- Qureshi, A. A., Suades, A., Matsuoka, R., Brock, J., McComas, S. E., Nji, E., et al. (2020). The molecular basis for sugar import in malaria parasites. *Nature* 578, 321–325. doi:10.1038/s41586-020-1963-z
- Santer, R., Groth, S., Kinner, M., Dombrowski, A., Berry, G. T., Brodehl, J., et al. (2002). The mutation spectrum of the facilitative glucose transporter gene SLC2A2 (GLUT2) in patients with Fanconi-Bickel syndrome. *Hum. Genet.* 110, 21–29. doi:10.1007/s00439-001-0638-6
- Santer, R., Schneppenheim, R., Dombrowski, A., Götze, H., Steinmann, B., and Schaub, J. (1997). Mutations in GLUT2, the gene for the liver-type glucose transporter, in patients with Fanconi-Bickel syndrome. *Nat. Genet.* 17, 324–326. doi:10.1038/ng1197-324
- Schmidl, S., Iancu, C. V., Choe, J.-Y., and Oreb, M. (2018). Ligand screening systems for human glucose transporters as tools in drug discovery. *Front. Chem.* 6, 183. doi:10.3389/fchem.2018.00183
- Schmidl, S., Iancu, C. V., Reifenrath, M., Choe, J.-Y., and Oreb, M. (2021). A label-free real-time method for measuring glucose uptake kinetics in yeast. *FEMS Yeast Res.* 21, foaa069. doi:10.1093/femsyr/foaa069
- Simpson, I. A., Carruthers, A., and Vannucci, S. J. (2007). Supply and demand in cerebral energy metabolism: The role of nutrient transporters. *J. Cereb. Blood. Flow. Metab.* 27, 1766–1791. doi:10.1038/sj.jcbfm.9600521
- Simpson, I. A., Dwyer, D., Malide, D., Moley, K. H., Travis, A., and Vannucci, S. J. (2008). The facilitative glucose transporter GLUT3: 20 years of distinction. *Am. J. Physiol. Endocrinol. Metab.* 295, E242–E253. doi:10.1152/ajpendo.90388.2008
- Slubowski, C. J., Funk, A. D., Roesner, J. M., Paulissen, S. M., and Huang, L. S. (2015). Plasmids for C-terminal tagging in *Saccharomyces cerevisiae* that contain improved GFP proteins. *Envy and Ivy. Yeast* 32, 379–387. doi:10.1002/yea.3065
- Smirnova, I., Kasho, V., Jiang, X., Pardon, E., Steyaert, J., and Kaback, H. R. (2014). Outward-facing conformers of LacY stabilized by nanobodies. *Proc. Natl. Acad. Sci. U.S.A.* 111, 18548–18553. doi:10.1073/pnas.1422265112
- Solis-Escalante, D., van den Broek, M., Kuijpers, N. G. A., Pronk, J. T., Boles, E., Daran, J.-M., et al. (2015). The genome sequence of the popular hexose-transport-deficient *Saccharomyces cerevisiae* strain EBY.VW4000 reveals LoxP/Cre-induced translocations and gene loss. *FEMS Yeast Res.* 15, fou004. doi:10.1093/femsyr/fou004
- Thorens, B. (2015). GLUT2, glucose sensing and glucose homeostasis. *Diabetologia* 58, 221–232. doi:10.1007/s00125-014-3451-1
- Tripp, J., Essl, C., Iancu, C. V., Boles, E., Choe, J.-Y., and Oreb, M. (2017). Establishing a yeast-based screening system for discovery of human GLUT5 inhibitors and activators. *Sci. Rep.* 7, 124. doi:10.1038/s41598-017-06262-4
- Uldry, M., Ibberson, M., Hosokawa, M., and Thorens, B. (2002). GLUT2 is a high affinity glucosamine transporter. *FEBS Lett.* 524, 199–203. doi:10.1016/s0014-5793(02)03058-2
- van't Klooster, J. S., Cheng, T.-Y., Sikkema, H. R., Jeucken, A., Moody, B., and Poolman, B. (2020a). Periprotein lipidomes of *Saccharomyces cerevisiae* provide a flexible environment for conformational changes of membrane proteins. *eLife* 9, e57003. doi:10.7554/eLife.57003
- van't Klooster, J. S., Cheng, T.-Y., Sikkema, H. R., Jeucken, A., Moody, D. B., and Poolman, B. (2020b). Membrane lipid requirements of the lysine transporter Lyp1 from *Saccharomyces cerevisiae*. *J. Mol. Biol.* 432, 4023–4031. doi:10.1016/j.jmb.2020.04.029
- Wieczorke, R., Dlugai, S., Krampe, S., and Boles, E. (2002). Characterisation of mammalian GLUT glucose transporters in a heterologous yeast expression system. *Cell. Physiol. Biochem.* 13, 123–134. doi:10.1159/000071863
- Wieczorke, R., Krampe, S., Weierstall, T., Freidel, K., Hollenberg, C. P., and Boles, E. (1999). Concurrent knock-out of at least 20 transporter genes is required to block uptake of hexoses in *Saccharomyces cerevisiae*. *FEBS Lett.* 464, 123–128. doi:10.1016/S0014-5793(99)01698-1
- Wu, X., Chi, R. J., Baskin, J. M., Lucast, L., Burd, C. G., De Camilli, P., et al. (2014). Structural insights into assembly and regulation of the plasma membrane phosphatidylinositol 4-kinase complex. *Dev. Cell* 28, 19–29. doi:10.1016/j.devcel.2013.11.012
- Wuest, M., Hamann, I., Bouvet, V., Glubrecht, D., Marshall, A., Trayner, B., et al. (2018). Molecular imaging of GLUT1 and GLUT5 in breast cancer: a multitracers positron emission tomography imaging study in mice. *Mol. Pharmacol.* 93, 79–89. doi:10.1124/mol.117.110007
- Yan, N. (2015). Structural biology of the major facilitator superfamily transporters. *Annu. Rev. Biophys.* 44, 257–283. doi:10.1146/annurev-biophys-060414-033901
- Zamora-Leon, S. P., Golde, D. W., Concha, I. I., Rivas, C. I., Delgado-Lopez, F., Baselga, J., et al. (1996). Expression of the fructose transporter GLUT5 in human breast cancer. *Proc. Natl. Acad. Sci. U.S.A.* 93, 1847–1852. doi:10.1073/pnas.93.5.1847
- Ziegler, G. C., Almos, P., McNeill, R. V., Jansch, C., and Lesch, K.-P. (2020). Cellular effects and clinical implications of SLC2A3 copy number variation. *J. Cell. Physiol.* 2020, 1–16. doi:10.1002/jcp.29753

Conflict of Interest: The authors declare that the research was conducted in the absence of any commercial or financial relationships that could be construed as a potential conflict of interest.

Copyright © 2021 Schmidl, Tamayo Rojas, Iancu, Choe and Oreb. This is an open-access article distributed under the terms of the Creative Commons Attribution License (CC BY). The use, distribution or reproduction in other forums is permitted, provided the original author(s) and the copyright owner(s) are credited and that the original publication in this journal is cited, in accordance with accepted academic practice. No use, distribution or reproduction is permitted which does not comply with these terms.

Supplementary Information

Functional expression of the human glucose transporters GLUT2 and GLUT3 in yeast offers novel screening systems for GLUT-targeting drugs

Sina Schmid¹, Sebastian A. Tamayo Rojas¹, Cristina V. Iancu², Jun-yong Choe^{2,3*} and Mislav Oreb^{1*}

¹Institute of Molecular Biosciences, Faculty of Biological Sciences, Goethe University Frankfurt, Frankfurt am Main, Germany

²Department of Chemistry, East Carolina Diabetes and Obesity Institute, East Carolina University, Greenville, NC, USA

³Department of Biochemistry and Molecular Biology, The Chicago Medical School, Rosalind Franklin University of Medicine and Science, North Chicago, IL, USA

*Corresponding authors

Mislav Oreb
Goethe University Frankfurt
Institute of Molecular Biosciences
Max-von-Laue Straße 9
60438 Frankfurt
Germany
Telephone +49 (0)69 798 29331
Telefax +49 (0)69 798 29527
E-Mail m.oreb@bio.uni-frankfurt.de

Jun-yong Choe
East Carolina University
Department of Chemistry
East Carolina Diabetes and Obesity Institute
105 Heart Drive
ECHI Rm 4114
Greenville, NC27834
USA
Telephone 1-252-744-3368
E-Mail Choej18@ecu.edu

Supplementary Table S1. Strains used in this study

Strain name	Relevant genotype	Reference
EBY.VW4000	<i>MATa leu2-3,112 ura3-52 trp1-289 his3-1 MAL2-8c SUC2 Δhxt1-17 Δgal2 Δstl1 Δagt1 Δmph2 Δmph3</i>	Wieczorke et al., 1999
EBY.S7	<i>MATa leu2-3,112 ura3-52 trp1-289 his3-Δ1 MAL2-8C SUC2 Δhxt1-17 Δgal2 Δagt1 Δstl1 fgy1-1</i>	Wieczorke et al., 2002
SDY.022	<i>MATa leu2- 3,112 ura3-52 trp1-289 his3-Δ1 MAL2-8C SUC2 Δhxt1-17 Δgal2 Δagt1 Δstl1 fgy1-1 erg4::kanMX</i>	Boles et al., 2004
CEN.PK2-1C	<i>MATa leu2-3,112 ura3-52 trp1-289 his3-Δ1 MAL2-8C SUC2</i>	Entian and Kötter, 2007

Supplementary Table S2. DNA sequences of the transporters GLUT2 and GLUT3

Shown are wild-type sequences or codon optimized sequences (opt) for expression in insect cells.

GLUT transporter	ORF sequence
GLUT2	ATGACAGAAGATAAGGTCACCTGGGACCCTGGTTTTTCACGTGCATCACTGCTGTGCTGGGTTCCCTCCAGTT TGGATATGACATTGGTGTGATCAATGCACCTCAACAGGTAATAATATCTCACTATAGACATGTTTTGGGTG TTCCACTGGATGACCGAAAAGCTATCAACAACATATGTTATCAACAGTACAGATGAAGTCCCAATCTCA TACTCAATGAACCCAAAACCAACCCCTTGGGGCTGAGGAAGAGACTGTGGCAGCTGCTCAACTAATCACCAT GCTCTGGTCCCTGTCTGTATCCAGCTTTGCAGTTGGTGGAAATGACTGCATCATTCTTTGGTGGGTGGCTTG GGACACACTTGGGAAGAATCAAAGCCATGTTAGTAGCAAACATTTGTCAATTAGTTGGAGCTCTCTTGATG GGTTTTTCAAATTTGGGACCATCTCATATACTTATAATTGCTGGAAGAAGCATATCAGGACTATATTGTGG GCTAATTTTCAAGCCCTGGTTCCTATGTATATCGGTGAAATTTGCTCCAACCGCTCTCAGGGGAGCACTTGGCA CTTTTCATCAGCTGGCCATCGTCACGGGCACTTCTTATTAGTCAGATTATTGGTCTTGAATTTATCTTGGG AATFATGATCTGTGGCACATCTGCTTGGCCCTGTCTGGTGTGCGAGCCATCCTTCAGTCTCTGCTACTCTT TTCTGTCCAGAAAAGCCCAAGATACCTTTACATCAAGTTAGATGAGGAAGTCAAAGCAAAACAAAGCTTGA AAAGACTCAGAGGATATGATGATGTCACCAAAGATATTAATGAAATGAGAAAAGAGAAGAAGCATCG AGTGAGCAGAAAGTCTCTATAATTCAGCTCTTCAACCAATTCAGCTACCGACAGCCTATTCTAGTGGCAGT GATGCTGCATGTGGCTCAGCAATTTTCCGGAATCAATGGCATTTTTTACTACTCAACCAGCATTTTTTCA CGGCTGGTATCAGCAAACCTGTTTATGCAACCATTTGGAGTTGGCGCTGTAACATGGTTTTTCACTGCTGTC TCTGTATTCTTGTGGAGAAGGCAGGGCGACGTTCTCTCTTTCTAATTGGAATGAGTGGGATGTTTGTGTTG TGCCATCTTCATGTCAGTGGGACTTGTGCTGCTGAATAAGTTCTCTTGGATGAGTTATGTGAGCATGATAG CCATCTTCTCTTTTGTAGCTTCTTTGAAATTTGGCCAGGCCGATCCCTGGTTCATGGTGGCTGAGTTT TTCAGTCAAGGACCAGTCCCTGCTGCTTTAGCAATAGCTGCATTCAGCAATTTGGACCTGCAATTTTCAATTGT AGCTCTGTGTTTTCCAGTACATTTGCGGACTTCTGTGGACCTTATGTGTTTTTCTCTTTTGTGGAGTGCTCC TGGCCTTTACCCTGTTTACATTTTTTAAAGTTCCAGAAACCAAAGGAAAGTCTTTTGGAGAAATTTGCTGCA GAATTTCAAAGAAGAGTGGCTCAGCCACAGGCCAAAAGCTGCTGTAGAAATGAAATTCCTAGGAGCTAC AGAGACTGTGTAA
optGLUT2	ATGACCGAAGACAAGTGACCGGTACTCTGGTGTTCACCGTGATTACCGCTGTTCTGGGTAGCTTCCAGTT CGGTATGATATTGGCGTTATCAACCGTCCGCAACAGGTCATCATAGCCACTATCGCCATGTGCTGGGTG TTCCACTGGATGATCGTAAAGCCATCAACAACATACGTTATCAACAGCACTGATGAAGTCCGACCATTAGC TATAGCATGAACCCAAAGCCGACCCCTGGGGCTGAAAGAAGAACTGTTGCCGCTGCCAGCTGATTAATA GCTGTGGAGCCTGAGCGTTAGCAGCTTCGCTGTTGGTGGTATGACCGCCAGCTTCTTCGGTGGTTGGCTGG GTGATACCTGGGTGATCAAAGCCATGCTGGTTGCCAACATCCTGTCTCTGGTTGGTGGTCTCTGCTGATG GGTTTTCTTAAACTGGGTCCATCTCACATCCTGATCATCGCTGGTCTTCTATCTCTGGTCTGTACTGTGG

	<p>TCTGATCTCTGGTCTGGTTCCAATGTACATCGGTGAAATCGCTCCAACCGCTCTGCGTGGTCTCTGGGTA CTTTCCACCAGCTGGCTATTGTTACCGGCATTCTGATCTCTCAGATCATTGGTCTGGAAATTCATCTGGGT AACTACGACCTGTGGCACATCTGCTGGGTCTGAGCGGTGTTCTGCTATCTCTGCAAAGCCTGCTGCTGTT CTTCTGCCCGAAAGCCCGCTTATCTGTATATCAAACCTGGATGAAGAAGTCAAAGCTAAACAGAGCCTGA AACGCTCTGCGTGGTTACGATGACGTGACCAAAGATATCAACGAAATGCGTAAAGAGCGCAAGAAGCTAGC AGCGAGCAGAAGGTTCTATCATTCAACTGTTCAACAACCTAGCTACCGCCAGCCGATCTGCTGCGCCCT GATGCTGCATGTGGCTCAGCAGTTACAGCGGTATTAACGGTATCTTCTATTATAGCACCTCCATTTTCCAGA CCGCTGGCATCTCTAAACCGGTTTATGCTACCATTGGTGTGGTGGCGGTTAACATGGTGTTCACCGCGTT AGCGTTTTCTGGTTGAAAAAGCCGGTCTGCTGTTCTCTGTTCTGATCGGTATGTTCTGGTATGTTCTGGTTG CGCT ATCTTCATGTCTGTGGTCTGGTTCTGCTGAACAAATTCTCTGGATGAGCTACGTTAGCATGATTGCCAT CTTCTGTTCTGTTAGCTTCTTCGAGATCGGTCCGGGTCGATTCCGTTGGTTCATGGTGGCTGAGTCTTCA GCCAAGGTCGCGTCCAGCTGCTCTGGCTATTGCTGCTTCTCCAACCTGGACCTGCAACTTCATCGTTGCT CTGTGTTTCCAATACATTGCTGACTTCTGTGGTCCGTACGTGTTCTTCTGTTCTGCTGGTGTCTGCTGGC TTTCAACCCTGTTACCTTCTTCAAGGTTCCAGAGACCAAAGGCAAGAGCTTCAAGAAATTGCTGCCGAAT TCCAAAAGAAGAGCGGTTCTGCCATCGCCGAAAGCCCGGTTGAGATGAAATTCTGGGTGCTACCGAA ACCGTTTTAA</p>
<p>GLUT3</p>	<p>ATGGGGACACAGAAGGTCACCCAGCTCTGATATTTGCCATCACAGTTGCTACAATCGGCTCTTTCCAATT TGGCTACAACACTGGGGTCATCAATGCTCTGAGAAGATCATAAAGGAATTTATCAATAAAACTTTGACGG ACAAGGGAAATGCCCCACCCCTGAGGTGCTGCTCACGCTCTCTGGTCCCTGTCTGTGGCCATATTTTCC GTCGGGGGTATGATCGGCTCCTTTCCGTCGGACTCTTCGTCACCCGCTTTGGCAGGCGCAATTCATGCT GATTGTCAACCTGTTGGCTGTCACTGGTGGCTGTTTATGGGACTGTGTAAGTAGCTAAGTCGGTTGAAA TGCTGATCTGGGTCGCTTGGTTATTGGCCTCTTCTGCGGACTCTGCACAGGTTTTGTGCCATGTACATT GGAGAGATCTGCCTACTGCCCTGCGGGGTGCCCTTGGCACTCTCAACCAGCTGGGCATCGTTGTTGGAAT TCTGGTGGCCAGATCTTGGTCTGGAAATTCATCTTGGGCTGTAAGAGCTATGGCCCTGCTACTGGGTT TTACCATCCTTCTGCTATCCTACAAAGTGCAGCCCTCCATTTTGCCTGAAAGTCCCAGATTTTGTGCTC ATTAACAGAAAAGAAGAGGAGAATGCTAAGCAGATCCTCCAGCGGTTGTGGGGCACCCAGGATGTATCCCA AGACATCCAGGAGATGAAAGATGAGAGTGCAAGGATGTACAAGAAAAGCAAGTCCCGTGTAGAGCTCT TTAGAGTGTCCAGCTACCGACAGCCCATCATCATTTCCATTTGTGCTCCAGCTCTCTCAGCAGCTCTCTGGG ATCAATGCTGTGTTCTATTACTCAACAGGAATCTCAAGGATGCAGGTGTTCAAGAGCCCATCTATGCCAC CATCGGCGGGGTGTGGTTAATACTATCTTCACTGTAGTTCTCTATTTCTGGTGGAAAGGGCAGGAAGAA GGACTCTGCATATGATAGGCCTTGGAGGATGGCTTTTTGTTCCACGCTCATGACTGTTTCTTTGTTATTA AAGGATAACTATAATGGGATGAGCTTTGTCTGTATTGGGGCTATCTTGGTCTTTGTAGCCTTCTTTGAAAT TGGACCAGGCCCATTCCTGGTTTTATGTGGCCGAACCTTTCAGCCAGGGCCCCGCCAGCTGCGATGG CAGTGGCCGGCTGCTCCAACCTGGACCTCCAACCTTCTAGTCGGATTGCTCTTCCCTCCGCTGCTCACTAT TTAGGAGCCTACGTTTTTATATCTTACCAGGCTTCTCATTACCTTCTTGGCTTTTACCTTCTCAAAGT CCTGAGACCCGTTGGCAGGACTTTTGGAGATATCACACGGGCTTTGAAGGGCAGGCACACGGTGCAGATA GATCTGGAAGGACGGGCTCATGGAGATGAACAGCATCGAGCCTGCTAAGGAGACCACCACCAATGTCTAA</p>
<p>optGLUT3</p>	<p>ATGGGTACTCAGAAAGTGACTCCAGCTCTGATCTTCCGCAATTACCGTTGCCACCATTGGCTCTTTCCAGTT CGGTTACAACACTGGTGTATCAACGCTCCAGAGAAGATCATCAAAGAGTTTCATCAACAAAACCCCTGACCG ATAAAGGCAACGCTCCGCGTCTGAAGTGTGCTGACCTCTCTGTGGTCTCTGTCCGTTGCCATCTTCTCT GTCGGTGGCATGATGGCTCCTTCTCTGTGGTCTGTTCCGTTAACCGCTTCGGTCTGCAACAGCATGCT GATCGTTAACTGCTGGCTGTACTGGTGGTTCATGGGCTCTGTGTAAGTTGCCAAGAGCGTTGAGA TGCTGATTCTGGTCTGTTATCGGCTGTTCTGTGGTCTGTGCACTGGTTCGTGCCGATGTATATC GGTGAGATCTCTCCACTGCTCTGCGTGGTGCCTTCGGCACCTGAACCAACTGGGATCGTGGTTGGCAT CCTGGTTGCCAGATCTTCCGCTGGAGTTCAATCTGGGTAGCGAGGAACCTGGCCCTGCTGCTGGGTT TCACCATTCTGCCAGTATTTCTGAGTCTGCTGCTCTGCCGTTCTGTCCAGAATCTCCGCTTTCTGCTG ATCAACCGTAAAGAGGAGGAGAACGCCAAAACAGATCTGCAACGCTGTGGGTAAGTACAGGACGTTAGCCA GGACATCCAGGAAATGAAAGACGAATCTGCTCGTATGTCTCAGGAGAAGCAGGTTACCGTCTGGAAGTGT TCCGTGTCTCTTACCCTCAGCCGATATCATCTCCATTGTTCTGCAGCTGAGCCAGCAGCTGTCTGGT ATCAACGCCGTTTTCTACTATTCTACTGGCATCTTCAAAGACGCTGGTGTTCAGGAACCGATTTACGCCAC CATCGGTGCTGGTGTGGTGAACACCATCTTACCCTGGTTAGCCTGTTCCGTTGAACGCTGCTGGTCTG GCACTCTGCACATGATGGTCTGGTGGTATGGCCTTCTGCTCTACCCTGATGACCGTTTCTGCTGCTG AAAGACAACATAACGGTATGCTTCTGTTTGCATCGGTGCCATCCTGGTGTTCGTTGCCTTCTTCGAGAT CGGTCCAGTCCGATTCGCTGGTTATCGTTGCTGAACGTTTTCAGCAAGGTTCCAGCTCCAGCTGCCATGG CTGTGGCTGGCTGTTCCAACCTGGACAGCAACTTCTGGTGGTCTGCTGTTCCGCTGCTGCTCACTAT CTGGGTGCTACGTGTTTCATCATCTTACCAGTTTCTGATCACCTTCTGCGCTTCCACTTCTCAAGGT TCCAGAAACCCGTTGGTCTGACCTTCAAGACATCACTGCTGCTTCAAGGTTCAAGCTACGGTGTGATC GCTCTGGCAAAGACGGTGTATGGAGATGAACAGCATCGAACCAGCCAAAGAAACCACTACCAACGTGTAA</p>

Supplementary Table S3. Primers used in this study

Primer name	Sequence 5'-3'	Application
MOP289	CAAGAACAAACAAGCTCAAC	Sequencing primer forward, binds in <i>HXT7</i> promoter region
MOP290	ACCTAGACTTCAGGTTGTC	Sequencing primer reverse, binds in <i>CYC1</i> terminator region
MOP425	CAAAAACAAAAAGTTTTTTTAAATTTTAAATCAAAAAATGACAGAAGATAAG GTCACTG	Amplification of GLUT2 constructs, overhang to <i>HXT7</i> promoter, forward
MOP426	ATGTAAGCGTGACATAACTAATTACATGACTCGAGTTACACAGTCTCTGT AGCTCCTAG	Amplification of GLUT2 constructs, overhang to <i>CYC1</i> terminator, reverse
MOP427	CACAAAAACAAAAAGTTTTTTTAAATTTTAAATCAAAAAATGACCGAAGACA AAGTG	Amplification of optGLUT2 constructs, overhang to <i>HXT7</i> promoter, forward
MOP428	GAATGTAAGCGTGACATAACTAATTACATGACTCGAGTTAAACGGTTTCG GTAGC	Amplification of optGLUT2 constructs, overhang to <i>CYC1</i> terminator, reverse
MOP429	CAAAAACAAAAAGTTTTTTTAAATTTTAAATCAAAAAATGGGGACACAGAAG GTCAC	Amplification of GLUT3 constructs, overhang to <i>HXT7</i> promoter, forward
MOP430	GAATGTAAGCGTGACATAACTAATTACATGACTCGAGTTAGACATTGGTG GTGGTC	Amplification of GLUT3 constructs, overhang to <i>CYC1</i> terminator, reverse
MOP431	ACAAAAACAAAAAGTTTTTTTAAATTTTAAATCAAAAAATGGGTACTIONAGAA AGTGACTC	Amplification of optGLUT3 constructs, overhang to <i>HXT7</i> promoter, forward
MOP432	GAATGTAAGCGTGACATAACTAATTACATGACTCGAGTTACACGTTGGTA GTGGTTTC	Amplification of optGLUT3 constructs, overhang to <i>CYC1</i> terminator, reverse
SSP18	AACTATGTTATCCAAAGTACAGATGAACTGC	Introduce mutation of glycosylation site (N62Q), forward
SSP17	GCAGTTCATCTGTACTTTGGATAACATAGTT	Introduce mutation of glycosylation site (N62Q), reverse
SSP1	CACCATGCTCTGGTCCCTGCTCRKRYTATKTTTGACAGTTGGTGGAATGA CTG	Degenerated primer to introduce a range of mutations in TM2 of GLUT2, forward
SSP2	CAGTCATTCCACCAACTGCAAAMATARYMAYAGACAGGGACCAGAGCATG GTG	Degenerated primer to introduce a range of mutations in TM2 of GLUT2, reverse
SSP3	GATTACTATGCTGTGGAGCCTGAGCRKRYTATKAGCAGCTTCGCTGTTG GTGGTATGAC	Degenerated primer to introduce a range of mutations in TM2 of optGLUT2, forward
SSP4	GTCATACCACCAACAGCGAAGCTGCTMATARYMAYGCTCAGGCTCCACAG CATAGTAATC	Degenerated primer to introduce a range of mutations in TM2 of optGLUT2, reverse

SSP11	CAGGGACCAGAGCATGGTGATTAGTTGAGCTTTTCGGTCATCCAGTGG	Introduction of Δ loop modification to GLUT2, reverse
SSP12	GTTTTGGGTGTTCCACTGGATGACCGAAAAGCTCAACTAATCACCATGCTC	Introduction of Δ loop modification to GLUT2, forward
SSP13	CAGGGACCAGAGCATGGTGATTAGTTGAGCAGATCGGTTCATCCAGTGG	Introduction of K55S_ Δ loop modification to GLUT2, reverse
SSP14	GTTTTGGGTGTTCCACTGGATGACCGATCTGCTCAACTAATCACCATGCTC	Introduction of K55S_ Δ loop modification to GLUT2, forward
SSP15	CAGGGACCAGAGCATGGTGATTAGTTGAGCAGATTTTCGGTCATCCAGTGG	Introduction of Δ loopS modification to GLUT2, reverse
SSP16	GTTTTGGGTGTTCCACTGGATGACCGAAAATCTGCTCAACTAATCACCATGCTC	Introduction of Δ loopS modification to GLUT2, forward
SRP306	ACTACACCTGTAAACAATTCCCTCGCCTTTAGACATCACAGTCTCTGTAGCTCCTAG	Amplification of GLUT2 constructs, overhang to <i>envyGFP</i> , reverse
SRP218	ATGTCTAAAGGCGAGGAATTG	Amplification of <i>envyGFP</i> , forward
SRP58	TAAGCGTGACATAACTAATTACATGACTCGAG	Amplification of <i>envyGFP</i> , URA3 overhang, reverse

Supplementary Table S4. Plasmids used in this study

Plasmid names	Relevant properties	Reference
p426H7	2μ , <i>URA3</i> , <i>Amp^r</i> , <i>HXT7p¹⁻³⁹²</i> , <i>CYC1t</i>	Mumberg et al., 1995 Hamacher et al., 2002
pRS62K	2μ , <i>kanMX</i> , <i>Amp^r</i> , <i>HXT7p¹⁻³⁹²</i> , <i>CYC1t</i>	Taxis and Knop, 2006; Farwick et al., 2013
pUCPY1	<i>CEN6/ARS4</i> , <i>URA3</i> , <i>Amp^r</i> , <i>HXT7p¹⁻³⁹²</i> , <i>CYC1t</i>	Fernando Garces Daza, Goethe Universität Frankfurt
SSV20	p426H7_ <i>Hxt1</i>	This study
SSV16	p426H7_ <i>GLUT1</i>	This study
SSV18	p426H7_ <i>optGLUT3</i>	This study
SSV19	p426H7_ <i>optGLUT3_{S66Y}</i>	This study
SSV21	p426H7_ <i>GLUT2</i>	This study
SSV23	p426H7_ <i>GLUT2Δloop</i>	This study
SSV26	p426H7_ <i>GLUT2_{K54S} Δloop</i>	This study
SSV43	p426H7_ <i>GLUT2ΔloopS</i>	This study
SSV28	p426H7_ <i>GLUT2ΔloopS_ Q455R</i>	This study
SSV45	pRS62K_ <i>Hxt1</i>	This study
SSV46	pRS62K_ <i>GLUT1</i>	This study
SSV47	pRS62K_ <i>GLUT2</i>	This study
SSV48	pRS62K_ <i>GLUT2ΔloopS</i>	This study
SSV49	pRS62K_ <i>GLUT2ΔloopS_ Q455R</i>	This study
SSV87	pRS62K_ <i>optGLUT3</i>	This study
SSV88	pRS62K_ <i>optGLUT3_{S66Y}</i>	This study
SSV89	pUCPY1_ <i>GLUT2_ <i>envyGFP</i></i>	This study
SSV90	pUCPY1_ <i>GLUT2ΔloopS_ <i>envyGFP</i></i>	This study
SSV91	pUCPY1_ <i>GLUT2ΔloopS_ Q455R_ <i>envyGFP</i></i>	This study

Supplementary Table S5. Growth rates and lag phases conferred by different constructs

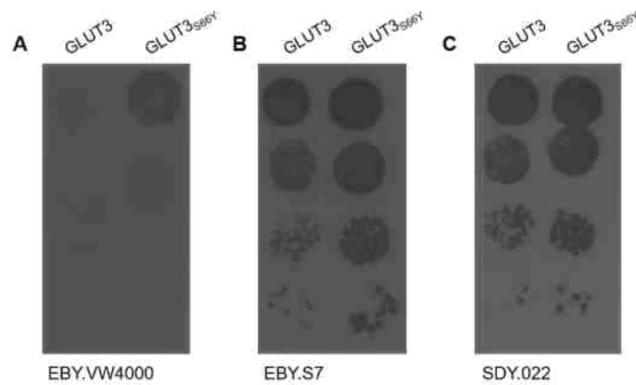
Apparent maximal growth rates (h^{-1}), calculated with the CGQuant software (Aquila Biolabs) as described previously (Bruder et al., 2016) and lag phases (h), determined from growth curves shown in Figure 1 and Figure 3 are listed. For growth rates, the mean values and standard deviation of triplicates are shown. The duration of lag phases did not differ within one position after decimal point between the replicates. The growth rates are significantly different between GLUT3 and GLUT3_{S66Y} as well as between GLUT2 Δ loopS and GLUT2 Δ loopS_Q455R (on both glucose and fructose). The significance was determined by a two-tailed unpaired *t*-test, $p < 0.05$.

Yeast strain	Sugar	Transporter	Max. growth rate (h^{-1})	Lag phase (h)
EBY.S7	0.2 % glucose	Hxt1	0.169 ± 0.036	4.3
		GLUT1	0.117 ± 0.017	7.6
		GLUT3	0.077 ± 0.010	10.7
		GLUT3 _{S66Y}	0.137 ± 0.002	8.5
		GLUT2 Δ loopS	0.049 ± 0.015	13.2
		GLUT2 Δ loopS_Q455R	0.084 ± 0.014	12.3
EBY.VW4000	0.2 % glucose	Hxt1	0.214 ± 0.026	3.4
		GLUT3 _{S66Y}	0.064 ± 0.002	9.9
		GLUT2 Δ loopS_Q455R	0.056 ± 0.011	8.5
EBY.S7	2 % fructose	GLUT2 Δ loopS	0.14 ± 0.029	12.8
		GLUT2 Δ loopS_Q455R	0.21 ± 0.01	17.9

Supplementary Table S6. Effect of phloretin on growth parameters of cells expressing different transporter constructs

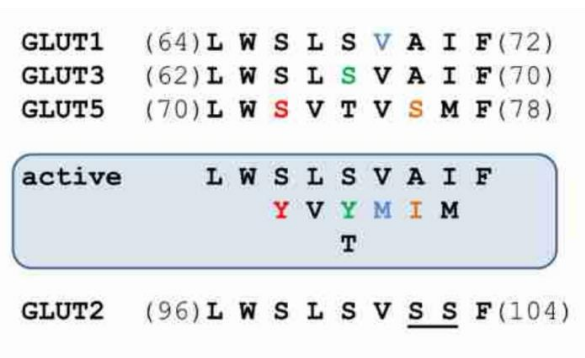
Apparent maximal growth rates (h^{-1}), calculated with the CGQuant software (Aquila Biolabs) as described previously (Bruder et al., 2016) and lag phases (h), determined from growth curves shown in Figure 5 (except for Hxt1; not shown) are listed. For growth rates, the mean values and standard deviation of duplicates were calculated. The duration of lag phases did not differ within one position after decimal point between the replicates. Both the growth rates and the lag phases are significantly affected in the presence of phloretin for GLUT2 Δ loopS_Q455R. In the case of GLUT3_{S66Y}, the growth rates are not significantly different, but the lag phases are. For Hxt1 (control), neither of the growth parameters was significantly affected by phloretin. The significance was determined by a two-tailed unpaired *t*-test, $p < 0.05$.

Yeast strain	Sugar / phloretin		Transporter	Max. growth rate (h^{-1})	Lag phase (h)
EBY.S7	0.2 % glucose	No phloretin	Hxt1	0.169 ± 0.036	4.7
		50 μ M phloretin		0.154 ± 0.012	4.7
EBY.S7	0.2 % glucose	No phloretin	GLUT2 Δ loopS_Q455R	0.099 ± 0.002	7.1
		50 μ M phloretin		0.049 ± 0.008	87.4
EBY.S7	0.2 % glucose	No phloretin	GLUT3 _{S66Y}	0.128 ± 0.016	6.1
		50 μ M phloretin		0.076 ± 0.013	15.6

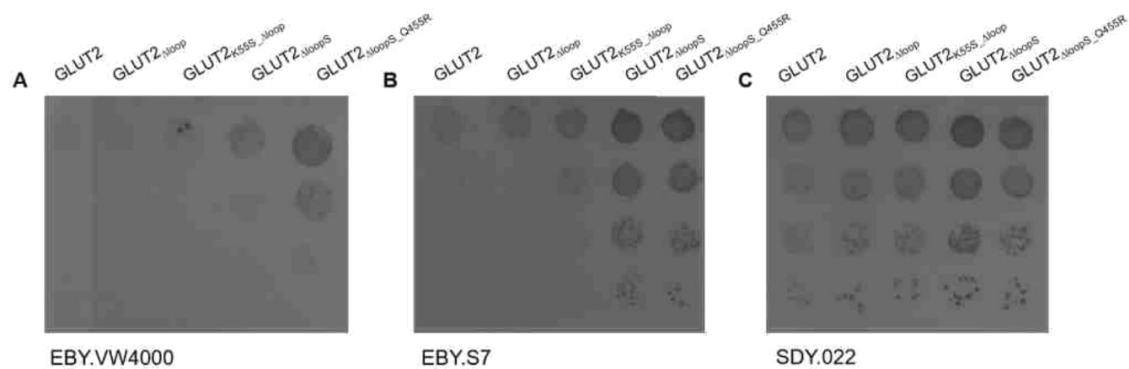


Supplementary Figure S7. Growth test of GLUT3 and GLUT3_{S66Y} expressing cells.

EBY.VW4000 (A), EBY.S7 (B) or SDY.022 (C) cells were grown over night in SC-URA medium containing 1 % maltose, washed and adjusted to an OD_{600nm} of 1 in ddH₂O. 4 µl of dilutions of OD_{600nm} 1, 0.1, 0.01 and 0.001 were dropped onto SC-URA agar plates with 0.2 % glucose. The plates were incubated at 30°C for 5 days.

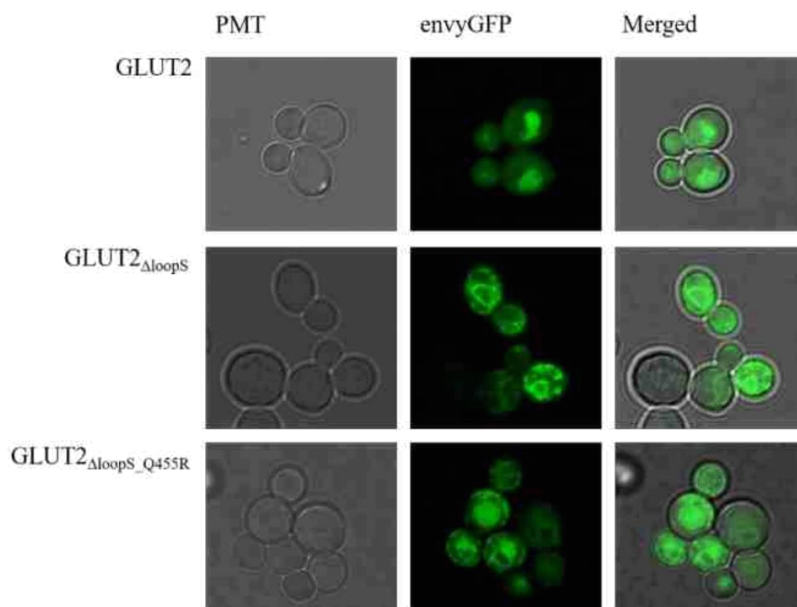


Supplementary Figure S8. Sequence comparison of the critical TM2 region. Amino acid sequence alignment of the TM2 region, in which mutations required for the functional expression of GLUT1, GLUT3, and GLUT5 in EBY.VW4000 cells frequently occurred. The mutated amino acids (colored) are V69M for GLUT1, S66Y for GLUT3, S72Y or S76I for GLUT5. A summary of the amino acids that occurred in at least one active variant at individual positions is shown in the blue box below the alignment. The most striking difference between GLUT2 and the other GLUT sequences - two consecutive serine residues that align to hydrophobic amino acids in the other three GLUTs - is underlined.



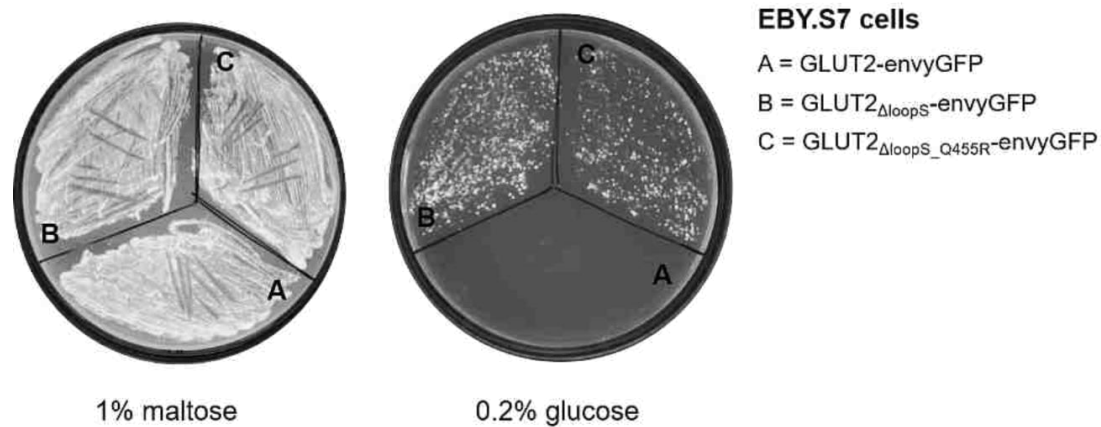
Supplementary Figure S9. Growth test of cells expressing the GLUT2 constructs.

EBY.VW4000 (A), EBY.S7 (B) or SDY.022 (C) cells expressing indicated constructs were grown over night in SC-URA medium containing 1 % maltose, washed and adjusted to an OD_{600nm} of 1 in ddH₂O. 4 μl of dilutions of OD_{600nm} 1, 0.1, 0.01 and 0.001 were dropped onto SC-URA agar plates with 0.2 % glucose. The plates were incubated at 30°C for 5 days.



Supplementary Figure S10. Subcellular localization of GLUT2, GLUT2_{ΔloopS} or

GLUT2_{ΔloopS_Q455R} in EBY.S7. envyGFP was fused to the C-termini of the three GLUT2 constructs. EBY.S7 cells, expressing the respective envyGFP construct, were grown in low fluorescent SC -URA medium containing 1% maltose. For immobilization 0.6 % low melt agarose was added to the suspension and localization was analyzed with the Confocal Laser Scanning Microscope (Zeiss LSM 780, Jena, Germany).



Supplementary Figure S11. Functional expression of the envyGFP-tagged transporter constructs. The C-terminal ends of GLUT2 (A), GLUT2_{ΔloopS} (B) and GLUT2_{ΔloopS_Q455R} (C) were fused to envyGFP. EBY.S7 cells expressing the respective envyGFP-tagged transporter construct on a pUCPY1 (CEN.ARS) plasmid were streaked out on solid SC -URA medium containing either 1 % maltose or 0.2 % glucose. The plates were incubated at 30°C for 5 days.

Supplementary References

- Boles, E., Dlugai, S., Mueller, G., and Voss, D. (2004). *Use of Saccharomyces cerevisiae ERG4 mutants for the expression of glucose transporters from mammals*. WO002004026907A3. Geneva: World Intellectual Property Organization.
- Bruder, S., Reifenrath, M., Thomik, T., Boles, E., and Herzog, K. (2016). Parallelised online biomass monitoring in shake flasks enables efficient strain and carbon source dependent growth characterisation of *Saccharomyces cerevisiae*. *Microb. Cell Fact.* 15, 127. doi: 10.1186/s12934-016-0526-3
- Entian, K. D. and Kötter, P. (2007). Yeast Genetic Strain and Plasmid Collections. *Method. Microbiol.* 36, 629–666. doi: 10.1016/S0580-9517(06)36025-4
- Farwick, A., Bruder, S., Schadeweg, V., Oreb, M. and Boles, E. (2013). Engineering of yeast hexose transporters to transport D-xylose without inhibition by D-glucose. *Proc. Natl. Acad. Sci. USA* 111, 5159–5164. doi: 10.1073/pnas.1323464111
- Hamacher T., Becker J., Gardonyi M., Hahn-Hagerdal B., Boles E. (2002). Characterization of the xylose-transporting properties of yeast hexose transporters and their influence on xylose utilization. *Microbiology* 148, 2783–2788. doi: 10.1099/00221287-148-9-2783
- Mumberg, D., Müller, R., Funk, M. (1995). Yeast vectors for the controlled expression of heterologous proteins in different genetic backgrounds. *Gene* 156, 119–122.
- Taxis, C., and Knop, M. (2006). System of centromeric, episomal, and integrative vectors based on drug resistance markers for *Saccharomyces cerevisiae*. *BioTechniques* 40, 73–78. doi: 10.2144/000112040
- Wieczorke, R., Dlugai, S., Krampe, S., and Boles, E. (2002). Characterisation of mammalian GLUT glucose transporters in a heterologous yeast expression system. *Cell. Physiol. Biochem.* 13, 123–134. doi: 10.1159/000071863
- Wieczorke, R., Krampe, S., Weierstall, T., Freidel, K., Hollenberg, C. P., and Boles, E. (1999). Concurrent knock-out of at least 20 transporter genes is required to block uptake of hexoses in *Saccharomyces cerevisiae*. *FEBS Lett.* 464, 123–128. doi: 10.1016/S0014-5793(99)01698-1

6.4 Identification of new GLUT2-selective inhibitors through *in silico* ligand screening and validation in eukaryotic expression systems

Declaration of author contributions to the publication:

Identification of new GLUT2-selective inhibitors through *in silico* ligand screening and validation in eukaryotic expression systems

Status: published, July 2021

Journal: Scientific Reports

Type of manuscript: research article

Contributing authors: Sina Schmidl (SS)*, Oleg Ursu (OU)*, Cristina V. Iancu (CVI), Mislav Oreb (MO), Tudor Oprea (TO) & Jun-yong Choe (JYC)

* Shared first authorship

Contributions of doctoral candidate and co-authors

(1) Concept and design

Doctoral candidate SS: 20%

Co-authors OU, CVI, MO, TO, JYC: 15%, 15%, 5%, 15%, 30%

(2) Conducting tests and experiments

Doctoral candidate SS: 25%, provision of yeast strains, screening with the yeast system

Co-authors OU, CVI, TO, JYC: 25%, 20%, 10%, 20%, structural modeling, *in silico* screening, screening with the yeast system

(3) Compilation of data sets and figures

Doctoral candidate SS: 20%

Co-author OU, CVI, JYC, TO: 25%, 25%, 25%, 5%

(4) Analysis and interpretation of data

Doctoral candidate SS: 25%

Co-authors OU, CVI, JYC: 20%, 25%, 30%

(5) Drafting of manuscript

Doctoral candidate SS: 70%

Co-authors OU, CVI, JYC: 10%, 10%, 10%



OPEN

Identification of new GLUT2-selective inhibitors through in silico ligand screening and validation in eukaryotic expression systems

Sina Schmidl^{1,7}, Oleg Ursu^{2,6,7}, Cristina V. Iancu³, Mislav Oreb¹, Tudor I. Oprea^{2,4,5} & Jun-yong Choe^{3,5}✉

Glucose is an essential energy source for cells. In humans, its passive diffusion through the cell membrane is facilitated by members of the glucose transporter family (GLUT, SLC2 gene family). GLUT2 transports both glucose and fructose with low affinity and plays a critical role in glucose sensing mechanisms. Alterations in the function or expression of GLUT2 are involved in the Fanconi-Bickel syndrome, diabetes, and cancer. Distinguishing GLUT2 transport in tissues where other GLUTs coexist is challenging due to the low affinity of GLUT2 for glucose and fructose and the scarcity of GLUT-specific modulators. By combining in silico ligand screening of an inward-facing conformation model of GLUT2 and glucose uptake assays in a hexose transporter-deficient yeast strain, in which the GLUT1-5 can be expressed individually, we identified eleven new GLUT2 inhibitors (IC₅₀ ranging from 0.61 to 19.3 μM). Among them, nine were GLUT2-selective, one inhibited GLUT1-4 (pan-Class I GLUT inhibitor), and another inhibited GLUT5 only. All these inhibitors dock to the substrate cavity periphery, close to the large cytosolic loop connecting the two transporter halves, outside the substrate-binding site. The GLUT2 inhibitors described here have various applications; GLUT2-specific inhibitors can serve as tools to examine the pathophysiological role of GLUT2 relative to other GLUTs, the pan-Class I GLUT inhibitor can block glucose entry in cancer cells, and the GLUT2/GLUT5 inhibitor can reduce the intestinal absorption of fructose to combat the harmful effects of a high-fructose diet.

Human glucose transporters (GLUTs), proteins of the *SLC2* gene family, facilitate the diffusion of hexoses into the cell and play a pivotal role in glucose homeostasis¹. Important diseases, including cancer² and diabetes^{3,4}, are related to the dysfunction or misregulation of these transporters, identifying them as potential drug targets¹. The 14 GLUT isoforms present in humans show an amino acid identity of 19–65% (homology of 42–81%)⁵ but differ in substrate specificity, affinity, and tissue distribution⁵. According to their sequence similarities, three classes of GLUTs have been defined⁷ with GLUT1-4 representing Class I, GLUTs 5, 7, 9, and 11 in Class II and GLUTs 6, 8, 10, 12, and 13 forming Class III^{6,7}.

All GLUTs are furthermore part of the large major facilitator superfamily (MFS) and display the MFS-typical structure of twelve transmembrane helices (TM1–TM12; Supplementary Fig. S1) organized in two halves (N-terminal half: TM1–TM6 and C-terminal half: TM7–TM12) with a central substrate cavity⁵. Proposed mechanisms for sugar transport are the alternating access mechanism⁸, in which the substrate binding site is open to either

¹Institute of Molecular Biosciences, Faculty of Biological Sciences, Goethe University Frankfurt, Frankfurt am Main, Germany. ²Translational Informatics Division, Department of Internal Medicine, The University of New Mexico School of Medicine, Albuquerque, NM 87131, USA. ³Department of Chemistry, East Carolina Diabetes and Obesity Institute, East Carolina University, Greenville, NC 27834, USA. ⁴UNM Comprehensive Cancer Center, The University of New Mexico, Albuquerque, NM 87131, USA. ⁵Department of Biochemistry and Molecular Biology, The Chicago Medical School, Rosalind Franklin University of Medicine and Science, North Chicago, IL 60064, USA. ⁶Present address: Computational and Structural Chemistry, Merck & Co., Inc., 2000 Galloping Hill Road, Kenilworth, NJ 07033, USA. ⁷These authors contributed equally: Sina Schmidl and Oleg Ursu. ✉email: toprea@salud.unm.edu; choej18@ecu.edu

the outside (exofacial, outward-facing) or inside (endofacial, inward-facing) space of the cell, and the fixed-site transporter with concurrent endo- and exo-facial substrate binding sites^{9,10}. A hybrid mechanism that combines features of both proposed mechanisms, and is consistent with structural, kinetic, and modeling data of GLUT1 suggests that this transporter is an oligomer of allosteric, alternating access transporters¹¹.

Three-dimensional structure determinations of GLUTs^{12–14} and their bacterial homologues^{5,15} have provided important information on the transport mechanisms and paved the way for structure-based drug design¹⁶, as exemplified by the discovery of a specific GLUT5 inhibitor¹⁷. For this, an extensive number of small compounds are screened *in silico* for binding to the respective transporter, as a first step¹⁷. Promising candidates can then be examined in an appropriate assay system¹⁶, and, if successful, be further developed into drugs.

Among GLUTs, GLUT2 is unique in its very low apparent affinity for glucose ($K_M = \sim 17$ mM)¹⁸, which significantly surpasses fasting blood glucose levels (~ 5.5 mM)¹⁹, and for the substrates fructose ($K_M = \sim 76$ mM)⁶, galactose ($K_M = \sim 92$ mM)⁶, and mannose ($K_M = \sim 125$ mM)⁶. The significance of GLUT2 lies in its regulatory functions such as glucose sensing³ and signaling^{20,21}. Evidently, GLUT2 plays a crucial role in maintaining glucose homeostasis in many human tissues, such as the intestine, liver, kidney, and brain^{20–25}.

Inactivating mutations in the GLUT2-encoding gene lead to the rare but severe Fanconi–Bickel syndrome²⁶. Patients suffering from this autosomal, recessive disease show very diverse symptoms²⁶, and its treatment is challenging due to the lack of effective drugs²⁷. The wide spectrum of Fanconi–Bickel syndrome symptoms, including many atypical ones, also make its diagnosis difficult, and more cases with unusual pathological reports are still discovered²⁶. Due to its many regulatory functions, a role of GLUT2 in the pathogenesis of diabetes is also discussed^{28–30}. Generally, glucose sensing processes are complex and the full extent of GLUT2 in them is not yet fully elucidated; therefore, an abnormal function of GLUT2 might be the still undiagnosed cause of more clinical signs. Hence, GLUT2 is an important pharmaceutical target, and specific effectors will allow a more tailored treatment for GLUT2-involving diseases and expand our knowledge about its physiological role when applied in relevant studies. Furthermore, identifying GLUT2-specific ligands might provide new ways to explore the basis of substrate specificity among GLUT members³¹.

Several compounds were discovered that effectively inhibit glucose uptake via GLUTs in cell lines³². Glupin and glutor, for example, are very potent inhibitors for GLUT1 and 3 or GLUT1–3, respectively; 2-deoxy-glucose uptake experiments with human cell lines revealed their high potency with IC_{50} values in the nanomolar range^{33,34}. Moreover, in presence of glupin or glutor the growth of several cancer cell lines was attenuated. Similarly, the pan-Class I inhibitor DRB18 showed potent anticancer activity³⁵, supporting Class I GLUT inhibitors as promising anticancer probes. Several flavonoids are known to have an inhibitory effect on GLUT2, including quercetin, phloretin, isoquercitrin, myricetin, fisetin, apigenin, and tiliroside^{36,37}. However, most show little potency ($IC_{50} > 60$ μ M)³⁶, and the more potent inhibitors quercetin and phloretin ($IC_{50} < 4$ μ M)³⁸ inhibit not only GLUT2 but also other GLUTs³⁸ or, in the case of quercetin, the Vitamin C transporter SVCT1³⁹. Identifying new, potent, and specific GLUT2 inhibitors is desirable but challenging due to GLUT2 low affinity for glucose and fructose and a background uptake of these substrates by other GLUT isoforms in human cell lines.

In this study, we used the recently established yeast cell-based system expressing human GLUT2³⁸ to screen 163 small compounds that have been selected by *in silico* ligand screening of a GLUT2 inward-facing conformation model. Eleven candidates showed a high potency ($IC_{50} < 20$ μ M) for inhibiting glucose uptake via GLUT2. Further examination of these GLUT2 inhibitors in the yeast cell-based systems expressing GLUT1⁴⁰, GLUT3³⁸, GLUT4⁴⁰, or GLUT5⁴¹, showed that nine inhibitors were GLUT2-selective, one inhibited all Class I GLUTs but not GLUT5, and another inhibited GLUT5 but not Class I GLUTs. These candidates are a valuable addition to already existing GLUT2 inhibiting compounds. They will promote the development of GLUT-targeting drugs and a better understanding of GLUT2 biological role in health and disease.

Results

In silico ligand screening against GLUT2 inward-facing conformation structural model. Depending on which side of the cell membrane the substrate cavity opens to, GLUTs have two major conformations captured by the crystal structures of some isoforms and GLUT bacterial homologs^{5,12–15}. For Class I GLUTs, inward-facing conformations have been determined for GLUT1¹², and outward-facing conformations for GLUT3¹³; three-dimensional structures for GLUT2 and GLUT4 are not available. *In silico* ligand screening requires a structural model for the protein target. Even in the absence of crystal structures, the homology modeling of GLUTs based on the available crystal structures has been used successfully to identify new specific ligands. For instance, *in silico* ligand screening with a GLUT5 model in the inward-facing conformation, generated based on the bacterial GLUT homolog GlcP_{se}⁵, produced the first potent and specific GLUT5 inhibitor¹⁷.

The structural model for the GLUT2 inward-facing conformation (Fig. 1) was modeled based on the crystal structure of GLUT1 (PDB ID: 4PYP) with the Molecular Operating Environment (MOE) software (<https://www.chemcomp.com/>). GLUT1 and GLUT2 share 52% and 68% protein sequence identity and similarity, respectively, as determined with Align function in MOE. The docking site, containing the substrate cavity without the substrate binding site, was prepared using OpenEye FRED software (<https://www.eyesopen.com/>). The ChemNavigator library of over 6 million commercially available compounds was prepared for docking using Omega2 and FRED software (<https://www.eyesopen.com/>). The docking studies were conducted using OpenEye FRED software. Docked compounds were scored using Chemgauss4 scoring function. The compounds docked in sites distinct from that of glucose, closer to the substrate cavity entrance (Fig. 1B). Considering commercial availability and affordability, we purchased 163 out of the top 200 scored compounds for experimental validation.

Screening of the lead candidates in the GLUT2-expressing *hxt*⁰ yeast system. To test the 163 compounds selected by *in silico* ligand screening, we utilized the *hxt*⁰ (hexose transporter-deficient) yeast

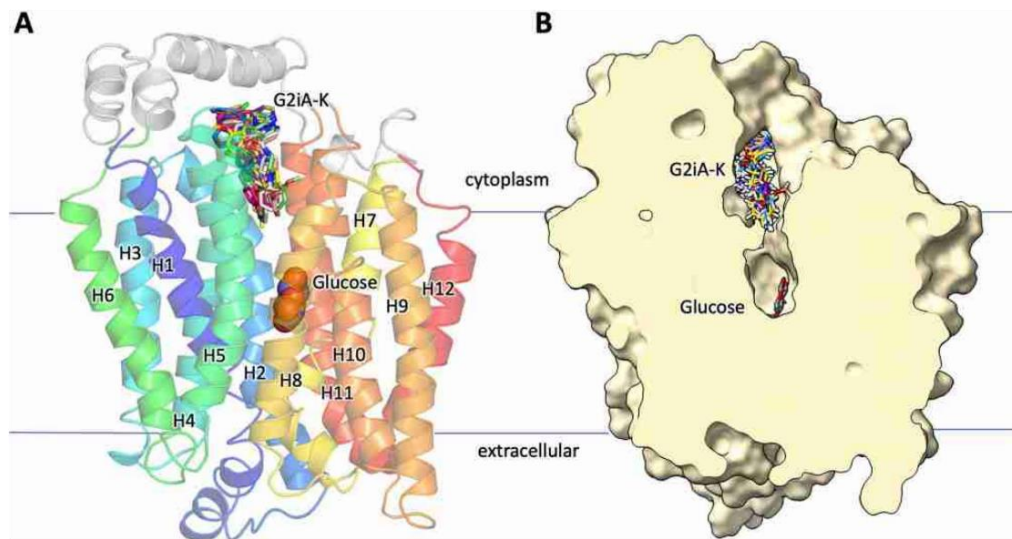


Figure 1. GLUT2 inward-facing conformation model and selected ligands from the virtual screening. The inward-facing conformation of GLUT2 showing the glucose binding site (glucose shown in sphere representation) and several ligands from the virtual screening (Table 1) bound above the glucose binding site (ligands shown as stick representation, in different colors). The homology model was generated based on the GLUT1 crystal structure (PDB ID: 4PYP). (A) GLUT2 model in ribbon diagram, with the transmembrane helices color-coded from blue (first transmembrane helix, H1) to red (last transmembrane helix, H12) (see also Fig. 4L). (B) Central slice through the GLUT2 isosurface showing the substrate cavity containing the glucose binding site and docked ligands. The figure was generated with ChimeraX Version 1.2 (<https://www.rbvi.ucsf.edu/chimera/>) and PyMOL Version 2.3.0 (<https://pymol.org/>).

system that expresses human GLUT2³⁸. Similar GLUT-specific *hxt*⁰ yeast systems are available for all Class I GLUTs and GLUT5^{38,40–42}, providing a convenient assay platform for these transporters' ligands¹⁶. For GLUT2, the applied yeast strain EBY.S7 is devoid of all its endogenous hexose transporters (*hxt*⁰) and carries the *fgy1* mutation³⁶ in the *EFR3* gene, proven to be beneficial for the heterologous expression of human GLUTs¹⁶. The active expression of the transporter required a GLUT2 version with a truncated loop between transmembrane regions TM1 and TM2 and an additional point mutation (GLUT2_{ΔloopS_Q455R})³⁸. GLUT2_{ΔloopS_Q455R} recapitulates the functional properties of GLUT2 closely. For example, GLUT2 expressed in *Xenopus laevis* oocytes had $K_{M, Glucose} = 17 \text{ mM}$ ¹⁸ and $K_{M, Fructose} = 66.7 \pm 18.3 \text{ mM}$ ⁴³, while GLUT2_{ΔloopS_Q455R} had $K_{M, Glucose} = 14.1 \pm 1.3 \text{ mM}$ and $K_{M, Fructose} = 87.0 \pm 8.2 \text{ mM}$ (Supplementary Fig. S2). Also, reported GLUT2 inhibitors, phloretin and quercetin³⁶, inhibited similarly GLUT2_{ΔloopS_Q455R}³⁸, confirming this system's applicability to screening GLUT2 inhibitors.

GLUT2 transport activity was determined as previously described³⁸. Pre-grown yeast cells were washed and resuspended in PBS buffer to an OD_{600nm} of ~10; 100 μl of this cell suspension constituted the assay mix. Uptake activity of GLUT2 was determined by adding C¹⁴-hexose (glucose or fructose), quenching after 10 min, filtering the cells, and measuring the radioactivity with a scintillation counter. Initial compound screening for GLUT2 inhibition was performed at 15 mM glucose concentration (i.e., ~ K_M) and 100 μM of each chemical. While none of the tested compounds mediated an increase in glucose uptake activity by GLUT2, several diminished it significantly (Fig. 2A). Among these, 11 compounds decreased GLUT2 activity by at least 60% and were further examined to determine their respective IC₅₀ value (Fig. 2B). All compounds are effective inhibitors (IC₅₀ < 20 μM); for simplicity, we named them G2i (from GLUT2 inhibitor) A–K in the order of decreasing inhibition potency (Table 1, Fig. 2). G2iA showed the strongest GLUT2 inhibition with an IC₅₀ of 0.61 μM, almost twice as strong as phloretin and five times more potent than quercetin³⁸.

Effect of GLUT2 inhibitors on the other Class I GLUTs and GLUT5. Establishing the selectivity of GLUT2 inhibitors for other GLUT isoforms, particularly its closely related Class I GLUTs, is crucial for future application of these inhibitors. Often several GLUTs coexist in the same tissue, and being able to modulate selectively an individual GLUT provides a powerful tool in unraveling its pathophysiological role. Therefore, to determine the selectivity of the identified GLUT2 inhibitors, we tested them for their effect on the GLUT homologs GLUT1, 3, 4, and 5. For this, *hxt*⁰ yeast cells actively expressing the respective transporter^{38,40–42} were incubated with 100 μM of the tested compound, and the transport activity was assayed in the same manner as for GLUT2 but at substrate concentrations close to the K_M in the respective GLUT (i.e., 5 mM glucose for GLUT1⁴⁴ and GLUT4⁴⁴, 1.5 mM glucose for GLUT3⁴³, 10 mM fructose for GLUT5⁴¹) (Fig. 3A). GLUT2 is more closely

www.nature.com/scientificreports/

GLUT2 inhibitor	Structure_ID	Chemical name	Structure	IC ₅₀ (μM)
G2iA	30865539	4-(5-(4-Fluorophenyl)-1-[[2-methyl-1H-indol-3-yl)sulfanyl]acetyl]-4,5-dihydro-1H-pyrazol-3-yl)phenyl methyl ether		0.61 ± 0.09
G2iB	121097081	N-Benzyl-N-(2-[[4-(4-chlorophenyl)-1-(3,4-dimethoxyphenyl)-1H-imidazol-2-yl]amino]-2-oxoethyl)-4-methylbenzamide		1.89 ± 0.52
G2iC	181278705	2-(5-Cyclopropyl-4-[[4-(2-methoxyphenyl)-1-piperazinyl]carbonyl]-1H-pyrazol-1-yl)-4-(2-thienyl)pyrimidine		2.87 ± 0.34
G2iD	466119877	2-[5-(Methoxymethyl)-4-[[4-(phenyl-1-piperazinyl)carbonyl]-1H-pyrazol-1-yl]-6,7-dihydro-5H-benzo[6,7]cyclohepta[1,2-d]pyrimidine		6.08 ± 1.52
G2iE	181349814	2-(4-(1-Benzothien-3-yl)-2-[[4-(2-pyridinyl)-1-piperazinyl]methyl]phenoxy)-N-(1,3-thiazol-2-ylmethyl)acetamide		6.32 ± 2.43
G2iF	182001206	5-Cyclopropyl-1-(5,6-dihydrobenzo[h]quinazolin-2-yl)-N-methyl-N-(5-quinolinylmethyl)-1H-pyrazole-4-carboxamide		7.07 ± 1.84
G2iG	34713223	N-(4-Isopropylphenyl)-3-[[4-(2-methoxyphenyl)-1-piperazinyl]carbonyl]-4-oxo-1,4-dihydro-6-quinolinesulfonamide		10.2 ± 2.0
G2iH	50759467	N-[2-(2-Chlorophenyl)-2-(1H-indol-3-yl)ethyl]-2-(1H-indol-3-yl)acetamide		10.5 ± 4.0
Continued				

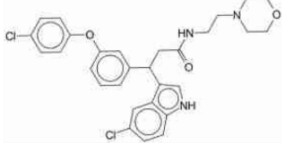
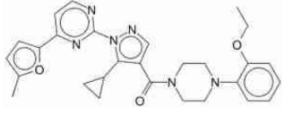
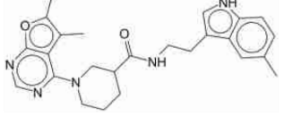
GLUT2 inhibitor	Structure_ID	Chemical name	Structure	IC ₅₀ (μM)
G2iI	332651912	3-(5-Chloro-1H-indol-3-yl)-3-[3-(4-chlorophenoxy)phenyl]-N-[2-(4-morpholinyl)ethyl]propanamide		13.3 ± 1.6
G2iJ	181305778	2-(5-Cyclopropyl-4-[[4-(2-ethoxyphenyl)-1-piperazinyl]carbonyl]-1H-pyrazol-1-yl)-4-(5-methyl-2-furyl)pyrimidine		15.9 ± 2.7
G2iK	111278730	1-(5,6-Dimethylfuro[2,3-d]pyrimidin-4-yl)-N-[2-(5-methyl-1H-indol-3-yl)ethyl]-3-piperidinecarboxamide		19.3 ± 7.9

Table 1. Structures and chemical names of potent (IC₅₀ < 20 μM) GLUT2 inhibitors. Structure_ID refers to the ChemNavigator structure identifier.

related to the other Class I GLUTs (52–65% sequence identity) than GLUT5 (Class II GLUT, 40% sequence identity)⁵. Nevertheless, most GLUT2 inhibitors seem to have only negligible inhibitory effects on the other GLUTs (Fig. 3A). Thus, only G2iF inhibits GLUT1, 3, and 4, whereas G2iI decreased just GLUT5 activity (Fig. 3A). However, G2iF IC₅₀ values were higher for other GLUTs (33 μM for GLUT1, 19 μM for GLUT3 and 14 μM for GLUT4) than for GLUT2 (7 μM); the same was found for the IC₅₀ of G2iI (23 μM for GLUT5 vs. 13 μM for GLUT2) (Fig. 3B–E). Importantly, all other tested compounds, including the most potent GLUT2 inhibitor G2iA appear not to significantly affect the other GLUTs tested, indicating that these are GLUT2-specific.

Docking sites of GLUT2 inhibitors. The virtual ligand screening showed that all 11 GLUT2 inhibitors docked to the inward-facing conformation of GLUT2 in sites distinct from that of glucose, closer to the substrate cavity entrance (Fig. 1B). The two most potent GLUT2 inhibitors, G2iA and G2iB, showed noncompetitive inhibition with glucose (Supplementary Fig. S3), consistent with their binding site being distinct from that of the substrate.

Protein–ligand interactions (Fig. 4 and Supplementary Fig. S4) include hydrogen-bonds with charged residues from the cytosolic loops or transmembrane (TM) helix ends (D120, R124, E178, R181, R185, R244, K249, E279, R280, R432), backbone carbonyls (G177, P433) or polar residues from TM helices (S112, Q193); hydrophobic or Van der Waals interactions (M174, A283, L436); and cation-π interactions with guanidinium groups (R244, R280). Among these, the residues that are not conserved in GLUT1-5 are D120, K249, R280, A283, W420, and L436 (Fig. 4L). G2iA is oriented in its pocket by hydrophobic interactions with M174 and L436, a hydrogen bond of its amino indole group with the sidechain of S112, a polar interaction of its phenyl fluorine with the R280 guanidinium group, as well as a cation-π interaction of the fluorophenyl group with the R280 sidechain (Fig. 4A). Hydrophobic interactions with M174 and L436 also contribute to the pockets of G2iB (Fig. 4B), G2iE (Fig. 4E), G2iH (Fig. 4H), and G2iI (Fig. 4I). R280 sidechain makes hydrogen bond interactions with oxygens from the methoxyl group of G2iB (Fig. 4B) or the sulfamide group of G2iG (Fig. 4G), and the sulfurs of the G2iC thienyl group (Fig. 4C) or of the G2iE thiazol group (Fig. 4E). It also has cation-π interaction with the G2iC thienyl group and G2iF quinoline moiety. The α-carbon of A283 comes close (3 Å) to G2iD (Fig. 4D); this inhibitor has Van der Waals interactions with the large cytosolic loop. In G2iF, besides the cation-π interaction with the quinoline, R244 also makes a hydrogen bond with the ligand's carbonyl, suggesting that positioning of R244 is essential for G2iF recognition.

Discussion

GLUT2 shares characteristic motifs and high similarity with the other Class I representatives GLUTs 1, 3, and 4⁷. In this group, it is the only transporter that also accepts fructose as a substrate⁸. This prompted us to test the identified GLUT2-inhibiting compounds against all Class I GLUTs and the Class II member GLUT5, a fructose-only transporter, to elucidate their specificity. Except for G2iF, which also inhibits other Class I GLUTs (although to a lesser extent: IC₅₀ in GLUT2 = 7 μM, IC₅₀ in other Class I GLUTs ≥ 14 μM), and G2iI which inhibits GLUT5 (IC₅₀ = 23 μM) less potently than GLUT2 (IC₅₀ = 13 μM), the other nine GLUT2 ligands did not show a significant effect on the tested transporters (Fig. 3). Although so far unknown effects on other human transporters cannot be ruled out completely, these data indicate that, for the first time, very potent and specific GLUT2 inhibitors were identified. For example, similarity search (Tanimoto > = 0.9, across the entire database, all the other options default) in PubChem for G2iA and G2iB returned 60 compounds with 34 bioactivity records and 409 compounds

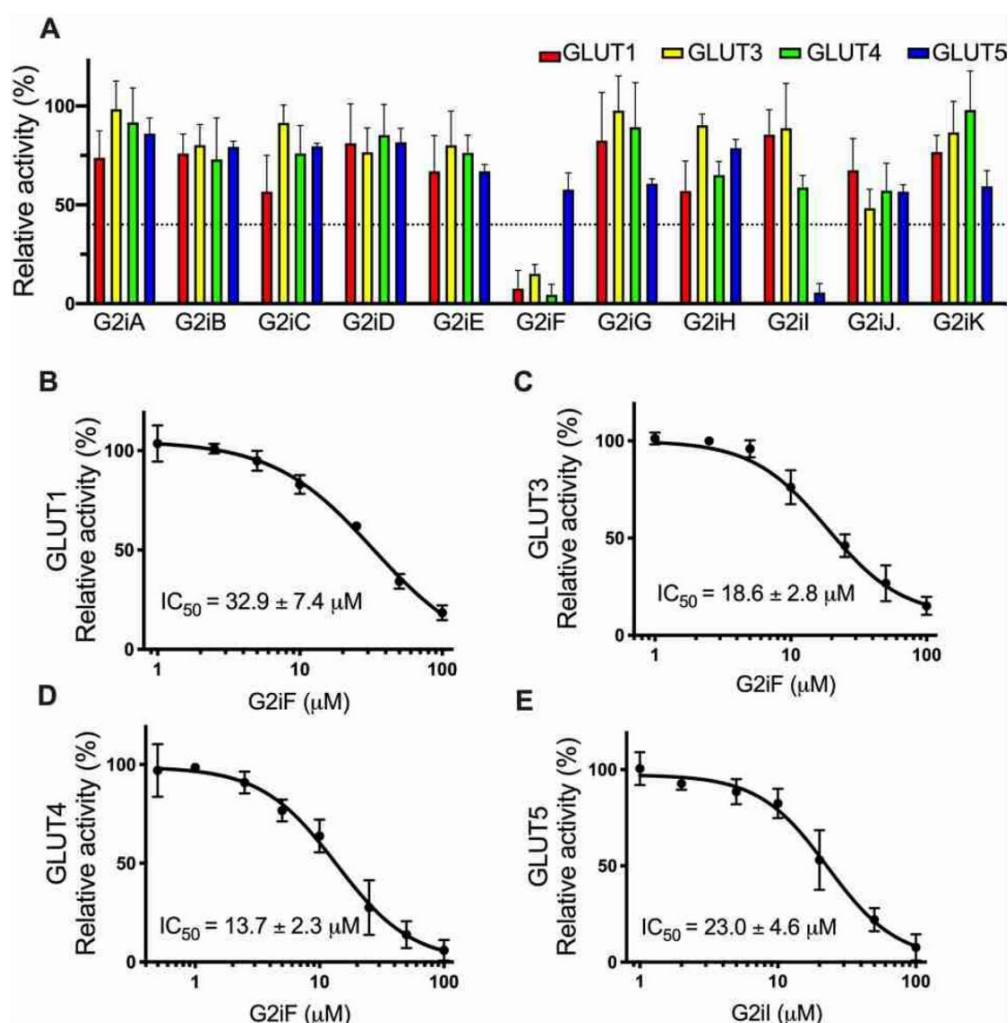


Figure 3. Effect of GLUT2 inhibitors on GLUT1, GLUT3, GLUT4, and GLUT5. (A) Relative transport activity of GLUT1 (red), GLUT3 (yellow), GLUT4 (green), and GLUT5 (blue) in the presence of 100 μM of GLUT2 inhibitors G2iA–G2iK. Dose–response curves for G2iF inhibition in GLUT1 (B), GLUT3 (C), and GLUT4 (D), and G2iI inhibition in GLUT5 (E). Substrate conditions for relative transport activity were: 1.5 mM glucose for GLUT3, 5 mM glucose for GLUT1 and GLUT4, and 10 mM fructose for GLUT5. Error bars show standard deviation from at least three independent measurements.

with 1 bioactivity record, respectively. The bioactivity records for all similar compounds are labeled as inactive. Identical searches with the exact similarity cutoffs, when performed on the ChEMBL database (<https://www.ebi.ac.uk/chembl/>), found no similar compounds. These results indicate that, based on current knowledge collated in two of the largest public databases, G2iA and G2iB are potentially selective for GLUT2 and can become valuable tools for probing and understanding GLUT2 biology.

A possible explanation for the high prevalence of GLUT2-selective inhibitors among the identified GLUT2 inhibitors may be that the inhibitors target the upper portion of the substrate cavity. All 11 inhibitors dock at the substrate cavity entrance, separately from the glucose binding site (Figs. 1, 4). As noted above, G2iA and G2iB are noncompetitive with glucose, confirming that the inhibitors bind at a different site than the substrate (Supplementary Fig. S3). The substrate cavity base containing the glucose binding site is made up of residues mostly conserved in Class I GLUTs (Supplementary Fig. S1A). The cytosolic entrance of the substrate cavity surrounded

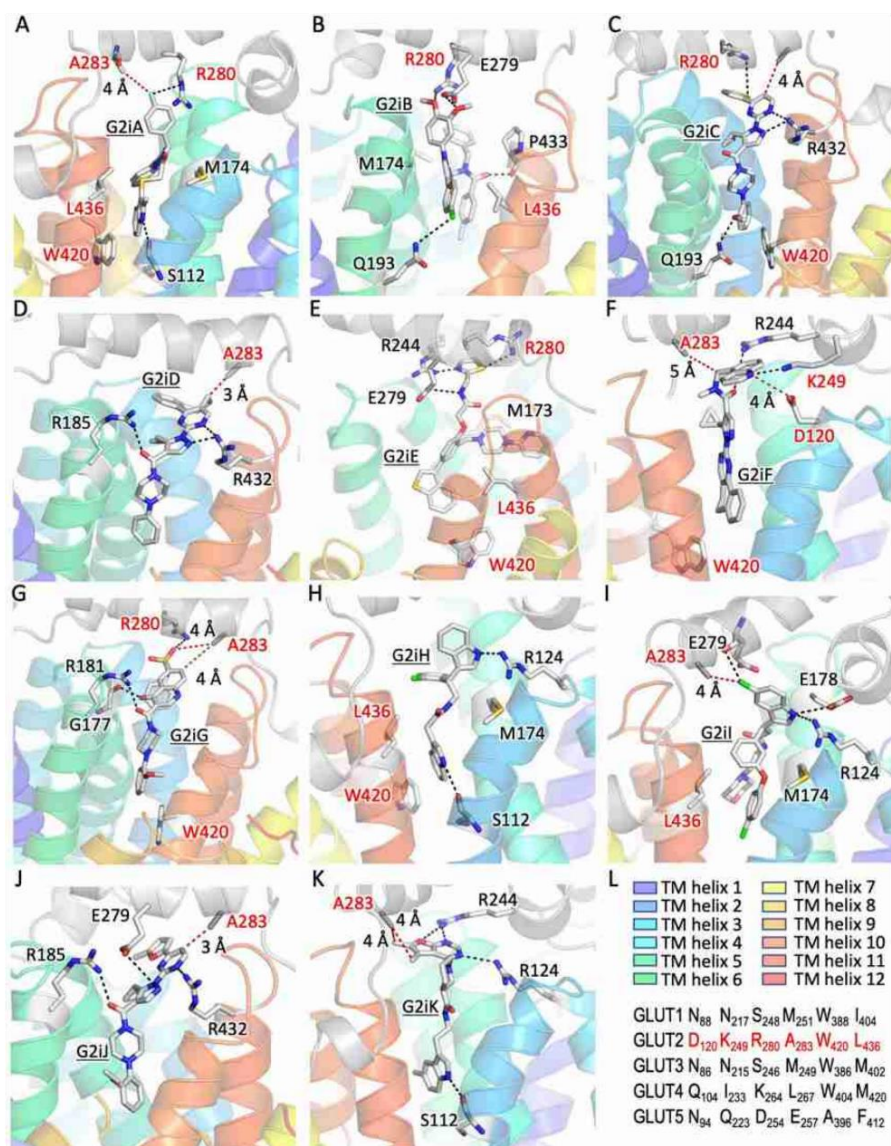


Figure 4. Docking sites of G2iA-G2iK in the inward-facing conformation GLUT2 model. G2iA-G2iK dock in the superior region of the substrate cavity, distinct from the glucose binding site (see Fig. 1B). Close-up views for the docked ligands: G2iA (A), G2iB (B), G2iC (C), G2iD (D), G2iE (E), G2iF (F), G2iG (G), G2iH (H), G2iI (I), G2iJ (J), and G2iK (K). Residues that are not conserved in GLUT1-5 are in red. (L) GLUT1-5 sequence alignment for unconserve protein residues interacting with G2iA-G2iK in the GLUT2 model. The color-code identification of transmembrane (TM) helices is the same as in Fig. 1A.

by soluble loops, especially the large loop connecting the N- and C-domains of the transporter (GLUT2 amino acid residues 240 -298), has much more variability in the protein sequence (Supplementary Fig. S1). Thus, the binding site location of the GLUT2 inhibitors is consistent with the GLUT2 selectivity exhibited by most of these

ligands and suggests that targeting the entrance of the substrate cavity, whether in the inward- or outward-facing conformations, for ligand screening may increase the chances of producing GLUT-specific ligands. Also, given the separation between glucose and such inhibitor sites, bridging the two sites by attaching a glucosyl group to these types of inhibitors may substantially improve inhibitor potency while maintaining selectivity. Additionally, such compounds could help to crystallize GLUTs whose structures are yet unknown, including GLUT2, as the combination of substrate and inhibitor would greatly stabilize the transporter conformation.

A significant difference in the substrate sites between Class I GLUTs and GLUT5 is W420_{GLUT2} (W388_{GLUT1}), conserved in Class I GLUTs but replaced by a smaller residue in Class II GLUTs (e.g., A396 in GLUT5). This substitution creates more space in the substrate cavity, changing the binding mode of ligands and substrate specificity³¹. For instance, GLUT5_{A396W} mutant became a transporter of both glucose and fructose, while the wild-type can only transport fructose. Therefore, it is likely that GLUT2 inhibitors adopt different binding modes in GLUT5 than those described for GLUT2.

Analysis of the docked GLUT2 inhibitors from the virtual ligand screening (Fig. 4) suggests that L436, R280, A283—residues not conserved in other Class I GLUTs or GLUT5—may play a role in the selectivity of GLUT2 inhibitors. The equivalent substitutions of R280 in other GLUTs (S248_{GLUT1}, S246_{GLUT3}, K264_{GLUT4}, D254_{GLUT5}) would decrease or abolish this residue's interactions with G2iA, G2iB, G2iC, G2iE, and G2iG (Fig. 4). A bulkier side chain in the position of A283 (M251_{GLUT1}, M249_{GLUT3}, L267_{GLUT4}, E257_{GLUT5}) could sterically interfere with the binding of G2iD, G2iG, G2iI, and G2iJ. L436 (I404_{GLUT1}, M402_{GLUT3}, M420_{GLUT4}, F412_{GLUT5}) may be important in shaping the hydrophobic interactions in the binding pockets for G2iA, G2iB, G2iE, G2iH, and G2iI. The recognition of G2iF, the pan-Class I GLUT inhibitor, relies mostly on R244, a conserved residue in GLUT1-5. This sidechain has hydrogen bond and cation- π interactions with G2iF, suggesting that the guanidinium group's position is critical. The quinoline nitrogen of G2iF makes a hydrogen bond with K249 (N217_{GLUT1}, N215_{GLUT3}, I233_{GLUT4}, Q223_{GLUT5}) and a weak interaction with D120 (N88_{GLUT1}, N86_{GLUT3}, Q104_{GLUT4}, N94_{GLUT5}). The equivalent substitutions in these positions for GLUT1-4 are still able to maintain interactions with G2iF. In GLUT4, the substitution of D120 with a glutamine residue would result in better interaction with G2iF, consistent with the lower IC₅₀ of this inhibitor for GLUT4, relative to the other Class I GLUTs (Fig. 3).

With this study, we present a range of molecules that will serve as valuable tools to investigate the physiological role of GLUT2 in health and disease and may evolve to therapeutic drugs in GLUT2-related diseases. Given their selectivity against other hexose transporters, we believe these compounds could serve as chemical probes for the in-depth study of GLUT2. Indeed, GLUT2 may play a role in several important diseases^{27,28,45,46}. It is upregulated in several cancer types like pancreatic, hepatic, micropapillary, or colon cancer⁴⁷. Inhibition of GLUT2 via the non-specific inhibitor phloretin has been shown to diminish tumor growth in colon cancer⁴⁸ and hepatocellular carcinoma⁴⁹. The Class I GLUTs 1 and 3 are also overexpressed in many cancer types and related to elevated tumor growth and poor survival⁵⁰. For cancer treatment, the non-specific inhibitor G2iF that inhibits Class I GLUTs but not GLUT5 might join phloretin as a putative drug⁴⁹. Furthermore, substantial overexpression of the fructose transporters GLUT2 and GLUT5 lead to the hypothesis that certain cancer cells use fructose as a preferential carbon source⁴⁷. In these cases, the here presented GLUT2/GLUT5 inhibiting compound G2iI might be a promising candidate in the combat against cancer and other high-fructose diet-related diseases⁵¹. Importantly, a potent and GLUT2-specific effector (e.g., G2iA) might further elucidate the particular role of GLUT2 in tumor pathogenesis and facilitate studies targeting GLUT2, thereby contributing to unravel complex cancer behavior further.

In healthy individuals, GLUT2 traffics to the apical side of the brush border membrane only after a meal, when glucose concentrations in the lumen are high, to support SGLT1 and accelerate glucose uptake²⁸. In morbidly obese humans, a consistent location of GLUT2 at the apical membrane, even in fasting states, was observed and related to insulin resistance⁵². This might result in higher glucose levels in the lumen in fasting states and an abnormal sugar supply could support bacterial growth which interferes with a healthy gut microbiome⁵². Specific inhibition of GLUT2 could mitigate such pathologies. An altered microbiome composition in mice with intestinal-specific GLUT2 deletion has been detected in previous studies⁵³, supporting the gut microbiome as a possible field of application for GLUT2 inhibitors. Also, Schmitt et al. showed that GLUT2 deletion in the murine intestine causes favorable effects like improved glucose tolerance and diminished body weight gain⁵³. This suggests that GLUT2 tailored inhibitors could lead to similar results and might be applied in morbidly obese patients or type 2 diabetic persons with beneficial health effects.

Interestingly, viral infections affect the expression of GLUT2. While the hepatitis C virus downregulates GLUT2 expression⁵⁴, the transmissible gastroenteritis virus upregulates the transporter's expression, enhancing intestinal glucose absorption, which promotes viral replication⁵⁵. Hence, GLUT2 inhibition could assist in the containment of certain viruses. Clearly, the role of GLUT2 in the metabolic processes is highly complex and not fully understood. Therefore, the application of GLUT2-specific inhibitors also bears high risks as it might have not only beneficial but also adverse effects, and more studies are necessary to increase our level of knowledge. However, accessibility of specific GLUT2 inhibitors represents a tremendous advantage over less-specific GLUT inhibitors in developing drugs with a defined effective spectrum and lower side effects.

These compounds are valuable tools in the efforts of answering many open questions concerning GLUT2. For instance, it is still unclear how GLUT2 is mobilized in response to glucose in various cell types and different pathologies⁵⁶. Possible players include the type of membrane lipids⁵⁷, protein partners^{56,58}, or glycosylation³. Distinct from other GLUTs, the extraordinary low affinity for glucose and fructose probably assigns special functions of glucose sensing⁵⁹ and signaling²¹ to GLUT2, but the detailed molecular functions remain to be elucidated. Furthermore, the Fanconi-Bickel syndrome due to GLUT2 malfunction²⁷ has various symptoms that indicate yet undiscovered physiological roles for GLUT2, and the transporter's role in certain cancer types remains unclear⁴⁷. Future studies will benefit from the existence of a range of easily accessible GLUT2-specific inhibitors with varying affinities.

Materials and methods

Yeast plasmids and *hxt⁰* strains were from Dr. Mislav Oreb and Dr. Eckhard Boles (Goethe University Frankfurt, Germany). The tested compounds were purchased from MilliporeSigma (St. Louis, MO, USA).

In silico ligand screening. GLUT2 homology models were built using Molecular Operating Environment (MOE) software (www.chemcomp.com). Based on sequence alignment between GLUT1 and GLUT2, with the crystal structure for GLUT1 inward-facing conformation (PDB ID: 4PYP) as a template, the initial model geometry was generated, followed by refinement of the sidechains and energy minimization with the MMFF94x force field. The model with the lowest interaction energy and RMSD was selected for docking studies. Molecular probing of inner cavities was done to identify potential binding sites. Two sites of interest were identified in the proximity of both ends of the transmembrane regions and used for receptor preparation with OpenEye FRED software⁶⁰ (<https://www.eyesopen.com>).

ChemNavigator collection (MilliporeSigma, St. Louis, MO, USA) of commercially available compounds (~6 million) was processed for docking studies using the following protocol: (i) remove all compounds that are not small organic molecules, (ii) remove salts counterions, (iii) normalize charges and select the most likely tautomer at pH 7, (iv) generate an ensemble of up to 400 molecular conformers for each compound using Omega2 software (<https://www.eyesopen.com>).

After completing the preparation steps, the virtual docking screen was performed with OpenEye FRED software on a Linux cluster. All conformer ensembles were docked into the selected sites described above, retaining only the best scoring pose based on the Chemgauss4 score for each compound. The top 200 best scoring compounds were extracted and selected for purchase and experimental validation. Due to availability and affordability issues, only 163 compounds were sourced and submitted for experimental validation.

Culturing of GLUT-expressing *hxt⁰* yeast cells for transport assay. Depending on the plasmid selection marker, the media for cell culturing was either YEP [1% (w/v) yeast extract and 2% (w/v) peptone] supplemented with 100 µg/ml geneticin (G418) or complete synthetic media without uracil (SC-uracil). Yeast cell culturing was done at 30 °C with shaking (180–220 rpm). The plasmids containing the functional constructs of GLUT1–5 (GLUT1, GLUT2^{ΔloopS_Q455R}, GLUT3^{366Y}, GLUT4, GLUT5^{S72Y}) were transformed in the corresponding *hxt⁰* strains (EBY.VW4000 for GLUT5, EBY.S7 for GLUT1–3, and EBY.S7 Δ *erg4* for GLUT4)^{38,40–42} and grown on 2% (w/v) agar plates of the respective media supplemented with 1% (w/v) maltose. An initial culture of ~10 ml was started with a few colonies and grown for 2–3 days if the media was SC-uracil with 1% (w/v) maltose (for GLUT1, GLUT3, and GLUT4) or 1–2 days if the media was YEP with 1% (w/v) maltose and 100 µg/ml G418 (for GLUT2 and GLUT5). Cells were washed once in the corresponding media in which maltose was substituted with 0.1–2% (w/v) hexose substrate for the expressing GLUT (i.e., SC-uracil, 2% (w/v) glucose for GLUT1; SC-uracil, 0.2% (w/v) glucose for GLUT3 and GLUT4; YEP, 0.2% (w/v) glucose, 100 µg/ml G418 for GLUT2; and YEP, 2% (w/v) fructose, 200 µg/ml G418 for GLUT5). Then, cells were transferred in the same media to OD_{600nm} ~ 0.5 and grown further for 1–2 days.

GLUT transport assay. Commercial providers for chemicals tested for GLUT2 inhibition are listed in Supplementary Table S1. C¹⁴-fructose and -glucose were from Moravek Inc (Brea, CA, USA). For transport activity assay, cells in the hexose media were centrifuged (1000×g, 5 min, room temperature), washed once with PBS buffer (10 mM Na₂HPO₄, 1.8 mM KH₂PO₄, 2.7 mM KCl, 137 mM NaCl, pH 7.4), and resuspended in PBS buffer at an OD_{600nm} ~ 10; each assay contained 100 µl of this cell solution. The transport activity assay was started by adding C¹⁴-hexose (5 mM glucose for GLUT1 or GLUT4, 1.5 mM glucose for GLUT3, 10 mM glucose for GLUT2, and 10 mM fructose for GLUT5). When determining the K_M for fructose and glucose in GLUT2, substrate concentrations were varied accordingly. Transport activity assay was stopped after 10 min by adding 3 ml ice-chilled Quench buffer (0.1 M KPi, 0.1 M LiCl, pH 5.5), followed by filtration through a glass fiber channel (GC50; Advantec, Tokyo, Japan) under vacuum and another wash with 3 ml Quench buffer and filtration. The filtration membranes were transferred into scintillation vials, combined with 10 ml of Scintillation Solution (BioSafeII; Research Products International, Mount Prospect, IL, USA), and vortexed briefly. The radioactivity was determined with a scintillation counter (Tri-carb 2900TR, Perkin Elmer, USA). The compounds were dissolved in dimethyl sulfoxide (DMSO) at 100× (i.e., ~10 mM) the final assay concentration. Controls for determining the relative transport activity included 1% (v/v) DMSO, representing the normal GLUT2 activity (100%), and known inhibitors 200 µM phloretin for GLUT1–4^{38,44}, and 100 µM N-[4-(methylsulfonyl)-2-nitrophenyl]-1,3-benzodioxol-5-amine (MSNBA) for GLUT5¹⁷, representing fully inhibited activity. Primary screening was done at 100 µM compound concentration (see Supplementary Table S1 for a list of all tested compounds). The IC₅₀ values were further determined for the compounds that diminished the relative transport activity by at least 60%. When determining the inhibition mode for the most potent GLUT2 inhibitors (IC₅₀ < 2 µM), G2iA and G2iB, transport activity at 7, 15, and 30 mM glucose concentrations were determined in the absence or presence of different inhibitor concentrations (0, 0.66 and 2 µM for G2iA or 0, 1.66, 5 µM for G2iB; Supplementary Fig. S3). Data were analyzed with GraphPad Prism (San Diego, CA, USA).

Received: 3 May 2021; Accepted: 14 June 2021
Published online: 02 July 2021

References

- Holman, G. D. Structure, function and regulation of mammalian glucose transporters of the SLC2 family. *Pflugers Arch.* **472**, 1155–1175 (2020).
- Barron, C. C., Bilan, P. J., Tsakiridis, T. & Tsiani, E. Facilitative glucose transporters: Implications for cancer detection, prognosis and treatment. *Metab. Clin. Exp.* **65**, 124–139 (2016).
- Ohtsubo, K. *et al.* N-Glycosylation modulates the membrane sub-domain distribution and activity of glucose transporter 2 in pancreatic beta cells. *Biochem. Biophys. Res. Commun.* **434**, 346–351 (2013).
- Hajjaghaalipour, F., Khalilpourfarshbafi, M. & Arya, A. Modulation of glucose transporter protein by dietary flavonoids in type 2 diabetes mellitus. *Int. J. Biol. Sci.* **11**, 508–524 (2015).
- Iancu, C. V., Zamoan, J., Woo, S., Aleshin, A. & Choe, J. Crystal structure of a glucose/H⁺ symporter and its mechanism of action. *Proc. Natl. Acad. Sci. U.S.A.* **110**, 17862–17867 (2013).
- Mueckler, M. & Thorens, B. The SLC2 (GLUT) family of membrane transporters. *Mol. Aspects Med.* **34**, 121–138 (2013).
- Joost, H. G. & Thorens, B. The extended GLUT⁻ family of sugar/polyol transport facilitators: Nomenclature, sequence characteristics, and potential function of its novel members. *Mol. Membr. Biol.* **18**, 247–256 (2001).
- Quistgaard, E. M., Löw, C., Guettou, F. & Nordlund, P. Understanding transport by the major facilitator superfamily (MFS): Structures pave the way. *Nat. Rev. Mol. Cell Biol.* **17**, 123–132 (2016).
- Baker, G. F. & Widdas, W. F. The asymmetry of the facilitated transfer system for hexoses in human red cells and the simple kinetics of a two component model. *J. Physiol.* **231**, 143–165 (1973).
- Carruthers, A. & Helgerson, A. L. Inhibitions of sugar transport produced by ligands binding at opposite sides of the membrane. Evidence for simultaneous occupation of the carrier by maltose and cytochalasin B. *Biochemistry* **30**, 3907–3915 (1991).
- Lloyd, K. P., Ojelabi, O. A., De Zutter, J. K. & Carruthers, A. Reconciling contradictory findings: Glucose transporter 1 (GLUT1) functions as an oligomer of allosteric, alternating access transporters. *J. Biol. Chem.* **292**, 21035–21046 (2017).
- Deng, D. *et al.* Crystal structure of the human glucose transporter GLUT1. *Nature* **510**, 121–125 (2014).
- Deng, D. *et al.* Molecular basis of ligand recognition and transport by glucose transporters. *Nature* **526**, 391–396 (2015).
- Nomura, N. *et al.* Structure and mechanism of the mammalian fructose transporter GLUT5. *Nature* **526**, 397–401 (2015).
- Sun, L. *et al.* Crystal structure of a bacterial homologue of glucose transporters GLUT1–4. *Nature* **490**, 361–366 (2012).
- Schmidl, S., Iancu, C. V., Choe, J.-Y. & Oreb, M. Ligand screening systems for human glucose transporters as tools in drug discovery. *Front. Chem.* **6**, 183 (2018).
- George Thompson, A. M. *et al.* Discovery of a specific inhibitor of human GLUT5 by virtual screening and in vitro transport evaluation. *Sci. Rep.* **6**, 24240 (2016).
- Uldry, M., Ibberson, M., Hosokawa, M. & Thorens, B. GLUT2 is a high affinity glucosamine transporter. *FEBS Lett.* **524**, 199–203 (2002).
- Jung, J. H., Wang, X. D. & Loeken, M. R. Mouse embryonic stem cells established in physiological-glucose media express the high KM Glut2 glucose transporter expressed by normal embryos. *Stem Cells Transl. Med.* **2**, 929–934 (2013).
- Stolarczyk, E. *et al.* Detection of extracellular glucose by GLUT2 contributes to hypothalamic control of food intake. *Am. J. Physiol. Endocrinol. Metab.* **298**, E1078–1087 (2010).
- Guillemain, G., Loizeau, M., Pinçon-Raymond, M., Girard, J. & Leturque, A. The large intracytoplasmic loop of the glucose transporter GLUT2 is involved in glucose signaling in hepatic cells. *J. Cell Sci.* **113**(Pt 5), 841–847 (2000).
- Kellett, G. L. The facilitated component of intestinal glucose absorption. *J. Physiol.* **531**, 585–595 (2001).
- Ghezzi, C., Loo, D. D. F. & Wright, E. M. Physiology of renal glucose handling via SGLT1, SGLT2 and GLUT2. *Diabetologia* **61**, 2087–2097 (2018).
- Patel, C. *et al.* Effect of dietary fructose on portal and systemic serum fructose levels in rats and in KHK^{-/-} and GLUT5^{-/-} mice. *Am. J. Physiol. Gastrointest. Liver Physiol.* **309**, G779–790 (2015).
- Koepsell, H. Glucose transporters in brain in health and disease. *Pflugers Arch.* **472**, 1299–1343 (2020).
- Santer, R. *et al.* The mutation spectrum of the facilitative glucose transporter gene SLC2A2 (GLUT2) in patients with Fanconi-Bickel syndrome. *Hum. Genet.* **110**, 21–29 (2002).
- Sharari, S., Abou-Alloul, M., Hussain, K. & Ahmad Khan, F. Fanconi-Bickel syndrome: A review of the mechanisms that lead to dysglycaemia. *Int. J. Mol. Sci.* **21**, 6286 (2020).
- Kellett, G. L. & Brot-Laroche, E. Apical GLUT2: A major pathway of intestinal sugar absorption. *Diabetes* **54**, 3056–3062 (2005).
- Thorens, B. GLUT2 in pancreatic and extra-pancreatic gluco-detection (review). *Mol. Membr. Biol.* **18**, 265–273 (2001).
- Eny, K. M., Wolever, T. M. S., Fontaine-Bisson, B. & El-Sohehy, A. Genetic variant in the glucose transporter type 2 is associated with higher intakes of sugars in two distinct populations. *Physiol. Genom.* **33**, 355–360 (2008).
- George Thompson, A. M., Iancu, C. V., Nguyen, T. T. H., Kim, D. & Choe, J.-Y. Inhibition of human GLUT1 and GLUT5 by plant carbohydrate products: insights into transport specificity. *Sci. Rep.* **5**, 12804 (2015).
- Reckzeh, E. S. & Waldmann, H. Development of glucose transporter (GLUT) inhibitors. *Eur. J. Org. Chem.* **2020**, 2321–2329 (2020).
- Reckzeh, E. S. *et al.* Inhibition of glucose transporters and glutamine synergistically impairs tumor cell growth. *Cell Chem. Biol.* **26**, 1214–1228.e25 (2019).
- Ceballos, J. *et al.* Synthesis of indomorphane pseudo-natural product inhibitors of glucose transporters GLUT-1 and -3. *Angew. Chem. Int. Ed. Engl.* **58**, 17016–17025 (2019).
- Shriwas, P. *et al.* A small-molecule pan-class I glucose transporter inhibitor reduces cancer cell proliferation in vitro and tumor growth in vivo by targeting glucose-based metabolism. *Cancer Metab.* **9**, 14 (2021).
- Kwon, O. *et al.* Inhibition of the intestinal glucose transporter GLUT2 by flavonoids. *FASEB J.* **21**, 366–377 (2007).
- Goto, T. *et al.* Tiliroside, a glycosidic flavonoid, inhibits carbohydrate digestion and glucose absorption in the gastrointestinal tract. *Mol. Nutr. Food Res.* **56**, 435–445 (2012).
- Schmidl, S., Tamayo Rojas, S. A., Iancu, C. V., Choe, J.-Y. & Oreb, M. Functional expression of the human glucose transporters GLUT2 and GLUT3 in yeast offers novel screening systems for GLUT-targeting drugs. *Front. Mol. Biosci.* **7**, 598419 (2020).
- Song, J. *et al.* Flavonoid inhibition of sodium-dependent vitamin C transporter 1 (SVC11) and glucose transporter isoform 2 (GLUT2), intestinal transporters for vitamin C and Glucose. *J. Biol. Chem.* **277**, 15252–15260 (2002).
- Wieczorke, R., Dlugai, S., Krampe, S. & Boles, E. Characterisation of mammalian GLUT glucose transporters in a heterologous yeast expression system. *Cell. Physiol. Biochem.* **13**, 123–134 (2003).
- Tripp, J. *et al.* Establishing a yeast-based screening system for discovery of human GLUT5 inhibitors and activators. *Sci. Rep.* **7**, 6197 (2017).
- Müller, G., Dlugai, S., Voss, D. & Boles, E. Use of *Saccharomyces cerevisiae* Erg4 mutants for the expression of glucose transporters from mammals. Patent number US8298812B2 (2004).
- Colville, C. A., Seatter, M. J., Jess, T. J., Gould, G. W. & Thomas, H. M. Kinetic analysis of the liver-type (GLUT2) and brain-type (GLUT3) glucose transporters in *Xenopus* oocytes: Substrate specificities and effects of transport inhibitors. *Biochem. J.* **290**, 701–706 (1993).
- Kasahara, T. & Kasahara, M. Characterization of rat Glut4 glucose transporter expressed in the yeast *Saccharomyces cerevisiae*: Comparison with Glut1 glucose transporter. *Biochim. Biophys. Acta* **1324**, 111–119 (1997).
- Thorens, B. GLUT2, glucose sensing and glucose homeostasis. *Diabetologia* **58**, 221–232 (2015).

46. Kim, Y. H. *et al.* SLC2A2 (GLUT2) as a novel prognostic factor for hepatocellular carcinoma. *Oncotarget* **8**, 68381–68392 (2017).
47. Godoy, A. *et al.* Differential subcellular distribution of glucose transporters GLUT1-6 and GLUT9 in human cancer: Ultrastructural localization of GLUT1 and GLUT5 in breast tumor tissues. *J. Cell. Physiol.* **207**, 614–627 (2006).
48. Lin, S.-T. *et al.* Apple polyphenol phloretin inhibits colorectal cancer cell growth via inhibition of the type 2 glucose transporter and activation of p53-mediated signaling. *J. Agric. Food Chem.* **64**, 6826–6837 (2016).
49. Wu, C.-H. *et al.* In vitro and in vivo study of phloretin-induced apoptosis in human liver cancer cells involving inhibition of type II glucose transporter. *Int. J. Cancer* **124**, 2210–2219 (2009).
50. Ancey, P.-B., Contat, C. & Meylan, E. Glucose transporters in cancer—from tumor cells to the tumor microenvironment. *FEBS J.* **285**, 2926–2943 (2018).
51. Tappy, L. & Lê, K.-A. Metabolic effects of fructose and the worldwide increase in obesity. *Physiol. Rev.* **90**, 23–46 (2010).
52. Ait-Omar, A. *et al.* GLUT2 accumulation in enterocyte apical and intracellular membranes: A study in morbidly obese human subjects and ob/ob and high fat-fed mice. *Diabetes* **60**, 2598–2607 (2011).
53. Schmitt, C. C. *et al.* Intestinal inactivation of the glucose transporter GLUT2 delays tissue distribution of glucose and reveals an unexpected role in gut homeostasis. *Mol. Metab.* **6**, 61–72 (2017).
54. Matsui, C. *et al.* Hepatitis C virus infection suppresses GLUT2 gene expression via downregulation of hepatocyte nuclear factor 1 α . *J. Virol.* **86**, 12903–12911 (2012).
55. Dai, L., Hu, W. W., Xia, L., Xia, M. & Yang, Q. Transmissible gastroenteritis virus infection enhances SGLT1 and GLUT2 expression to increase glucose uptake. *PLoS One* **11**, e0165585 (2016).
56. Cohen, M. *et al.* Live imaging of GLUT2 glucose-dependent trafficking and its inhibition in polarized epithelial cysts. *Open Biol.* **4**, 140091 (2014).
57. Jennemann, R. *et al.* Gangliosides modulate insulin secretion by pancreatic beta cells under glucose stress. *Glycobiology* **30**, 722–734 (2020).
58. Rogers, R. C., Burke, S. J., Collier, J. J., Ritter, S. & Hermann, G. E. Evidence that hindbrain astrocytes in the rat detect low glucose with a glucose transporter 2-phospholipase C-calcium release mechanism. *Am. J. Physiol. Regul. Integr. Comp. Physiol.* **318**, R38–R48 (2020).
59. Ohtsubo, K. *et al.* Dietary and genetic control of glucose transporter 2 glycosylation promotes insulin secretion in suppressing diabetes. *Cell* **123**, 1307–1321 (2005).
60. McGann, M. FRED pose prediction and virtual screening accuracy. *J. Chem. Inf. Model* **51**, 578–596 (2011).

Acknowledgements

We thank Andrea Adams, Valerie Riehl, and Drew Neuffer for technical support. This work was supported by NIH Grant R01-GM123103 (to M.O., T.O., J.C.). We thank OpenEye Scientific Software for granting access to their software under an academic license.

Author contributions

T.O. and J.C. conceived the project. S.S., O.U., C.V.I., and J.C. performed the experiments. All authors analyzed the data and wrote the manuscript.

Competing interests

The authors declare no competing interests.


Additional information

Supplementary Information The online version contains supplementary material available at <https://doi.org/10.1038/s41598-021-93063-5>.

Correspondence and requests for materials should be addressed to T.I.O. or J.C.

Reprints and permissions information is available at www.nature.com/reprints.

Publisher's note Springer Nature remains neutral with regard to jurisdictional claims in published maps and institutional affiliations.

 **Open Access** This article is licensed under a Creative Commons Attribution 4.0 International License, which permits use, sharing, adaptation, distribution and reproduction in any medium or format, as long as you give appropriate credit to the original author(s) and the source, provide a link to the Creative Commons licence, and indicate if changes were made. The images or other third party material in this article are included in the article's Creative Commons licence, unless indicated otherwise in a credit line to the material. If material is not included in the article's Creative Commons licence and your intended use is not permitted by statutory regulation or exceeds the permitted use, you will need to obtain permission directly from the copyright holder. To view a copy of this licence, visit <http://creativecommons.org/licenses/by/4.0/>.

© The Author(s) 2021

SUPPLEMENTARY INFORMATION**Identification of new GLUT2-selective inhibitors through *in silico* ligand screening and validation in eukaryotic expression systems**

Sina Schmidl^{1,#}, Oleg Ursu^{2,3,#}, Cristina V. Iancu⁴, Mislav Oreb¹,
Tudor Oprea^{2,5*} and Jun-yong Choe^{4,6,*}

¹ Institute of Molecular Biosciences, Faculty of Biological Sciences, Goethe University Frankfurt, Frankfurt am Main, Germany.

² Translational Informatics Division, Department of Internal Medicine, The University of New Mexico School of Medicine, Albuquerque, NM 87131, USA.

³ Present address: Computational and Structural Chemistry, Merck & Co., Inc., 2000 Galloping Hill Road, Kenilworth, NJ 07033, USA.

⁴ Department of Chemistry, East Carolina Diabetes and Obesity Institute, East Carolina University, Greenville, NC 27834 USA.

⁵ UNM Comprehensive Cancer Center, The University of New Mexico, Albuquerque, NM 87131, USA.

⁶ Department of Biochemistry and Molecular Biology, The Chicago Medical School, Rosalind Franklin University of Medicine and Science, North Chicago, IL 60064 USA.

These authors contributed equally.

*Corresponding authors: Jun-yong Choe, E-mail: choej18@ecu.edu
Tudor Oprea, E-mail: toprea@salud.unm.edu

Supplementary Figure S1

Supplementary Figure S2

Supplementary Figure S3

Supplementary Figure S4

Supplementary Table S1

with the sequence alignment color-coded; blue regions show sequence conservation, red ones show the highest sequence variation. GLUT2 is more closely related to GLUT1, 3, and 4 (52-65% sequence identity) as compared with GLUT5 (40% sequence identity); however, the loop between the two halves of the transporter (highlighted by a red dotted ellipse) shows a higher variation (the sequence identity among GLUT1, 2, 3, and 4 is 33-61%, and that between GLUT2 and 5 is 35%). The yellow ellipse labeled G2i shows the approximate location of GLUT2 inhibitors. (A) Homology model showing the sequence conservation (blue) for GLUT1, 2, 3, and 4. (B) Homology model showing the sequence conservation (blue) between GLUT2 and 5. (C) Amino acid sequence alignment (<https://www.ibi.vu.nl/programs/pralinewww/>) of GLUT1-5 shows three unconserved areas: 1) between TM helices 1 and 2 in which GLUT2 has extra ~35 amino acid residues compared with the other GLUTs; 2) between TM helices 6 and 7 (the large cytoplasmic loop highlighted by the red ellipse in A-B); and 3) after TM helix 12.

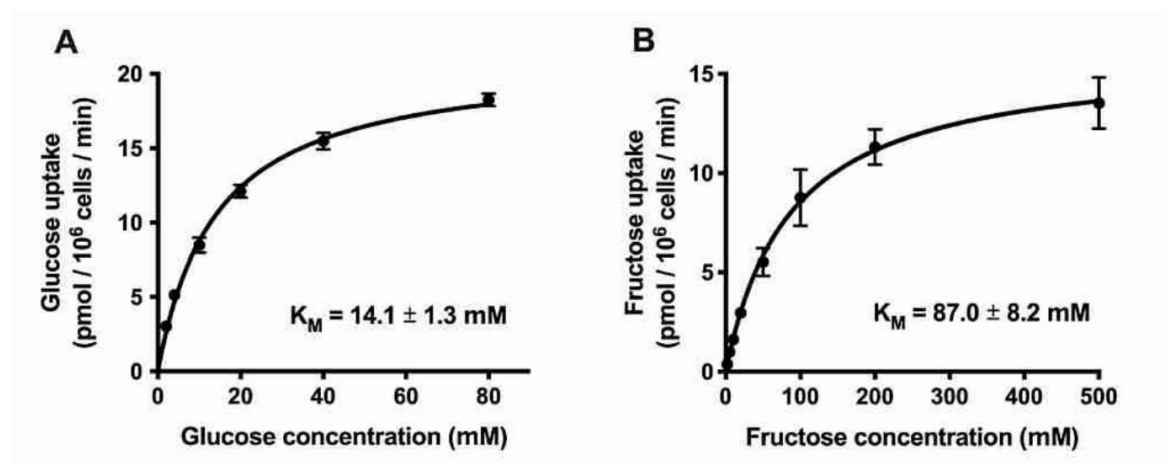


Figure S2. Michaelis-Menten curves for glucose and fructose transport in GLUT2-expressing *hxt⁰* yeast system. Glucose (A) and fructose (B) transport activity by GLUT2 $_{\Delta\text{loopS_Q455R}}$ in EBY.S7 yeast cells. Transport activity was initiated by the addition of C¹⁴-hexose (glucose or fructose) to cells in the PBS buffer. After 10 mins, transport activity was stopped, and the radioactivity accumulated in cells was measured. See Materials and Methods for details. Error bars represent standard deviation from three independent measurements. Data analysis for calculating K_M values and the graphs were generated with GraphPad Prism (<https://www.graphpad.com>).

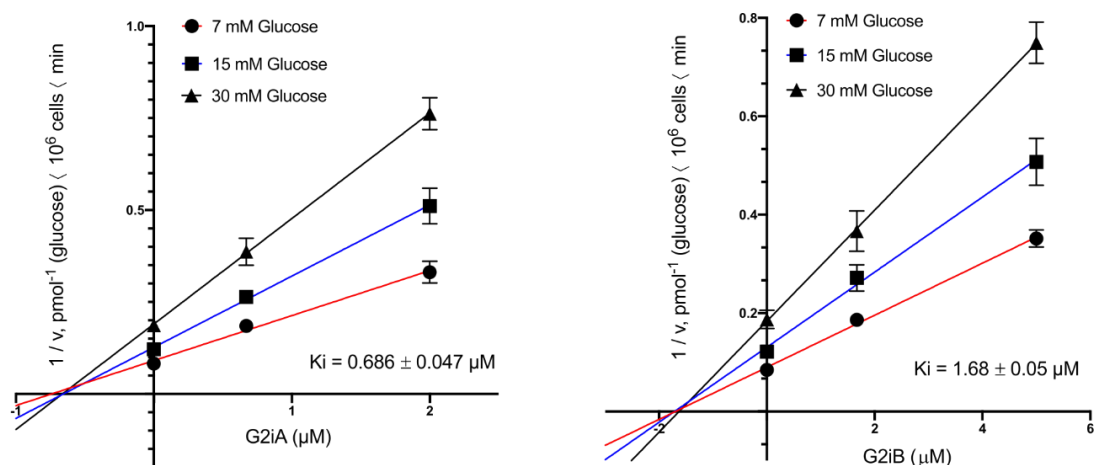
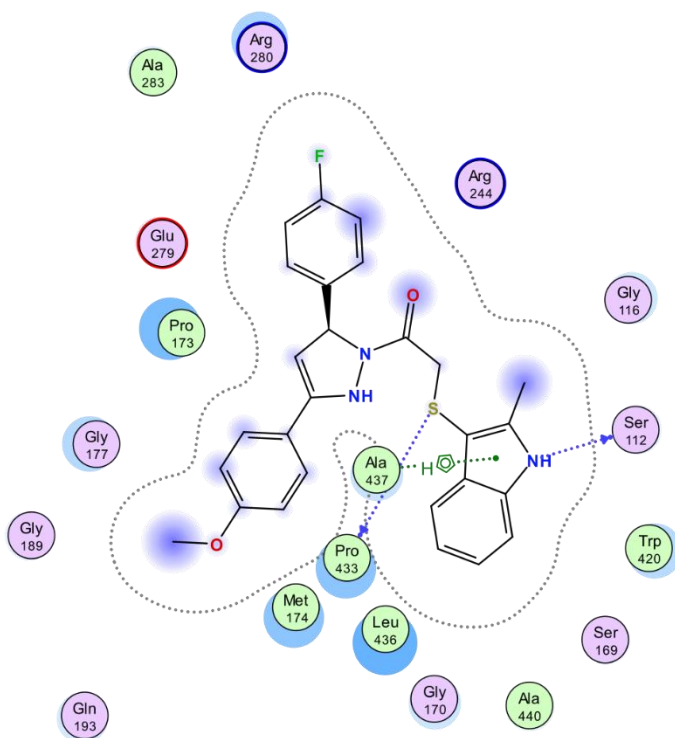
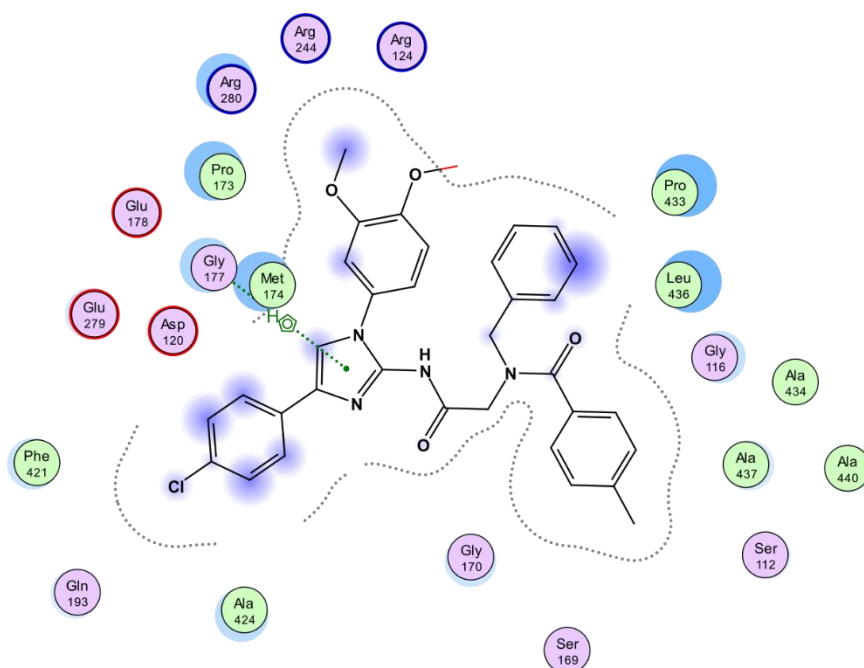


Figure S3. Dixon plots for GLUT2 glucose transport inhibition by G2iA (left) and G2iB (right). Glucose transport activity by GLUT2 $_{\Delta\text{loopS_Q455R}}$ in EBY.S7 yeast cells was determined at 7, 15, and 30 mM glucose, in the absence or presence of different inhibitor concentrations. Transport activity was initiated by the addition of C¹⁴- glucose to cells in the PBS buffer. After 10 mins, transport activity was stopped, and the radioactivity accumulated in cells was measured. See Materials and Methods for details. Data analysis for calculating K_i values and the graphs were generated with GraphPad Prism (<https://www.graphpad.com>). Error bars represent standard deviation from three measurements.

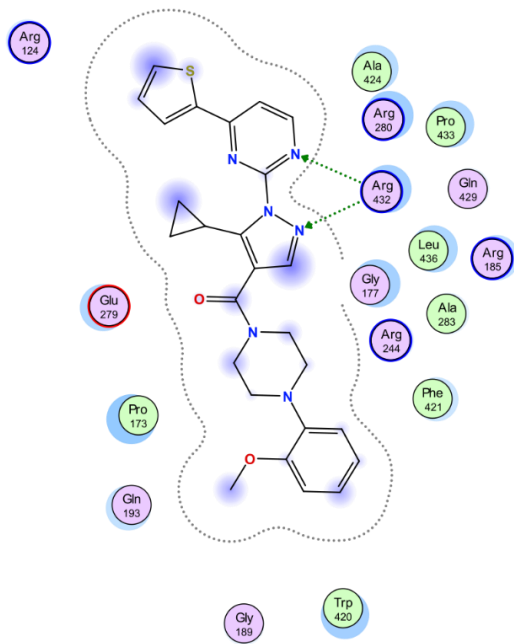
A. G2iA



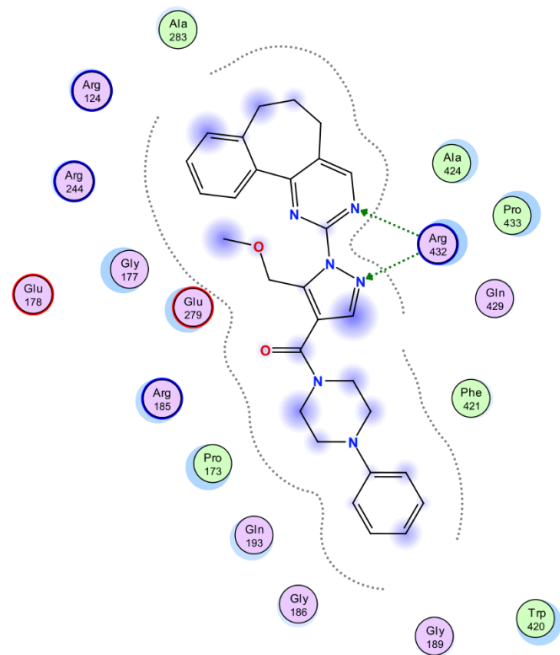
B. G2iB



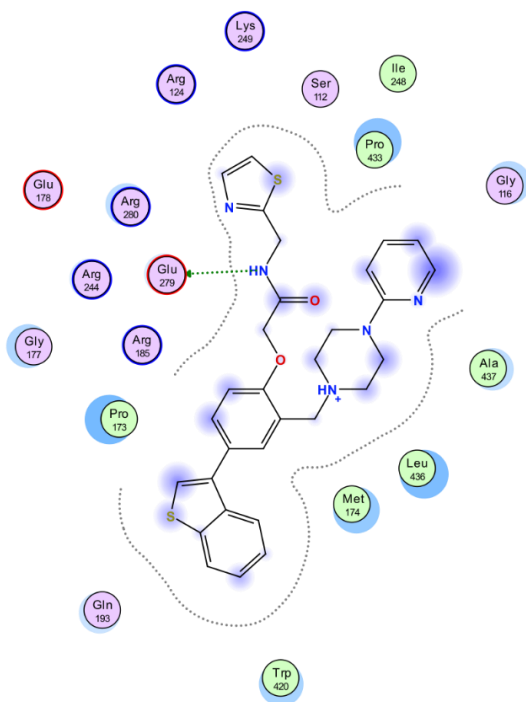
C. G2iC



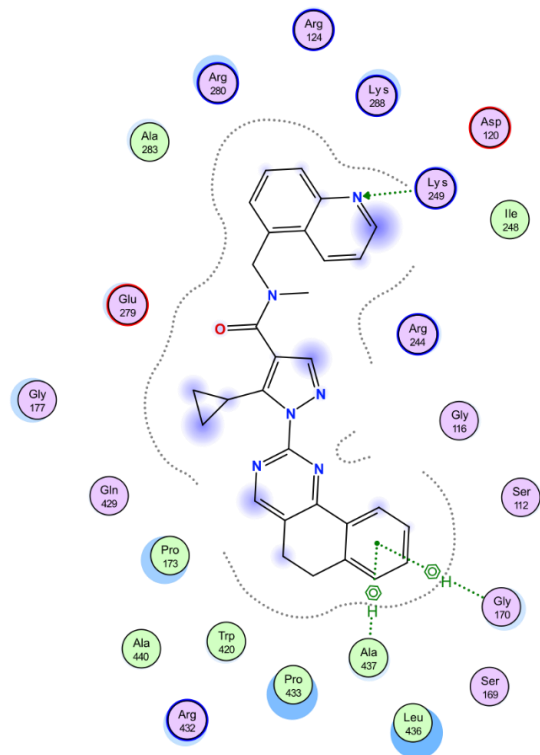
D. G2iD



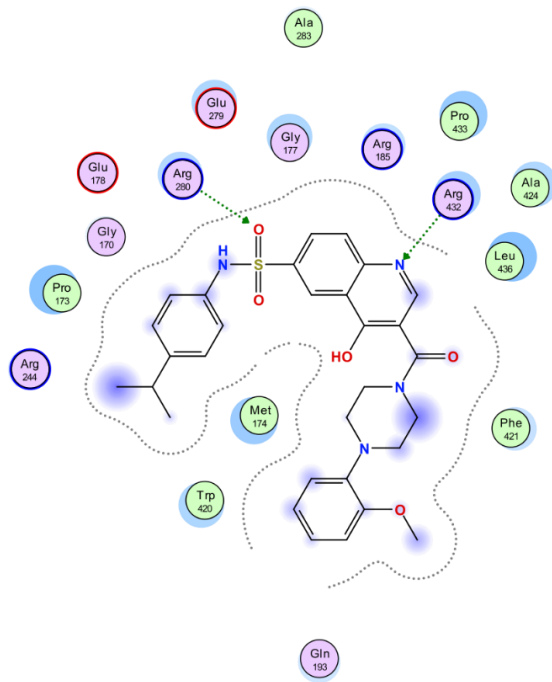
E. G2iE



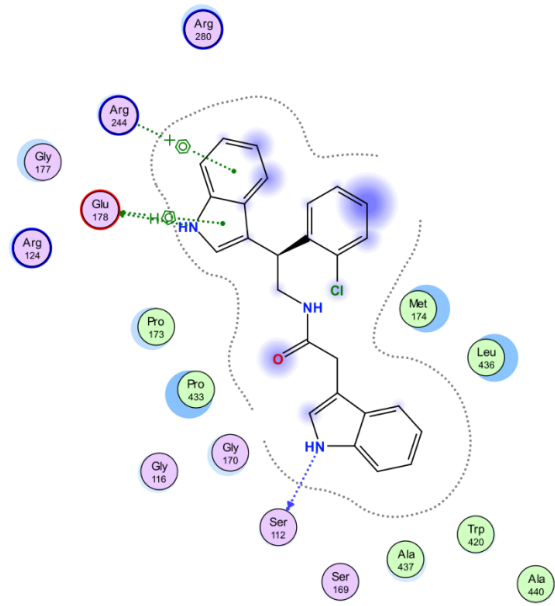
F. G2iF



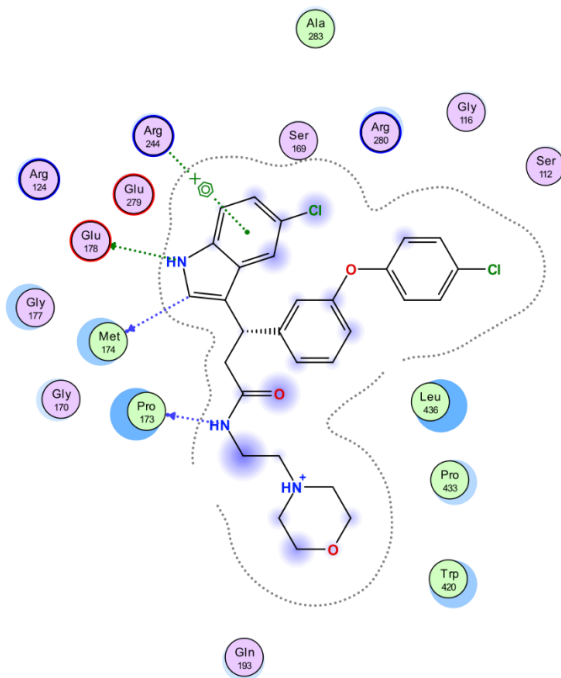
G. G2iG



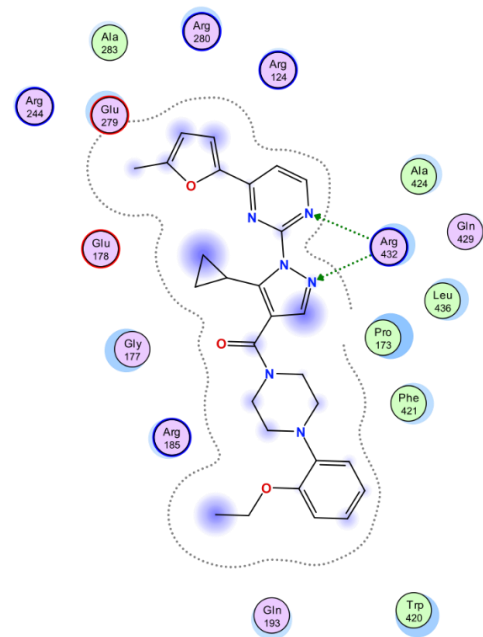
H. G2iF



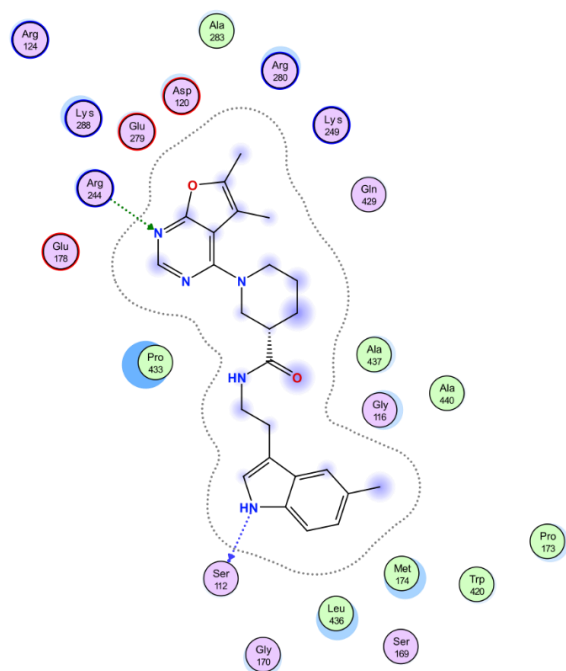
I. G2iI



J. G2iJ



K. G2iK



L. Legend

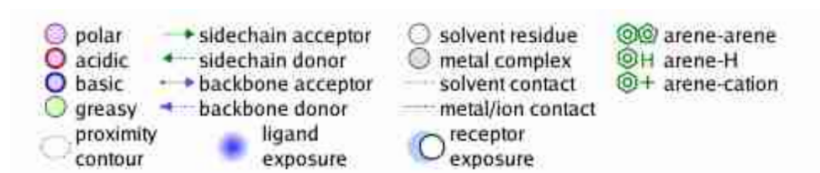


Figure S4. Protein-ligand interactions for docked GLUT2 inhibitors to the inward-facing conformation GLUT2 model. The ligand-protein interaction diagrams for G2iA (A), G2iB (B), G2iC (C), G2iD (D), G2iE (E), G2iF (F), G2iG (G), G2iH (H), G2iI (I), G2iJ (J), and G2iK (K), were generated in MOE (www.chemcomp.com) with the program “Ligand Interactions”. (L) Legend for the type of residues and ligand-protein interactions in (A-K).

Table S1. *In silico* ligand screening candidates tested for GLUT2 transport inhibition. The structure identifier (STRUCTURE_ID), commercial information (SUPPLIER and CATALOG #), chemical name (CHEM_NAME), SMILES code (SMILES), and the molecular formula (MF) are indicated for each compound (except for some unavailable chemicals' names). Identified potent GLUT2 inhibitors (G2iA-K) are in bold, red font.

STRUCTURE_ID	SUPPLIER	SUPPLIER_CATALOG #	CHEM_NAME	SMILES	MF
448434472	Ark Pharm	AK242035		<chem>N1(CCN(CC1)c2ncc(cc2)c3cc4[n](cc(c4c(c3)C(=O)Nc5c(nc(cc5)C)O)C)C)C)C</chem>	C31H38O2N6
403941836	Ark Pharm	AK317596	5-(ethyl(tetrahydro-2H-pyran-4-yl)amino)-N-((2-hydroxy-4,6-dimethylpyridin-3-yl)methyl)-4-methyl-4'-(morpholinomethyl)-[1,1'-biphenyl]-3-carboxamide	<chem>N5(CCOCC5)Cc1ccc(cc1)c2cc(c(c2)C(=O)Nc4c(nc(cc4)C)O)C)N(C3CCOCC3)CC</chem>	C34H44O4N4
407639426	Target Molecule Corp.	T1905	1-cyclopentyl-N-((2-hydroxy-4,6-dimethylpyridin-3-yl)methyl)-6-(4-(morpholinomethyl)phenyl)-1H-indazole-4-carboxamide	<chem>N6(CCOCC6)Cc1ccc(cc1)c2cc3[n](ncc3c(c2)C(=O)Nc5c(nc(cc5)C)O)C4CCCC4</chem>	C32H37O3N5
27829088	ChemBridge Corporation	5340763	2-(3,5-diphenyl-4,5-dihydro-1H-pyrazol-1-yl)-4-(4-fluorophenyl)-6-phenylpyrimidine	<chem>Fc1ccc(cc1)c2nc(nc(c2)c6ccccc6)N3NC(=CC3c5ccccc5)c4ccccc4</chem>	C31H23N4F1
30023243	ChemBridge Corporation	5720478	4-(4-benzhydryl-1-piperazinyl)-1-phenyl-6-(1-piperidinyl)-1H-pyrazolo[3,4-d]pyrimidine	<chem>N3(CCN(CC3)c4nc(nc6[n](ncc64)c7ccccc7)N5CCCC5)C(c2ccc(cc2)c1ccccc1</chem>	C33H35N7
466119877	ChemBridge Corporation	77390155	2-[5-(methoxymethyl)-4-[(4-phenyl-1-piperazinyl)carbonyl]-1H-pyrazol-1-yl]-6,7-dihydro-5H-benzo[6,7]cyclohepta[1,2-d]pyrimidine (G2iD)	<chem>[n]4(ncc(c4COC)C(=O)N5CCN(C5)c6ccccc6)c1nc2c(cn1)CCCc3c2ccccc3</chem>	C29H30O2N6
549939793	ChemBridge Corporation	94887258		<chem>FC(F)(F)c1cc(ccc1)OC[C@@H]2CN(C[C@@H](C2)C(=O)NCCc4c5c([nH]c4)cccc5)CCc3ccccc3</chem>	C32H34O2N3 F3
549930126	ChemBridge Corporation	26385775		<chem>N2(C[C@H])(C[C@H](C2)C(=O)NCCc5c6c([nH]c5)cccc6)COc3c4c(cc3)CCC4)Cc1cc(c(cc1)OC)OC</chem>	C35H41O4N3
347006762	ChemBridge Corporation	40266327	(3R,5S)-5-[(2,3-dihydro-1H-inden-5-yl)oxy)methyl]-1-(2-naphthylmethyl)-N-(2-phenylethyl)-3-piperidinecarboxamide	<chem>N3(C[C@H])(C[C@H](C3)C(=O)NCCc6ccccc6)COc4cc5c(cc4)CC5)Cc1cc2c(cc1)cccc2</chem>	C35H38O2N2
181925102	ChemBridge Corporation	18817511	3-(1-benzothien-7-yl)-1-(cyclopropylmethyl)-6-[(4,6-dimethyl-2-oxo-1,2-dihydro-3-pyridinyl)carbonyl]-5,6,7,8-tetrahydro[1,6]naphthyridin-2(1H)-one	<chem>[s]1c2c(cc1)cccc2C3=CC4=C(N(C3=O)CC6CC6)CCN(C4)C(=O)c5c(nc(cc5)C)O</chem>	C28H27O3N3 S1
181950723	ChemBridge Corporation	42621764	N-benzyl-N,1-dimethyl-5-(spiro[indene-1,4'-piperidin]-1'-yl)-4,5,6,7-tetrahydro-1H-indazole-3-carboxamide	<chem>[n]1(nc(c3c1CCC(C3)N4CCCC(C4)c6c(cccc6)C=C5)C(=O)N(Cc2ccccc2)C)C</chem>	C30H34O1N4

Publications

181921786	ChemBridge Corporation	16753878	1,8-bis(2-phenylethyl)-3-(3-pyridinylmethyl)-1,3,8-triazaspiro[4.5]decane-2,4-dione	N2(C4(CCN(CC4)CCc5cccc5)C(=O)N(C2=O)Cc3cnccc3)CCc1cccc1	C29H32O2N4
181940757	ChemBridge Corporation	32425739	8-(2,6-dimethyl-5-heptenyl)-1-(2-phenylethyl)-3-(3-pyridinylmethyl)-1,3,8-triazaspiro[4.5]decane-2,4-dione	N2(C4(CCN(CC4)CC(CCC=C(C)C)C)C(=O)N(C2=O)Cc3cnccc3)CCc1cccc1	C30H40O2N4
181915466	ChemBridge Corporation	12052429	1-(4-methoxybenzyl)-4-((1R,2R)-2-phenylcyclopropyl)carbonyl]-6-(3-pyridinylmethoxy)-1,4-diazepan-2-one	N3(CC(CN(C(=O)C3)Cc5ccc(cc5)OC)OCc4cnccc4)C(=O)[C@H]1[C@@H](C1)c2cccc2	C29H31O4N3
182070366	ChemBridge Corporation	94419756	8-(1H-indol-3-ylmethyl)-3-isobutyl-1-[2-(4-methoxyphenyl)ethyl]-1,3,8-triazaspiro[4.5]decane-2,4-dione	[nH]1c2c(c(c1)CN3CCC4(N(C(=O)N(C4=O)CC(C)C)CCc5ccc(cc5)OC)CC3)cccc2	C29H36O3N4
181349814	ChemBridge Corporation	57791277	2-(4-(1-benzothien-3-yl)-2-((4-(2-piperazinyl)methyl)phenoxy)-N-(1,3-thiazol-2-ylmethyl)acetamide (G2iE)	[s]1c(ncc1)CNC(=O)COc2c(cc(c2)c5c6c([s]c5)cccc6)CN3CCN(CC3)c4ncccc4	C30H29O2N5S2
466125339	ChemBridge Corporation	87775506		[s]1c(c(cc1C)c2nc(ncc2)[n]3ncc(c3C5CC5)C(=O)N(Cc4cc(ccc4)OC)C)C	C26H27O2N5S1
181305778	ChemBridge Corporation	26258872	2-(5-cyclopropyl-4-((4-(2-ethoxyphenyl)-1-piperazinyl)carbonyl)-1H-pyrazol-1-yl)-4-(5-methyl-2-furyl)pyrimidine (G2i)	[n]3(ncc(c3C6CC6)C(=O)N4CCN(CC4)c5c(ccc5)OCC)c1nc(ccn1)c2[o]c(cc2)C	C28H30O3N6
181336555	ChemBridge Corporation	47200727	methyl 3-[4-{1-[(2-methyl-1H-indol-3-yl)methyl]-4-piperidinyl}-2-(4-pyridinyl)-5-pyrimidinyl]phenyl ether	N3(CCC(CC3)c4nc(ncc4c6cc(ccc6)OC)c5ccncc5)Cc1c2c([nH]c1C)cccc2	C31H31O1N5
181267787	ChemBridge Corporation	11197728	2-[2,5-dioxo-3-phenyl-1-(3-pyridinylmethyl)-3-pyrrolidinyl]-N-methyl-N-[2-(trifluoromethyl)benzyl]acetamide	FC(F)(F)c1c(cccc1)CN(C)C(=O)C3(CC(=O)N(C3=O)Cc4cnccc4)c2cccc2	C27H24O3N3F3
181971369	ChemBridge Corporation	68833669	{4-[[4-(2,5-dimethylphenyl)-1-piperazinyl]carbonyl]-1-[4-(2-thienyl)-2-pyrimidinyl]-1H-pyrazol-5-yl]methyl methyl ether	[s]1c(ccc1)c2nc(ncc2)[n]3ncc(c3COC)C(=O)N4CCN(CC4)c5c(cc(c5)C)C	C26H28O2N6S1
181931148	ChemBridge Corporation	23777777	3-((3-[4-(2-methoxyphenyl)-1-piperazinyl]-1-piperidinyl)carbonyl)-4,6-dimethyl-2(1H)-pyridinone	N3(CCN(CC3)c4c(cccc4)OC)C1CN(CCC1)C(=O)c2c(nc(c2C)C)O	C24H32O3N4
181278705	ChemBridge Corporation	15094108	2-(5-cyclopropyl-4-((4-(2-methoxyphenyl)-1-piperazinyl)carbonyl)-1H-pyrazol-1-yl)-4-(2-thienyl)pyrimidine (G2iC)	[s]1c(ccc1)c2nc(ncc2)[n]3ncc(c3C6CC6)C(=O)N4CCN(CC4)c5c(cccc5)OC	C26H26O2N6S1
181284072	ChemBridge Corporation	16803568	6-[(4'-methyl[1,1'-biphenyl]-4-yl)carbonyl]-1-[4-(2-pyridinyl)-1-piperazinyl]carbonyl]-6-azaspiro[2.5]octane	N2(CCN(CC2)C(=O)C3C4(CCN(C4)C(=O)c5ccc(cc5)c6ccc(cc6)C)C3)c1ncccc1	C31H34O2N4
181268085	ChemBridge Corporation	11381046	2-(5-cyclopropyl-4-((4-phenyl-1-piperazinyl)carbonyl)-1H-pyrazol-1-yl)-4-(3-methoxyphenyl)pyrimidine	[n]3(ncc(c3C6CC6)C(=O)N4CCN(CC4)c5cccc5)c1nc(ccn1)c2cc(ccc2)OC	C28H28O2N6
181962616	ChemBridge Corporation	56596371	2-[4-[[4-cyclopentyl-1-piperazinyl]carbonyl]-5-(methoxymethyl)-1H-pyrazol-1-yl]-4-(2,5-dimethyl-3-thienyl)pyrimidine	[s]1c(c(cc1C)c2nc(ncc2)[n]3ncc(c3COC)C(=O)N4CCN(CC4)C5CCC5)C	C25H32O2N6S1

182001206	ChemBridge Corporation	88168217	5-cyclopropyl-1-(5,6-dihydrobenzo[h]quinazolin-2-yl)-N-methyl-N-(5-quinolinylmethyl)-1H-pyrazole-4-carboxamide (G2iF)	[n]4(ncc(c4C7CC7)C(=O)N(Cc5c6(ncccc6)ccc5)C)c1nc2c(cn1)CCc3c2cccc3	C30H26O1N6
181149526	ChemBridge Corporation	35941485	N-([3-(1-benzofuran-2-yl)-1-benzyl-1H-pyrazol-4-yl]methyl)-2-(3,5-dimethyl-1H-pyrazol-4-yl)-N-methylethanamine	[n]2(nc(c(c2)CN(Cc5c([nH]nc5C)C)C)c3[o]c4c(c3)cccc4)Cc1cccc1	C27H29O1N5
181121814	ChemBridge Corporation	24355885	3-[(3-{3-oxo-3-[4-(2-pyridinyl)-1-piperazinyl]propyl}-1-piperidinyl)carbonyl]-1H-indazole	N2(CCN(CC2)C(=O)CCC3CN(CC3)C(=O)c4n[nH]c5c4cccc5)c1ncccc1	C25H30O2N6
947315724	ChemBridge Corporation	78029423		[s]1c2c(c(c1)C(=O)N3CCNC(=O)[C@@H](NC(=O)[C@@H](N(C(=O)[C@@H](NC(=O)C3)Cc5c6c([nH]c5)cccc6)C)C)c4cccc4)C(C)C2	C37H42O5N6 S1
258707156	Princeton BioMolecular Research, Inc.	OSSL_325802	5-(4-methylphenyl)-2-phenyl-7-[4-[2-(4-pyridinyl)ethyl]-1,4-diazepan-1-yl][1,3]oxazolo[4,5-d]pyrimidine	N2(CCN(CCC2)c3nc(nc5nc([o]c53)c6cccc6)c4ccc(cc4)C)CCc1cnccc1	C30H30O1N6
34977075	Princeton BioMolecular Research, Inc.	OSSL_392390	7-[3-(1,3-benzothiazol-2-ylsulfanyl)propyl]-3-methyl-8-(4-phenyl-1-piperazinyl)-3,7-dihydro-1H-purine-2,6-dione	[s]1c2c(nc1SCCC[n]3c4c(nc3N5CCN(CC5)c6cccc6)N(C(=O)NC4=O)C)cccc2	C26H27O2N7 S2
35943973	Princeton BioMolecular Research, Inc.	OSSL_575565	2-(3-[1,1'-biphenyl]-4-yl-1-[(5-(5-chloro-2-thienyl)-7-(trifluoromethyl)pyrazolo[1,5-a]pyrimidin-2-yl]carbonyl)-4,5-dihydro-1H-pyrazol-5-yl)phenol	FC(F)(F)C1=CC(=Nc3[n]1nc(c3)C(=O)N4NC(=CC4c7c(ccc7)O)c5ccc(cc5)c6cccc6)c2[s]c(cc2)Cl	C33H21O2N5 Cl1S1F3
63176616	Princeton BioMolecular Research, Inc.	OSSL_586205	2-[3,5-bis(2,4-dimethoxyphenyl)-1H-pyrazol-1-yl]-4-(4-fluorophenyl)-6-(trifluoromethyl)pyrimidine	FC(F)(F)c1nc(nc(c1)c5ccc(cc5)F[n]2nc(cc2c4c(cc(cc4)OC)OC)c3c(cc3)OC)OC	C30H24O4N4 F4
63178386	Princeton BioMolecular Research, Inc.	OSSL_587015	2-[3,5-bis(3,4-dimethoxyphenyl)-1H-pyrazol-1-yl]-4-(4-fluorophenyl)-6-(trifluoromethyl)pyrimidine	FC(F)(F)c1nc(nc(c1)c5ccc(cc5)F[n]2nc(cc2c4cc(c(cc4)OC)OC)c3cc(c(cc3)OC)OC	C30H24O4N4 F4
63178397	Princeton BioMolecular Research, Inc.	OSSL_589046	2-[3,5-bis[4-(difluoromethoxy)phenyl]-1H-pyrazol-1-yl]-4-phenyl-6-(trifluoromethyl)pyrimidine	FC(F)(F)c1nc(nc(c1)c5cccc5)[n]2nc(cc2c4ccc(cc4)OC(F)F)c3cc(c(cc3)OC(F)F	C28H17O2N4 F7
40904376	Princeton BioMolecular Research, Inc.	OSSL_768205	N-benzyl-1-(1H-indol-3-ylmethyl)-N-(2-phenylethyl)-4-piperidinamine oxalate	N3(CCC(CC3)N(Cc5cccc5)Cc4cccc4)Cc1c2c([nH]c1)cccc2.OC(=O)C(=O)O	C31H35O4N3
35085263	Scientific Exchange, Inc.	M-033644	6-amino-3-(1-naphthyl)-4-[4-(1-naphthylmethoxy)phenyl]-1,4-dihydropyrano[2,3-c]pyrazole-5-carbonitrile	[nH]1nc(c4c1OC(=C(C4c5ccc(cc5)OCc6c7c(ccc6)ccc7)C#N)N)c2c3c(ccc2)cccc3	C34H24O2N4
27659180	Specs	AG-205/11132108	2-(3-{2-[3-(4-fluorophenyl)-5-(4-isopropylphenyl)-2,5-dihydro-1H-pyrazol-1-yl]-1,3-thiazol-4-yl}phenyl)-1H-isoindole-1,3(2H)-dione	Fc1ccc(cc1)C2=CC(N(N2)c4[s]cc(n4)c5cc(ccc5)N6C(=O)c7c(ccc7)C6=O)c3ccc(cc3)C(C)C	C35H27O2N4 S1F1
27916761	Specs	AG-690/13508135	4-(4-tert-butylphenyl)-2-[[2-oxo-2-(10H-phenothiazin-10-yl)ethyl]sulfanyl]-6-phenylnicotinonitrile	S1c2c(cccc2)N(c6c1cccc6)C(=O)CS3c3nc(cc3C#N)c5ccc(cc5)C(C)C)c4cccc4	C36H29O1N3 S2

Publications

27824288	Specs	AG-690/40750941	N-(4-chlorobenzyl)-N-(1-naphthyl)-2-[(2-phenyl-4-quinazoliny)sulfany]acetamide	S(CC(=O)N(Cc6ccc(cc6)Cl)c4c5c(ccc4)cccc5)c1nc(nc3c1cccc3)c2cccc2	C33H24O1N3Cl1S1
27883605	Specs	AG-690/40753767	2-phenoxyethyl 4-[2-(benzyloxy)phenyl]-7-(3,4-dimethoxyphenyl)-2-methyl-5-oxo-1,4,5,6,7,8-hexahydro-3-quinolinecarboxylate	N1C2=C(C(C(=C1C)C(=O)OCCOc6cccc6)c4c(ccc4)OCc5cccc5)C(=O)CC(C2)c3cc(c(cc3)OC)OC	C40H39O7N1
27659184	Specs	AG-205/11132170	N-(4-{2-[3-(4-fluorophenyl)-5-(4-isopropylphenyl)-2,5-dihydro-1H-pyrazol-1-yl]-1,3-thiazol-4-yl}phenyl)-4-methylbenzenesulfonamide	Fc1ccc(cc1)C2=CC(N(N2)c4[s]cc(n4)c5ccc(cc5)N[S](=O)(=O)c6c(cc6)C)c3ccc(cc3)C(C)C	C34H31O2N4S2F1
27644832	Specs	AN-919/14712055	4-(4-methoxyphenyl)-2-(10H-phenothiazin-10-ylcarbonyl)-6-phenylthieno[2,3-b]pyridin-3-amine	[s]1c2nc(cc2c(c1C(=O)N5c6c(cccc6)Sc7c5cccc7)N)c4ccc(cc4)OC)c3cccc3	C33H23O2N3S2
35975457	InterBioScreen Ltd.	STOCK75-69659	(8S,8aR,11aS)-10-(2-naphthyl)-9,11-dioxo-N-[3-(trifluoromethyl)phenyl]-8a,9,10,11,11a,11b-hexahydro-8H-pyrrolo[3',4':3,4]pyrrolo[2,1-a]isoquinoline-8-carboxamide	FC(F)(F)c1cc(ccc1)NC(=O)[C@H]2N3C([C@@H]5[C@H]2C(=O)N(C5=O)c6cc7c(cc6)cccc7)c4c(ccc4)C=C3	C32H22O3N3F3
29332280	InterBioScreen Ltd.	STOCK75-68264	3-benzhydryl 1-methyl (1S,2R,3R)-1-cyano-2-[4-(dimethylamino)phenyl]-1,2,3,10b-tetrahydropyrrolo[2,1-a]isoquinoline-1,3-dicarboxylate	N21[C@H]([C@@H]([C@@H]([C@H]2c6c(ccc6)C=C1)(C(=O)OC)C#N)c5ccc(cc5)N(C)C(=O)OC(c4cccc4)c3cccc3	C37H33O4N3
29351964	InterBioScreen Ltd.	STOCK75-65756	benzhydryl (8S,8aR,11aS)-10-(4-methoxyphenyl)-9,11-dioxo-8a,9,10,11,11a,11b-hexahydro-8H-pyrrolo[3',4':3,4]pyrrolo[2,1-a]isoquinoline-8-carboxylate	N21[C@@H]([C@H]5[C@H]([C@H]([C@H]2c7c(ccc7)C=C1)C(=O)N(C5=O)c6ccc(cc6)OC)C(=O)OC(c4cccc4)c3cccc3	C35H28O5N2
29728600	Life Chemicals Inc.	F0417-2422	ethyl 5-({(4-benzoylbenzoyl)amino)benzoyl}oxy)-2-methyl-1-phenyl-1H-indole-3-carboxylate	[n]2(c3c(c(c2C)C(=O)OCC)cc(cc3)OC(=O)c4c(ccc4)NC(=O)c5cc(c(cc5)C(=O)c6cccc6)c1cccc1	C39H30O6N2
30865539	Life Chemicals Inc.	F0575-0046	4-(5-(4-fluorophenyl)-1-((2-methyl-1H-indol-3-yl)sulfanyl)acetyl)-4,5-dihydro-1H-pyrazol-3-yl)phenyl methyl ether (G2iA)	Fc1ccc(cc1)C2N(NC(=C2)c5ccc(cc5)OC)C(=O)CSc3c4c([NH]c3C)cccc4	C27H24O2N3S1F1
29791344	Life Chemicals Inc.	F0721-0768	N-([5-([2-(3,4-dihydro-1(2H)-quinolinyl)-2-oxoethyl)sulfanyl]-4-(2-methoxyphenyl)-4H-1,2,4-triazol-3-yl)methyl]-4-[[dimethylamino)sulfonyl]benzamide	[S](=O)(=O)(N(C)C)c1ccc(cc1)C(=O)NCc2[n](c(nn2)SCC(=O)N4CCc5c4cccc5)c3c(ccc3)OC	C30H32O5N6S2
30335515	Life Chemicals Inc.	F0913-4612	3-([4-(2,5-dimethylphenyl)-1-piperazinyl]carbonyl)-6-([4-(4-fluorophenyl)-1-piperazinyl]sulfonyl)-4(1H)-quinolinone	Fc1ccc(cc1)N2CCN(CC2)[S](=O)(=O)c3cc4c(ncc(c4O)C(=O)N5CN(CC5)c6c(ccc(c6)C)C)cc3	C32H34O4N5S1F1
29793191	Life Chemicals Inc.	F0737-0110	N-[3-(1,3-benzothiazol-2-yl)-6-methyl-4,5,6,7-tetrahydro-1-benzothien-2-yl]-4-(2,3-dihydro-1H-indol-1-yl)sulfonylbenzamide	[S](=O)(=O)(N6CCc7c6cccc7)c1ccc(cc1)C(=O)Nc2[s]c3c(c2c4[s]c5c(n4)cccc5)CCC(C3)C	C31H27O3N3S3
29606176	Labotest	LT01321967	N-(2-benzoyl-4-bromophenyl)-4-[(6-chloro-4-phenyl-2-quinazoliny)amino]benzamide	Brc1cc(c(cc1)NC(=O)c3ccc(cc3)Nc4nc5c(c(n4)c6cccc6)cc(cc5)Cl)C(=O)c2cccc2	C34H22O2N4Cl1Br1
65382808	Otava	7006549	4-[4-(benzyloxy)phenyl]-3-(2-hydroxyphenyl)-5-(3-pyridinylmethyl)-4,5-	[nH]1nc(c3c1C(=O)N(C3c5ccc(c5)OCc6cccc6)Cc4cnccc4)c2c(ccc2)O	C30H24O3N4

			dihydropyrrolo[3,4-c]pyrazol-6(1H)-one		
77016607	Pharmeks LTD.	PHAR335882	4-(bis(3-hydroxy-5-methyl-1H-pyrazol-4-yl)methyl)phenyl 4-fluorobenzoate	Fc1ccc(cc1)C(=O)Oc2ccc(cc2)C(c4c([nH]nc4O)C)c3c([nH]nc3O)C	C22H19O4N4F1
458452454	Pharmeks LTD.	PHAR363782		N3(C(=CC(=O)C(C3=O)C(CC(=O)OC)c4[o]c(cc4)c5c(ccc5)C(=O)O)C)CCc1c2c([nH]c1)cccc2	C31H28O7N2
34979766	Pharmeks LTD.	PHAR083314	8-benzoyl-4-(4-bromobenzoyl)-2-(3,5-dichlorophenyl)-3a,4,9a,9b-tetrahydro-1H-pyrrolo[3,4-a]indolizine-1,3(2H)-dione	Brc1ccc(cc1)C(=O)C2N3C(C5C2C(=O)N(C5=O)c6cc(cc(c6)Cl)Cl)C=C(C=C3)C(=O)c4cccc4	C30H19O4N2Cl2Br1
29363082	Pharmeks LTD.	PHAR089794	(11beta)-11,17-dihydroxy-3,20-dioxopregna-1,4-dien-21-yl 4-[[2-(2,2-dimethyl-4-phenyltetrahydro-2H-pyran-4-yl)ethyl]amino]-4-oxobutanoate	N(CCC6(CC(OCC6)(C)C)c5cccc5)C(=O)CCC(=O)OCC(=O)[C@@]1([C@@]2(C(C3C([C@@]4(C(C=CC(=O)C=C4)CC3)C)[C@H](C2)O)CC1)C)O	C40H53O8N1
50759467	Enamine	Z30131423	N-[2-(2-chlorophenyl)-2-(1H-indol-3-yl)ethyl]-2-(1H-indol-3-yl)acetamide (G2iH)	Clc1(ccccc1)C(CNC(=O)Cc4c5c([nH]c4)cccc5)c2c3c([nH]c2)cccc3	C26H22O1N3Cl1
95817411	Enamine	Z109718458	5-[1,1'-biphenyl]-4-yl-N-[(4,6-dimethyl-2-oxo-1,2-dihydro-3-pyridinyl)methyl]-2-thiophenecarboxamide	[s]1c(ccc1C(=O)NCc4c(nc(cc4C)C)O)c2ccc(cc2)c3cccc3	C25H22O2N2S1
30206540	Enamine	T0513-5507	2-({2-[2,5-dimethyl-1-(2-phenylethyl)-1H-pyrrol-3-yl]-2-oxoethyl}sulfanyl)-6-methyl-5-(4-methylphenyl)-3-phenylthieno[2,3-d]pyrimidin-4(3H)-one	[s]1c2c(c(c1C)c6ccc(cc6)C)C(=O)N(C(=N2)SCC(=O)c4c([n]c(c4)C)CCc5cccc5)C)c3cccc3	C36H33O2N3S2
29399326	Enamine	Z19304338	N-(9-ethyl-9H-carbazol-3-yl)-2-[[5-(1H-indol-3-yl)-1,3,4-oxadiazol-2-yl]sulfanyl]acetamide	S(CC(=O)Nc4cc5c([n]c6c5cccc6)CC)cc4c1nnc([o]1)c2c3c([nH]c2)cccc3	C26H21O2N5S1
155920809	Enamine	Z244415796	3-(1-((2E)-3-[2-(4-fluorophenyl)-1,3-thiazol-4-yl]-2-propenoyl)-1,2,3,6-tetrahydro-4-pyridinyl)-1H-pyrrolo[2,3-b]pyridine	Fc1ccc(cc1)c2[s]cc(n2)\C=C\C(=O)N3CCC(=CC3)c4c5c([nH]c4)nc5	C24H19O1N4S1F1
27082796	Enamine	T5603758	N-(2-benzoyl-4-methylphenyl)-4-[(6-methyl-4-phenyl-2-quinazolyl)amino]benzamide	N(c4ccc(cc4)C(=O)Nc5c(cc(cc5)C)C(=O)c6cccc6)c1nc2c(c(n1)c3cccc3)cc(cc2)C	C36H28O2N4
112921324	Enamine	Z220595048	N-(1-isoquinolylmethyl)-4-[5-(4-methoxyphenyl)-3-phenyl-4,5-dihydro-1H-pyrazol-1-yl]-4-oxobutanamide	N3(NC(=CC3c5cc(cc5)OC)c4ccc4)C(=O)CCC(=O)NC1nccc2c1cccc2	C30H28O3N4
371582429	Enamine	Z1446647643	3-[1-(3-fluorobenzoyl)-5-(4-fluorophenyl)-2,5-dihydro-1H-pyrazol-3-yl]-6-methyl-4-phenyl-2-quinolinol	Fc1cc(ccc1)C(=O)N2NC(=CC2c6ccc(cc6)F)c3c(nc4c(c3c5cccc5)cc(cc4)C)O	C32H23O2N3F2
947324579	Enamine	Z2858952890		[s]1c(ccc1C(=O)O)CN(C5CC6(N(C5)C(=O)OC(C)(C)C)CCCC6)C(=O)OCC2c3c(ccc3)c4c2cccc4	C36H42O6N2S1
113915710	Enamine	Z234513220	3-([1-(1,3-diphenyl-1H-pyrazol-5-yl)carbonyl]-1,2,3,6-tetrahydro-4-pyridinyl)-1H-pyrrolo[2,3-b]pyridine	[n]2(nc(cc2C(=O)N4CCC(=CC4)c5c6c([nH]c5)nccc6)c3cccc3)c1cccc1	C28H23O1N5
388606908	Enamine	Z1558581164	N-(2-(1-(6-chloro-4-phenylquinazolin-2-yl)-5-(4-(dimethylamino)phenyl)-	[S](=O)(=O)(Nc1c(ccc1)C2=CC(N(N2)c4nc5c(c(n4)c6cccc6)cc(c5)Cl)c3ccc(cc3)N(C)C	C32H29O2N6Cl1S1

Publications

			2,5-dihydro-1H-pyrazol-3-yl)phenyl)methanesulfonamide		
33510957	Enamine	Z18699620	2-(1H-indol-3-yl)-2-oxoethyl 3-[(2-methyl-2,3-dihydro-1H-indol-1-yl)sulfonyl]benzoate	[S](=O)(=O)(N4C(Cc5c4cccc5)C)c1cc(ccc1)C(=O)OCC(=O)c2c3c([nH]c2)cccc3	C26H22O5N2 S1
118879125	Enamine	Z243366928	2-[hexyl(4-phenyl-1,3-thiazol-2-yl)amino]-2-oxoethyl 6-(1H-1,2,4-triazol-1-yl)nicotinate	[s]1c(nc(c1)c4cccc4)N(CCCCCC)C(=O)COC(=O)c2cnc(cc2)[n]3nnc3	C25H26O3N6 S1
428762224	Enamine	Z1891749033		Clc1cc(ccc1)N2CCN(CC2)C(=O)c3ccc(cc3)Nc4nc5c(c(n4)c6ccc(c6)Cl)cccc5	C31H25O1N5 Cl2
30846314	Enamine	Z19316401	methyl 4-{3-phenyl-1-[(4-quinazoliny)sulfonyl]acetyl}-4,5-dihydro-1H-pyrazol-5-yl)phenyl ether	S(CC(=O)N3NC(=CC3c5ccc(cc5)OC)c4cccc4)c1ncnc2c1cccc2	C26H22O2N4 S1
37807463	Enamine	Z25492200	2-[[4-(3,4-dimethylphenyl)-1-phenyl-1H-imidazol-2-yl]sulfonyl]-1-(2-methyl-1H-indol-3-yl)ethanone	S(CC(=O)c4c5c([nH]c4C)cccc5)c1[n](cc(n1)c3cc(c(cc3)C)C)c2cccc2	C28H25O1N3 S1
29606134	Enamine	T5605033	N-(2-benzoyl-4-bromophenyl)-3-[(6-bromo-4-phenyl-2-quinazoliny)amino]benzamide	BrC1cc(c(cc1)NC(=O)c3cc(ccc3)Nc4nc5c(c(n4)c6cccc6)cc(cc5)Br)C(=O)c2cccc2	C34H22O2N4 Br2
29116573	Enamine	T0513-8000	2-([2-[2,5-dimethyl-1-(2-phenylethyl)-1H-pyrrol-3-yl]-2-oxoethyl]sulfonyl)-3,6-diphenylthieno[2,3-d]pyrimidin-4(3H)-one	[s]1c2c(cc1c6cccc6)C(=O)N(C(=N2)SCC(=O)c4c([n](c(c4)C)CCc5cccc5)C)c3cccc3	C34H29O2N3 S2
388606909	Enamine	Z1558581147	6-chloro-2-(5-(4-ethoxyphenyl)-3-(m-tolyl)-2,5-dihydro-1H-pyrazol-1-yl)-4-phenylquinazoline	Clc1cc2c(nc(nc2c6cccc6)N3NC(=CC3c5ccc(cc5)OCC)c4cc(ccc4)C)cc1	C32H27O1N4 Cl1
406070290	Enamine	EN300-117175	4-(N-(4-cyclohexylbenzyl)-2-((2,3,4,5,6-pentafluoro-N-methylphenyl)sulfonamido)acetamido)-2-hydroxybenzoic acid	Fc1c(c(c(c1F)F)[S](=O)(=O)N(C(=O)N(Cc3ccc(cc3)C4CCCC4)c2cc(c(cc2)C(=O)O)O)C)F	C29H27O6N2 S1F5
28678113	Vitas-M Laboratory, Ltd.	STK269113	2-[1,1'-biphenyl]-4-yl-2-oxoethyl 2-[1,1'-biphenyl]-4-yl-6-methyl-4-quinolinecarboxylate	n1c2c(c(cc1c5ccc(cc5)c6cccc6)C(=O)OCC(=O)c3ccc(cc3)c4cccc4)cc(cc2)C	C37H27O3N1
34885276	Vitas-M Laboratory, Ltd.	STK296037	1,3-dioxo-2-[3-[(3-phenoxyanilino)carbonyl]phenyl]-N-(3-phenoxyphenyl)-5-isoindolinecarboxamide	N4(C(=O)c5c(ccc(c5)C(=O)Nc6cc(ccc6)Oc7cccc7)C4=O)c1cc(c(cc1)C(=O)Nc2cc(ccc2)Oc3cccc3	C40H27O6N3
36012691	Vitas-M Laboratory, Ltd.	STK279195	4,4'-((3-bromo-4-(naphthalen-1-yl)methoxy)phenyl)methylene)bis(3-methyl-1H-pyrazol-5-ol)	BrC1c(ccc(c1)C(c5c([nH]nc5C)O)c4c([nH]nc4C)O)OCc2c3c(ccc2)cccc3	C26H23O3N4 Br1
63176574	Vitas-M Laboratory, Ltd.	STK313895	2-[3,5-bis(3,4-dimethoxyphenyl)-1H-pyrazol-1-yl]-4-(2-thienyl)-6-(trifluoromethyl)pyrimidine	FC(F)(F)c1nc(nc(c1)c5[s]ccc5)[n]2nc(cc2c4cc(c(cc4)OC)OC)c3cc(c(cc3)OC)OC	C28H23O4N4 S1F3
63176613	Vitas-M Laboratory, Ltd.	STK313915	2-[3,5-bis(3,4-dimethoxyphenyl)-4-ethyl-1H-pyrazol-1-yl]-4-(4-fluorophenyl)-6-(trifluoromethyl)pyrimidine	FC(F)(F)c1nc(nc(c1)c5ccc(cc5)F)[n]2nc(c(c2c4cc(c(cc4)OC)OC)C)c3cc(c(cc3)OC)OC	C32H28O4N4 F4
63176630	Vitas-M Laboratory, Ltd.	STK313922	2-[3,5-bis(3,4-dimethoxyphenyl)-4-ethyl-1H-pyrazol-1-yl]-4-phenyl-6-(trifluoromethyl)pyrimidine	FC(F)(F)c1nc(nc(c1)c5cccc5)[n]2nc(c(c2c4cc(c(cc4)OC)OC)CC)c3cc(c(cc3)OC)OC	C32H29O4N4 F3
63178383	Vitas-M Laboratory, Ltd.	STK314253	2-[3,5-bis(3,4-dimethoxyphenyl)-4-methyl-1H-pyrazol-1-yl]-4-(3-methoxyphenyl)-6-(trifluoromethyl)pyrimidine	FC(F)(F)c1nc(nc(c1)c5cc(ccc5)OC)[n]2nc(c(c2c4cc(c(cc4)OC)OC)C)c3cc(c(cc3)OC)OC	C32H29O5N4 F3

28394210	Vitas-M Laboratory, Ltd.	STK038146	N-benzyl-N-(4,5-diphenyl-1,3-thiazol-2-yl)-2-[(4-hydroxy-6-phenyl-2-pyrimidinyl)sulfanyl]acetamide	[s]1c(nc(c1c6cccc6)c5cccc5)N(Cc4cccc4)C(=O)CSc2nc(ccn2)c3cccc3)O	C34H26O2N4 S2
29999180	Vitas-M Laboratory, Ltd.	STK053875	2-(4-tert-butylphenoxy)-N-(2-[[[4-tert-butylphenoxy]acetyl]anilino]ethyl)-N-phenylacetamide	N(CCN(c4cccc4)C(=O)COc3ccc(cc3)C(C)(C)(c2cccc2)C(=O)COc1ccc(cc1)C(C)(C)C	C38H44O4N2
28414872	Vitas-M Laboratory, Ltd.	STK392050	1-(9H-fluoren-2-yl)-2-[[5-(2-furyl)-4-phenyl-4H-1,2,4-triazol-3-yl]sulfanyl]ethanone	S(CC(=O)c4cc5c(cc4)c6c(cccc6)C5)c1[n](c(nn1)c3[o]ccc3)c2cccc2	C27H19O2N3 S1
27806338	Vitas-M Laboratory, Ltd.	STK043440	N-[1-(4-methoxybenzoyl)-2-methyl-1,2,3,4-tetrahydro-4-quinolinyl]-4-pentyl-N-phenylbenzamide	N2(C(CC(c5c2cccc5)N(c4cccc4)C(=O)c3ccc(cc3)CCCC)C)C(=O)c1ccc(cc1)OC	C36H38O3N2
39750226	Vitas-M Laboratory, Ltd.	STL052698	9a-((E)-2-[4-[3-(3-chloro-4-methoxyphenyl)-1-phenyl-1H-pyrazol-4-yl]phenyl]ethenyl)-9,9-dimethyl-9,9a-dihydro-1H-imidazo[1,2-a]indol-2(3H)-one	Clc1c(ccc(c1)c2n[n](cc2c4ccc(c4)\C=C\C65N(CC(=O)N6)c7c(ccc7)C5(C)C)c3cccc3)OC	C36H31O2N4 Cl1
158573473	Vitas-M Laboratory, Ltd.	STK636849	N-(2-[5-(benzyloxy)-1H-indol-3-yl]ethyl)-3-(4-pyridinyl)-1,2,4-oxadiazole-5-carboxamide	[nH]1c2c(c(c1)CCNC(=O)c4nc(n[o]4)c5cnc5)cc(cc2)OCc3cccc3	C25H21O3N5
31278512	Vitas-M Laboratory, Ltd.	STK681999	2-[[4-(1-adamantyl)-1-piperazinyl]carbonyl]-5,7-diphenylpyrazolo[1,5-a]pyrimidine	[n]21nc(cc2N=C(C=C1c8cccc8)c7cccc7)C(=O)N3CCN(CC3)C54CC6CC(C5)CC(C4)C6	C33H35O1N5
47635094	Vitas-M Laboratory, Ltd.	STK686647	4-(4-chlorophenyl)-1-(4-isopropylphenyl)-N-(3-methoxyphenyl)-5,6,7,8-tetrahydro-2a,4a-diazacyclopenta[cd]azulene-2-carboxamide	Clc1ccc(cc1)C2=C[n]3c4c(c(c3C(=O)Nc6cc(ccc6)OC)c5ccc(cc5)C(C)C)CCCCN42	C33H32O2N3 Cl1
47635071	Vitas-M Laboratory, Ltd.	STK782131	4-(3,4-dimethylphenyl)-N-(4-methoxyphenyl)-1-(4-methylphenyl)-5,6,7,8-tetrahydro-2a,4a-diazacyclopenta[cd]azulene-2-carboxamide	[n]21c3c(c(c2C(=O)Nc6ccc(cc6)OC)c5ccc(cc5)C)CCCCN3C(=C1)c4cc(c(cc4)C)C	C33H33O2N3
27366974	Vitas-M Laboratory, Ltd.	STK528173	ethyl 3-[[[1-[[1,3-dioxo-1,3-dihydro-2H-isoindol-2-yl)methyl]-3,4-dihydro-2(1H)-isoquinolinyl]acetyl]amino]-5-methoxy-1H-indole-2-carboxylate	[nH]1c2c(c(c1C(=O)OCC)NC(=O)CN3CCc4c(ccc4)C3CN5C(=O)c6c(ccc6)C5=O)cc(cc2)OC	C32H30O6N4
27546167	Vitas-M Laboratory, Ltd.	STK717513	4-ethyl-2-[4-(4-methyl-1,3-thiazol-2-yl)-1H-pyrazol-3-yl]-5-(1-naphthylmethoxy)phenol	[s]1c(nc(c1)C)c2c[nH]nc2c3c(cc(c3)CC)OCc4c5c(ccc4)cccc5)O	C26H23O2N3 S1
27304178	Vitas-M Laboratory, Ltd.	STK526378	ethyl 6-amino-2-[[[4-(4-chlorophenyl)-3-cyano-6-(2-thienyl)-2-pyridinyl]sulfanyl]methyl]-5-cyano-4-(3-pyridinyl)-4H-pyran-3-carboxylate	[s]1c(ccc1)c2nc(c(c2)c5ccc(cc5)Cl)C#N)SCC3=C(C(C(=O)N)C#N)c4cnc4)C(=O)OCC	C31H22O3N5 Cl1S2
27348341	Vitas-M Laboratory, Ltd.	STK528432	N-(4-fluorobenzyl)-N'-(1-naphthyl)-N-[4-(9H-thioxanthen-9-yl)phenyl]urea	Fc1ccc(cc1)CN(c4ccc(cc4)C5c6c(ccc6)Sc7c5cccc7)C(=O)Nc2c3c(cc2)cccc3	C37H27O1N2 S1F1
27558683	Vitas-M Laboratory, Ltd.	STK532121	4-(3-methoxyphenyl)-1-(phenethylthio)-4H-spiro[benzo[h][1,2,4]triazolo[4,3-a]quinazoline-6,1'-cyclohexan]-5(7H)-one	S(CCc7cccc7)c1[n]2c(nn1)N(C(=O)C4=C2c5c(ccc5)CC64CCCC6)c3cc(ccc3)OC	C33H32O2N4 S1
48658033	Vitas-M Laboratory, Ltd.	STK597215	4-(3,4-dimethylphenyl)-1-(4-ethylphenyl)-N-(3-methylphenyl)-5,6,7,8-tetrahydro-2a,4a-	[n]21c3c(c(c2C(=O)Nc6cc(ccc6)C)c5ccc(cc5)CC)CCCCN3C(=C1)c4cc(c(cc4)C)C	C34H35O1N3

Publications

			diazacyclopenta[cd]azulene-2-carboxamide		
28869109	Vitas-M Laboratory, Ltd.	STK065789	4-[bis(5-hydroxy-3-methyl-1H-pyrazol-4-yl)methyl]-2-ethoxyphenyl 2-chlorobenzoate	Clc1c(cccc1)C(=O)Oc2c(cc2)C(c4c([nH]nc4C)O)c3c([nH]nc3C)O)OCC	C24H23O5N4 Cl1
27462543	Vitas-M Laboratory, Ltd.	STK084760	N-(2-methyl-1-[(2-naphthylloxy)acetyl]-1,2,3,4-tetrahydro-4-quinolinyl)-2-(2-naphthylloxy)-N-phenylacetamide	N3(C(CC(c7c3cccc7)N(c6cccc6)C(=O)COc4cc5c(cc4)cccc5)C(C(=O)COc1cc2c(cc1)cccc2	C40H34O4N2
30738164	ChemDiv, Inc	5867-4076	N-[3-(1,3-benzothiazol-2-yl)phenyl]-3-[(5-phenyl[1,3]thiazolo[2,3-c][1,2,4]triazol-3-yl)sulfanyl]propanamide	S1c2[n](c(nn2)SCCC(=O)Nc4cc(ccc4)c5[s]c6c(n5)cccc6)C(=C1)c3cccc3	C26H19O1N5 S3
40756209	ChemDiv, Inc	C797-0522	1-[1-(2,5-dimethylbenzyl)-1H-benzimidazol-2-yl]-N-[2-(1H-indol-3-yl)ethyl]-4-piperidinecarboxamide	N4(CCC(CC4)C(=O)NCCc5c6c([nH]c5)cccc6)c1[n](c3c(n1)cccc3)Cc2c(ccc(c2)C)C	C32H35O1N5
40768166	ChemDiv, Inc	C797-0834	4-([3-(4-methoxybenzyl)-3H-imidazo[4,5-c]pyridin-2-yl)sulfanyl)methyl)-N-(4-methylbenzyl)benzamide	S(Cc4ccc(cc4)C(=O)NCc5ccc(cc5)C)c1[n](c3c(n1)ccnc3)Cc2ccc(cc2)OC	C30H28O2N4 S1
61639904	ChemDiv, Inc	C878-1784	3-[4-(2,3-dihydro-1H-indol-1-ylcarbonyl)benzyl]-2-[(4-methylbenzyl)sulfanyl]-3H-imidazo[4,5-c]pyridine	S(Cc6ccc(cc6)C)c1[n](c5c(n1)ccnc5)Cc2ccc(cc2)C(=O)N3CCc4c3cccc4	C30H26O1N4 S1
61602513	ChemDiv, Inc	D016-1208	1-[5-(3-[4-(5-chloro-2-methylphenyl)-1-piperazinyl]-2-hydroxypropoxy)-2-methyl-1-(4-methylphenyl)-1H-indol-3-yl]ethanone	Clc1cc(c(cc1)C)N2CCN(CC2)CC(=O)COc3cc4c([n](c4C(=O)C)C)c5ccc(cc5)C)cc3	C32H36O3N3 Cl1
30295813	ChemDiv, Inc	C096-0092	2-(5-[(4-(2-methoxyphenyl)-1-piperazinyl)sulfonyl]-6-methyl-4-oxothieno[2,3-d]pyrimidin-3(4H)-yl)-N-methyl-N-[2-(2-pyridinyl)ethyl]acetamide	[S](=O)(=O)(N4CCN(CC4)c5c(cc5)OC)c1c2c([s]c1C)N=CN(C2=O)CC(=O)N(CCC3NCCCC3)C	C28H32O5N6 S2
64190611	ChemDiv, Inc	C794-1611	1-[5-{2-[(4-ethoxyanilino)methyl]-1H-pyrrol-1-yl}-1,3,4-thiadiazol-2-yl)-N-[2-(1H-indol-3-yl)ethyl]-4-piperidinecarboxamide	[s]1c(nnc1N4CCC(CC4)C(=O)NCc5c6c([nH]c5)cccc6)[n]2c(ccc2)CNc3ccc(cc3)OCC	C31H35O2N7 S1
111269525	ChemDiv, Inc	F154-0105	4-({2-[(4-chlorobenzyl)sulfanyl]-3H-imidazo[4,5-c]pyridin-3-yl)methyl)-N-cyclooctylbenzamide	S(Cc5ccc(cc5)Cl)c1[n](c4c(n1)ccnc4)Cc2ccc(cc2)C(=O)NC3CCCCCCC3	C29H31O1N4 Cl1S1
111269527	ChemDiv, Inc	F154-0109	4-({2-[(2-chloro-4-fluorobenzyl)sulfanyl]-3H-imidazo[4,5-c]pyridin-3-yl)methyl)-N-cyclooctylbenzamide	Fc1cc(c(cc1)C)Sc2[n](c5c(n2)ccn5)Cc3ccc(cc3)C(=O)NC4CCCCC4)Cl	C29H30O1N4 Cl1S1F1
111269549	ChemDiv, Inc	F154-0183	4-chlorobenzyl 3-[4-(2,3-dihydro-1H-indol-1-ylcarbonyl)benzyl]-3H-imidazo[4,5-c]pyridin-2-yl sulfide	S(Cc6ccc(cc6)Cl)c1[n](c5c(n1)ccnc5)Cc2ccc(cc2)C(=O)N3CCc4c3cccc4	C29H23O1N4 Cl1S1
111269574	ChemDiv, Inc	F154-0254	4-({2-[(3-chlorobenzyl)sulfanyl]-3H-imidazo[4,5-c]pyridin-3-yl)methyl)-N-(2,4-dimethylphenyl)benzamide	S(Cc5cc(ccc5)Cl)c1[n](c4c(n1)ccnc4)Cc2ccc(cc2)C(=O)Nc3c(ccc3)C)C	C29H25O1N4 Cl1S1
111269732	ChemDiv, Inc	F154-0645	N-(2-methylbenzyl)-4-[(2-[(3-(trifluoromethyl)benzyl)sulfanyl]-3H-imidazo[4,5-c]pyridin-3-yl)methyl]benzamide	FC(F)(F)c1cc(ccc1)C)Sc2[n](c5c(n2)ccnc5)Cc3ccc(cc3)C(=O)NCc4(ccc4)C	C30H25O1N4 S1F3

182707700	ChemDiv, Inc	G430-1653	(1-(2-(3,4-dimethylphenyl)pyrazolo[1,5-a]pyrazin-4-yl)piperidin-3-yl)(4-phenylpiperazin-1-yl)methanone	[n]21nc(cc2C(=NC=C1)N4CCC(CC4)C(=O)N5CCN(CC5)c6cccc6)c3cc(c(cc3)C)C	C30H34O1N6
30335059	ChemDiv, Inc	K781-0391	3-(4-(tert-butyl)benzamido)-N-(3-chlorobenzyl)-4-(8-oxo-1,5,6,8-tetrahydro-2H-1,5-methanopyrido[1,2-a][1,5]diazocin-3(4H)-yl)benzamide	Clc1cc(ccc1)CNC(=O)c2cc(c(cc2)N4CC5CN6C(=CC=CC6=O)C(C4)C5)NC(=O)c3ccc(cc3)C(C)C	C36H37O3N4 Cl1
30335319	ChemDiv, Inc	K781-1690	ethyl 4-(4-(8-oxo-1,5,6,8-tetrahydro-2H-1,5-methanopyrido[1,2-a][1,5]diazocin-3(4H)-yl)-3-(3-(trifluoromethyl)benzamido)benzamido)piperidine-1-carboxylate	FC(F)(F)c1cc(ccc1)C(=O)Nc2c(cc(c2)C(=O)NC6CCN(CC6)C(=O)OCC)N3CC4CN5C(=CC=CC5=O)C(C3)C4	C34H36O5N5 F3
30335447	ChemDiv, Inc	K781-1931	N-(5-(4-benzylpiperidine-1-carbonyl)-2-(8-oxo-1,5,6,8-tetrahydro-2H-1,5-methanopyrido[1,2-a][1,5]diazocin-3(4H)-yl)phenyl)-3-(trifluoromethyl)benzamide	FC(F)(F)c1cc(ccc1)C(=O)Nc2c(cc(c2)C(=O)N6CCC(CC6)C7c7ccc(cc7)N3CC4CN5C(=CC=CC5=O)C(C3)C4	C38H37O3N4 F3
34713223	ChemDiv, Inc	K788-1241	N-(4-isopropylphenyl)-3-[[4-(2-methoxyphenyl)-1-piperazinyl]carbonyl]-4-oxo-1,4-dihydro-6-quinolinesulfonamide (G2iG)	[S](=O)(=O)(Nc5ccc(cc5)C(C)C)c1cc2c(ncc(c2O)C(=O)N3CCN(C3)c4c(cccc4)OC)cc1	C30H32O5N4 S1
111278730	ChemDiv, Inc	F228-0561	1-(5,6-dimethylfuro[2,3-d]pyrimidin-4-yl)-N-[2-(5-methyl-1H-indol-3-yl)ethyl]-3-piperidinecarboxamide (G2iK)	N3(CC(CCC3)C(=O)NCCc4c5c([nH]c4)ccc(c5)C)c1ncnc2[o]c(c1c21)C	C25H29O2N5
185953192	ChemDiv, Inc	G435-0034	(4-(2,5-dimethylphenyl)piperazin-1-yl)(1-(2-phenylpyrazolo[1,5-a]pyrazin-4-yl)piperidin-4-yl)methanone	[n]21nc(cc2C(=NC=C1)N4CCC(CC4)C(=O)N5CCN(CC5)c6c(ccc(c6)C)C)c3cccc3	C30H34O1N6
237221619	ChemDiv, Inc	G435-0553	(1-(2-(2,4-dimethylphenyl)pyrazolo[1,5-a]pyrazin-4-yl)piperidin-4-yl)(4-(2-methoxyphenyl)piperazin-1-yl)methanone	[n]21nc(cc2C(=NC=C1)N4CCC(CC4)C(=O)N5CCN(CC5)c6c(cccc6)OC)c3c(cc(cc3)C)C	C31H36O2N6
237187975	ChemDiv, Inc	L390-0507	N-(2-(1H-indol-3-yl)ethyl)-7-(3,4-dimethylphenyl)pyrazolo[1,5-a]pyrimidine-3-carboxamide	[n]21ncc(c2N=CC=C1c5cc(c(cc5)C)C)C(=O)NCCc3c4c([nH]c3)ccc4	C25H23O1N5
237189315	ChemDiv, Inc	L483-0680	4-(4-(4-benzylpiperidine-1-carbonyl)piperidin-1-yl)-6-ethoxyquinoline-3-carbonitrile	N3(CCC(CC3)C(=O)N4CCC(CC4)Cc5cccc5)c1c2c(ncc1C#N)ccc(c2)OCC	C30H34O2N4
90394475	ChemDiv, Inc	V005-9064	6-methoxy-2-[4-(trifluoromethoxy)benzoyl]-1-[5-[2-(trifluoromethyl)phenyl]-2-furyl]-2,3,4,9-tetrahydro-1H-beta-carboline	FC(F)(F)Oc1ccc(cc1)C(=O)N2CCc3c4c([nH]c3C2c5[o]c(cc5)c6c(cccc6)C(F)(F)F)ccc(c4)OC	C31H22O4N2 F6
90317639	ChemDiv, Inc	V007-0482	8-(4-[[[2-tert-butylphenyl)sulfanyl]methyl]benzoyl]-3-(2-isopropylphenoxy)-8-azabicyclo[3.2.1]octane	S(Cc2ccc(cc2)C(=O)N3C4CCC3C(C4)Oc5c(ccc5)C(C)C)c1c(ccc1)C(C)C	C34H41O2N1 S1
121116441	ChemDiv, Inc	V003-6571	4-fluoro-N-isobutyl-N-[2-oxo-2-(4-phenyl-1-[4-(trifluoromethyl)phenyl]-1H-imidazol-2-yl)amino]ethyl]benzamide	FC(F)(F)c1ccc(cc1)[n]2c(nc(c2)C4cccc4)NC(=O)CN(CC(C)C)C(=O)c3ccc(cc3)F	C29H26O2N4 F4
121285335	ChemDiv, Inc	V007-7958	6-benzyl-4-{4-[(4-tert-butylphenyl)sulfonyl]-1-piperazinyl}-	[S](=O)(=O)(N2CCN(CC2)c3nc(nc5[n](ncc53)c6cc(ccc6)Cl)Cc4ccc4)c1ccc(cc1)C(C)C	C32H33O2N6 Cl1S1

Publications

			1-(3-chlorophenyl)-1H-pyrazolo[3,4-d]pyrimidine		
234347154	ChemDiv, Inc	V008-7832	N,3-bis(4-fluorobenzyl)-8-(trifluoromethyl)-2,3,4,4a,5,6-hexahydro-1H-pyrazino[1,2-a]quinoline-5-carboxamide	FC(F)(F)c1cc2c(cc1)N3C(CN(CC3)Cc5ccc(cc5)F)C(C)C(=O)Ncc4ccc(cc4)F	C28H26O1N3 F5
49282656	ChemDiv, Inc	V009-0402	N-(4-tert-butylbenzyl)-2-[(4-chlorobenzyl)(cyclopropyl)amino]-N-[2-(1H-indol-3-yl)ethyl]acetamide	Clc1ccc(cc1)CN(C5CC5)CC(=O)N(CCC3c4c([nH]c3)cccc4)Cc2cc(c(cc2)C(C)C)C	C33H38O1N3 Cl1
154638968	ChemDiv, Inc	V009-3943	2-[[[4-tert-butylbenzyl)(3,3-diphenylpropyl)amino]methyl]-N-(2-furylmethyl)-1,3-thiazole-4-carboxamide	[s]1c(nc(c1)C(=O)NCc5[o]ccc5)CN(CCC(c4cccc4)c3cccc3)Cc2ccc(cc2)C(C)C	C36H39O2N3 S1
90386568	ChemDiv, Inc	V011-3487	1-([1-[3',5'-bis(trifluoromethyl)[1,1'-biphenyl]-4-yl]-1H-imidazol-5-yl]carbonyl)-4-(4-tert-butylbenzyl)piperidine	FC(F)(F)c1cc(cc(c1)c2ccc(cc2)[n]3cncc3C(=O)N4CCC(CC4)Cc5ccc(cc5)C(C)C)C(F)F	C34H33O1N3 F6
154930032	ChemDiv, Inc	V014-0753	2-[[3-(benzyloxy)-2-hydroxypropyl](butyl)amino]-N-(4-tert-butylbenzyl)-N-[2-(1H-indol-3-yl)ethyl]acetamide	[nH]1c2c(c(c1)CCN(Cc4ccc(cc4)C(C)C)C)C(=O)CN(CC(O)COCc3cccc3)CCCC)cccc2	C37H49O3N3
121204288	ChemDiv, Inc	V014-1570	2-methyl-N-(2-[[1-(4-methylphenyl)-4-phenyl-1H-imidazol-2-yl]amino]-2-oxoethyl)-N-[2-(4-morpholinyl)ethyl]benzamide	[n]2(c(nc(c2)c5cccc5)NC(=O)CN(CCN4CCOCC4)C(=O)c3c(cccc3)C)c1ccc(cc1)C	C32H35O3N5
234333487	ChemDiv, Inc	V014-8901	1-benzhydryl-4-[[1-(2,5-dimethylphenyl)-3-(3-methoxyphenyl)-1H-pyrazol-5-yl]carbonyl]piperazine	[n]2(nc(cc2C(=O)N4CCN(CC4)C(c6cccc6)c5cccc5)c3cc(ccc3)OC)c1c(ccc(c1)C)C	C36H36O2N4
372736109	ChemDiv, Inc	V015-4774	(4-(2-fluorophenyl)piperazin-1-yl)(4-(5-isopropyl-4-p-tolyl-4H-1,2,4-triazol-3-ylthio)methyl)phenylmethanone	Fc1c(cccc1)N2CCN(CC2)C(=O)c3ccc(cc3)CSc4[n](c(nn4)C(C)C)c5ccc(cc5)C	C30H32O1N5 S1F1
154643154	ChemDiv, Inc	V020-4178	4-fluoro-N-isobutyl-N-([1-[3-(trifluoromethyl)benzyl]-4-[3-(trifluoromethyl)phenyl]-3-pyrrolidinyl]methyl)benzamide	FC(F)(F)c1cc(ccc1)C2CN(CC2CN(C(C)C)C(=O)c4ccc(cc4)F)Cc3cc(ccc3)C(F)F	C31H31O1N2 F7
344693638	ChemDiv, Inc	V025-8637	3-([4-[(4-fluorophenyl)acetyl]-1-piperazinyl]methyl)-6-(3-methylphenyl)-2-phenylimidazo[1,2-a]pyridine	Fc1ccc(cc1)CC(=O)N2CCN(CC2)Cc3[n]4c(nc3c6cccc6)C=CC(=C4)c5ccc(cc5)C	C33H31O1N4 F1
121097081	ChemDiv, Inc	V025-9097	N-benzyl-N-2-[[4-(4-chlorophenyl)-1-(3,4-dimethoxyphenyl)-1H-imidazol-2-yl]amino]-2-oxoethyl)-4-methylbenzamide (G2iB)	Clc1ccc(cc1)c2nc([n](c2)c5cc(c(c5)OC)OC)NC(=O)CN(Cc4cccc4)C(=O)c3ccc(cc3)C	C34H31O4N4 Cl1
344695929	ChemDiv, Inc	V026-6880	2-[[4-[[2-(4-chlorophenyl)-6-(3-methylphenyl)imidazo[1,2-a]pyridin-3-yl]methyl]-1-piperazinyl]sulfonyl]benzotriazole	[S](=O)(=O)(N2CCN(CC2)Cc3[n]4c(nc3c6ccc(cc6)Cl)C=CC(=C4)c5cc(ccc5)C)c1c(cccc1)C#N	C32H28O2N5 Cl1S1
344693629	ChemDiv, Inc	V027-0500	2-(4-methylphenyl)-3-([4-[4-(trifluoromethyl)benzoyl]-1-piperazinyl]methyl)-6-[3-(trifluoromethyl)phenyl]imidazo[1,2-a]pyridine	FC(F)(F)c1cc(ccc1)C2=C[n]3c(nc(c3CN5CCN(CC5)C(=O)c6ccc(cc6)C(F)F)F)c4ccc(cc4)C)C=C2	C34H28O1N4 F6
344693828	ChemDiv, Inc	V027-0530	6-(3-ethoxyphenyl)-3-[[4-(3-fluorobenzoyl)-1-piperazinyl]methyl]-	Fc1cc(ccc1)C(=O)N2CCN(CC2)Cc3[n]4c(nc3c6ccc(cc6)C)C=CC(=C4)c5ccc(cc5)OCC	C34H33O2N4 F1

			2-(4-methylphenyl)imidazo[1,2-a]pyridine		
344693645	ChemDiv, Inc	V027-1389	3-({4-[(4-fluorophenyl)acetyl]-1-piperazinyl)methyl}-2-(3-methoxyphenyl)-6-[3-(trifluoromethyl)phenyl]imidazo[1,2-a]pyridine	FC(F)(F)c1cc(ccc1)C2=C[n]3c(nc(c3CN5CCN(CC5)C(=O)Cc6ccc(c6)F)c4cc(ccc4)OC)C=C2	C34H30O2N4 F4
344693525	ChemDiv, Inc	V027-1402	6-(1-benzothien-2-yl)-2-(4-chlorophenyl)-3-[[4-[[3-(trifluoromethyl)phenyl]sulfonyl]-1-piperazinyl)methyl]imidazo[1,2-a]pyridine	FC(F)(F)c1cc(ccc1)[S](=O)(=O)N2CCN(CC2)Cc3[n]4c(nc3c7ccc(c7)Cl)C=CC(=C4)c5[s]c6c(c5)ccc6	C33H26O2N4 Cl1S2F3
154821145	ChemDiv, Inc	V027-1461	2-(4-chlorophenyl)-3-({4-[(4-fluorophenyl)sulfonyl]-1-piperazinyl)methyl}-6-phenylimidazo[1,2-a]pyridine	Fc1ccc(cc1)[S](=O)(=O)N2CCN(CC2)Cc3[n]4c(nc3c6ccc(cc6)Cl)C=CC(=C4)c5cccc5	C30H26O2N4 Cl1S1F1
344693835	ChemDiv, Inc	V027-4749	4-(6-(1-benzothien-2-yl)-3-[(4-(3-fluorobenzoyl)-1-piperazinyl)methyl]imidazo[1,2-a]pyridin-2-yl)phenyl methyl ether	Fc1cc(ccc1)C(=O)N2CCN(CC2)C c3[n]4c(nc3c7ccc(cc7)OC)C=CC(=C4)c5[s]c6c(c5)cccc6	C34H29O2N4 S1F1
90368846	ChemDiv, Inc	V027-7169	1-(diphenylacetyl)-4-(3,5-diphenyl-1H-pyrazol-1-yl)piperidine	[n]4(nc(cc4c6cccc6)c5cccc5)C1CCN(CC1)C(=O)C(c3cccc3)c2cccc2	C34H31O1N3
344696025	ChemDiv, Inc	V029-3339	6-(3-ethoxyphenyl)-2-(4-fluorophenyl)-3-({4-[(4-fluorophenyl)sulfonyl]-1-piperazinyl)methyl}imidazo[1,2-a]pyridine	Fc1ccc(cc1)[S](=O)(=O)N2CCN(CC2)Cc3[n]4c(nc3c6ccc(cc6)F)C=CC(=C4)c5cc(ccc5)OCC	C32H30O3N4 S1F2
332647939	ChemDiv, Inc	V029-3540	3-[4-(benzyloxy)phenyl]-3-[1-(4-fluorobenzyl)-1H-indol-3-yl]-N-[2-(2-pyridinyl)ethyl]propanamide	Fc1ccc(cc1)C[n]2c3c(c(c2)C(CC(=O)NCCc6ncccc6)c4ccc(cc4)OC c5cccc5)cccc3	C38H34O2N3 F1
344693512	ChemDiv, Inc	V029-8627	3-[[4-(4-tert-butylbenzoyl)-1-piperazinyl)methyl]-6-(2,5-dimethylphenyl)-2-phenylimidazo[1,2-a]pyridine	[n]21c(nc(c2CN5CCN(CC5)C(=O)c6ccc(cc6)C(C)C)c4cccc4)C=CC(=C1)c3c(ccc(c3)C)C	C37H40O1N4
154819933	ChemDiv, Inc	V029-9895	8-[[4-[[2-(4-chlorophenyl)-6-phenylimidazo[1,2-a]pyridin-3-yl]methyl]-1-piperazinyl]sulfonyl]quinoline	[S](=O)(=O)(N3CCN(CC3)Cc4[n]5c(nc4c7ccc(cc7)Cl)C=CC(=C5)c6cccc6)c1c2ncccc2ccc1	C33H28O2N5 Cl1S1
332651912	ChemDiv, Inc	V030-0484	3-[5-(chloro-1H-indol-3-yl)-3-[3-(4-chlorophenoxy)phenyl]-N-[2-(4-morpholinyl)ethyl]propenamide (G2ii)]	Clc1ccc(cc1)Oc2cc(ccc2)C(CC(=O)NCCN5CCOCC5)c3c4c([nH]c3)ccc(c4)Cl	C29H29O3N3 Cl2
372880764	ChemDiv, Inc	V030-1419	(3-((4-(4-fluorophenyl)-5-(furan-2-yl)-4H-1,2,4-triazol-3-ylthio)methyl)phenyl)(4-(2-fluorophenyl)piperazin-1-yl)methanone	Fc1c(cccc1)N2CCN(CC2)C(=O)c3cc(ccc3)CSc4[n](c(nn4)c6[o]cc6)c5ccc(cc5)F	C30H25O2N5 S1F2
344693633	ChemDiv, Inc	V030-2174	6-(1-benzothien-2-yl)-2-(4-chlorophenyl)-3-({4-[(trifluoromethyl)benzoyl]-1-piperazinyl)methyl}imidazo[1,2-a]pyridine	FC(F)(F)c1ccc(cc1)C(=O)N2CCN(CC2)Cc3[n]4c(nc3c7ccc(cc7)Cl)C=CC(=C4)c5[s]c6c(c5)cccc6	C34H26O1N4 Cl1S1F3
344696239	ChemDiv, Inc	V030-2573	1-[4-[3-({4-[(2-chloro-5-nitrophenyl)sulfonyl]-1-piperazinyl)methyl}-2-	[S](=O)(=O)(N2CCN(CC2)Cc3[n]4c(nc3c6cccc6)C=CC(=C4)c5cc(c(cc5)C(=O)C)c1c(ccc(c1)[N+](=O)[O-])Cl	C32H28O5N5 Cl1S1

Publications

			phenylimidazo[1,2-a]pyridin-6-yl]phenyl)ethanone		
344696238	ChemDiv, Inc	V030-2628	3-({4-[(2-chloro-5-nitrophenyl)sulfonyl]-1-piperazinyl)methyl}-2-(3-methoxyphenyl)-6-(3-methylphenyl)imidazo[1,2-a]pyridine	[S](=O)(=O)(N2CCN(CC2)Cc3[n]4c(nc3c6cc(ccc6)OC)C=CC(=C4)c5cc(ccc5)C)c1c(ccc(c1)[N+](=O)[O-])Cl	C32H30O5N5 Cl1S1
344696332	ChemDiv, Inc	V030-2674	2-(4-fluorophenyl)-3-({4-[(3-nitrophenyl)sulfonyl]-1-piperazinyl)methyl}-6-[3-(trifluoromethyl)phenyl]imidazo[1,2-a]pyridine	FC(F)(F)c1cc(ccc1)C2=C[n]3c(nc(c3CN5CCN(CC5)[S](=O)(=O)c6cc(ccc6)[N+](=O)[O-]))c4ccc(cc4)F)C=C2	C31H25O4N5 S1F4
344696242	ChemDiv, Inc	V030-2685	3-({4-[(2-chloro-5-nitrophenyl)sulfonyl]-1-piperazinyl)methyl}-2-(4-fluorophenyl)-6-(3-methylphenyl)imidazo[1,2-a]pyridine	Fc1ccc(cc1)c2nc3[n](c2CN5CCN(CC5)[S](=O)(=O)c6c(ccc(c6)[N+](=O)[O-])Cl)C=C(C=C3)c4cc(ccc4)C	C31H27O4N5 Cl1S1F1
332657079	ChemDiv, Inc	V030-2767	3-[3-(4-chlorophenoxy)phenyl]-3-(1H-indol-3-yl)-N-(4-pyridinylmethyl)propanamide	Clc1ccc(cc1)Oc2cc(ccc2)C(CC(=O)NCc5ccncc5)c3c4c([nH]c3)ccc4	C29H24O2N3 Cl1
344696288	ChemDiv, Inc	V030-5887	N-4-({4-[(6-(3-chlorophenyl)-2-(4-chlorophenyl)imidazo[1,2-a]pyridin-3-yl)methyl]-1-piperazinyl)sulfonyl]phenyl)acetamide	[S](=O)(=O)(N2CCN(CC2)Cc3[n]4c(nc3c6ccc(cc6)Cl)C=CC(=C4)c5cc(ccc5)Cl)c1ccc(cc1)NC(=O)C	C32H29O3N5 Cl2S1
344693611	ChemDiv, Inc	V030-8097	3-({4-[(benzyloxy)acetyl]-1-piperazinyl)methyl}-6-(2,5-dimethylphenyl)-2-(4-nitrophenyl)imidazo[1,2-a]pyridine	[N+](=O)([O-])c1ccc(cc1)c2nc3[n](c2CN5CCN(CC5)C(=O)COCc6ccccc6)C=C(C=C3)c4c(ccc(c4)C)C	C35H35O4N5
117452839	ChemDiv, Inc	L227-0253	1-(2-(4-chlorophenyl)-5-methylene-4,5-dihydropyrazolo[1,5-a]pyrimidin-7-yl)-N-((3-methyl-1H-pyrazol-4-yl)methyl)piperidine-4-carboxamide	Clc1ccc(cc1)c2n[n]3c(c2)NC(=C)C=C3N4CCC(CC4)C(=O)NC5c([nH]n)5C	C24H26O1N7 Cl1
40717273	ChemDiv, Inc	C380-0602	10-(2-chloro-6-fluorobenzyl)-8-(3,4-dihydro-2(1H)-isoquinolinylcarbonyl)dibenzo[b,f][1,4]thiazepin-11(10H)-one	Fc1c(c(ccc1)Cl)CN2c3c(ccc(c3)C(=O)N5CCc6c(cccc6)C5)Sc4c(ccc4)C2=O	C30H22O2N2 Cl1S1F1

7 Deutsche Zusammenfassung

Menschliche Glukosetransporter (GLUTs) sind eine Familie von spezialisierten Membranproteinen die den Transport von Hexosen über Membranen, entlang eines Konzentrationsgefälles, ermöglichen. Die Aminosäuresequenzen der 14 Isoformen weisen hohe Ähnlichkeiten auf, doch unterscheiden sich die Proteine in ihrer Substratspezifität und -affinität und sind in verschiedenen Geweben unterschiedlich stark vertreten. Anhand ihrer Strukturähnlichkeiten werden GLUTs in drei Klassen unterteilt, wobei die am besten untersuchten Isoformen GLUTs1-4 zur Klasse 1 zählen. Abweichungen in der Funktion von verschiedenen GLUTs wurden mit unterschiedlichen Krankheiten assoziiert, darunter auch die Volkskrankheiten Krebs und Diabetes. Folglich sind GLUTs Gegenstand intensiver Forschung und erhebliche Anstrengungen werden unternommen, um Liganden zu identifizieren, die spezifisch mit einzelnen GLUTs interagieren. Diese könnten als Hilfsmittel in Studien eingesetzt werden, die anstreben die genauen Funktionen der einzelnen GLUTs weiter aufzuklären und haben das Potenzial, als pharmazeutisch aktive Substanzen eingesetzt zu werden.

In dem Hexose Transporter-freiem („hxt⁰“) Hefestamm EBY.VW4000 wurden sämtliche endogene Hexose Transporter Gene (*HXT1-16* und *GAL2*) und einige Maltose Transporter Gene (*AGT1*, *MPH2* und *MPH3*) deletiert, was dazu führte, dass dieser Stamm nicht mehr auf Glukose oder einer ähnlichen Hexose wachsen kann. Wachstum kann jedoch auf Maltose-haltigem Medium erreicht werden, da dieses Disaccharid immer noch über spezialisierte Maltose Symporter der Malx1 Familie aufgenommen werden kann. Dieser Stamm eignet sich sehr gut für die Untersuchung von heterologen Transportern, wie bereits durch verschiedene Studien, mit Transportern aus unterschiedlichen Organismen, gezeigt werden konnte. Die funktionelle Expression von GLUTs in der Hefe ist jedoch nicht ohne bestimmte Modifikationen möglich, die entweder den Transporter selbst betreffen, oder den hxt⁰ Hefestamm, in dem dieser exprimiert werden soll. Einzelne Punktmutationen in GLUT1 und GLUT5 führten zu deren funktioneller Expression im EBY.VW4000 Stamm und der unveränderte GLUT1 Transporter ist aktiv im hxt⁰ Stamm EBY.S7, der die *fgy1* Mutation in seinem Genom trägt. Diese Mutation bewirkt eine C-terminale Verkürzung des Efr3 Proteins, welches, über C-terminale Interaktionen, die Rekrutierung der Phosphatidylinositol-4-phosphat (PI4P) Kinase

Stt4 zur Plasmamembran vermittelt. Es wird daher angenommen, dass der Gehalt an PI4P in der Membran von EBY.S7 reduziert ist. GLUT4 konnte im hxt⁰ Stamm SDY.022 aktiv exprimiert werden, der ebenfalls die *fgy1* Mutation besitzt und in dem außerdem *ERG4* deletiert wurde. Erg4 ist eines der letzten Enzyme des Ergosterol Synthesewegs, weswegen eine veränderte Sterol Zusammensetzung in der Membran von SDY.022 angenommen wird.

Ziel dieser Arbeit war die funktionelle Expression von GLUT2 und GLUT3 in einem hxt⁰ Hefestamm, um so ein geeignetes System für das Screening von Molekülen zu erschaffen, die die Aktivität dieser Transporter beeinflussen. Ein, durch PCR entstandener, Aminosäureaustausch in der zweiten Transmembranregion von GLUT3 (S66Y) führte zu seiner funktionellen Expression im EBY.VW4000 Stamm, während das unveränderte GLUT3 Protein auch im EBY.S7 Stamm aktiv war. Die Funktionalität von GLUT2 in Hefe konnte durch rationales Design erreicht werden. Der extrazelluläre Bereich (Loop), der die Transmembranregionen 1 und 2 verbindet, ist in GLUT2 signifikant länger, im Vergleich zu den anderen GLUTs der Klasse 1. Durch eine gezielte Kürzung dieses Loops um 34 Aminosäuren und den Austausch eines Alanins gegen ein Serin wurde ein GLUT3-ähnlicher Loop in das GLUT2 Protein eingebaut. Durch Fluoreszenzmikroskopie konnte gezeigt werden, dass dieses Konstrukt mit verkürztem Loop (GLUT2_{ΔloopS}), nicht jedoch das GLUT2 Protein in voller Länge, korrekt an der Plasmamembran lokalisiert. Dies deutet darauf hin, dass der auffallend große Loop das Protein Trafficking verhindert. Dieses Konstrukt (GLUT2_{ΔloopS}) war bereits aktiv im EBY.S7 Stamm. Eine weitere Mutation in der Transmembranregion 11, die zufällig durch PCR-Amplifikation eingebaut wurde, ermöglichte schließlich auch die Funktionalität von GLUT2_{ΔloopS_Q455R} in EBY.VW4000. Es wurde vermutet, dass die beiden Mutationen, die für die funktionelle Expression von GLUT2 bzw. GLUT3 in der Hefe vorteilhaft sind (Q455R bzw. S66Y), eine Destabilisierung der nach innen gerichteten Konformation bewirken, was die nach außen gerichtete Konformation begünstigt. Dadurch könnte die Substratbindestelle für Substrate außerhalb der Zelle besser zugänglich werden, was eine mögliche Erklärung für die gesteigerte Aktivität der Mutationen-tragenden Transporter in der Hefe ist. Die jeweilige Zugabe der bekannten GLUT Inhibitoren phloretin und quercetin erzeugte eine verminderte Transport Aktivität für die GLUT2 und GLUT3 Konstrukte im

Hefesystem, was durch Aufnahme- und Wachstumstests gezeigt werden konnte. Dies bestätigte, dass die beiden Systeme für Screening Experimente geeignet sind.

Das GLUT2 Hefesystem wurde im Anschluss auch für diesen Zweck verwendet. Eine Auswahl an Substraten, die zuvor durch *in silico* Screening selektiert worden waren, wurden auf ihren Einfluss auf die GLUT2 Aktivität im Hefesystem getestet. Dadurch konnten elf wirkungsvolle GLUT2 Inhibitoren identifiziert werden, die IC₅₀ Werte im Bereich von 0.61 und 19.3 µM aufwiesen, und mit absteigender Wirkstärke als G2iA- G2iK bezeichnet wurden. Durch den Einsatz der anderen GLUT Hefesysteme wurde untersucht ob diese Komponenten ebenfalls Einfluss auf die Aktivität von GLUT1, GLUT3, GLUT4 oder GLUT5 haben. Diese Untersuchungen zeigten, dass neun Liganden spezifisch auf GLUT2 wirkten, während einer sämtliche GLUTs der Klasse 1 (GLUTs1-4) beeinflusste und ein weiterer die Fruktose transportierenden Transporter GLUT2 und GLUT5 inhibierte. Eine virtuelle Analyse der Liganden-Transporter Interaktionen zeigte außerdem, dass die identifizierten Inhibitoren an den äußeren Rand der Substrat Aushöhlung des GLUT2 Proteins binden. An dieser Stelle ist die hohe Sequenzähnlichkeit, die zwischen GLUT2 und anderen Klasse 1 GLUTs herrscht, weniger ausgeprägt als an der zentralen Glukosebindestelle, was vermutlich die hohe Spezifität der neun GLUT2-spezifischen Inhibitoren ermöglicht. Die Liganden stellen nützliche Werkzeuge für Studien dar, die eine weitere Aufklärung der metabolischen Rolle von GLUT2 im menschlichen Organismus anstreben. Außerdem sind sie potenzielle Substrate für die Therapie von GLUT2-asoziierten Krankheiten, wie das Fanconi-Bickel Syndrom, Diabetes oder bestimmte Tumore.

Der positive Effekt der vermutlich veränderten Sterol Zusammensetzung (durch Deletion von *ERG4*) in der Membran von SDY.022 auf die funktionelle Expression von GLUT4, führte zu der Hypothese, dass die Anwesenheit des menschlichen Hauptsterols Cholesterol oder Cholesterol-ähnlicher Sterole, ebenfalls vorteilhaft für die Funktionalität von GLUTs in Hefe sein könnte. Daher wurde im Rahmen dieser Arbeit die Erzeugung von hxt⁰ Stämmen angestrebt, die diese Sterole synthetisieren, indem Modifikationen am Ergosterol Biosyntheseweg vorgenommen wurden. Durch diese Experimente entstanden mehrere hxt⁰ Stämme die vermutlich verschiedene Hauptsterole in ihrer Membran enthalten.

Tropftests auf Glukose Medium mit diesen Stämmen die GLUT1 oder GLUT4 exprimierten zeigten, dass die Deletion von *ERG6* für die funktionelle Expression von GLUT1 (aber nicht von GLUT4) vorteilhaft ist. Dies deutet darauf hin, dass die Methylgruppe an der Seitenkette des Ergosterols (eine Methylengruppe wird durch Erg6 eingefügt und durch Erg4 reduziert) einen negativen Effekt auf die Aktivität von GLUT1 hat. Der Effekt der *ERG6* Deletion war jedoch weniger ausgeprägt als der putativ reduzierte Gehalt von PI4P in der Membran vom EBY.S7 Stamm. Das Membranprotein Sfk1 vermittelt, ähnlich wie Efr3 über C-terminale Interaktionen, eine korrekte Lokalisation von Stt4 an der Plasmamembran. Wie in dieser Arbeit gezeigt, führte eine Überexpression von Sfk1, nicht jedoch von einem Sfk1 Konstrukt mit verkürztem C-Terminus, in EBY.S7 zu einer verminderten Aktivität von GLUT1. Diese Ergebnisse unterstützen die Annahme, dass ein verminderter PI4P Gehalt vorteilhaft für die funktionelle Expression einiger GLUTs in der Hefe ist. Eine weitergehende Regulation der Phospholipid Zusammensetzung in der Plasmamembran könnte demnach ein vielversprechender Ansatz sein, um *hxt*⁰ Stämme zu konstruieren, in denen (weitere) GLUTs aktiv sind.

Des Weiteren wurde in dieser Arbeit eine neue Methode entwickelt, um Glukose Transportraten von, im *hxt*⁰ Hefesystem exprimierten, Transportern zu bestimmen und somit deren kinetische Charakterisierung zu erleichtern. Hierfür wurde die pH-sensitive GFP (*green fluorescent protein*) Variante pHluorin als Biosensor verwendet. Mit diesem Sensor kann der zytosolische pH-Wert der Zelle (pH_{cyt}) bestimmt werden, indem das Verhältnis der Emissionsintensitäten bei 512 nm bei zwei verschiedenen Anregungswellenlängen (390 und 470 nm) ermittelt wird ($R_{390/470}$). Zellen, denen die Zuckerzufuhr für einige Stunden entzogen wird, weisen einen leicht sauren pH_{cyt} auf, da die ATP Produktion nachlässt und somit die Aktivität von ATP-abhängigen Protonenpumpen reduziert wird. Wenn Zucker, wie z.B. Glukose, wieder zugeführt wird, steigt der pH_{cyt} mit der Zeit wieder auf ein normales Niveau von etwa 7 an, da die ATP Produktion wieder hergestellt wird. In den ersten ~10 Sekunden nach der Glukosezufuhr sinkt der pH_{cyt} jedoch zunächst rapide weiter. Dies ist durch den ersten Schritt der Glykolyse zu erklären, in dem Glukose durch eine Hexokinase zu Glukose-6-Phosphat phosphoryliert wird, wobei ein ATP hydrolysiert wird, was ein Proton freisetzt, welches das Zytosol weiter ansäuert. Es wurde entdeckt, dass die Geschwindigkeit dieser anfänglichen

Ansäuerung, unter bestimmten Voraussetzungen, direkt proportional zur Glukose Aufnahmerate des jeweils getesteten Transporters ist. Der lineare Abfall des pH_{cyt} wurde infolgedessen als Parameter für die Zuckeraufnahmegeschwindigkeit benutzt und für die Michaelis Menten Gleichung verwendet. Somit konnten verlässlich die K_M Werte von ausgewählten Transportern bestimmt werden. Diese Methode bietet einen klaren Vorteil gegenüber dem klassischen C^{14} -Glukose Aufnahmetest, da sie auf den Einsatz von radioaktiv markierter Glukose verzichtet. Ihre Anwendung ist dadurch kostengünstiger, da die Beschaffung und die Entsorgung von radioaktiven Substanzen teuer sind, und birgt ein geringeres gesundheitliches Risiko für den Anwender. Neben der kinetischen Charakterisierung der Transporter, könnten pHfluorin-basierte Tests auch für qualitative Aktivitätsmessungen eingesetzt werden, z.B. zur Überprüfung der Aktivität eines heterologen Glukosetransporters im hxt^0 Hefesystem oder zum Screening von potenziellen Inhibitoren. Als konzeptioneller Beweis dafür, wurde in dieser Arbeit anhand von Messungen mit GLUT1 exprimierenden hxt^0 Zellen gezeigt, dass der inhibitorische Effekt von phloretin auch in der, deutlich langsamer verlaufenden, Erholungsphase, in dem der pH_{cyt} auf ein neutrales Niveau ansteigt, sichtbar wird. Da eine besonders schnelle Messung dann nicht nötig ist, kommen diese Experimente auch mit der langsameren Datenerfassung eines Mikroplatten Lesegeräts aus, wodurch eine Voraussetzung für ein Hochdurchsatzscreening gegeben ist.

Zusammenfassend konnte das hxt^0 Hefesystem in dieser Arbeit um die beiden wichtigen Transporter GLUT2 und GLUT3 erweitert werden. Dadurch wurde ein geeignetes Screening System erschaffen, welches die Suche nach Liganden, die spezifisch mit diesen Transportern interagieren, erleichtert. Das GLUT2 System kam in dieser Arbeit bereits erfolgreich zum Einsatz, wodurch elf wirkungsstarke Inhibitoren identifiziert wurden, von denen neun sehr wahrscheinlich spezifisch auf GLUT2 wirken. Außerdem wurde eine neue Methode entwickelt, um die kinetischen Eigenschaften von Transportern zu bestimmen, die auf den Einsatz von radioaktiv markierter Glukose verzichtet. Diese innovative Entwicklung ist eine wertvolle Ergänzung zu bestehenden Methoden und wird die Forschung an Zuckertransportern bedeutend unterstützen.